DXN074510.

Fibre Bragg Grating Temperature Sensors for High-Speed Machining Applications.

by

Frédéric Bezombes

A thesis submitted in partial fulfilment of the
requirements of Liverpool John Moores University
for the degree of Doctor of Philosophy.

February 2004

General Engineering Research Institute
Liverpool John Moores University

Acknowledgements.

The first and main thanks goes to Professor M. J. Lalor and Professor D. R. Burton for their patience, help, guidance and encouragement throughout the period of this work.

A very big thank you also goes to the EPSRC for providing a studentship.

The author would also like to thank all the people working within the General Engineering Research Institute (GERI) for their help and support particularly Dr. D. Allanson, Dr. F. Lilley, Mr F. Cristino, Dr. D. Tipper and Mr S. Anderson. This work would not have been possible without the useful help of Mr L. Douglas and Mr. T. Dunmore from the manufacturing group of the School of Engineering and also Mr. T. Scargill, Mr. M. Noord and Dr. M. Morgan from the Advanced Manufacturing Technology and Tribology Research Laboratory (part of GERI) for their help with the grinding application.

The author is also grateful to Mrs. M. Sutton for her help and kindliness.

A special thanks goes to the author's friends who had to deal with him throughout the stressful writing-up time and finally the author would like to thank his parents and his family for their support.

Abstract.

In high-speed grinding research, it is required to measure temperature within the workpiece. Present techniques are thermocouple based, and often suffer from excessive electrical noise on the signal. This thesis presents a number of novel and existing optical sensing devices that overcome this limitation and also, in some cases, offer greater performance. The optical sensors are fibre Bragg grating based and the optical techniques used to interrogate that sensor include DWDM, WDM, athermic grating, tuneable grating and coupler. Optical fibre devices are simpler to place in situ prior to the machining tests and they offer faster response and greater sensitivity than was previously possible. Results are presented from machining tests and the new devices are compared with each other and thermocouple based techniques. A method to relate internal measured temperature to machined surface temperature is also demonstrated in the context of high-speed machining.

Contents.

Symbols list.

Optic.

Grating.

I	the optical power in *dBm*.
n_{eff}	the effective index of the core.
ξ	the thermo-optic coefficient of the fibre.
λ_B	the Bragg wavelength in *nm*.
λ	the wavelength in *nm*.
$\Delta\lambda_{BT}$	wavelength shift in *nm*.
ΔT	temperature change in *°C*.
Λ	the Bragg grating period in nm.

Signal prediction.

I_L	the insertion loss in *dB*.
P_i	the optical power input to the optical network in *mW*.
P_o	the optical power output to the optical network in *mW*.

Photodetectors.

C_J	the diode junction capacitance in *pF*.
f_{BW}	the bandwidth in *Hz*.
$R(\lambda)$	the detector responsivity, in *A/W*.
R_{LOAD}	the external load resistance in Ω.
T_R	the rise time response in *s*.
V_0	the output voltage in *V*.

Heat transfer.

A	the crossectional area in m^2.
c	the specific heat in $kJ.kg^{-1}.°C^{-1}$.
k	the thermal conductivity in $W.m^{-1}.°C^{-1}$.
y	the distance in m.
n	the position along y.
p	the instant.
q_0	the heat transfer rate in $k.s^{-1}$.
τ	the time in s.
T	the temperature in $°C$.
T_l	the steady state temperature also, in normal conditions, the ambient temperature in $°C$.
T_n^p	the nodal temperature at position n and instant p.
α	the thermal diffusivity in $m^2.s^{-1}$.
ρ	the density in $kg.m^{-3}$.

Machining parameters.

f	the feed rate per tooth in $mm.tooth^{-1}$.
F	the feed rate in $mm.min^{-1}$.
n	the number of teeth of the cutter.
RPM	the rotational spindle speed in $rev.min^{-1}$.
s	the peripheral speed in $m.min^{-1}$.

Chapter 1: Introduction.

1. Introduction.

Tools are essential for our long-term survival because they allow us to build objects that would be impossible to build by hand. The evolution of early wooden tools, to the most sophisticated machine tool, has been motivated by the need to improve our standard of living. Since the stone age (over 50000 years ago), men have developed different type of tool to satisfy their needs. First stones, wood or bones were used as tools and weapons.

The harnessing of fire created a major improvement in human's standard of living. First, fire was used to warm up, protect or cook, and then later, it was used to extract metal from copper ore. This resulted in the bronze age (over 6500 years ago), during which time humans produced copper and bronze tools that are more easy to shape and stronger than the previous stone tools.

Later, as fire was more understood, high temperature furnaces were created allowing extraction of iron from iron ores. During the iron age (over 3400 years ago) humans learned to temper and hardened it. Iron soon replaced copper and bronze due to its properties creating a very important improvement of tools and weapons. Humans also started to domesticate animals and soon, the first animal powered tools replaced the human powered tools.

Around 300 years ago (machine age), new sources of energy were investigated. Humans started to develop the first machines that used the elements of nature such as water instead of human power or animal power. This was the birth of the first machines, production increased and better machines were built, helping the manufacture of the first viable steam

engine in 1776 by James Watt. This new source of energy rapidly led to the industrial revolution during which old machines were improved and new ones created using that new source of high power. This created a major improvement in humans' standard of living. The first railways, steamboats and also steam driven tractors rapidly appeared. Around the same period, a way to produce static electricity was discovered by Otto von Guericke in 1660, then a few years later, in 1800, Volta developed the first battery producing the first continuous source of electricity. A few years later, the battery was mass-produced and the first electrical lamp was in use. Later inventors like André-Marie Ampère (1775-1836) and Michael Faraday (1791-1867) developed new ways to produce electricity. All these new discoveries rapidly led to the first electrical machine tool. In turn, this rapid progress in building new and better machines, led to the creation of diesel and gasoline engines.

Since day one, humans' need to create new and better weapons was primary. World War I (1914-1918) and World War II (1939-1945) were the catalysts of industrial growth and development since better machines were urgently needed to produce weapons and machine to high quantity. This resulted in today's technology and machine tools.

There are three main different type of machining that have been developed throughout the years:

- Turning where the workpiece is rotating horizontally while the tool is translating horizontally. This process allows the creation of cylindrical forms.

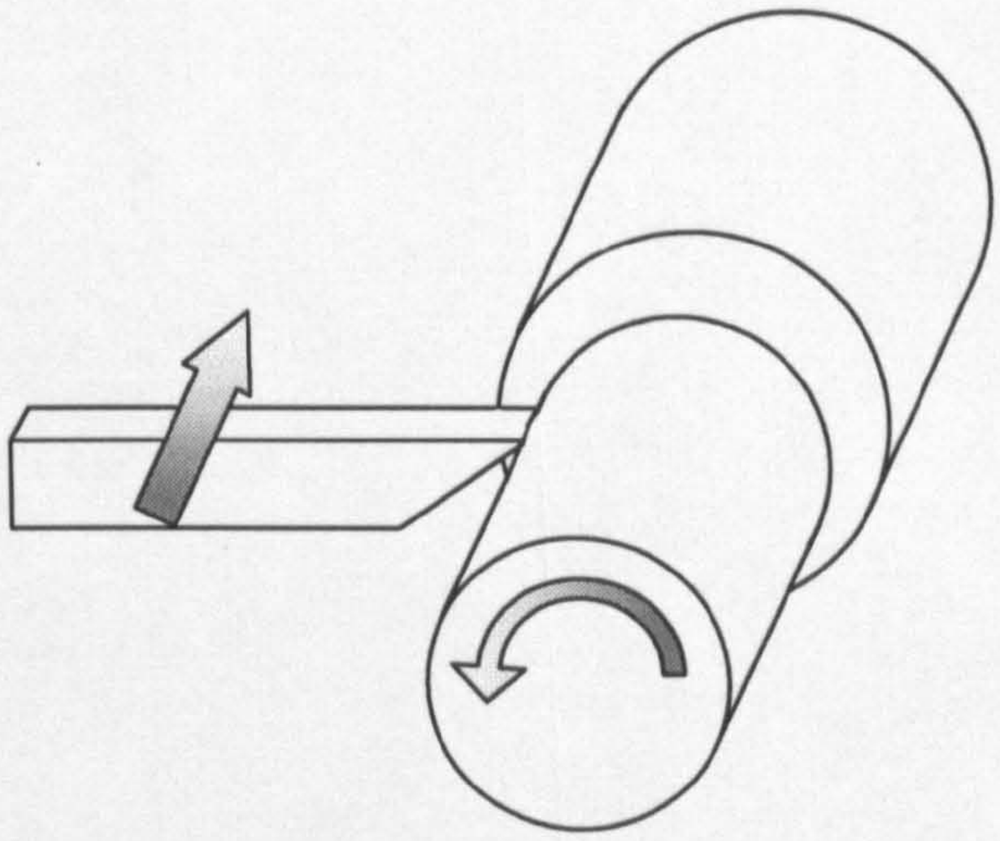

***Figure 1.1**: Standard turning process description.*

- Milling where the tool is rotating vertically while the workpiece is moving horizontally. This process is used for creating flat horizontal and/or vertical surfaces.

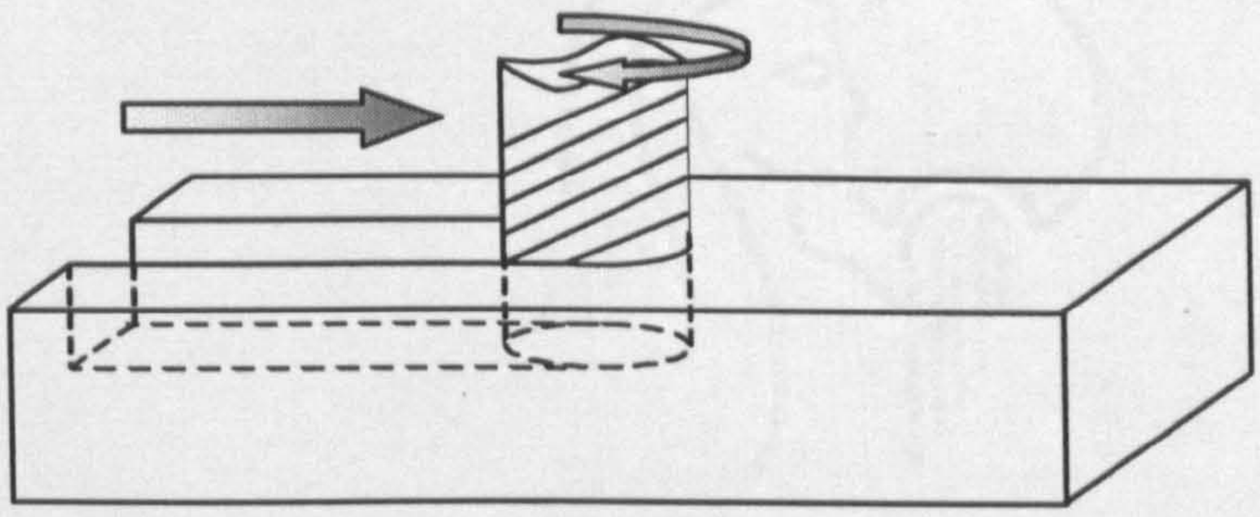

***Figure 1.2.:** Standard milling process description.*

- Grinding which is similar to milling except that the tool is rotating vertically removing just a thin layer of material at the time. This is used when high quality surface finish is needed.

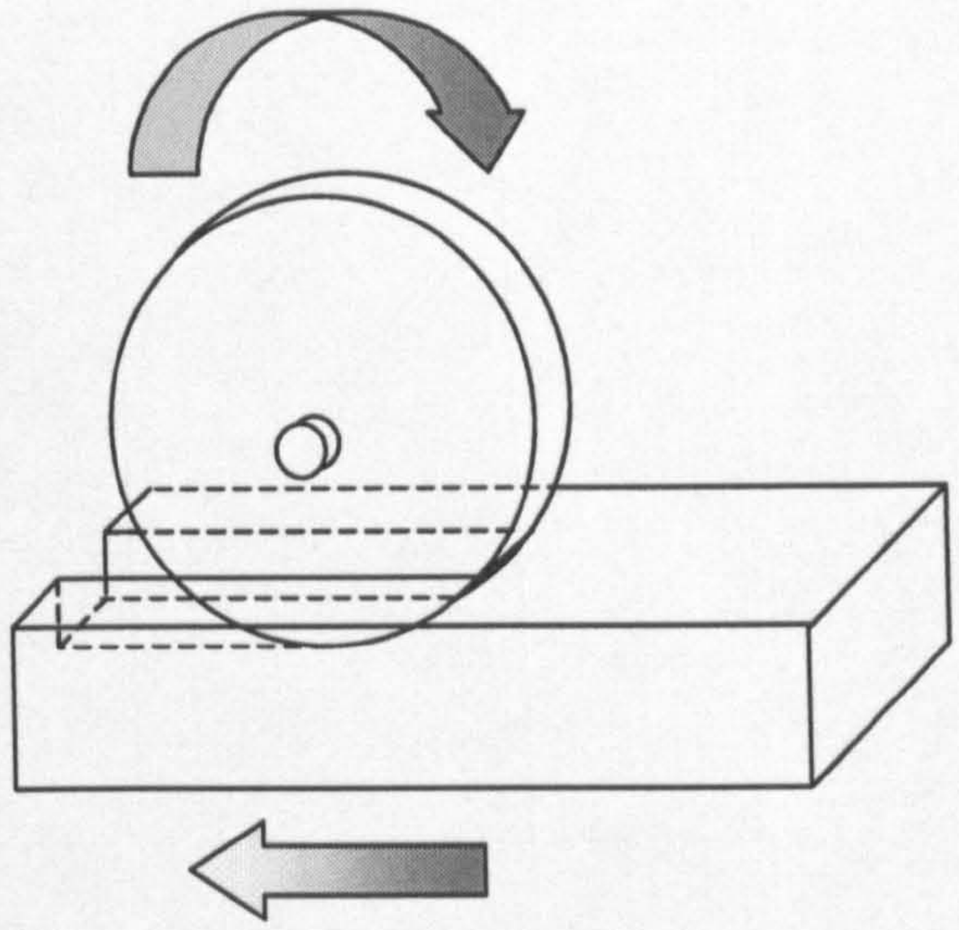

Figure 1.3.: *Standard grinding process description.*

1.1. Background.

Previous work within the School of Engineering has investigated the correlation between workpiece material damage, such as tempering, re-hardening, surface cracking and residual stress levels, with the temperatures achieved during the grinding process [1,2].

Theoretical heat transfer models have predicted the temperature generated on the workpiece surface during a grinding process [3]. However, there still remains a need to validate the predicted temperatures for the wide range of workpieces and grinding wheel geometries encountered in industry. Validation of the theoretical models [4] would allow the optimisation of the process to provide more productive and yet safe metal removal rates without the need for temperature measurement.

Work undertaken by Rowe, Morgan, Black et al [1,3,5,6] has to date concentrated on the measurement of machining temperatures using thermocouple techniques. Extensive experience [4] has been gained in the application of thermocouples for temperature measurement during machining operations, however there are still problems with signal reliability. The effects of machining coolant on thermocouple junctions, thermocouple calibration and high noise levels limit the accuracy, repeatability and reliability of thermocouple techniques [5].

The most successful thermocouple technique uses a fine single pole thermocouple embedded in the workpiece [6]. During grinding, the workpiece material is smeared over the surface of the thermocouple wire forming a temporary junction which gives rise to the measured temperature signal. Formation of the junction is dependent on the material properties of the workpiece as some materials are more ductile and the probability of smearing and junction formation is enhanced.

Complex workpiece geometries often require the measurement of temperatures at four or more locations, in these cases, the thermocouple technique is difficult to use. The difficulties arise, as each thermocouple has to be assembled into the workpiece by hand. To facilitate insertion of a thermocouple, the test workpiece is fabricated from two sections, between which the thermocouples are sandwiched. Each pole has to be laid in a shallow groove and insulated by a thin (less that 10μm) layer of mica. To complete the workpiece the two sections are brought together sandwiching the thermocouple poles in their required positions. This assembly process

may take from one to three days to complete and the complexity of thermocouple installation makes it difficult to guarantee a successful outcome. As a consequence, an experimental investigation of grinding temperatures on the surface of a complex geometry requires a significant period of time.

Formation of a thermocouple junction by smearing the workpiece material onto the thermocouple wire has one undesirable side effect; the measurement circuit becomes directly (electrically) coupled to the chassis of the machine tool. As the typical machine tool environment is electrically noisy, problems are encountered with the signal to noise ratio of the temperature signal. This can be reduced somewhat, by insulating the workpiece from the body of the machine tool, a requirement that is difficult to achieve reliably when the working area of the machine tool is bathed in copious quantities of water based coolant. Since the amplitude of the unconditioned thermocouple signal is very small (for example, a K-type thermocouple unconditioned voltage is 0.397mV at 10°C and 3.266mV at 80°C, taken from the manufacturer's data), therefore the thermocouple signal is very sensitive to the addition of electrical noise; in particular the noise generated by the machine components. In addition, the temperature signal compensation and amplification system is also prone to radio frequency interference generated by the motor control systems used on modern computer controlled machine tools.

The use of an optical fibre grating as a temperature sensor offers a potential solution to this difficult and time-consuming measurement process.

Operating on a completely different principle than electrical temperature sensors, such as thermocouples, the optical sensing system is electrically isolated from the machine tool and will not be subject to the effects of electro-magnetic interference and the effects caused by the electrical coupling of the measurement system to the machine tool (a particular problem when using a single pole thermocouple configuration).

1.2. Temperature sensing during machining.

High productivity and high quality levels are two very important and yet conflicting factors in modern manufacturing.

The drive for improved productivity cannot be allowed to jeopardise product quality. Many ground components are being used under more extreme conditions of loading and the need for surfaces of high integrity is becoming more crucial for success. There is therefore a need to understand the behaviour of the manufacturing processes and their impact on the integrity of the generated surface. This requires that controlling parameters such as surface finish, cutting force, heat generation and surface/subsurface temperatures etc are measured and strategies for process control developed.

For this purpose, different techniques were developed throughout the years to monitor changes in important parameters during machining processes. There are three main machining processes that create a surface by cutting,

these are: turning, milling and grinding. Techniques for monitoring these processes are described by Dragos Axinte in "Sensor Applications for Monitoring High Speed Cutting" [7a] and in "Sensor Applications for Grinding Process Monitoring" [7b].

Temperature is one of the most important outputs of the machining process since elevated temperatures can increase tool wear i.e. decrease tool life and produce thermal deformations [8]. Also in some cases, the heat generated during machining needs to be controlled to avoid the tempering of the workpiece material. This is of particular concern to the manufacturers of heavily loaded ground components such as those found in the fuel injection and rolling element-bearing industries. In-order to control the heat developed within the surface of a machined component, it is necessary to measure both the heat transfer into the surface and the subsurface temperatures. The main techniques that have been developed to measure the heat generated during machining processes are:

- **Thermocouple technique.**

Thermocouples are the most common transducers used to measure temperature during machining. A variety of thermocouple based temperature measurement systems have been employed on a range of machining processes.

A thermocouple-based system was successfully developed by Chen and Tsao for measuring the temperature of the tool rake face [8]. During turning the relative motion between the workpiece and the cutting tool is generated

by rotating the workpiece and controlling the axial and radial position of the cutting tool. Since the cutting tool is clamped and does not rotate during turning, it is relatively easy to insert sensors below the tool cutting face. This was achieved by machining a groove in the tool chip breaker and by inserting the thermocouple in it. This experiment showed that it was possible to measure the temperature generated during a turning operation and it was also possible to show that the tests results were in "reasonable agreement" with the theoretical results also described in this publication [8]. Other attempts for measuring temperature during grinding using thermocouples were successful [5,6] using the techniques previously described. The main limitation encountered during the experiments being caused by the electrical noise interference picked up by the thermocouple and by the unreliability of the thermocouple signal in wet grinding [6]. To avoid such undesirable effects, good insulation of the thermocouple is necessary and this makes the setting up of experiments, long and difficult.

- **Infrared radiation technique.**

A previous attempt at using an optical method to sense grinding temperature, used an optical fibre to collect the infrared radiation being generated by the newly ground workpiece surface [9,10]. The infrared radiation was then transmitted to an InAs (Indium Arsenide) based infrared detector. This technique allowed measurement of the heat pulses generated by the individual cutting grains during a grinding process. The method was first used to determine the temperature of cutting grains on a

grinding wheel just after cutting [9]. The work was further extended and the same system was used to measure the inner temperature of the workpiece [10]. A small blind hole was drilled towards the workpiece surface. An optical fibre was inserted into the hole to collect the black body radiation generated in the resulting cavity. The spectrum of the infrared radiation was then used to calculate the temperature of the cavity. Different types of pyrometer were tested and these results were then compared with the results given by thermocouples. The optical systems described can detect brief heat pulses that cannot be detected by the thermocouple with its slower response time. InAs-infrared radiation pyrometer was found to be the most suitable detection technique since it has a time response of in the order of 1μs [10]. Dictionaries' definition of response time is "the time a system takes to react to a given input". This system was successfully used to measure the temperature inside the workpiece [10] and also of the tool abrasive grains [9] during grinding.

Other commercially available techniques used to measure temperature during machining processes are:

- **Thermal imaging systems.**

A camera is used to detect and display the infrared radiation emitted by the machined surface. This technique is limited by the reaction time of the camera and also by the fact that the camera cannot detect the heat

at the point of contact between the tool and the workpiece during milling and grinding as the contact point is hidden by the tool.

- **Thermo sensitive painting.**

  This technique uses the property of a special type of paint (thermo sensitive paint) to change colour with temperature. It is an approximate method and the workpiece temperature achieved during the machining can only be read after the event.

In order to avoid some of the aforementioned limitations, it was decided to investigate the application of optical fibre based temperature measurement systems to the problem of grinding temperature measurement. To-date there have been no attempts at measuring milling or grinding temperatures using an embedded optical fibre Bragg grating. In some cases, optical sensors offer significant advantages over more conventional sensors such as greater sensitivity, wide dynamic range, electrical passiveness, both point and distributed configuration, freedom from electromagnetic interference multiplexing capabilities [11].

The programme of work described in this thesis attempts to determine the benefits achievable when adopting an optical approach to the measurement of machining temperatures.

1.2. Aim and Objectives.

The aim of the research program was to investigate the feasibility of measuring grinding temperature using fibre based optical sensors. This was achieved through the following objectives:

- Review of existing optical temperature measurement systems.
- Design and development of prototype optical temperature measurement systems based on in-fibre Bragg gratings.
- Development of a basic heat transfer model to predict the temperature at the surface of interest.
- Development of a workpiece for testing of the optical fibre temperature measurement systems during high-speed machining.
- Comparison of temperatures measured by optical fibre based sensors and the existing thermocouple techniques during high-speed machining tests.

References.

1. McCormack D. F., Rowe W. B., Morgan M. N., Mills B. and Pettit J. A. P., "Prevention of Material Damage During Grinding", Proc. 4th International Conference of Materials in Machining: Opportunities and Prospects for Improved Operations, p 238-247, 1998.

2. McCormack D. F., Rowe W. B., Chen X., Bouzina A., Fitzpatrick M. E. and Edward L., "Characterising the Onset of Tensile Residual Stresses in Ground Components", Proc. 6th International Conference on Residual Stresses (ICRS-6), Oxford University, p 225-232, 2000.

3. Black S C E, "The effect of abrasive properties on the surface integrity of ground ferrous materials", Ph.D. Liverpool John Moores University Thesis, 1996.

4. Tan Jin, Carmona Diaz E, Baldwin A, Corbett J, Stephenson D J, "A new grinding regime – thermal limitations to material removal by grinding", Review of progress, School of industrial and manufacturing science, Cranfield University, 2002.

5. Rowe W. B., Mills B. and Black S. C. E., "Temperature Control in CBN Grinding", The International Journal of Advanced Manufacturing Technology, p 387-392, 1996.

6. Black S. C. E., Rowe W. B., Qi H. S. and Mills B., "Temperature Measurement in Grinding", Proc. 31st International MATADOR Conference, p 409-413, 1995.

7. a. Dragos Axinte, "Sensor Applications for Monitoring High Speed Cutting", Sponsored by: CNR - NATO fellowship programme, http://www.lapt.unina.it/Axinte2.html.

7. b. Dragos Axinte, "Sensor Applications for Grinding Process Monitoring", Sponsored by: CNR - NATO fellowship programme, http://www.lapt.unina.it/Axinte3.html.

8. Chen W C and Tsao C C, "Determination of temperature distributions on the rake face of cutting tools using a remote method", Int. Comm. Heat Mass Transfer, Vol. 24, No. 2, p 161-170, 1997.

9. Ueda T., Hosokawa A. and Yamamoto A., "Studies of Temperature of Abrasive Grains in Grinding – Application of Infrared Radiation Pyrometer", Trans. ASME, J. of Eng. for Ind., vol. 107, p 127-133, 1985.

10. Ueda T., Hosokawa A. and Yamamoto A., "Measurement of grinding temperature using infrared radiation pyrometer with optical fiber", Trans. ASME, J. of Eng. for Ind., vol. 108 , p 247-251, 1986.

11. Keck D. B., "Optical Sensors and Specialty Fibers", Japanese technologies evaluation center, Loyola College, http://www.wtec.org/loyola/opto/, 1996.

Chapter 2: Background:
Optical sensors technology.

2. Background. Optical sensors technology.

There are two options for optical fibre based temperature measurement; *remote pyrometry*, where the fibre transmits the signal from an external source to an external detector, and *embedded sensors* where the sensing element is embedded in the fibre and it is interrogated by an external light source and detector.

By definition, a fibre based optical sensor system uses a light source to probe for an external perturbation of a fibre or fibre grating. Optical fibres are used to transmit the resulting signal from the sensing area/volume to the detector. Optical fibres use the principle of total internal reflection to transmit the optical signal. The principle of total internal reflection in its simplest form states that: "when the angle of incidence exceeds a critical value, light cannot get out of the glass; instead the light is reflected back in". Thus the principle of total internal reflection makes it possible to transmit light through an optical fibre along one or more optical paths to and from the sensing element.

Many different techniques have been developed in recent years for the optical sensing of temperature, the main ones of interest for this research programme are:

2.1. Fabry-Pérot interferometer.

Fabry-Pérot interferometers are made of materials such as glass, or zinc selenide calcite for which the thermal expansion coefficient and refractive

index are well known. A temperature change will induce a change in the optical path length of a short piece of material [1a]. The change in that path length is detected using a spectrometer. Then, knowing the thermal properties of the material used for building the interferometer, it is possible to relate the changes in wavelength detected with changes in temperature. Due to the materials used, these sensors are limited to a maximum temperature of approximately 600°C [1b]. The sensor described in this paper was successfully used for the monitoring of aircraft engine exhausts temperature.

2.2. Remote pyrometry.

In this technique, the optical fibres are used "to telemeter the black-body spectrum of a small piece of material such as sapphire to an appropriate measurement site" [2] where the temperature can be determined directly from the observed spectrum. The remote pyrometry technique is mainly used for high temperature applications. Examples of work using remote pyrometry [3a,3b] for the measurement of machining temperatures have been previously discussed (chapter 1: Introduction, paragraph 1.2.). In these experiments, the optical fibres were used to transmit the infrared radiation from an object to an infrared detector InAs.

2.3. Fluorescence emission.

In this type of device, a suitable laser source pumps a pulse of light to a fluorescent material sensor via optical fibre. The fluorescence and luminescence signal of the material exhibits both temporal and spectral change in response to temperature change. This allows the fluorescent material to be used as a temperature-sensing probe. By exploiting the temporal change and examining the changes in decay time of the reflected fluorescence signal, it is possible to measure temperature [4,5]. This system is illustrated in figure 2.1..

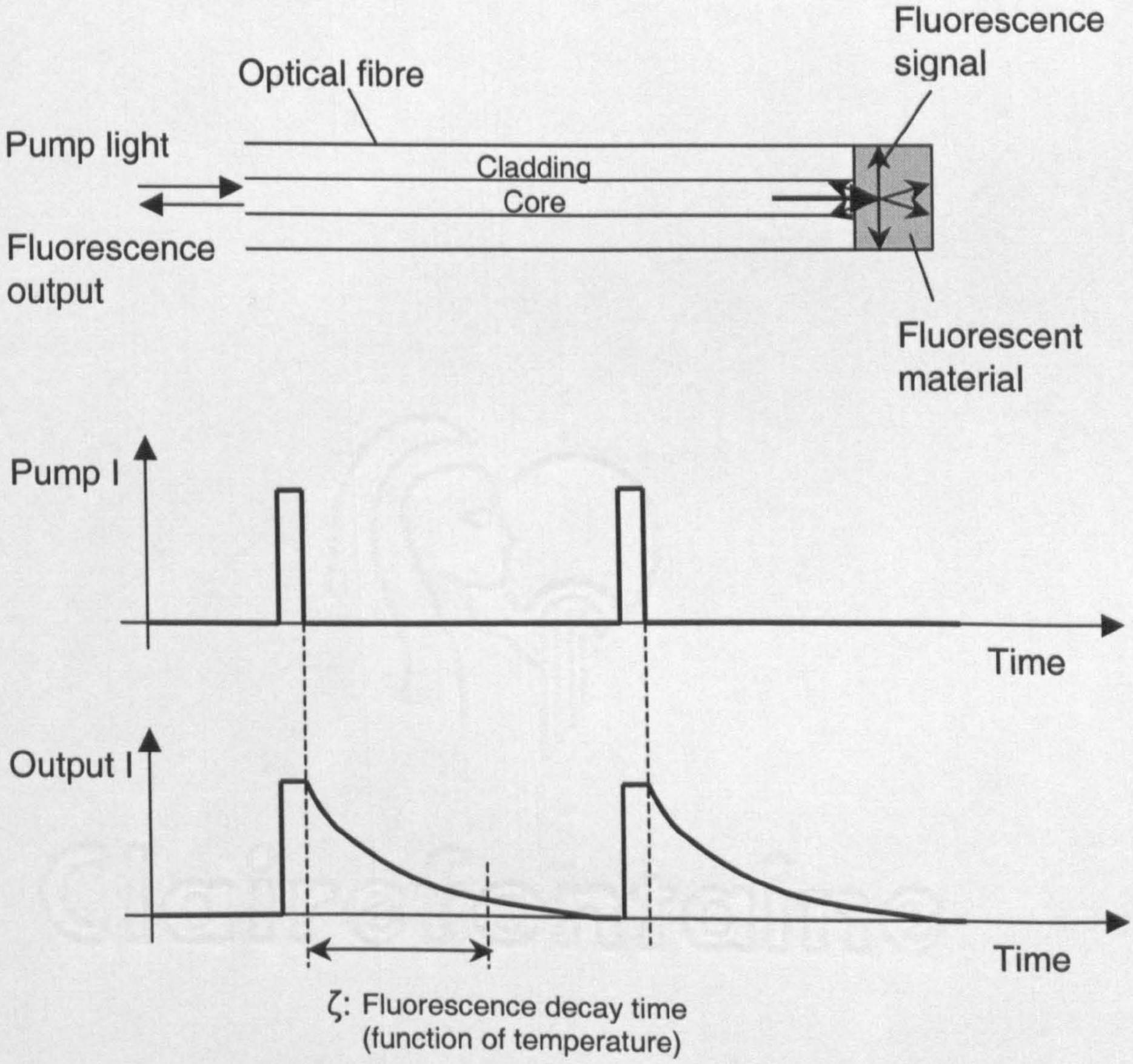

Figure 2.1.: *Fluorescence sensor, probe and operation [6].*

2.4. Bragg grating.

An increasingly used method of sensing temperature, strain etc. is the use of fibre Bragg gratings. Fibre Bragg techniques have been demonstrated by several research groups [7a]. One of the benefits of using intrinsic optical fibre sensors such Bragg gratings or fluorescent emission is that the sensing element is intrinsic to the fibre, as a result the light never leaves the fibre and this removes the need for the use of an optical bench. This is particularly important for the measurement of temperatures within a manufacturing environment, where the equipment will be subject to a relatively dirty environment.

The most common way for manufacturing a fibre Bragg gratings is by laterally exposing the core of a single-mode fibre to an ultraviolet (UV) radiation through a phase mask or an interferometer [8a]. The UV exposure creates a fixed refractive index modulation of the core of the fibre producing a fibre Bragg grating [8a]. A fibre Bragg grating is an interferometric sensor as it is based on the "relative phase difference between two or more rays". The light propagating through a periodic fibre Bragg grating is subjected to periodic changes in refractive index. At each refractive index change, a small amount of light is reflected back towards the source and the reflected rays interfere constructively producing a large reflection at a particular wavelength, which is called the Bragg wavelength λ_B.

The Bragg wavelength is defined by Bragg's law that states that:

$$\lambda_B = 2 \times n_{eff} \times \Lambda \qquad (1)$$

where n_{eff} is the effective refractive index of the core and Λ is the Bragg grating period [7a] as illustrated on figure 2.2..

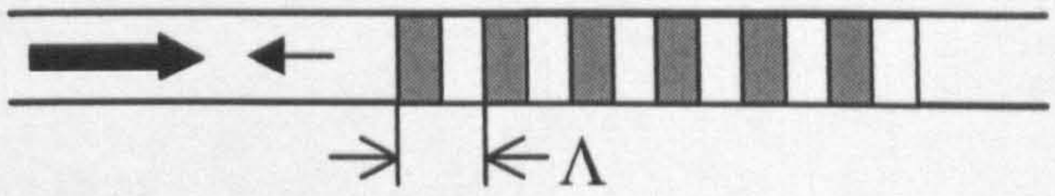

Figure 2.2.: *Fibre Bragg grating [8b].*

Reflection of other components of the source spectrum having wavelengths other than the Bragg wavelength are not phase matched and interfere destructively giving little reflected energy so it is possible to say that at these wavelengths the grating is essentially transparent. Therefore, most light from a broadband source will propagate through the grating with negligible attenuation and only those wavelengths that satisfy the Bragg condition are strongly reflected. Hence the spectrum of the light passing through the grating will be attenuated at the Bragg wavelength [7a].

Figure 2.3. illustrates the principle of the Bragg grating. The figure shows spectrum of light entering the grating, the spectrum of the light transmitted through the grating and the spectrum of the light reflected by the grating.

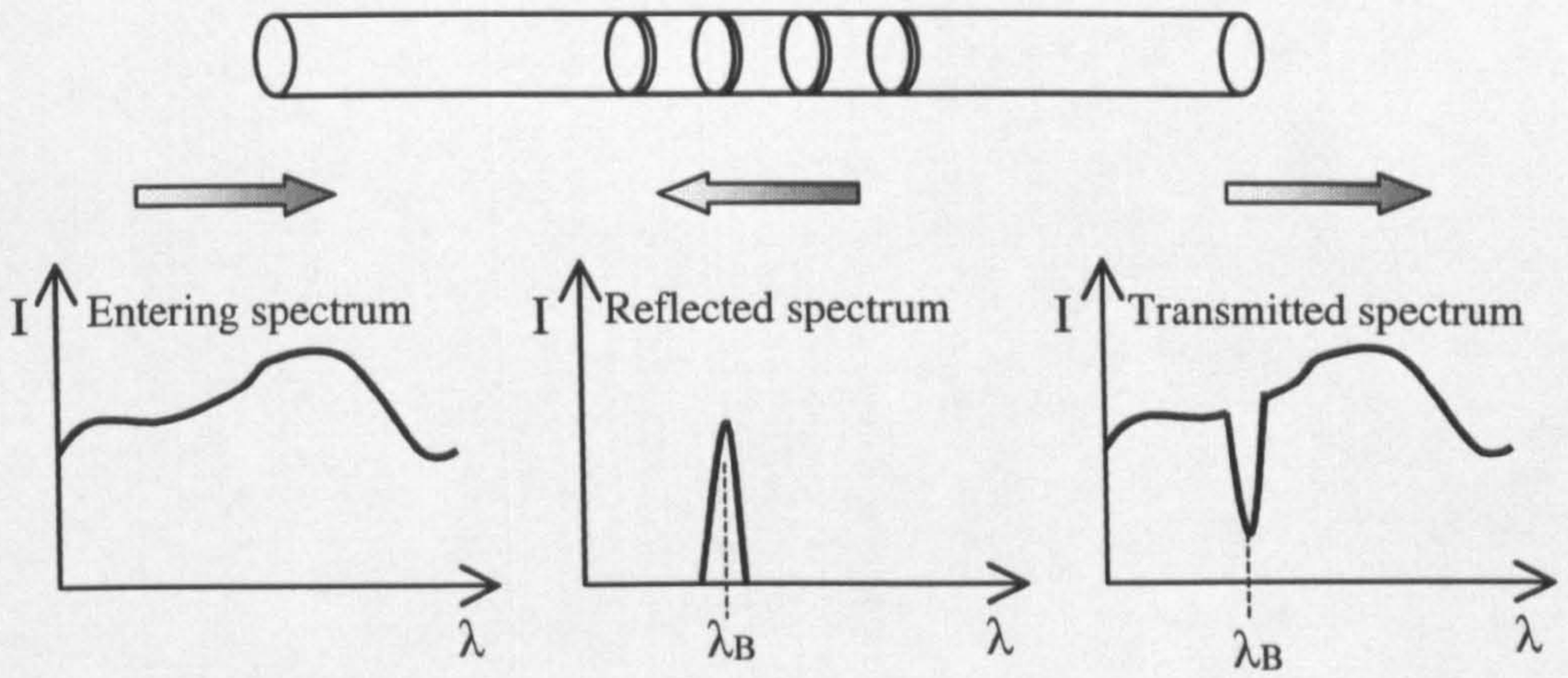

Figure 2.3.: *Bragg grating properties.*

The Bragg wavelength of a given fibre grating depends on the period of the grating and the refractive index of the material (Braggs Law). Both of these parameters are sensitive to mechanical strain and the temperature field within the grating [7b] and any change in strain or temperature will modify the spacing between the gratings of a Bragg sensor and the refractive index of the core of the fibre.

Note:

A positive temperature change will result in increasing the Bragg wavelength to longer wavelengths that will induce a positive change of the refractive index of the core. [8a]

If the grating can be isolated from the effects of mechanical strain, the geometry changes will be entirely due to the applied temperature field and the temperature dependence of the fibre material. Hence an external perturbation of the temperature field within the grating will cause a change in the Bragg wavelength of the grating and the reflected light will change in wavelength. By detecting that wavelength change, the temperature within

the grating may be detected. The wavelength shift $\Delta\lambda_{BT}$ for a temperature change of ΔT is given by the following expression:

$$\Delta\lambda_{BT} = \lambda_B \times (1+\xi) \times \Delta T \qquad (2)$$

Where ξ is the thermo-optic coefficient of the fibre. [7a]

In recent years, Bragg gratings have been used to measure temperature in harsh environments where conventional temperature sensing elements would fail. Bragg grating temperature sensors for harsh environments like nuclear environment or in the oil industry for example have been developed and successfully tested [9,10].

- **Problems encountered.**

The main problem encountered, in all the fibre Bragg grating temperature measurement applications, is the discrimination of different measurands. The sensing of one measurand is quite straightforward when the temperature and strain are not created by the same factor. It is difficult to separate the wavelength fluctuations caused by the temperature change from wavelength fluctuations caused by other disturbances, for example by the stress on the fibre [11]. In some cases, further calibrations [12] and investigation will need to be undertaken to discriminate changes due to temperature from the ones due to strain [13,14,15]. It is possible to use a reference FBG to separate the effects of changes in strain and temperature. The separation of measurands can be achieved by using a reference grating that is not subjected to both measurands [7a]. Results given by the

reference grating can then be subtracted from the reading of the sensing grating. This leaves solely the results due to the measurand of interest. Separation of the measurands can also be achieved by practical calibration tests.

Assuming that the effect of temperature can be isolated from the effect of mechanical strain or vice versa using the techniques described above, then an effective method of detecting the wavelength change in the reflected light is required. Many different methods have been developed throughout the years to detect the change in wavelength induced by the change in measurand [6,7a]. The interrogation methods of interest are described in the following section.

2.4.1. Interrogation of Bragg grating sensors.

There are a number of different techniques that are commonly used to interrogate a fibre Bragg grating sensor. A good sensing interrogation technique has to accurately detect the wavelength shift induced by the change in measurand of the sensing grating. There are many different ways to detect that wavelength shift. Rao Yun-Jiang in "In-fibre Bragg grating sensors" [7a], Martin Christiansen in his Ph.D. thesis entitled "Spectrometer with CMOS Demodulation of Fiber Optic Bragg Grating Sensors" [16] and Alan Kersey in "Optical fiber sensors" [6] discuss them in detail. The techniques described by these three authors include:

2.4.1.a. Optical spectrum analyser or wavelength meter.

The most common device used to detect a wavelength or a change in wavelength is an optical spectrum analyser (OSA) [12,14,17,18]. OSAs measure the intensity of the light as a function of wavelength. OSAs offer the advantage of displaying the spectrum of the optical spectrum detected (intensity vs. wavelength) which is very useful to test an optical device, for the fabrication of Bragg gratings and also for sensing purposes since the wavelength change can be read and easily displayed. A temperature measurement system utilising an OSA to measure wavelength shift is illustrated in figure 2.4. OSAs main drawbacks are that they are very expensive. The cheapest OSA found costing $14,995 (2003) at an operating wavelength of 1519-1620 nm (L-band) and having an optical resolution of approximately 0.16nm. With a limited speed of approximately 5Hz such devices not suitable for real time detection (from the technical data of OPM-LC manufactured by Ocean Optic Ltd) [19]. As high-speed temperature measurement is necessary for machining applications and the high price of the optical system makes it uncompetitive with the existing thermocouple technique, the OSA technique has found to be not suitable for the measurement of temperature during a high-speed machining application.

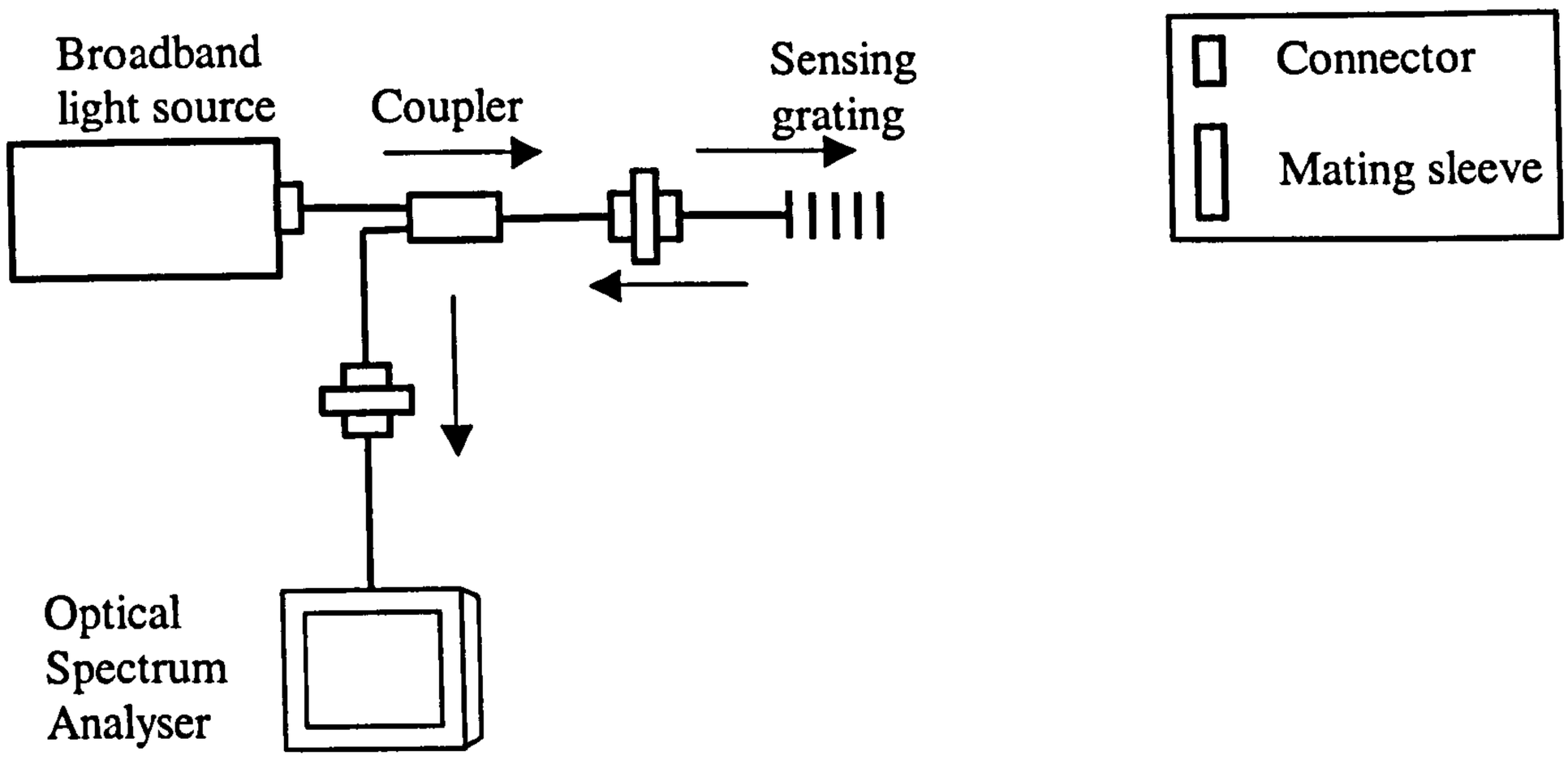

Figure 2.4.: *Optical Spectrum Analyser based system.*

Since the price, resolution and speed of OSAs is a problem, other ways to detect a wavelength shift have been developed in recent years. The main techniques used are:

2.4.1.b. Wavelength Division Multiplexer (WDM) fibre coupler.

The origin and development of this system are discussed in details by Yun-Jiang Rao in "In-fibre Bragg grating sensors" [7a]. The basic mode of operation is as follow:

A broadband optical spectrum is launched into the fibre by a stabilised light source. A coupler is then used to divide the signal, part of the signal enters the sensing grating and the remainder is lost from the system. Of the light that arrives at the sensing grating, a component corresponding to the Bragg wavelength is reflected back to the coupler where it is divided and a

proportion of it propagates to the WDM. Figure 2.5. illustrates schematically the layout of a WDM based interrogation system.

WDMs are usually used for telecommunications purposes to multiplex signals of different wavelengths down a single fibre or demultiplex an optical signal into signals of different wavelengths.

To achieve the above, WDMs use "frustrated internal reflection to couple intensity to the output fibres based on the wavelength of the input light" [16]. This allows them to separate or reconstitute the optical signal. If only one wavelength is entering the WDM coupler, then any changes in that wavelength will result in a change of the output intensity of each branch. By making use of the wavelength sensitivity of a WDM, the signal reflected back from the sensing grating may be interrogated.

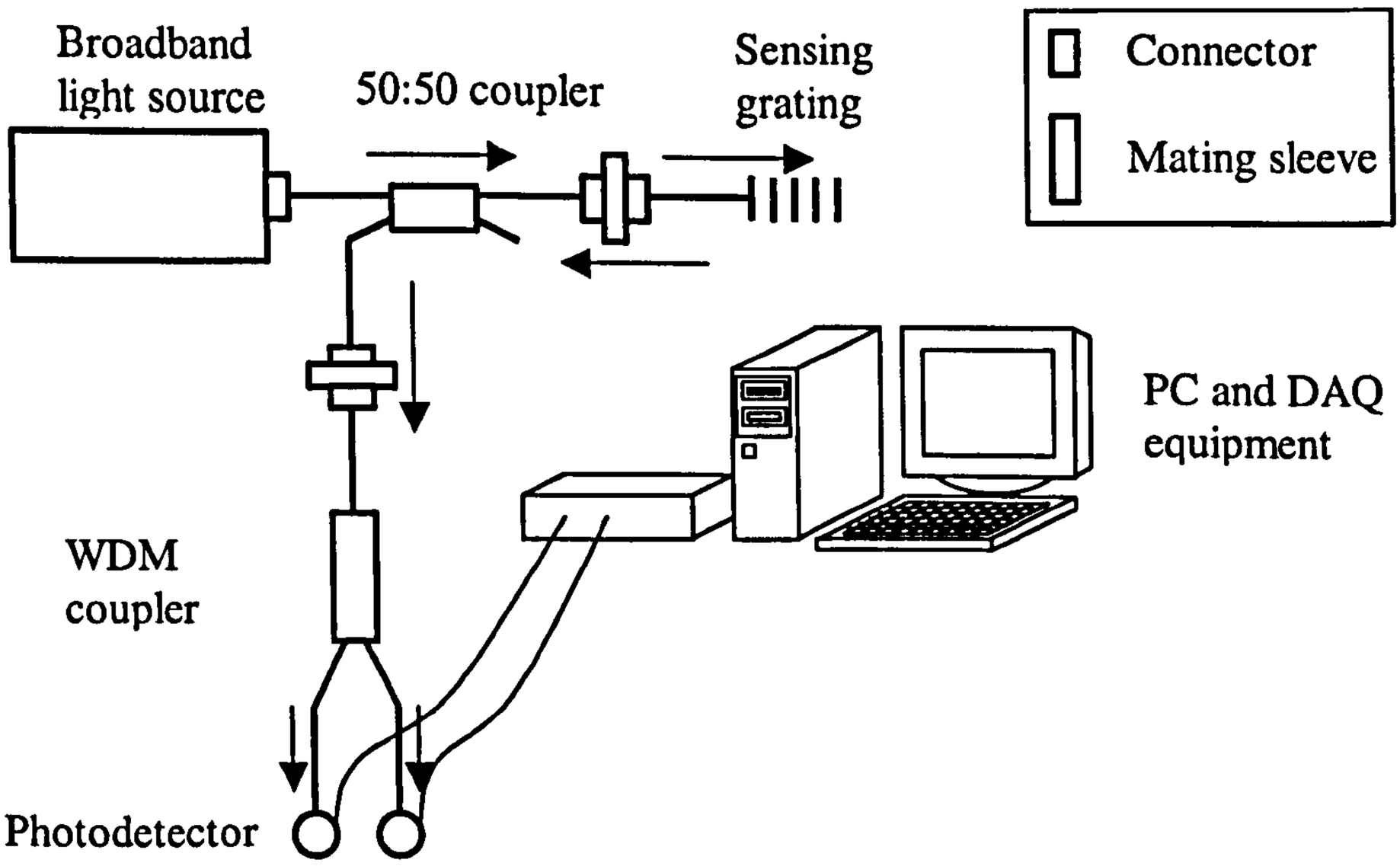

Figure 2.5: *WDM coupler system. [7]*

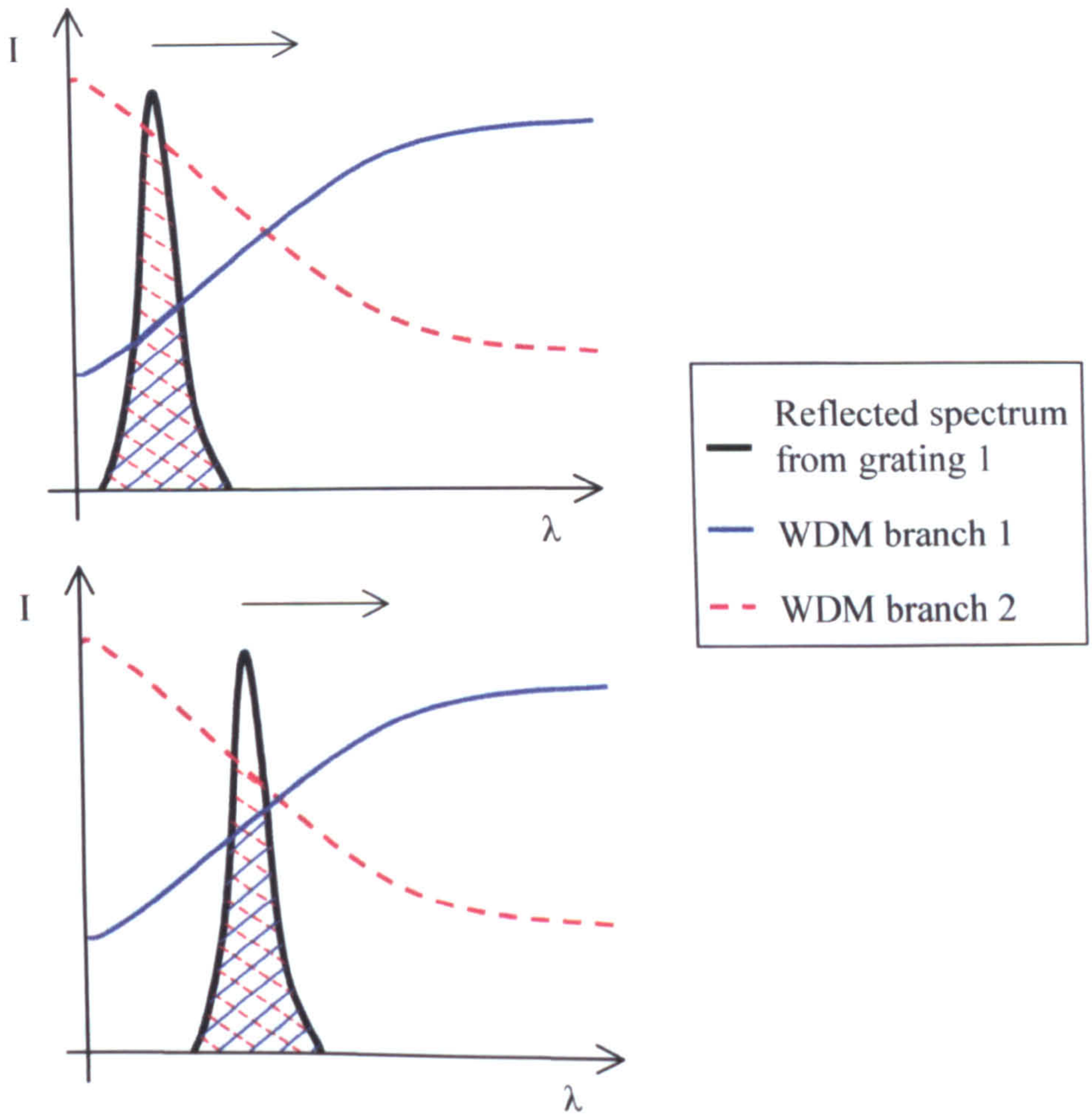

Figure 2.6: *Power in WDM coupler branches.*

When a measurand is applied on the grating, the reflected Bragg wavelength changes causing a change in intensity at the outputs of the WDM coupler. Figure 2.6. illustrates this principle. The WDM curves shown are based on typical WDM spectrum. The two curves show how at a given wavelength, the optical signal is distributed between the two output branches of the WDM. Thus any change in wavelength of the input signal will result in a redistribution of energy between the two output channels. So as the wavelength changes, this causes less intensity to be coupled out of branch 2 of WDM coupler, while the intensity out of branch 1 increases as illustrated figure 2.6. above.

2.4.1.c. Fibre Bragg Grating (FBG) - based filters.

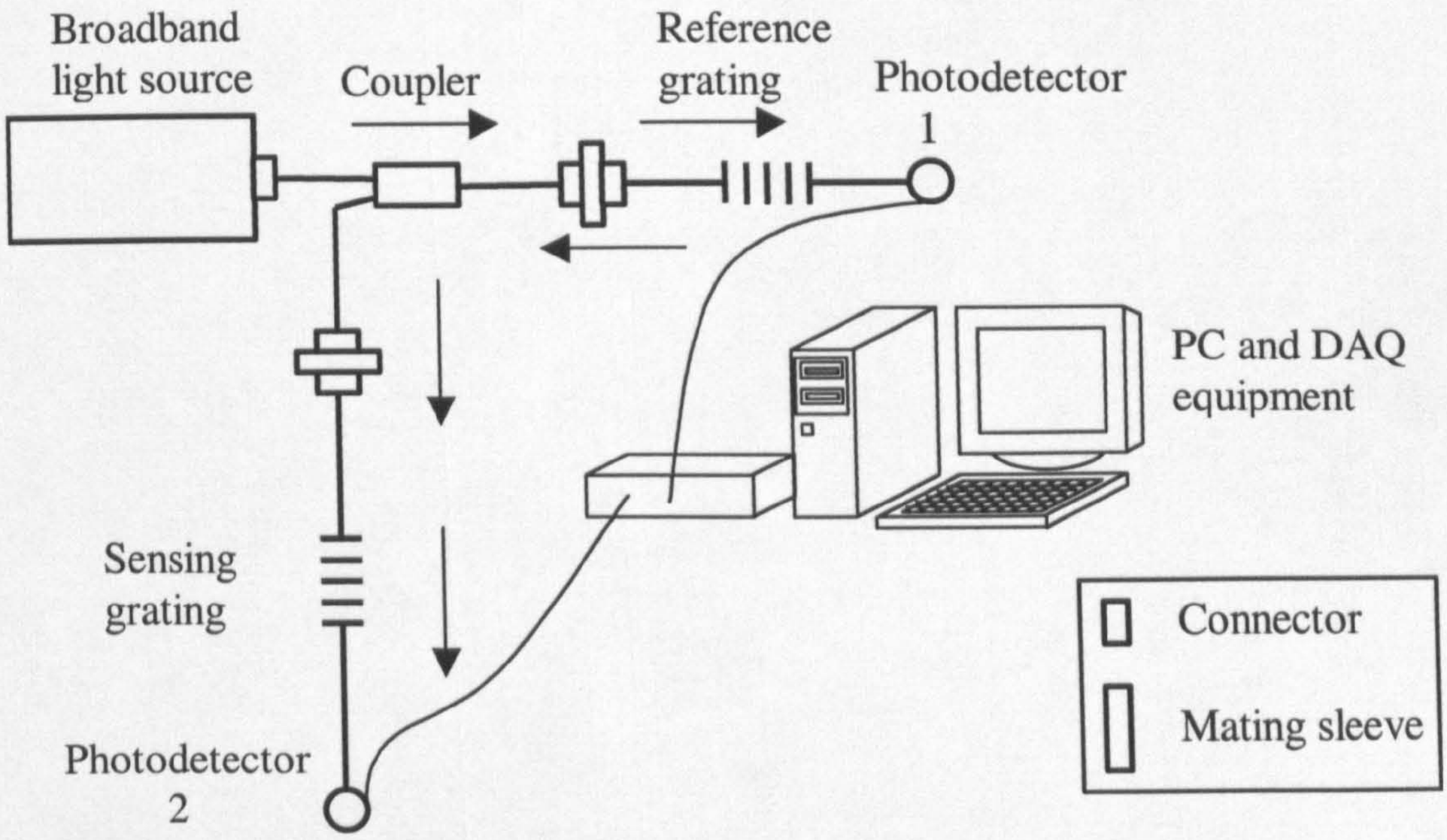

Figure 2.7: *Two gratings system. [20]*

This system, illustrated in figure 2.7., uses the ability of the fibre Bragg grating to reflect a narrow band of light. A broadband signal is launched in the optical system after passing through the 50:50 coupler, a portion of the signal is reflected by a fibre Bragg grating. This reflected peak signal from the reference grating is used as a reference signal since it provides a steady and known spectrum for the sensing grating. The signal reflected from the reference grating then goes through another sensing grating. The sensing grating spectrum truncates the reflected spectrum from the reference grating, this allows the wavelength change to be related to the intensity reaching the second detector as illustrated in figure 2.8..

Note:

The signal propagating through the reference grating is monitored by the first photodetector. This allows any changes in source intensity to be detected and allowed for.

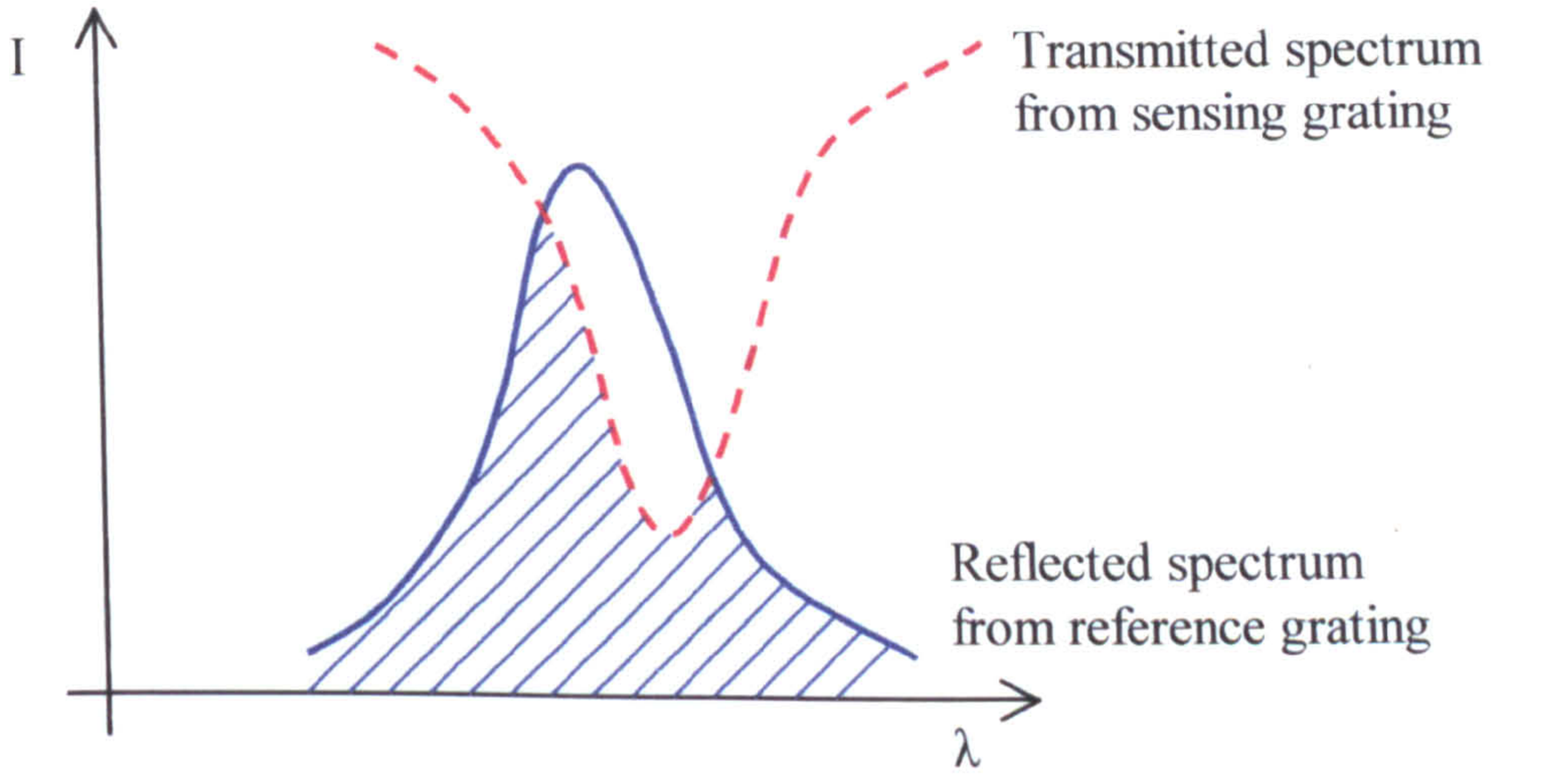

Figure 2.8.: *Intensity change of the grating filter system.*

Figure 2.8. shows that when the sensing grating is disturbed, causing its Bragg wavelength to vary, the area below the intersecting spectra changes and this results in a change in intensity detected by the second detector.

A similar system has been successfully used as a strain sensor to monitor "the frequency spectrum of the respiration process" [20].

2.4.1.d. Fabry-Perot interferometer.

The Fabry-Perot property described above (Chapter 2.1.) has been applied to interrogate a Bragg grating sensor. The reflected signal from the grating is truncated by a tuneable Fabry-Perot bandpass filter [16]. This principle is the same as the signal truncation principle used by the fibre Bragg grating - based filters of chapter 2.4.1.c. and described in figure 2.8. above. This allows relating the wavelength change to the intensity change. The intensity change is then detected by a photodetector.

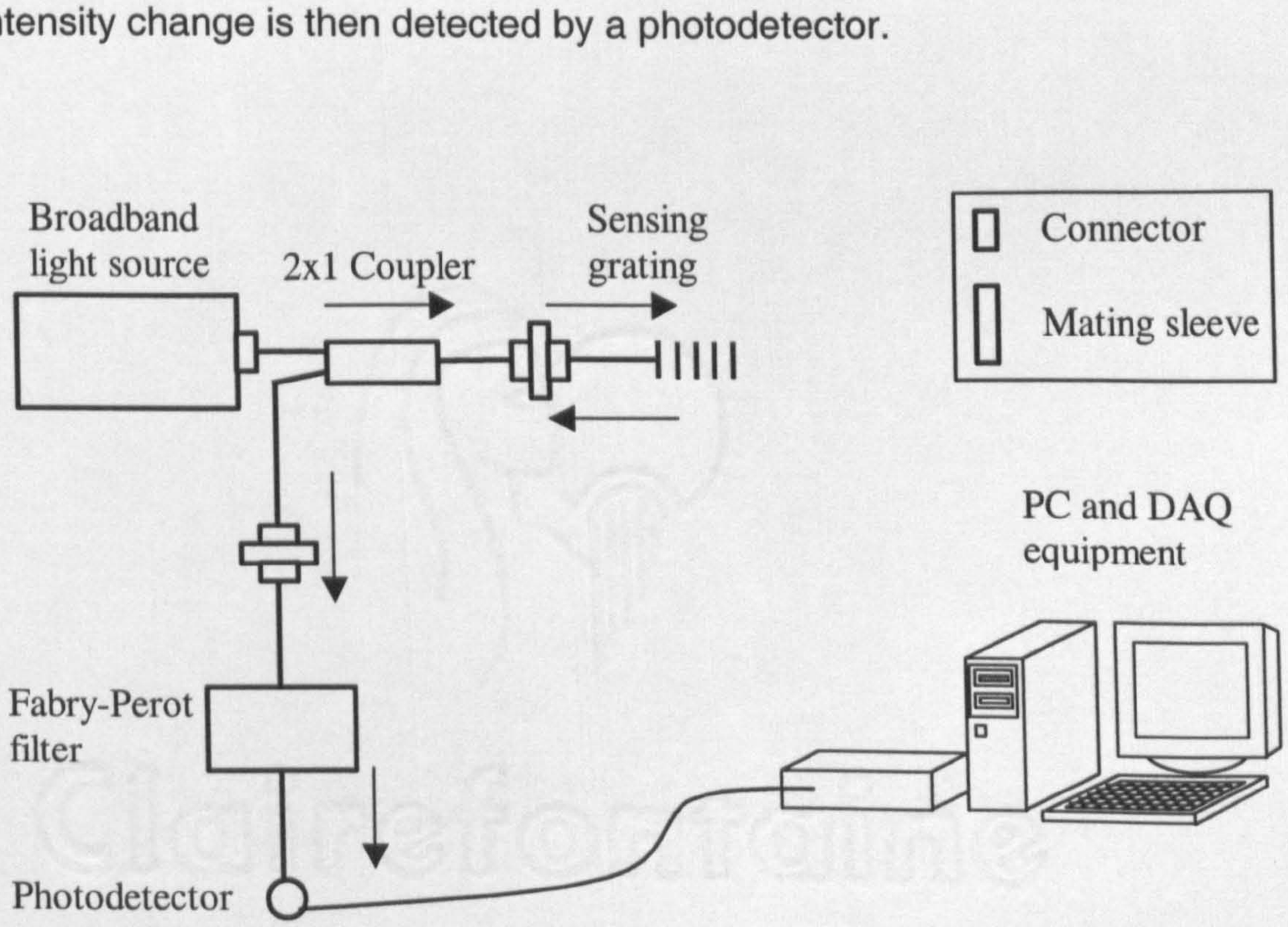

Figure 2.9.: *Fabry-Perot system. [16]*

Application of a Fabry-Perot filter used for interrogating a Bragg grating have been investigated. The sensor displayed a wavelength shift due to temperature of 10.3pm/°C that is very similar to that of general fibre Bragg grating [21].

2.5. Conclusion.

To date most of the interrogation techniques have been used to detect changes in wavelength associated with measuring mechanical strain. For a temperature sensing application, the most suitable technique to employ, appears to be the WDM fibre coupler scheme and the grating filter scheme. This is because both those techniques offer a favourable comprise between operating range and accuracy when compared to other techniques. It is also the case that the WDM method and the grating filter method have lower costs than many others and are relatively easy to use.

References.

1. a. Lee E. C and Taylor H. F., "Fiber-optic Fabry-Perot temperature sensor using a low-coherence light source", Journal of lightwave technology, vol. 9, No. 1, p 129-134, 1991.

1. b. Lewis Research Center, "Fabry-Perot fiber-optic temperature sensor", http://www.nasatech.com/briefs/jan99/LEW16610.html, 1999.

2. Keck D. B., "Optical Sensors and Specialty Fibers", Japanese technologies evaluation center, Loyola College, http://www.wtec.org/loyola/opto/, 1996.

3. a. Ueda T., Hosokawa A. and Yamamoto A., "Studies of Temperature of Abrasive Grains in Grinding – Application of Infrared Radiation Pyrometer", Trans. ASME, J. of Eng. for Ind., 107, p 127-133, 1985.

3. b. Ueda T., Hosokawa A. and Yamamoto A., "Measurement of grinding temperature using infrared radiation pyrometer with optical fiber", Trans. ASME, J. of Eng. for Ind., 108 , p 247-251, 1986.

4. McIntyre T. J., Allison S. W., Maxey L. C. and Cates M. R., "Fiber optic temperature sensors for PEM fuel cells", Hydrogen, fuel cells and infrastructure technologies, FY2003, Progress report, http://www.eere.energy.gov/hydrogenandfuelcells/pdfs/viib8_mcintyre.pdf, 2003.

5. Stokes J. and Palmer G., "A fiber-optic temperature sensor". Sensor technology and design, http://www.sensorsmag.com/articles/0802/28/main.shtml, 2002.

6. Kersey A. D., "Chapter 8: Optical fiber sensors", p 217-254, "Optical measurement techniques and applications", publisher: Pramod Rastogi; 1997.

7. a. Rao Y J, "In-fibre Bragg grating sensors", Meas. Sci. Technol.8, p 355-375, 1997.

7. b. Leiderman R., Matos C. J. S., Braga A. M. D., Margulis W. and Valente L. C. G., "Interrogation methods for fiber Bragg grating sensors", SPIE Vol. 3666, p 554-560, 1999.

8. a. Kashyap R., "Fiber Bragg gratings", Optic and photonics, Academic Press, 1999.

8. b. Lee B., "Review of the present status of optical fiber sensors", Optical Fiber Technology 9, p 57-79, 2003.

9. Fernandez F. A., Gusarov A., Brichard B., Bodart S., Lammens K., Berghmans F., Décreton M., Mégret P., Blondel M., and Delchambre A., "Temperature monitoring of nuclear reactor cores with multiplexed fibre Bragg grating sensors", Optical Engineering, vol. 41, no. 6, p 1246-1254, 2002.

10. Schroeder R J and Yamate T, "High pressure and temperature sensing for the oil industry using fiber Bragg gratings written onto a side hole single mode fiber", proc. SPIE 3746, p 42–45, 1999.

11. Van Steenkiste R. J. and Springer G. S., "Strain and Temperature Measurement with Fibre Optic Sensors", Ed. Technomic, 1997.

12. Haran F. M., Rew J. K. and Foote P. D., "A strain-isolated fibre Bragg grating sensor for temperature compensation of fibre Bragg grating strain sensors", Meas. Sci. Technol. 9, p 1163–1166, 1998.

13. Song M., Lee S. B., Choi S. S. and Lee B., "Simultaneous measurement of temperature and strain using two fiber Bragg gratings embedded in a glass tube", Optical fiber technology 3, p 194-196, 1997.

14. Jung J., Nam H., Lee J. H., Park N. and Lee B., "Simultaneous measurement of strain and temperature by use of a single-fiber Bragg grating and an erbium-dopes fiber amplifier", Applied Optics, Vol. 38, No. 13, p 2749-2751, 1999.

15. Tanaka N., Okabe Y. and Takeda N., "Temperature-compensated strain measurement using fiber Bragg grating sensors embedded in composite laminates", Institute of physics publishing smart materials and structures, Smart Mater. Struct. 12, p 940–946, 2003.

16. Christiansen M., "Spectrometer with CMOS Demodulation of Fiber Optic Bragg Grating Sensors", Ph.D. Thesis University of Maryland, 2001.

17. Degrieck J. and De Waele W., "Embedded optical fibre sensors for the permanent monitoring of filament wound pressure vessels", NDT.net, Vol. 4, No. 3, 18, http://www.ndt.net/article/v04n03/5/5.htm, 1999.

18. Morse T. F., He Y. and Luo L., "An optical fiber sensor for the measurement of elevated temperatures", IEICE Trans. Electron., Vol. E83-C, No. 3, p 298-302, 2000.

19. Ocean Optics website, OPM-series Optical Performance Monitors http://www.oceanoptics.com/products/opm.asp.

20. Wehrle G, Kalinowski H J, Torres P I and Valente L C G, "Fibre optic Bragg grating strain sensor used to monitor the respiratory spectrum", Proceedings of SPIE, Vol. 4185, p 310-313, 2000.

21. Hirayama N. and Sano Y., "Fibre Bragg grating temperature sensor for practical use", ISA Transactions 39, p 169-173, 2000.

Chapter 3: Optical system design.

3. Optical system design.

3.1. Design considerations.

The design considerations of the optical temperature measurement system are based on many factors.

- **Cost:** One of the main constraints is the price of the complete system. From an engineering point of view, the optical system has to be reasonably competitive with the price of the thermocouple technique. Although as previously mentioned reduced set-up times/costs could be offset against more expensive hardware.

- **Range:** The measuring range of the system has to be larger than the temperature range encountered inside the workpiece during the machining process (10-80°C). The temperature range was first measured using thermocouples (chapter 5). These initial experiments although not accurate due to presence of electrical noise gave a good idea of the maximum temperature experienced and therefore allowed the determination of the minimum temperature range the optical system should achieve.

- **Accuracy:** An optical system was selected to replace the existing thermocouple. This was mainly to overcome the problems in reading the thermocouple signal when electrical noise, produced by the

machine and/or its surroundings, having a drastic effect on the thermocouple signal, is present. When making measurements optically, the signal to noise ratio of the optical sensor signal had to be better than the equivalent thermocouple signal. This was an important factor because it has an influence on the accuracy of the results. Accuracy of ±1 degree or better is necessary for a good comparison of the optical sensor with the thermocouple technique.

- **Response speed:** The response speed is limited by the time required for heating up and cooling down of a typical optical fibre. This reaction time can then be compared with the thermocouple reaction time by experiment. If the optical system is to offer improved performance over the thermocouple system, then the speed of response must be at least comparable.

- **The optical system should be user-friendly.** A competent machine operator should be able to use the optical system even with no optical fibre knowledge.

3.2. Optical system design.

As previously explained in chapter 2, the most basic requirements of an optical fibre Bragg grating temperature sensor are a light source, a coupler connected to a fibre Bragg grating and a spectrometer (or other instrument that detects spectral changes) to measure the spectral properties of the reflected signal. With a spectrometer or a wavelength-meter, the wavelength shift, induced by the temperature change on the sensing grating, is easily detectable. However as discussed before, spectrometers are expensive and their detection speed and accuracy may not be suitable for high-speed machining applications. It was therefore necessary to develop alternative methods of detecting a wavelength or a wavelength shift. Of the existing techniques discussed in chapter 2, the WDM coupler technique and the grating filter technique were identified as the most promising for use in measuring machining temperature.

In addition to the two existing techniques, two new methods, developed by the author, are proposed giving four techniques worthy of further investigation. All four techniques were investigated experimentally and theoretically and their performances compared. The four techniques were:

- WDM coupler.
- Coupler.
- DWDM.
- Two grating.

3.2.1. WDM coupler technique.

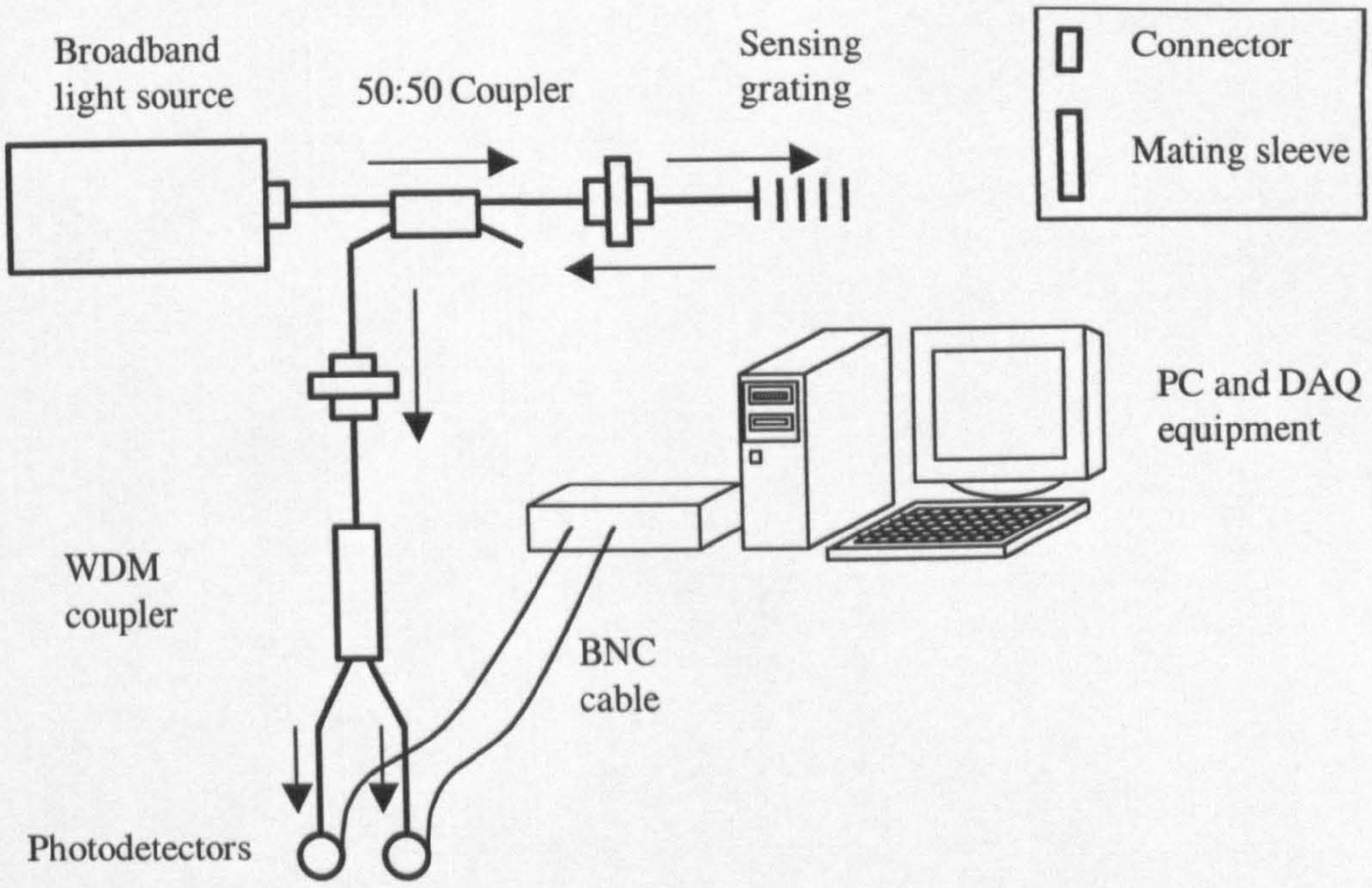

Figure 3.1.: *WDM coupler system. [1]*

As previously explained in chapter 2, a wavelength division multiplexer (WDM) can be used to detect a wavelength change. As the wavelength of the light reflected from the sensing grating changes, the intensity transmitted into each branch of the WDM coupler changes.

The above system was tested because it is an existing established technique and it allows comparison with the new designs proposed.

Two main changes were made:

- The light source was replaced by a stabilised light source therefore there is no need to measure the reference signal, nor to use ratiometric techniques nor to correct the input signal.
- Also, to minimise the optical system insertion loss and therefore improve its sensitivity, the signal was split using a circulator instead of a coupler. The circulator is a passive junction consisting of three ports in this

case. When a signal arrives to the first port, it is then transferred to the next port.

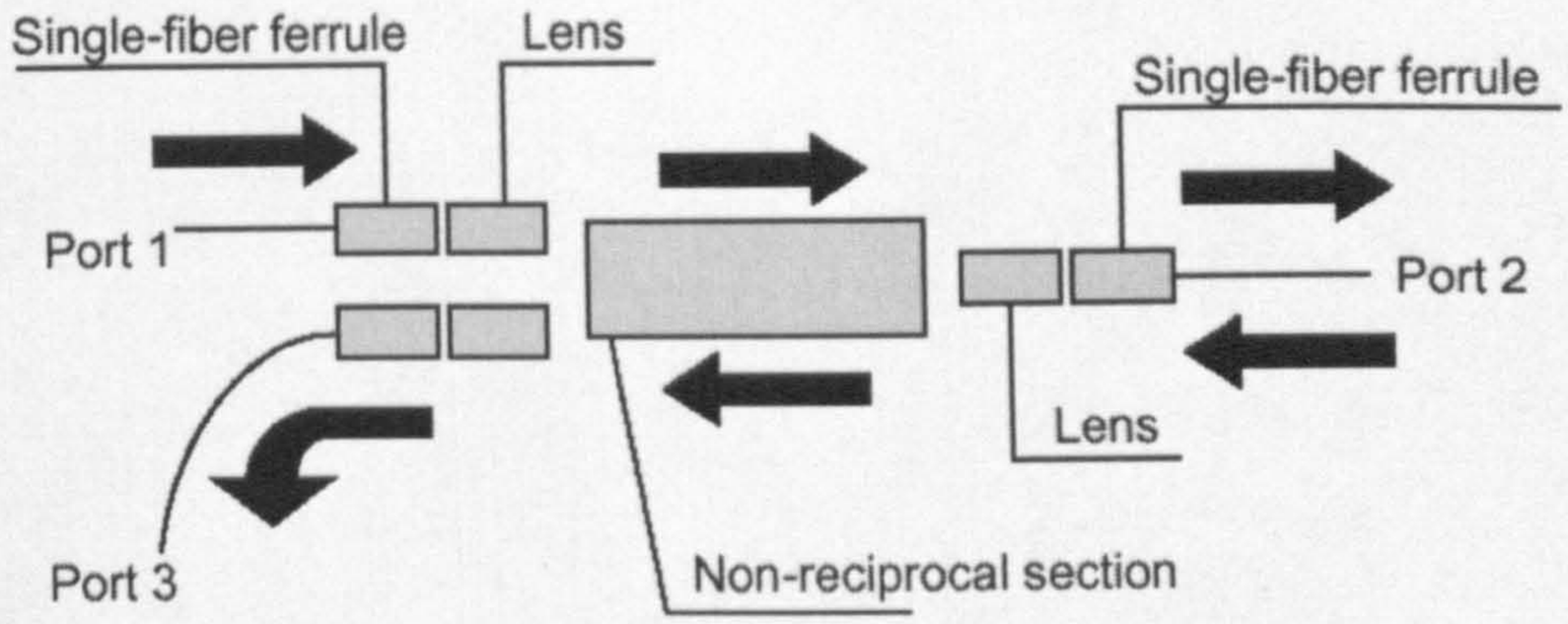

Figure 3.2.: *Newly developed low-loss optical circulator [2].*

A circulator makes the signal circulate while the coupler has a strong effect on the transmitted intensity of the signal. A 50:50 coupler splits the intensity as shown in the figure 3.3..

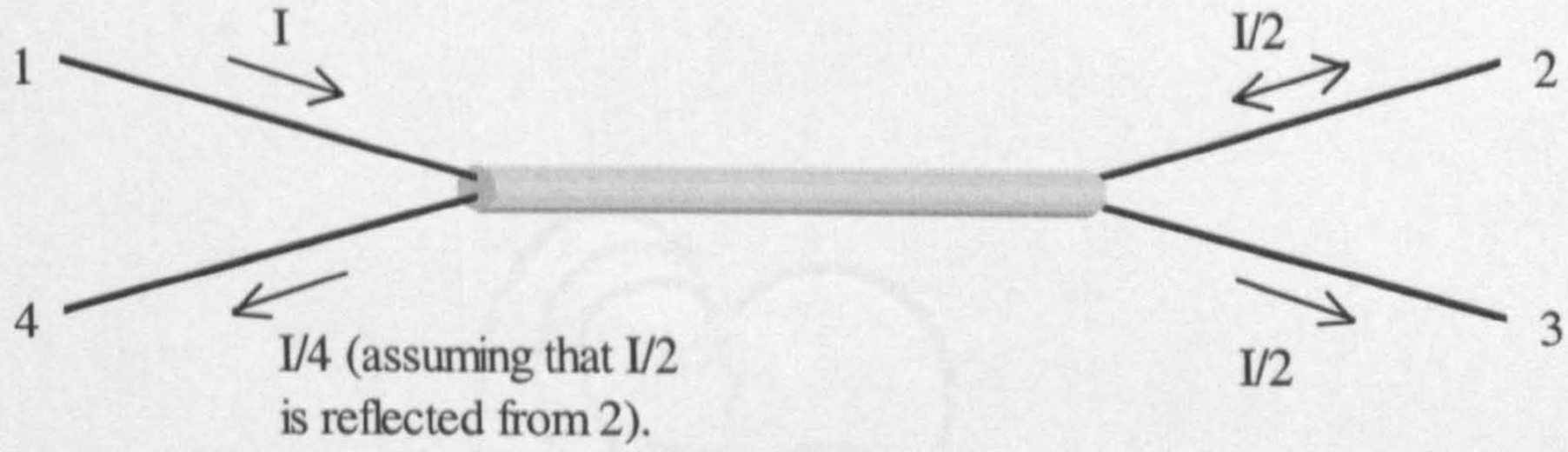

Figure 3.3.: *50:50 coupler effect on signal intensity.*

By comparing figure 3.2. and figure 3.3., it is possible to say that the intensity of the circulator output signal is ideally four times stronger than the output from the coupler. Since the optical noise is unchanged, it is possible to say that the signal to noise ratio is highly improved by the change and also a greater sensitivity can be expected.

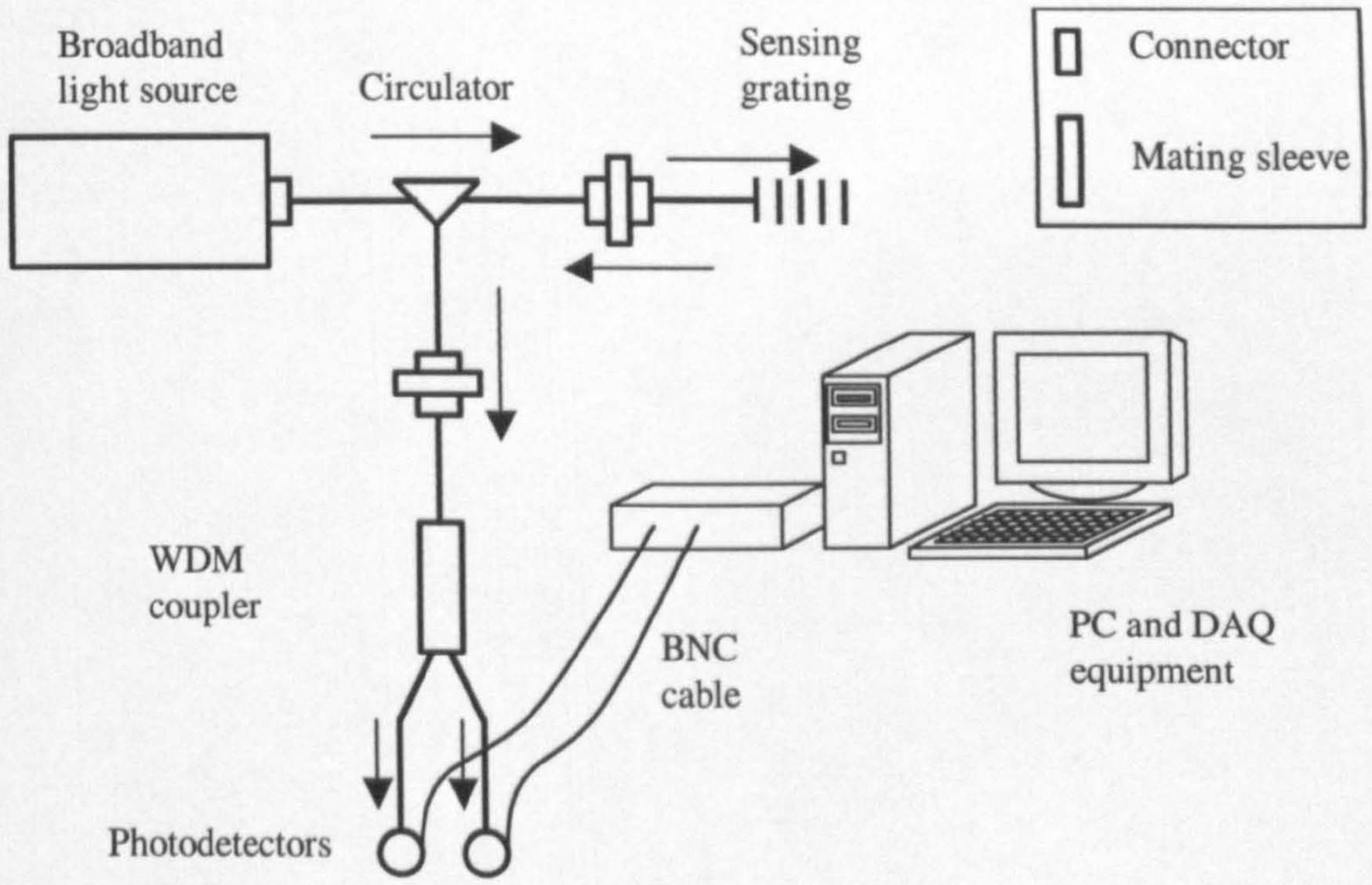

Figure 3.4.: *Modified WDM coupler system.*

Figure 3.4. illustrates schematically the modified layout of a WDM based interrogation system. This technique offers the potential to measure a wide range of temperatures. The actual range achieved, depends on the wavelength band supported by the WDM coupler. In this case, it is 1510 to 1550nm used with a grating centred at 1530.2nm. This gives a range of around ±20nm, which in temperature terms would mean the possibility to measure over a temperature range of approximately 2000°C. However, the maximum temperature detectable by this system is limited by the maximum temperature that the grating can sustain without suffering permanent deformation or destruction.

3.2.2. Coupler technique.

One of the standard assumptions made while designing a fibre based optical system is that: the intensity of the light transmitted through a standard coupler is independent of its wavelength. However during the early stages of this research programme, the author noticed that in a low quality (low cost) 50:50 coupler, the intensity of the light varies slightly with its wavelength. It was realised that this property could be exploited to detect changes in wavelength and therefore to measure temperature. Figure 3.5. shows the layout of a temperature measuring system exploiting this behaviour.

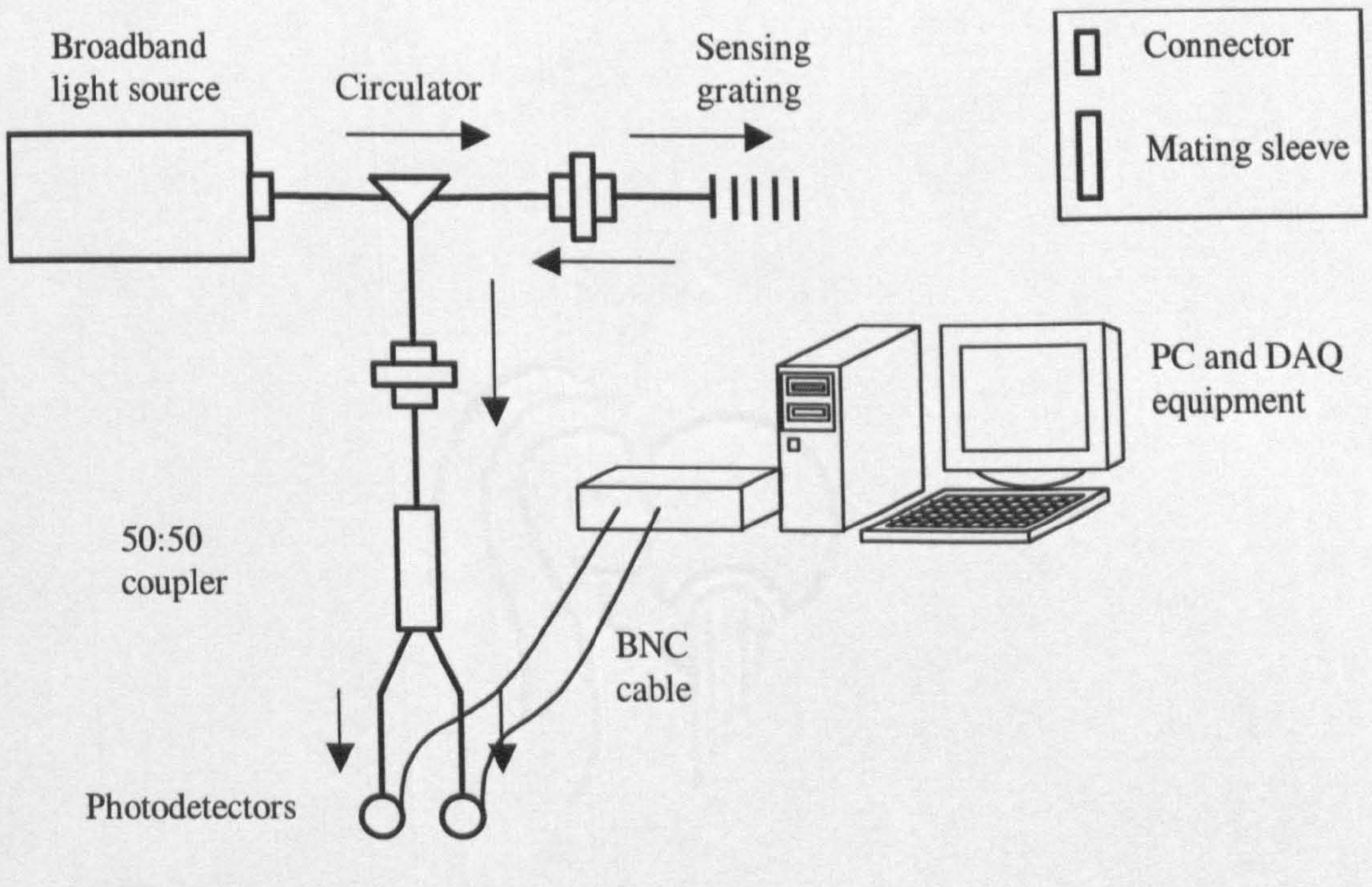

Figure 3.5.: *50:50 coupler system.*

The optical signal is launched into the system by a broadband light source. After passing through the circulator, the sensing Bragg grating reflects a spectral peak of this signal; that reflected signal propagates back to the

circulator towards the coupler. As the centre wavelength of the grating changes due to the applied temperature field, the intensity of the light transmitted in each output arm of the coupler changes. This change can be detected and used to measure the temperature applied on the sensing grating.

The maximum possible temperature range for this type of system is limited by the maximum temperature rating of the grating (approximately 100°C) before permanent deformation or even destruction of the grating (see section 4.14. for more details). The coupler system is the least sensitive of the four optical systems, since ideally, standard couplers do not relate intensity to wavelength change.

3.2.3. Division wavelength demultiplexer (DWDM) technique.

The system using thin film dense Division Wavelength DeMultiplexer (DWDM) technique is a major improvement on the WDM technique. The 50:50 coupler of the above system was replaced by a circulator as described in section 3.2.1.. The circulator produces less insertion losses than the 50:50 coupler and does not divide the signal but just makes it circulate. Secondly, the WDM coupler was replaced by a thin film dense DWDM. Thin film dense DWDMs are commonly used in telecommunication systems to mutiplex (combine) or demultiplex (separate) an optical signal, this allows signals of different wavelengths to share one single fibre. A thin film DWDM was selected to replace a WDM coupler because the DWDM

channels offer a steeper intensity response for the same wavelength variation (figure 3.6.). A DWDM based system technique should therefore be more sensitive to wavelength changes than the WDM based system.

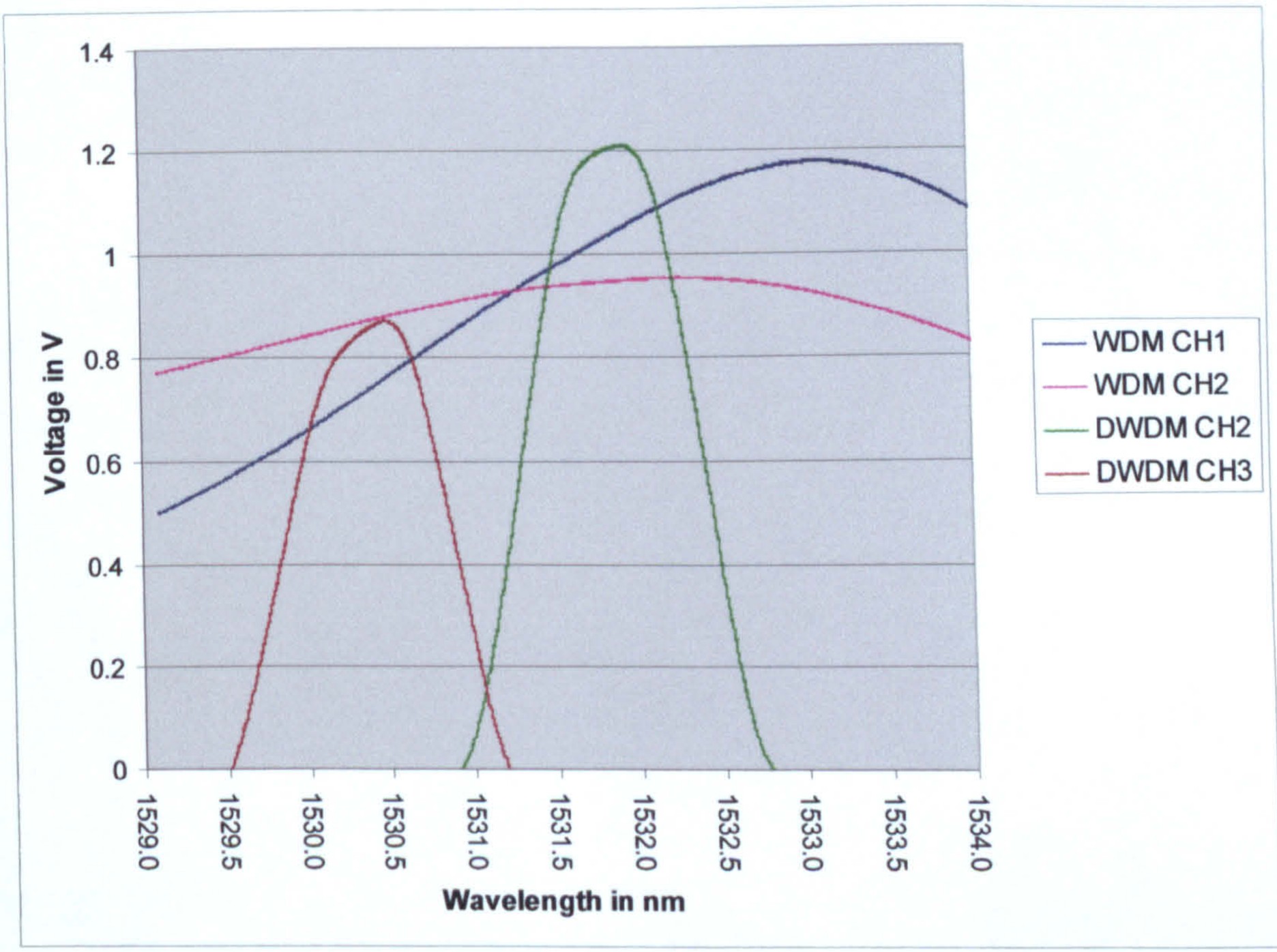

Figure 3.6.: *WDM / DWDM characteristic transmission spectra.*

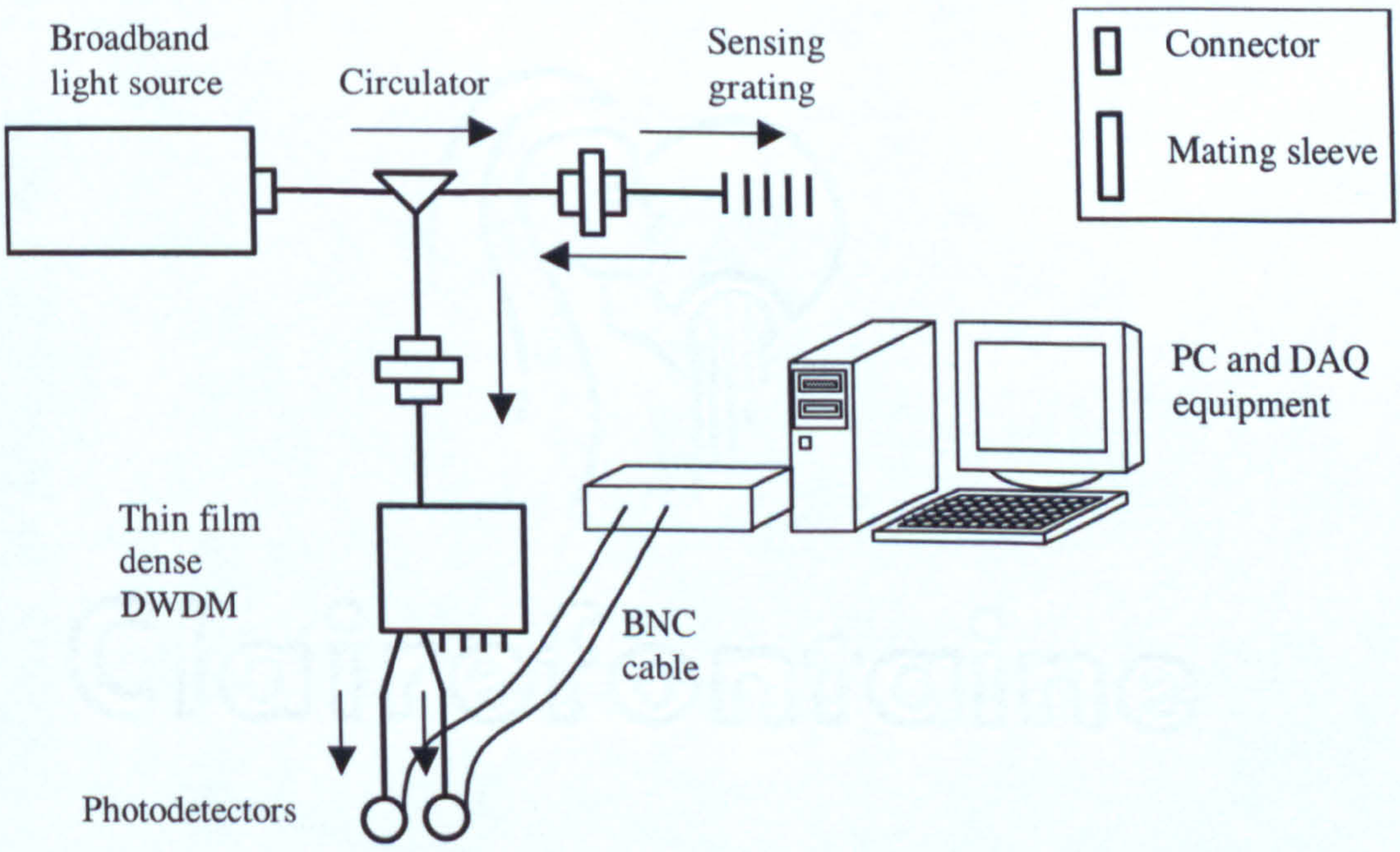

Figure 3.7.: *Thin film dense DWDM system.*

The DWDM system layout is shown in figure 3.7.. The optical signal is launched into the system by the broadband light source. After passing through the circulator; the sensing Bragg grating reflects a peak of the optical signal; the reflected signal propagates back through the circulator and enters the DWDM. The DWDM is used in this case to relate wavelength and intensity as explained before. The DWDM also offers a choice of a small number of different channels each covering a few nanometers of wavelength range (figure 3.8.); this property allows the user to make a first good initial assessment of the reflected wavelength range and thus the temperature range. Using a photodetector on each channel of the DWDM would allow a temperature range of approximately 1200°C to be achieved. However this assumes that the sensing fibre grating could endure such a temperature without sustaining permanent damage.

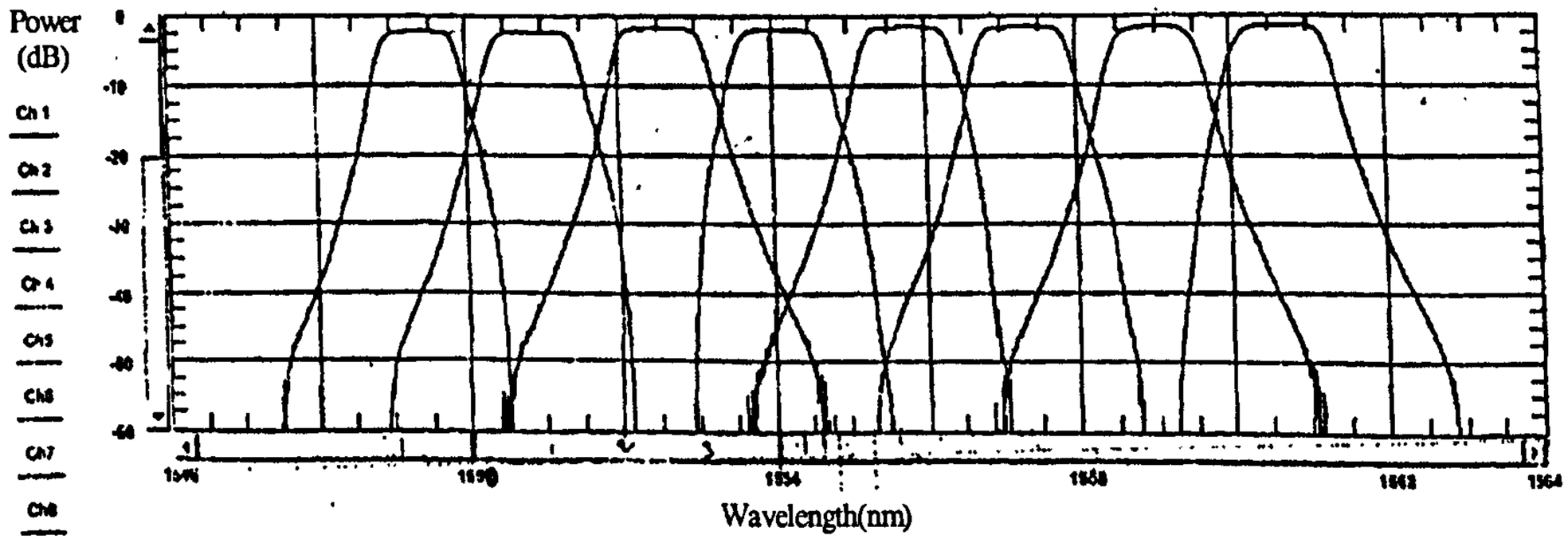

Figure 3.8.: *8 channels thin film dense DWDM standard spectrum.*

Using the spectral specifications given by the manufacturer of the DWDM, it is possible to relate the optical power (transformed into voltage by the photodetectors) to the reflected wavelength and therefore the temperature.

This process is discussed in detail in chapter 4. However the basic idea is illustrated in figure 3.9..

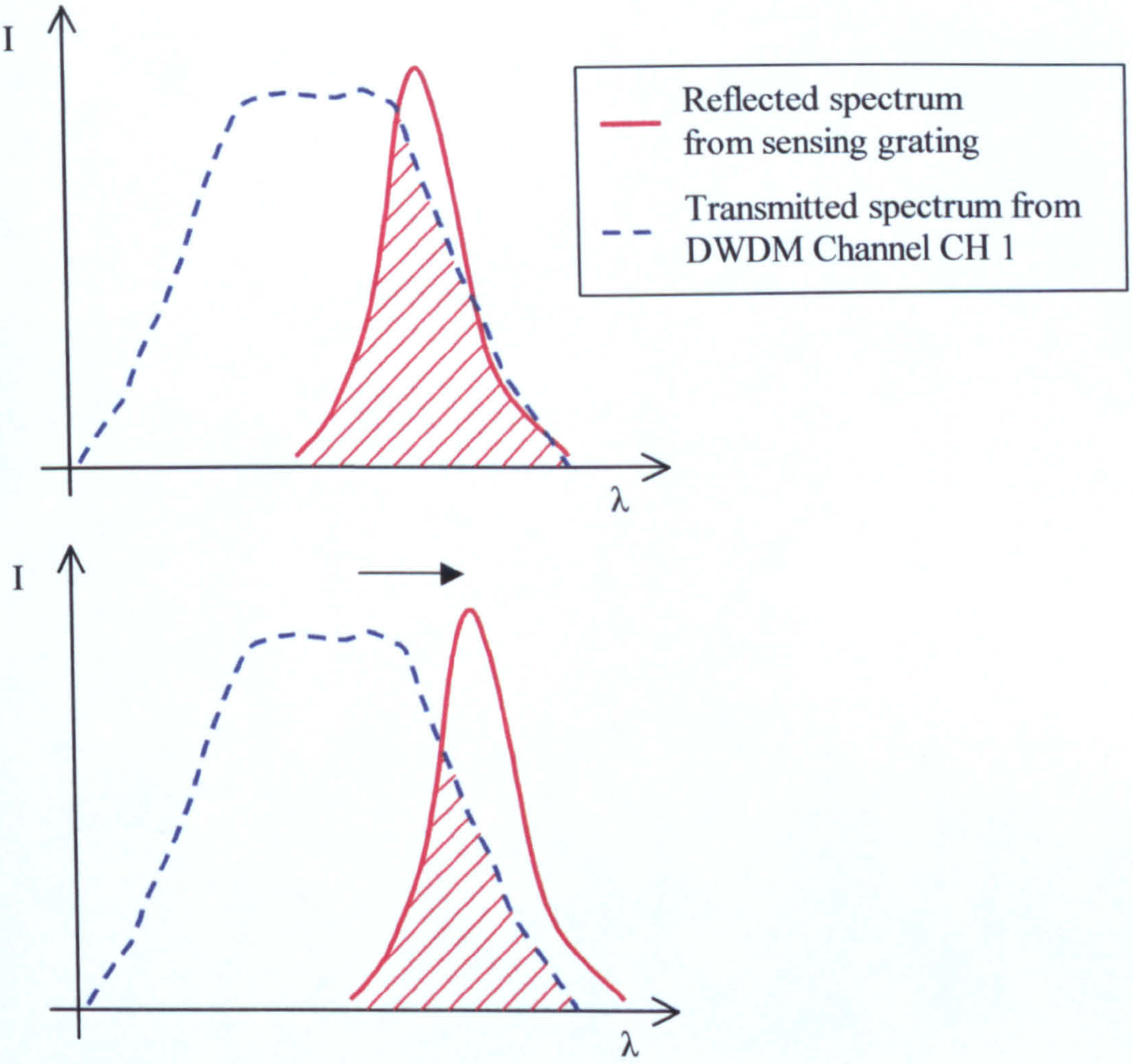

Figure 3.9.: *DWDM principle (one channel).*

As the temperature sensed increases, the wavelength of the sensing grating (dotted line) increases. Since the spectrum of the DWDM channel is steady, it results in a decrease in the intensity output on that channel (area below and between the two spectra). Figure 3.9. illustrates the principle.

As the reflected spectrum shift to the right in figure 3.10., the intensity of the output power decreases in channel 1, the intensity output of channel 2 increases. This principle is illustrated in figure 3.10..

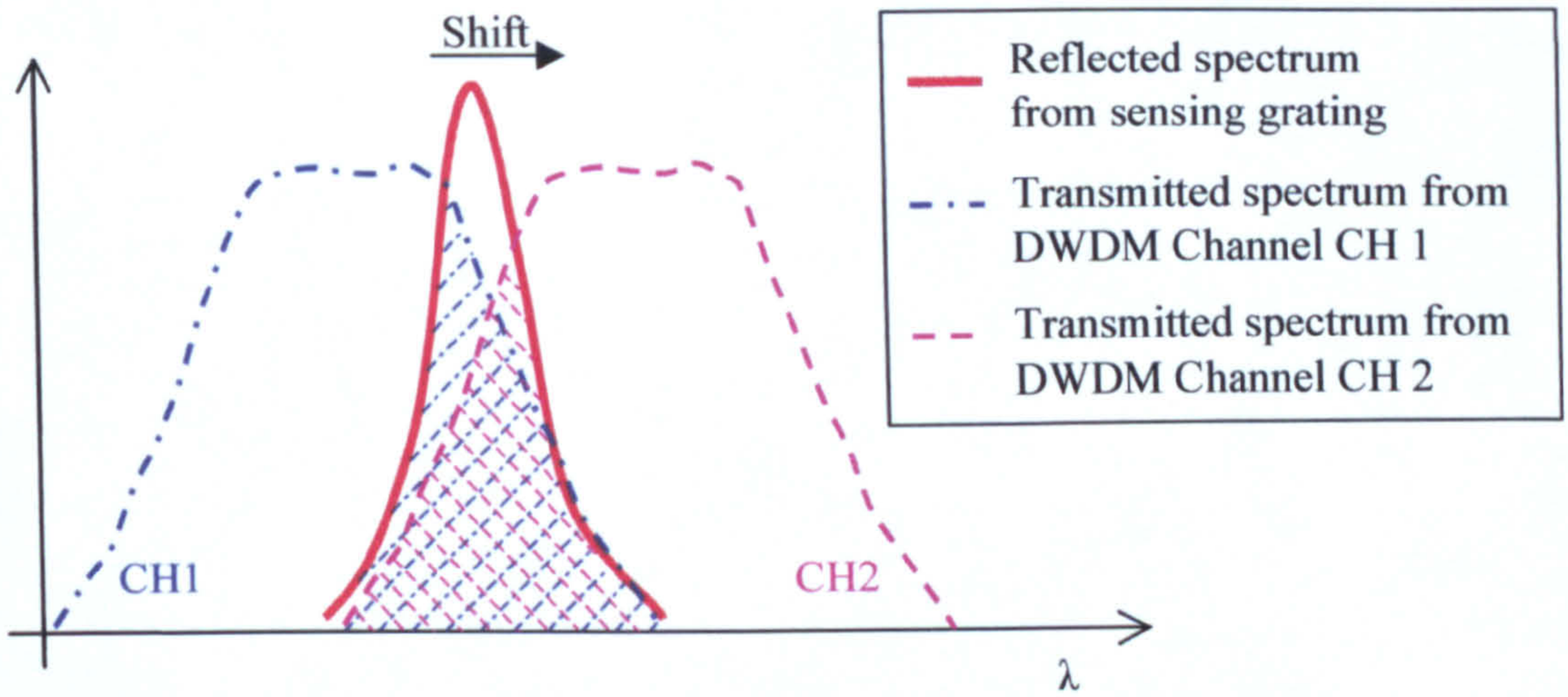

Figure 3.10.: *DWDM principle on 2 channels.*

3.2.4. Two-gratings technique.

This technique is based on the fibre Bragg grating based filtering technique discussed in section 2.4.1.c. with two main modifications: a stabilised light source was used to avoid the need of measuring the reference signal for compensating the sensed signal and a circulator has replaced the previously used coupler for the reasons discussed before.

Since the spectrum of light arriving at the sensing grating is known (from the spectrum of the reference or athermic grating) and the "missing peak" is also known (from the spectrum of the sensing grating), it is possible to determine the change in temperature knowing the change in intensity of the

measured signal. This is explained in more details in chapter 4. As the temperature changes, the Bragg wavelength of the sensing grating changes. As a result, the peak is moving along the athermic-grating spectrum causing a large change in intensity for a small change in wavelength. The layout and theory of this system are described in figures 3.11. and 3.12..

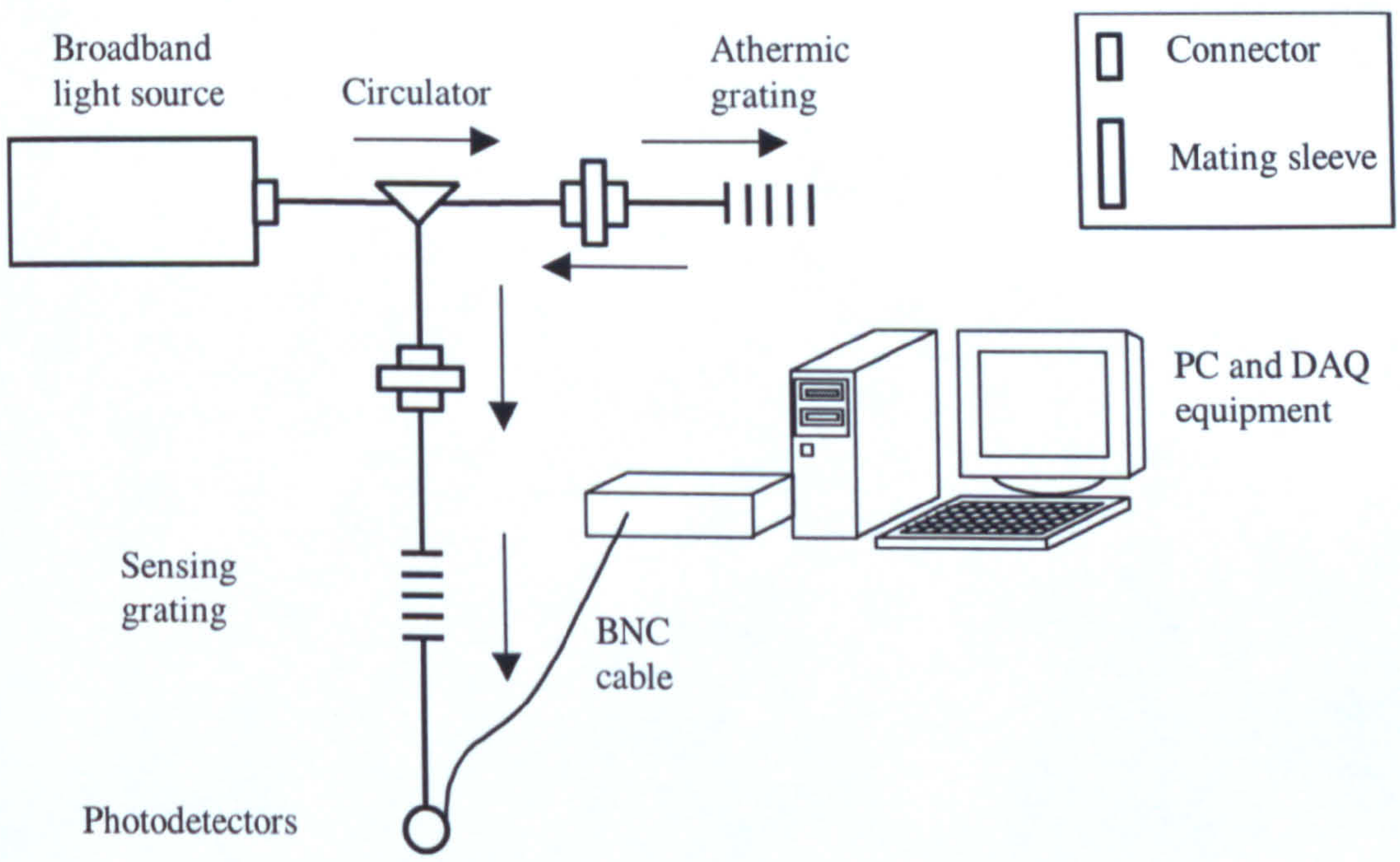

Figure 3.11.: *Two gratings system layout.*

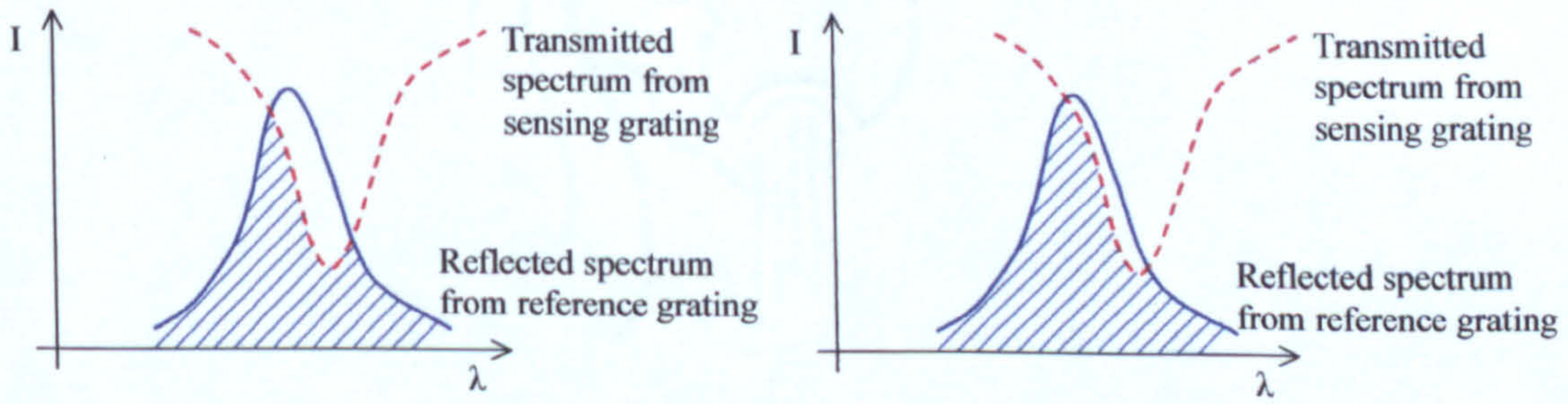

Figure 3.12.: *Two gratings system theory.*

Note:

Since it is quite difficult to manufacture two matching gratings, a tuneable grating can be used to replace the athermic grating. Hence the tuneable grating is tuned by strain (an electrical step index motor stretches the grating) exactly to the desired wavelength so it matches the sensing grating.

3.3. Conclusion.

Two existing techniques for workpiece temperature measurement, have been found worthy of further investigations. However new modifications to these techniques have been proposed that should offer improved performances.

In addition, two entirely new techniques have also been proposed. One of the new methods offers improved performances over existing systems.

As four techniques were selected for further testing, it was then necessary to select the appropriate equipment that would be suitable for use in all four optical systems.

For the systems described above the following equipment is required:

- A broadband light source to launch a broadband spectrum in the optical fibres.
- A circulator to split the signal while inserting low power loss.

- A 50:50 coupler that can be used either as a beam splitter or as an interrogation device for the sensing Bragg grating.
- A pair of standard Bragg gratings for sensing.
- An athermic FBG to be used as a good reference reflected signal.
- A tuneable grating to be used for the same role as the athermic grating and also used for spectrometry purposes as explained in detail in chapter 4.
- A WDM coupler to interrogate the sensing Bragg grating.
- A thin film DWDM demultiplexer to interrogate the sensing Bragg grating.
- Photodetectors for transforming the optical power into an electrical signal capable of being logged by computer.
- A PC equipped with a data acquisition card and compatible data acquisition software to acquire, process and save the data.

The following chapter describes the selection of all this equipment.

References.

1. Rao Y J, "In-fibre Bragg grating sensors", Meas. Sci. Technol.8, p 355-375, 1997.

2. Makiuchi Y and Matsuura H, "Development of a Low-Loss Optical Circulator", Furukawa Review, No. 22, p 1-4, http://www.furukawa.co.jp/review/fr022/fr22_09.pdf, 2002.

Chapter 4: Equipment selection.

4. Equipment selection.

4.1. Fibre Bragg Grating (FBG) selection.

4.1.1. Wavelength.

The performance of the temperature measurement system is highly dependant on the selection of the fibre Bragg grating (FBG). The sensitivity of the grating to temperature change is mainly dependant on the material used for the core of the fibre. Since wavelength has an effect on the sensitivity of the grating [1] (figure 4.1.), it is important to select the most suitable wavelength region for a particular temperature sensing application.

Wavelength (nm)	Temperature sensitivity (pm/°C)	Strain sensitivity (pm/με)
830	~ 6.8	~ 0.64
1300	~ 10	~ 1
1550	~ 13	~ 1.2

Figure 4.1.: *Temperature and strain sensitivity of a fibre Bragg grating sensor in silica fibre at different wavelengths [1].*

Note:

The manufacturer AOS (Advanced Optics Solutions GmbH) specify that for an FBG at 1530nm in SMF28 (standard telecommunication single mode

fibre), the FBG centre wavelength dependency is 11.8pm/°C at 1530nm ±10nm. This temperature sensitivity is produced by the average index change correlated to the temperature change and the effect of the physical expansion.

Figure 4.1. shows that, the highest the wavelength the most sensitive it is to measurands (strain, temperature) therefore a wavelength in the 1540nm ±10nm region is the most suitable for a temperature measurement application since the fibre is more sensitive to temperature at this wavelength. The change in wavelength due to temperature changes is approximately of 13pm/°C for a silica fibre at 1550nm. High temperature sensitivity gives a greater measurement resolution over a relatively small temperature range. The wavelength selected is also influenced by the availability of broadband light sources. In this investigation, a broadband light source with a peak wavelength of 1530nm was selected. Consequently a grating wavelength of 1530nm was selected. At this wavelength the optical power launched in the optical system is at its maximum (section 4.2. and figure 4.7.b.) thus reducing the effect of losses.

Note:

There are two main kinds of optical fibre: multimode and single mode. To date, only single mode fibres are available at this wavelength (1550nm).

4.1.2. Reflectivity.

The reflectivity of the grating is also an important factor. The reflectivity required depends mainly on the position of the grating in the optical circuit, if the optical system measures the reflected light the reflectivity needs to be high (around 22dB), however if the measurement is based on transmission then the reflectivity should be low (around 12.5dB).

4.1.3. Bandwidth.

Other factors such as the –3dB bandwidth have also to be considered. For the two gratings techniques, the temperature measuring range depends on the bandwidth of the athermic grating. For the other systems considered, the bandwidth of the grating will determine the resolution of the system. A standard FBG that has a simple non-chirped structure allows a bandwidth range of 0.1nm to 1nm as standard. However the bandwidth depends on the grade of the reflectivity. If the reflectivity of a Bragg grating becomes stronger, then its bandwidth increases. This can be compensated by changing the length of the fibre Bragg grating: the longer the FBG becomes, the smaller is the bandwidth. Length, reflectivity, and bandwidth of a FBG are dependent on each other.

4.1.4. Resistance to temperature.

Since temperature is to be measured by the fibre Bragg grating, it is necessary that the fibre can withstand the maximum temperature to be measured without sustaining any damage. If the temperature experienced by the grating is greater than the maximum temperature the grating can sustain, then the grating will deform to such an extent that it will not shrink back into its initial condition upon cooling and will be permanently damaged. Standard non-treated optical fibre can withstand temperatures up to 100+°C. Different treatments can allow temperature measurement up to 300+°C made by Indigo photonics and other companies such as ACREO AB can produce gratings able to withstand 1000+°C. It is therefore important to define quite accurately the maximum temperature that the fibre Bragg grating will measure before starting the measurement. However, for this low temperature sensing application (15-80°C) standard telecom optical fibre may be used. The standard material of the fibres are: silica (Ge+ doped) for the core (9µm in diameter), silica for the cladding (125µm in diameter) and acrylate for the coating (250µm in diameter).

4.1.5. Grating selection.

Taking the previously mentioned factors into account, the athermic grating was selected with a 1530.1nm peak wavelength, a reflectivity of 12.7dB and a –3dB bandwidth of 0.4nm (figure 4.2.). Since the reflected signal was

used as the reference signal in the two gratings technique, it was important to have a good reflected signal. However selection of the reflectivity was a compromise between having a good reflected signal whilst avoiding saturation of the photodetector. A wide bandwidth was chosen so it was easier to match with the sensing grating and also provided a wider operating range.

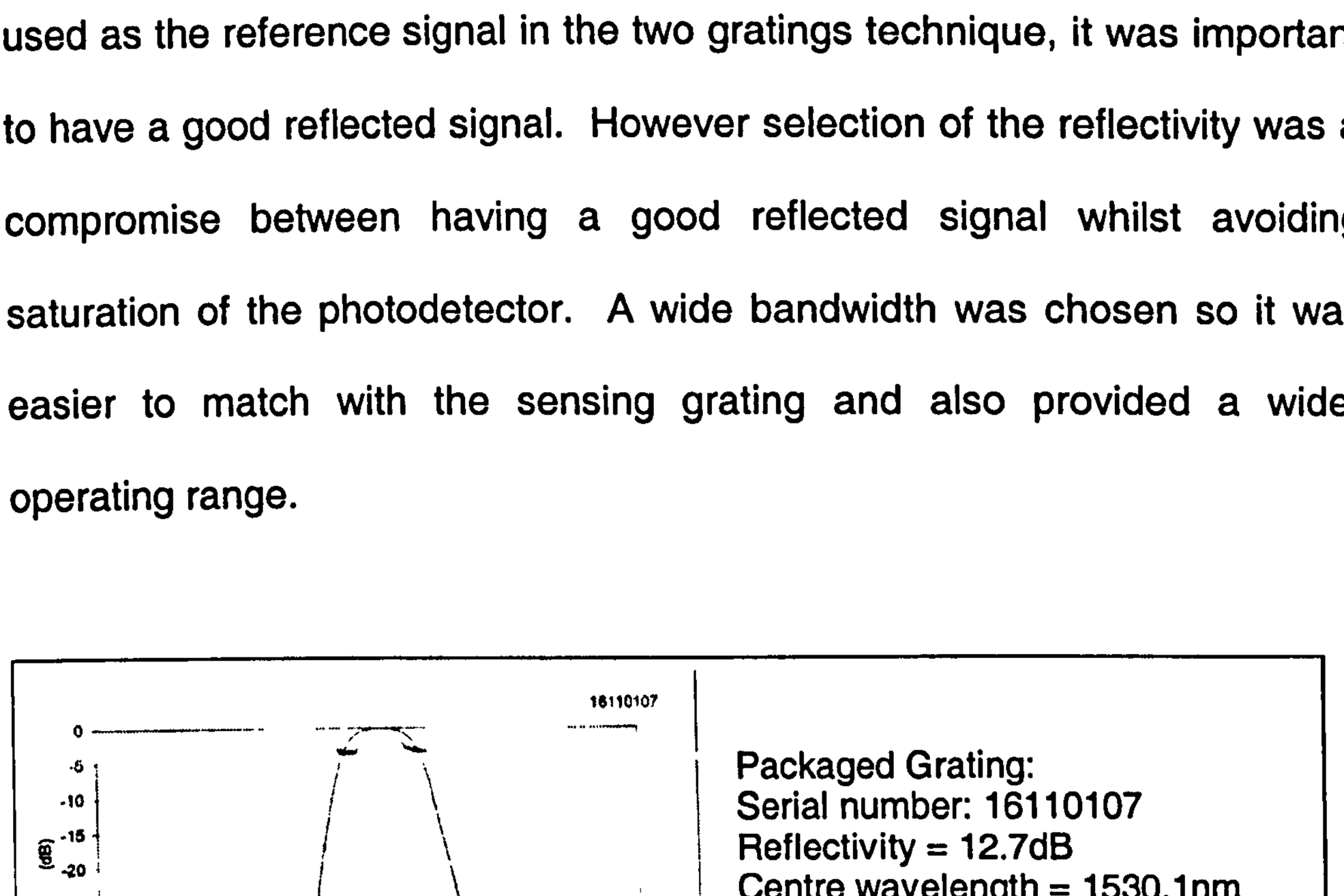

Figure 4.2.: *Athermic grating characteristic spectra.*

For the sensing element, a non-treated grating was selected with a peak wavelength of 1530.3nm, a reflectivity of 12.5dB and a –3dB bandwidth of 0.43nm (figure 4.3.). This grating was used for sensing in the two gratings technique. Its characteristics were almost matched to those of the athermic grating so that when their reflected wavelengths are aligned a minimum signal is passed through the sensing grating to the detector. The wavelength was selected such that the peak in the spectrum of the sensing

grating was on the slope of the reference spectrum as shown in figure 4.4.. This provides a linear response of intensity vs. wavelength and therefore, this system will be easier to calibrate.

Note:

Losses are the amount of light that is lost in an optical component or system. It is expressed in decibels or dB.

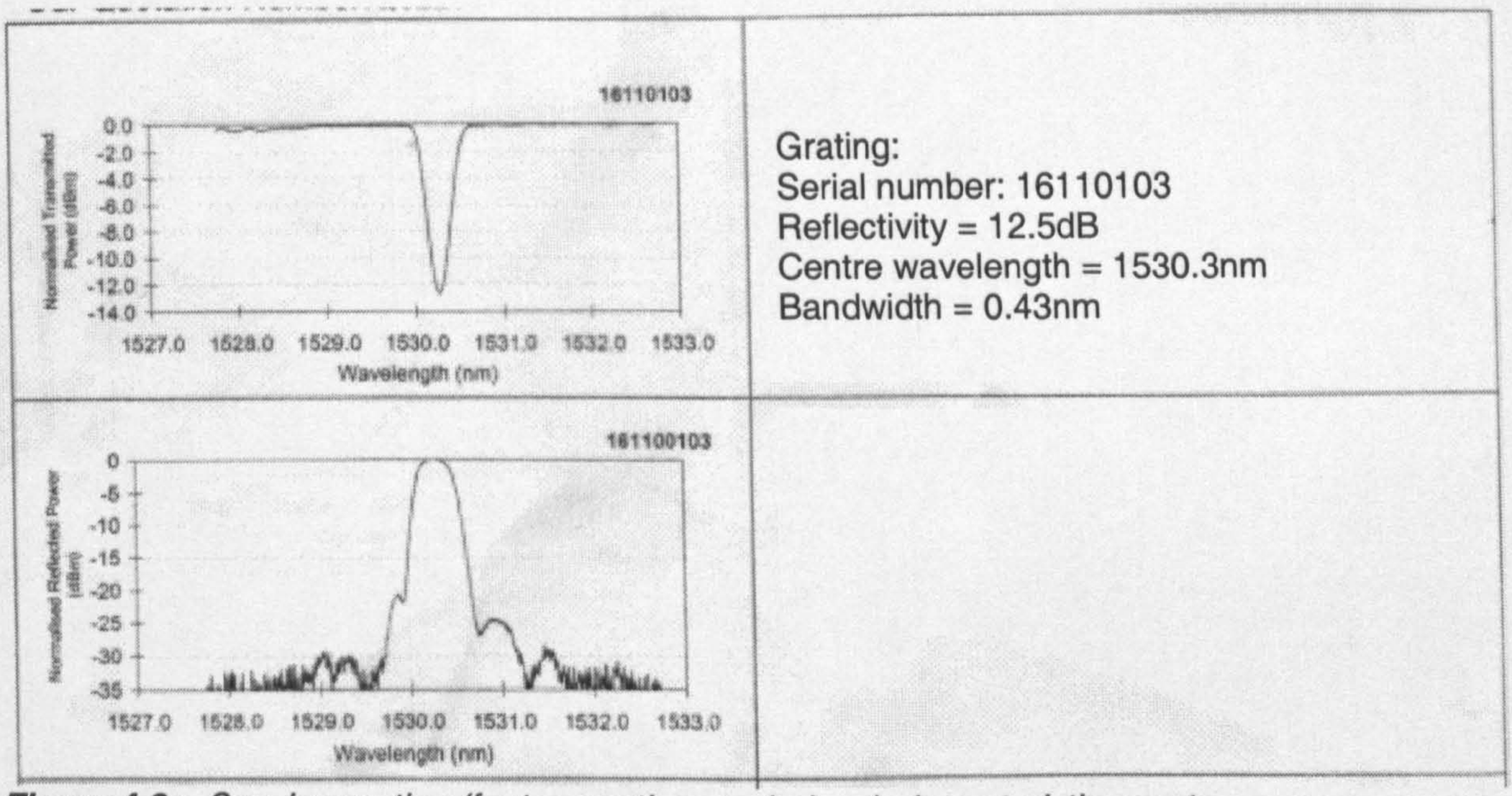

Figure 4.3.: *Sensing grating (for two gratings technique) characteristic spectra.*

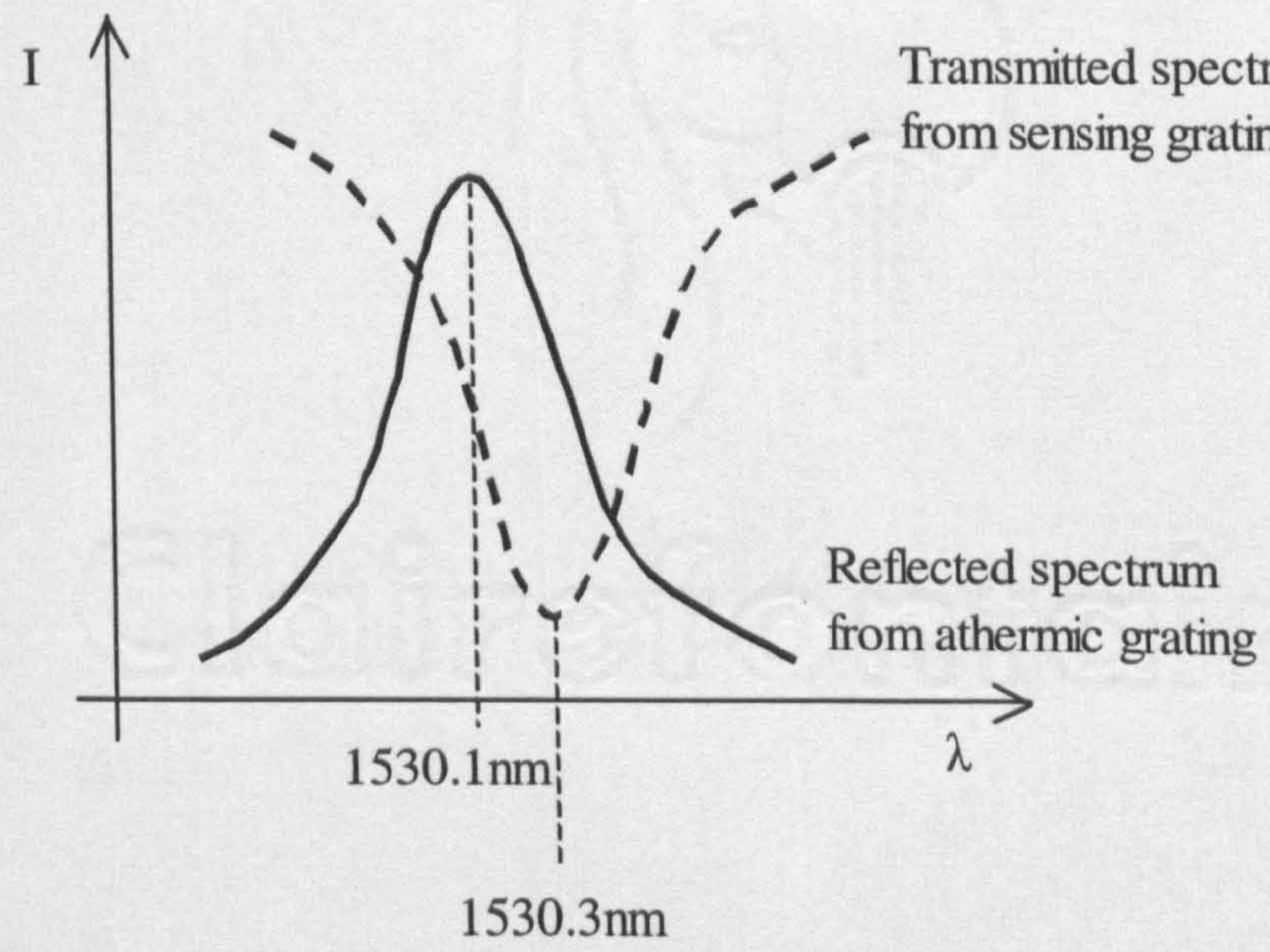

Figure 4.4.: *Position of the spectra (two gratings technique).*

A third grating was selected for the DWDM application. This grating had a Bragg wavelength of 1530.8nm, a reflectivity of 22dB and a –3dB bandwidth of 0.46nm (figure 4.5.). For this measuring system, maximum reflectivity was selected since the interrogation devices produce higher insertion losses. The wavelength was selected so that at standard temperature (20°C), its spectrum was positioned at the beginning of the slope of the DWDM CH2 as shown in figure 4.6.. This grating was also to be used for the WDM technique and the coupler technique, as both techniques require a high reflectivity.

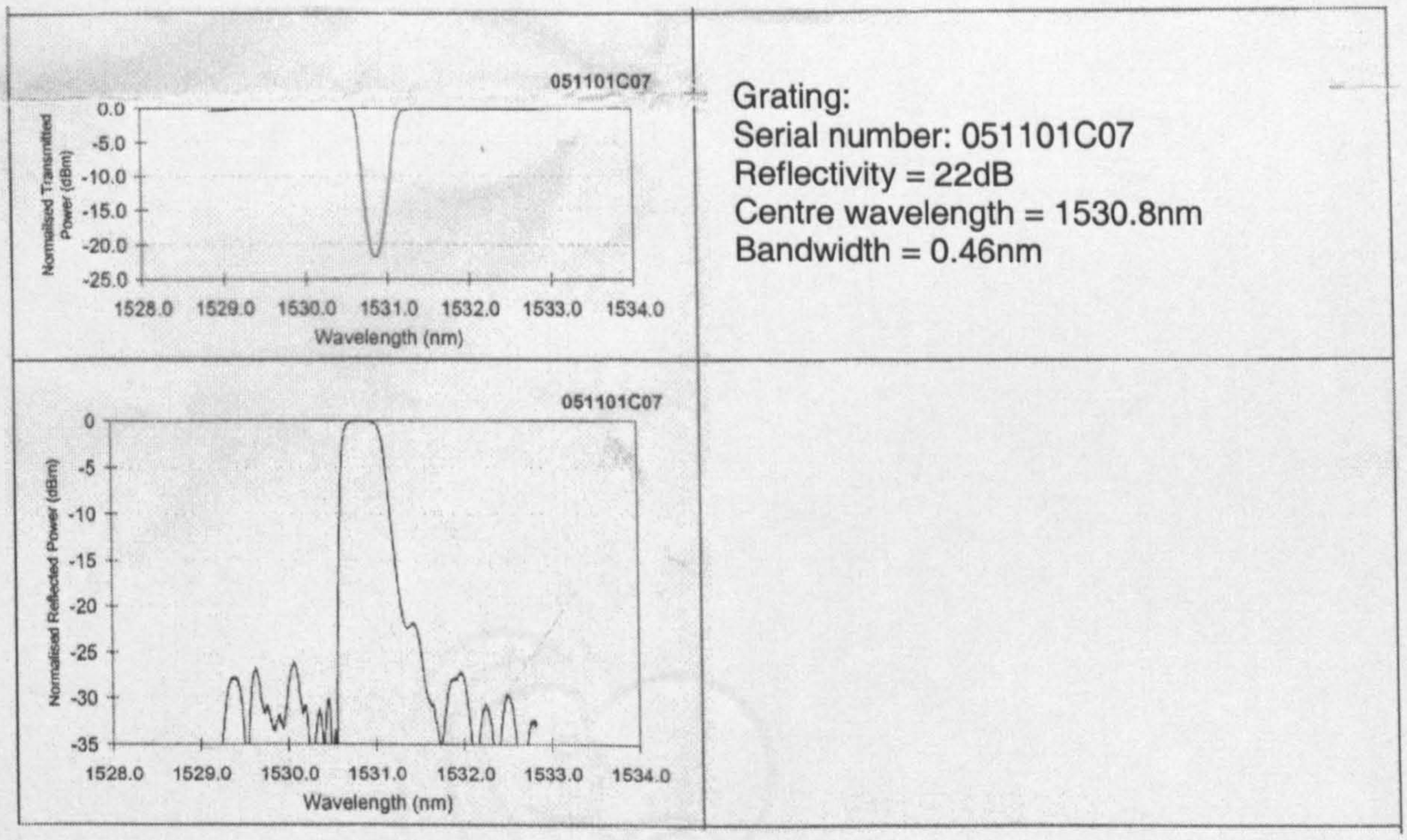

Figure 4.5.: *Sensing grating characteristic spectra (for DWDM, WDM and coupler technique).*

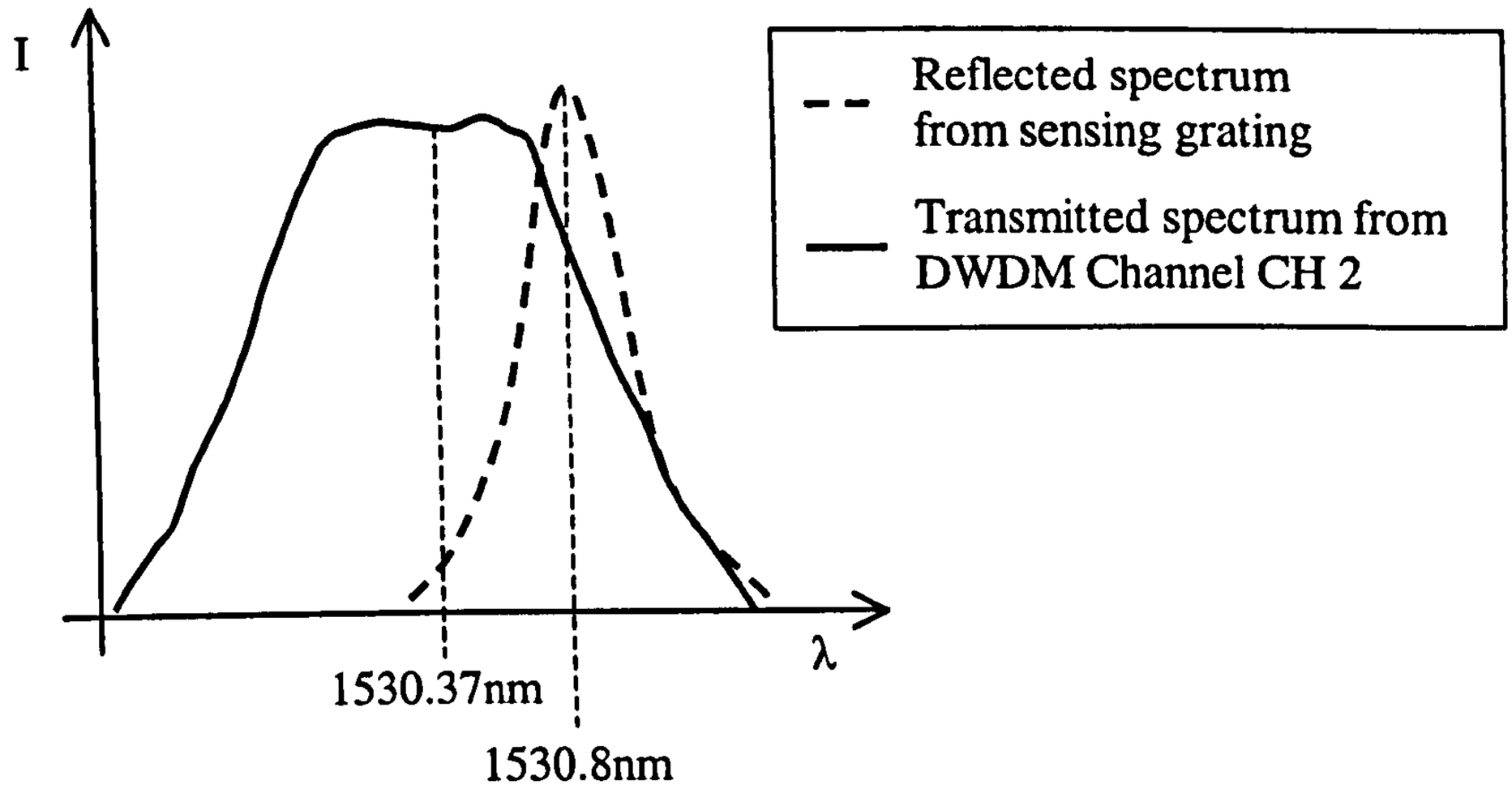

Figure 4.6.: *DWDM technique spectra positioning.*

4.2. Broadband Light Source (BLS) selection.

The main factors that had to be considered when choosing a BLS were:

4.2.1. Band size.

Standard telecoms broadband light sources are readily available in three different bands: C band (1520nm-1575nm), L band (1570nm-1620nm) and C+L band (1525nm-1615nm).

The minimum bandwidth for the sensing system can be determined from knowledge of the temperature sensitivity at the selected wavelength (11.8pm/°C) and the temperature change to be measured.

For this application, a maximum temperature of 300°C (maximum temperature before destruction of a treated grating (used for the DWDM,

WDM and coupler systems) was selected and this gave a minimum bandwidth of 3.9nm. This requirement was satisfied by a C-Band source operating in the 1550nm wavelength region.

4.2.2. Output power.

A broadband source manufactured by O-Net Communications (SZ) Ltd was selected. The source, type FOS-AC-13-3, has an optical output power in the region of 13.7dBm. The source operates on Amplified Spontaneous Emission (ASE) principle and is based on "the self-emitting amplification of Er^{3+} in erbium-doped fibre" [2]. The output of the source is non-polarised and is fibre based (like a standard connector (FC/APC in this case) mating sleeve). This maximise the output power since the coupling to a fibre creates minimal losses (approximately 0.1dB).

Note:

Optical power can be expressed in Watts or decibel values. However, decibel values are more commonly used because they make the calculation of the optical power going through an optical system easier than if using mW. This is because the logarithmic nature of decibel units translates the multiplication and division associated with gains and losses into addition and subtraction. The used unit is dBm, which stands for decibels relative to 1 mW of power.

The optical power units: dBm and mW are related as expressed in the following equations:

$$P(dBm) = 10 \times \log\left(P(mW)\right) \tag{1}$$

$$P(mW) = 10^{\frac{P(dBm)}{10}} \tag{2}$$

Where P is the optical power.

4.2.3. Power stability.

For this particular temperature measurement sensing application, it was very important that the light source output power was stabilised. A steady output power level allowed for reliable calibration and accurate measurement since the optical systems designed relied on the detection of changes in intensity.

Figure 4.7.a. tabulates the characteristics of the selected light source and figure 4.7.b. shows the characteristic spectrum of an ASE based light source.

Parameters	Value	Remark
Peak wavelength	1557.8nm	
Total output power	13.7dBm (23.44mW)	
Output stability*	0.01dB	15 minutes
Output stability*	0.01dB	1 hour
Lasting stability*	0.02dB	24 hours
Wavelength range	1523.2nm ~ 1572.3nm	Over –30dBm / 0.1nm
Adapter type	FC/APC	

*: After one hour of warm up.

Figure 4.7.a.: *Light source characteristics for the FOS-AC-13-3 source from O-Net Communications (SZ) Ltd.*

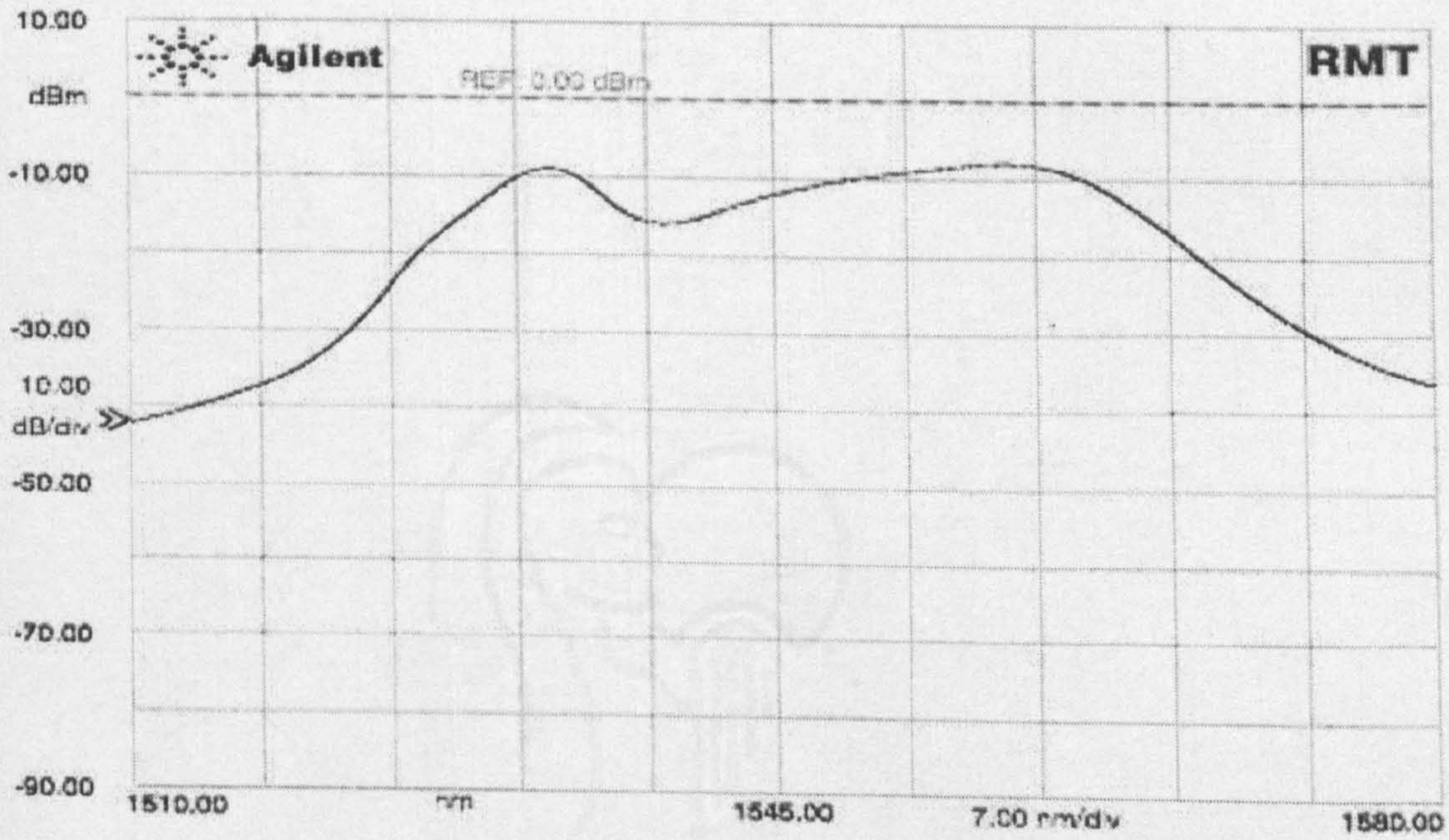

Figure 4.7.b.: *Characteristic spectrum of an ASE based light source from O-Net Communications (SZ) Ltd.*

4.3. Circulator selection.

The circulator was chosen for its very small insertion loss at the wavelength range used (approximately 1530nm). An additional advantage of using a circulator is that despite the fact of transmitting almost maximum signal to the next branch (as explained before in chapter 3.2.1.), the circulator also acts as a very good isolator avoiding the problems caused by the reflected signal returning to the light source and eventually causing damage. Figure 4.8. tabulates the characteristics of the circulator used.

Insertion Loss (dB)	1530nm	1550nm	1570nm	1590nm	1610nm
1→2	0.69	0.70	0.74	0.76	0.89
2→3	1.03	0.99	1.07	1.10	1.16
Isolation (dB)	1530nm	1550nm	1570nm	1590nm	1610nm
2→1	63	65	61	53	48
3→2	63	64	63	54	49

Figure 4.8.: *Circulator characteristics.*

4.4. WDM selection.

A 1510nm/1550nm WDM was chosen because its characteristic transmission curves crossed in the 1530nm region. This reduced any confusion in interpreting the signal since the centre wavelength of the

sensing grating was above the 1530nm crossover. It also mean that one intensity level read on any branches corresponds to one wavelength only (see figure 4.9.). For example, if this WDM was used with a grating centred at 1529.5nm, the same intensity could be read on branch 1 at 1529.8nm and on branch 2 at 1530.2nm (these values are randomly taken as an example).

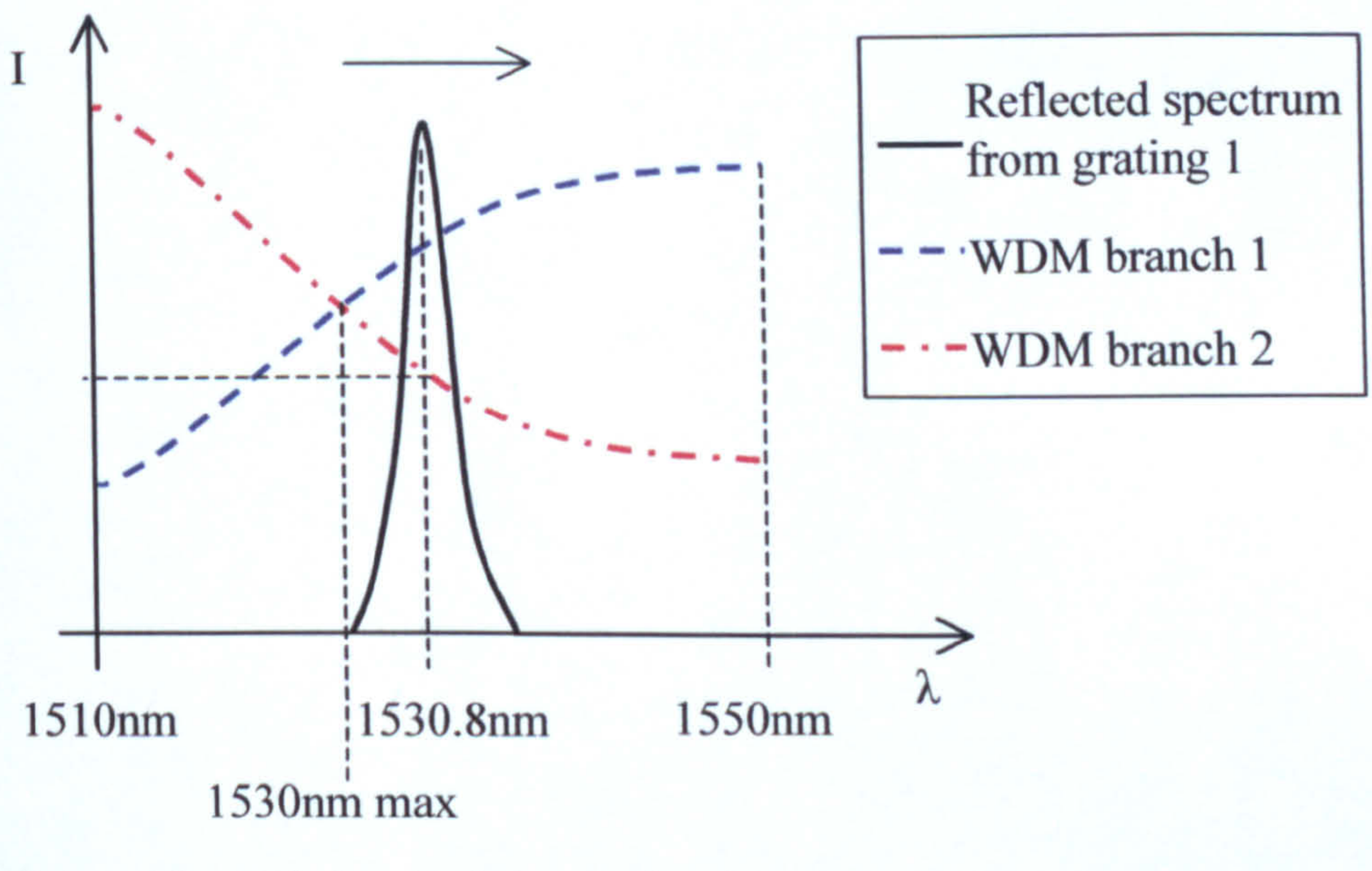

Figure 4.9.: *Relationship between the characteristic transmission curves and the reflected spectrum.*

4.5. DWDM selection.

One of the reasons for using a thin film dense DWDM was for its steep wavelength vs. intensity response. Figure 4.10. below shows the characteristics of each channel.

Insertion Loss (dB)	CH61	1.82	CH53	1.94
	CH59	1.81	CH51	2.35
	CH57	1.7	CH49	2.46
	CH55	1.86	CH47	2.76
Centre wavelength (nm)	CH61	1528.78	CH53	1535.06
	CH59	1530.37	CH51	1536.66
	CH57	1531.92	CH49	1538.2
	CH55	1533.44	CH47	1539.69
Passband at 0.5dB (nm)	CH61	0.97	CH53	0.91
	CH59	0.89	CH51	0.96
	CH57	0.88	CH49	0.89
	CH55	0.89	CH47	0.87

Figure 4.10.: *Characteristics of the different channels of the used thin film dense DWDM.*

The channel spacing (2nm) is small but ideal for this application, since the temperature range measured is relatively small and the steep response of the DWDM allows a higher sensitivity. This allows accurate measurement to be achieved since the intensity vs. wavelength curve for the DWDM with 2nm channel spacing is steeper than for a DWDM using 6nm channel spacing as illustrated in figure 4.11..

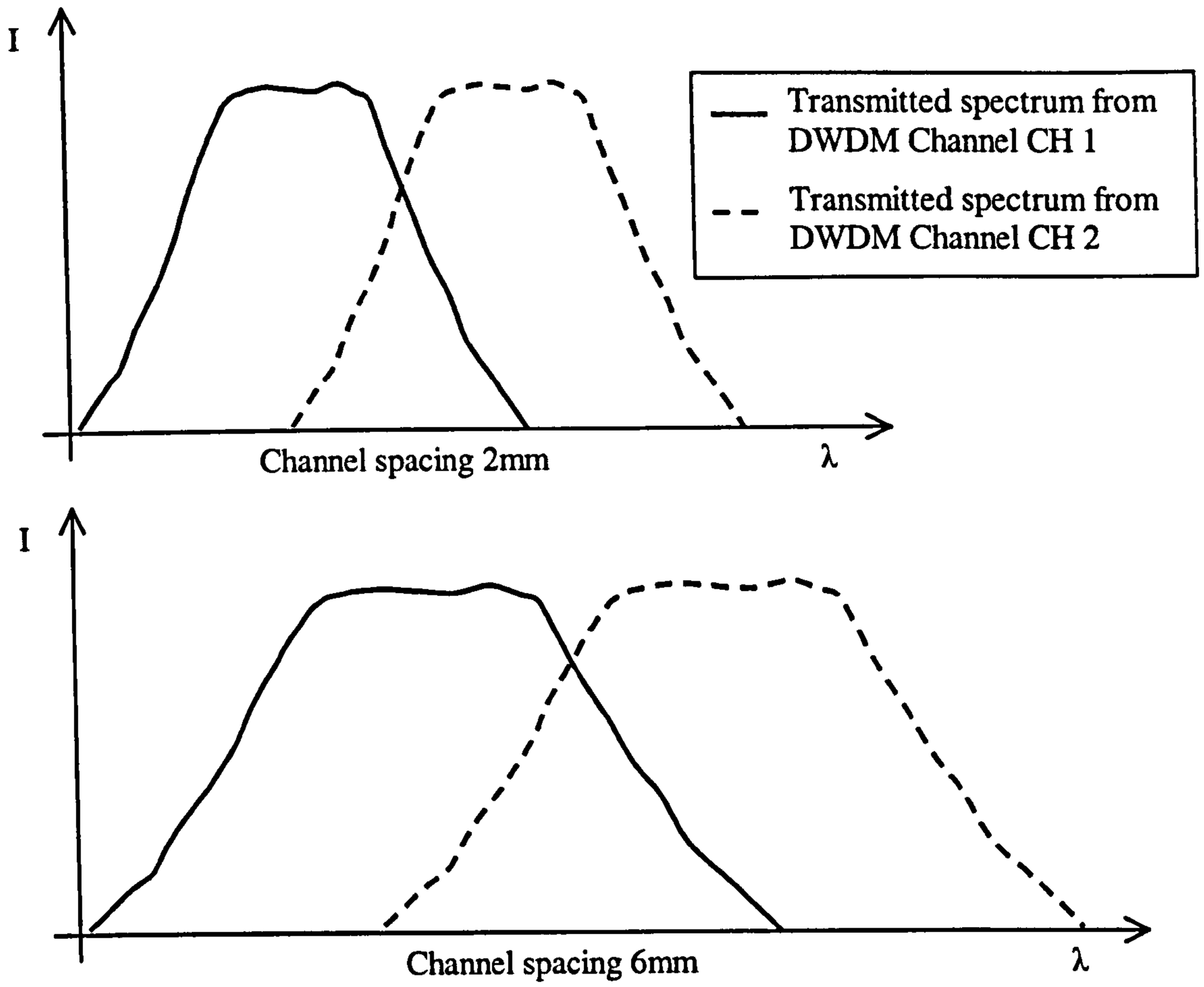

Figure 4.11.: *Effect of channel spacing on two DWDM channels spectra.*

4.6. Coupler selection.

For the coupler technique, a standard coupler matching the wavelength range of interest was selected. A 50:50 ratio was chosen since a 50:50 coupler splits the input signal into two equal output signals, the power transmitted to the output branches is therefore equal in each branch. This principle is illustrated in figure 4.12..

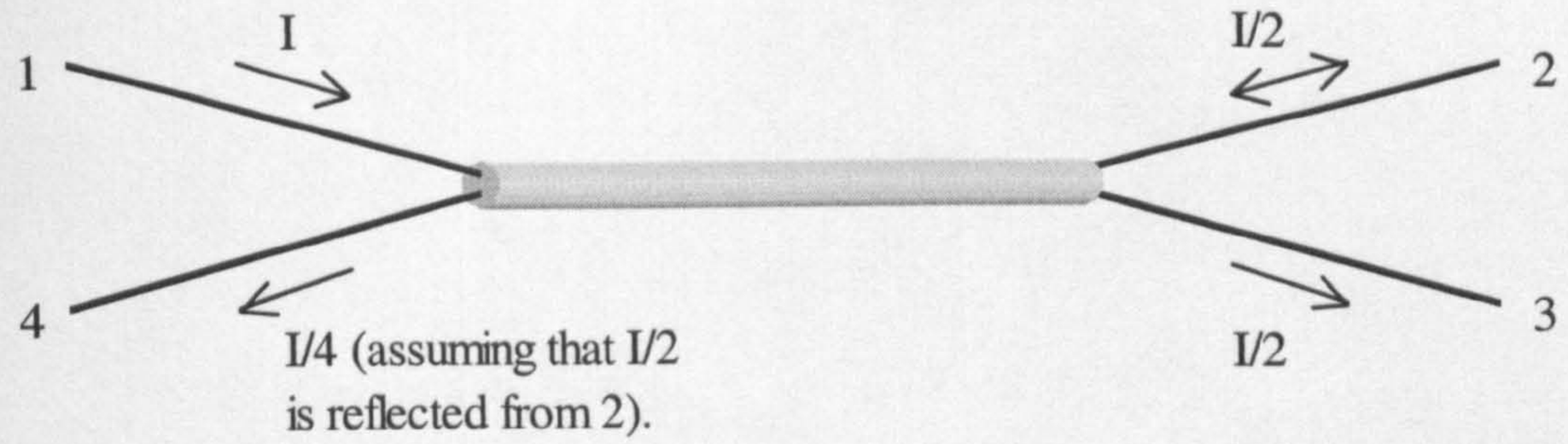

Figure 4.12.: *50:50 coupler.*

4.7. Photodetector selection.

An optical detector converts the optical energy delivered by a fibre into an electrical signal that is suitable for input into a data acquisition card. The basic detection circuit consists mainly of a photodiode, a load resistance and an amplifier. In a photodetector, when one photon of light becomes in contact with the active area of the photodiode, it releases one electron that is detected via an electronic circuitry. This creates a change in the electrical current in the circuit. This current is "the direct photocurrent out of the photodiode anode and is a function of the incident light power and the wavelength" [3]. Therefore, to avoid any potential source of error, it is necessary to select a photodetector so that its responsivity versus wavelength is constant and equal to 1 at the wavelength region of interest (1525nm-1540nm). The output signal is the voltage drop across the load resistor and this can be input into a suitable data acquisition card.

There are three main factors used to determine the right photodetector:

- The lowest luminosity that the device can detect.
- The spectral range over which the detector operates.
- The rise time, i.e. the time interval required for the detector to respond to a step input in the signal intensity.

Therefore prior to selecting the right photodetector, it was necessary to determine the characteristics of the output power produced by the different temperature measurement techniques.

4.7.1. Determination of the power out of the optical system.

4.7.1.a. Theory.

For a given optical arrangement, the knowledge of insertion loss of each device, the spectral characteristics of the gratings and the insertion loss formulas, allowed a good approximation of the minimum power arriving to the photodetectors. The calculations were used to determine if the power launched into the system by the broadband light source (BLS) was sufficient and also to determine the minimum intensity that had to be detected by the photodetectors. The results were also used later on in the investigation for calibration purposes.

The general insertion loss formula states that:

$$I_L(dB) = 10 \times \log\left(\frac{P_o}{P_i}\right) \qquad (3)$$

Where P_o and P_i are the optical power out and into, respectively, of the optical network in mW and I_L is the insertion loss in dB.

The insertion loss is the total optical power loss caused by the insertion of an optical component; it is a characteristic that is provided by the manufacturer for every device. The total insertion loss, for a given system, can be calculated by adding all the insertion losses (if all losses are given in dB). It was therefore important to choose components with small insertion losses since the measurement was based on intensity change at the end of the optical system and high insertion losses would reduce the energy incident on the detector.

For example, the following are typical insertion losses for the components required for the temperature measurement systems:

A single mode fibre losses approximately	I_{LF} = 0.2dB/km (negligible).
Fixed FC/APC connector:	I_{LFC} = 0.1dB
2 FC/APC connectors+fibre and 1 sleeve:	I_{LFC+F} = 0.36dB (selected for their low losses).
Mating sleeves:	I_{LS} = 0.16dB
Circulator at 1530nm:	$I_{LC\ 1\rightarrow 2}$ = 0.69dB
	$I_{LC\ 2\rightarrow 3}$ = 1.03dB

Grating: I_{LG} = 1dB (if the signal is transmitted).

I_{LGR} = 0.5dB (if the light is reflected (I_{LG}/2)).

Note:

The data, quoted above, were provided by the equipment manufacturers. However, the values were checked by performing practical experiments and by measuring the power loss with a power meter. The insertion loss formula is quite straightforward when used with standard optical equipment, however the insertion of a grating, into an optical system, is a more complex problem and requires further discussion. This discussion is given in the following section.

4.7.1.b. Basic configuration.

Use of the insertion loss figures combined with detailed data on the spectral response of selected components, allowed the determination of the optical power at any point of the optical system. The three suggested optical measurement systems layouts start as shown in figure 4.13..

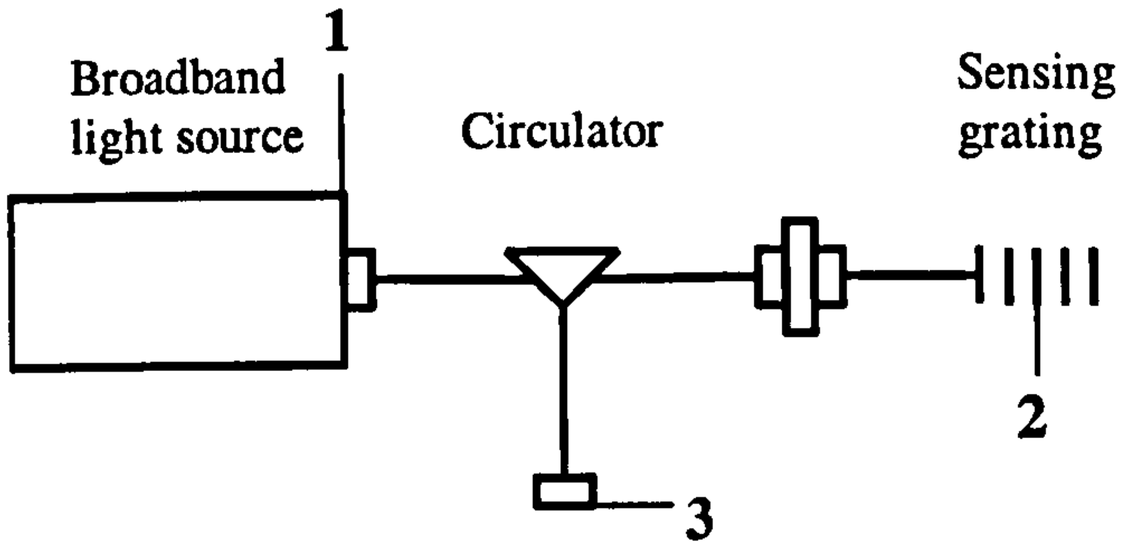

Figure 4.13.: *Point of references.*

The BLS launches the optical signal into the system (1) (section 4.2.2.), then a circulator transmits the optical signal to the athermic grating in the case of the two gratings technique (2) (or to the sensing grating for the DWDM, WDM and/or coupler technique). The reflected signal from the grating then returns in the other branch of the circulator to (3) where the different types of equipment to relate wavelength and intensity of the signal are to be inserted.

As the spectra for the BLS and gratings, provided by the equipment manufacturers, are not defined by standard mathematical functions, the spectra were enlarged and data was read from figure 4.7.b..

%LIGHT SOURCE VALUES

LambdaLS = [1514 1520 1526 1532...]'; wavelength values of the light source (nm).

PowerLS1 = [-35 -33.01 -18 -10...]'; corresponding intensity values (dBm).

%dB

PowerLS2 = (PowerLS1+7.95);

This was included because the spectrum given by the manufacturer was suspect. When calculating the area below the spectrum of figure 4.7.b. and comparing the result (5.75dBm) to the real output power of the light source (13.7dBm), it was possible to realise that the spectrum provided by the manufacturer was for a 6dBm light source and not for a 13dBm light source. And by adding this 7.95dBm value to each point of the scanned spectrum it was possible to plot the real characteristics of the light (figure 4.14.).

After determining the coordinates of the light source spectral curves, it was possible to fit a curve passing through all the data points. This was achieved using the following Matlab code whose output is shown graphically in figure 4.14.:

%Curve fitting

hLS=1523.2:0.01:1572.3; first a range and a step were defined.

tLS1=interp1(LambdaLS,PowerLS2,hLS,'cubic'); Then it was possible to fit a curve using a 1-D cubic interpolation.

Numerical integration of the BLS spectrum allowed its power output to be checked. The output power was found to be 23.02mW or 13.62dBm. The following Matlab code was used to calculate the power.

%at 1 (power out the light source).

tLS10=10.^(tLS1/10); to transform the plotted values of the light source spectrum from dBm into mW.

area1 = trapz(hLS,tLS10); to calculate that area below the spectrum curve (result in mW). The function *trapz* does the trapezoidal integration of the area under *tLS10 = f(hLS)* given data point in hLS and tLS10.

*Power1=10*log10(area1)* to transform the previous value in dBm.

Note:

As the area, below the spectral curve of the light source, represents the power out of the light source, it was necessary to calculate the area in mW first since the dB unit is only useful for insertion loss purpose.

This gives the following plot and values:

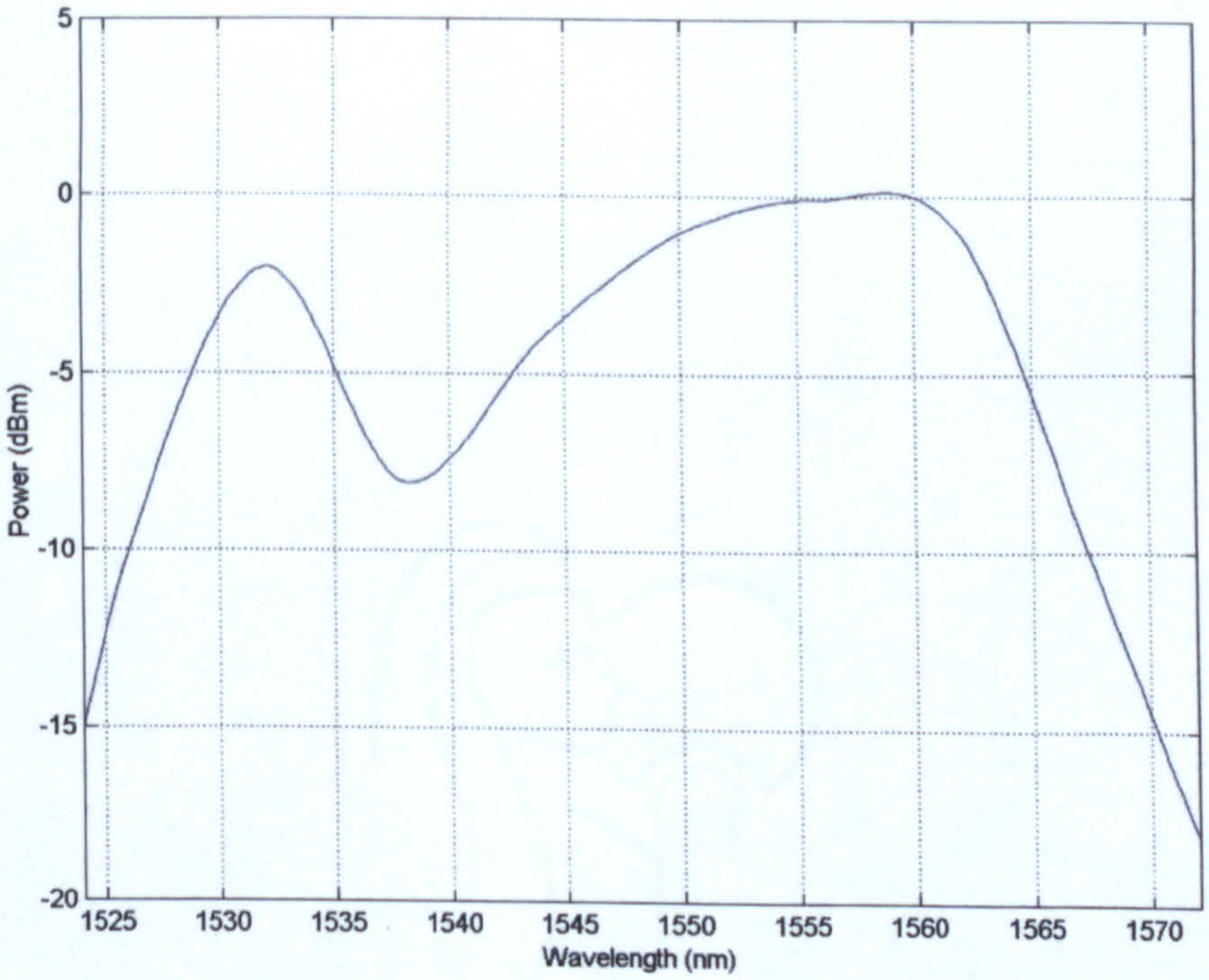

Figure 4.14.: *Broadband light source spectrum.*

The optical power output calculated from the above algorithm was: 13.62dBm. This value compared favourably with the value of 13.7dBm determined by experiment at the same position.

Once that the source power was defined, it was possible to work out the losses through the rest of the optical system. The insertion losses of the different devices between the light source and the athermic grating were subtracted from the light source spectrum since they damp the optical signal.

```
%Losses between 1&2 LS and grating in dB are 0.69 for circulator, 0.36 for
connectors and fibre and 0.5 + 0.1 for 1/2 grating and 1 connector as shown
in figure 4.15..
This gives a total loss of:
tLS2=tLS1-(0.18+0.69+0.18+0.1+0.5);
```

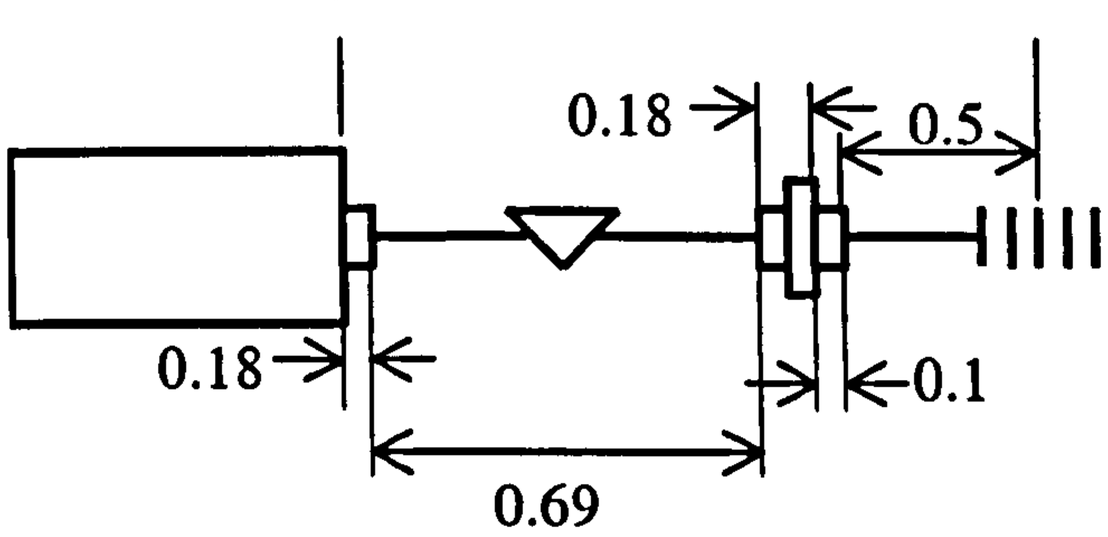

Figure 4.15.: *Losses between (1) and (2) (all values in dB).*

The reflected signal from the athermic grating was then plotted and a curve was fitted through these points using the following code:

```
%REFLECTED SIGNAL FROM THE ATHERMIC GRATING
%Values
LambdaAR = [1520 1525 1527.9 1528 1528.1 1528.2...]'; %nm
PowerAR1 = [-35  -35  -35  -35  -35  -35...]';  %dBm
```

%CURVE FITTING

tAR1=interp1(LambdaAR,PowerAR1,hLS,'spline'); to fit a curve using 1_D cubic spline interpolation.

The output from this is shown graphically in figure 4.16..

Since the grating only reflects the optical power that enters it, it is necessary to define the real reflected spectrum. It is a mix of the damped signal from the light source (light source original signal minus the losses encounter by the light signal between the light source and the grating) and of the reflected spectrum from the grating.

%INTERSECTION LIGHT SOURCE AND GRATING

s2 = size(tLS2); size matrix.

a2 = tLS2 <= tAR1 ; Condition if the values of the spectrum of the grating are greater than the values of the spectrum coming in the grating.

Then the resulting curve *tAR2* is defined as follow:

tAR2=tLS2;

for i=1:1:s2(2),

if a2(1,i) == 0 if the condition is false

tAR2(1,i) = tAR1(1,i); then the real reflected signal is the same as the one from the grating.

else tAR2(1,i) = tLS2(1,i); in any other case, the real reflected signal is the same as the one from the signal entering the grating.

end

end

The output from this algorithm is shown graphically in figure 4.17..

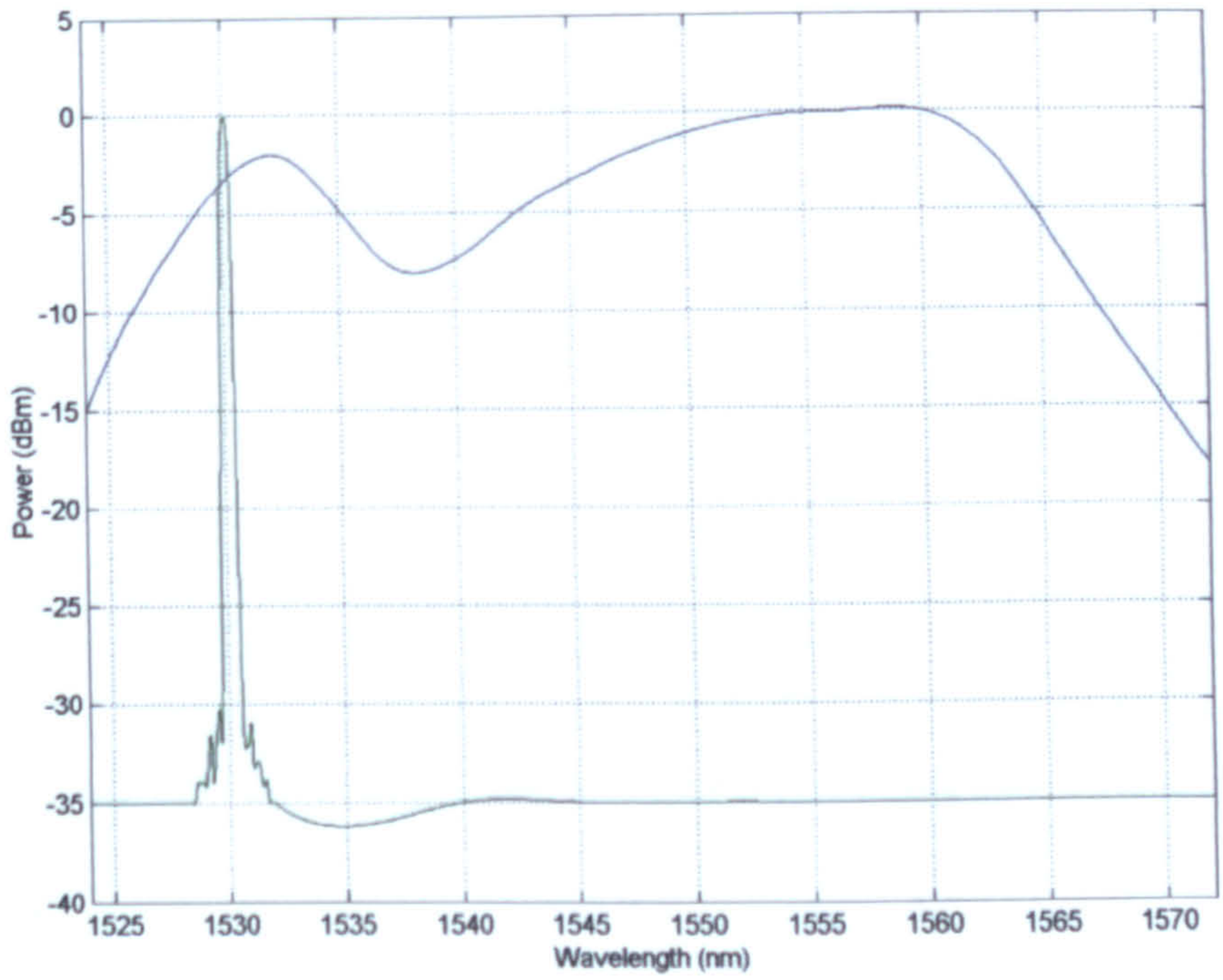

Figure 4.16.: *Light source + reflected grating spectra.*

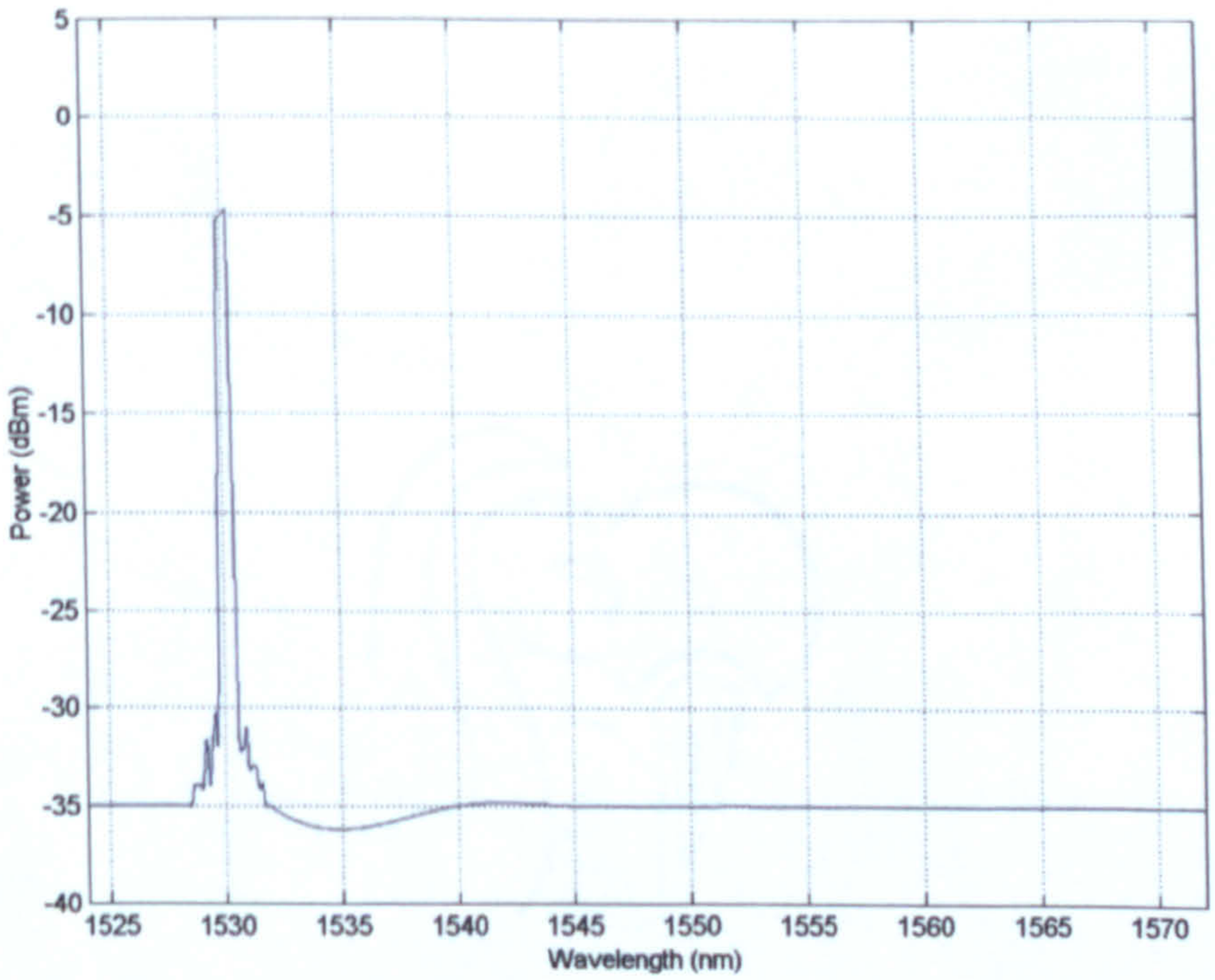

Figure 4.17.: *Mix of light source + reflected grating.*

4.7.1.c. Verification.

This reflected signal is guided back to the circulator which diverts it toward (3) in figure 4.18..

Losses from device between (2) and (3) were then deducted from the signal.

%Losses between 2&3 in dB=(0.5 + 0.1 for 1/2 grating and connector)+(1.03 for circulator)+(0.36 for connectors and fibre)+(0.1 for connector) as shown figure 4.18..

tLS3=tLS2-(0.5+0.1+0.18+1.03+0.18);

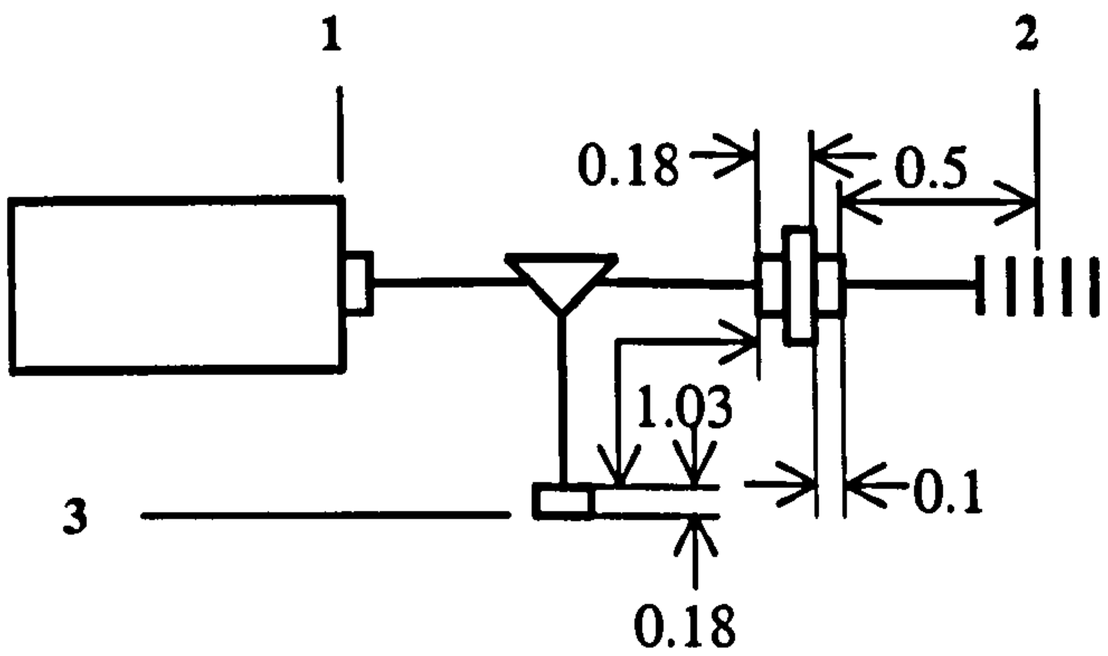

Figure 4.18.: *Losses between (2) and (3) (All units in dB).*

To check the calculations, it was possible to calculate the power at (3) and directly compare it to the value measured experimentally at some point.

To determine the power at (3), it was again necessary to intersect the spectrum of the total optical power minus all the losses and the spectrum of the signal reflecting from the athermic grating. This was simulated using the following Matlab code:

```
%INTERSECTION LIGHT SOURCE NEW LS3 AND GRATING

s3 = size(tLS3);

a3 = tLS3 <= tAR2 ;

tAR3=tLS3;

for i=1:1:s3(2),

  if a3(1,i) == 0

    tAR3(1,i) = tAR2(1,i);

  else tAR3(1,i) = tLS3(1,i);

  end

end
```

The output of this is shown in figure 4.19..

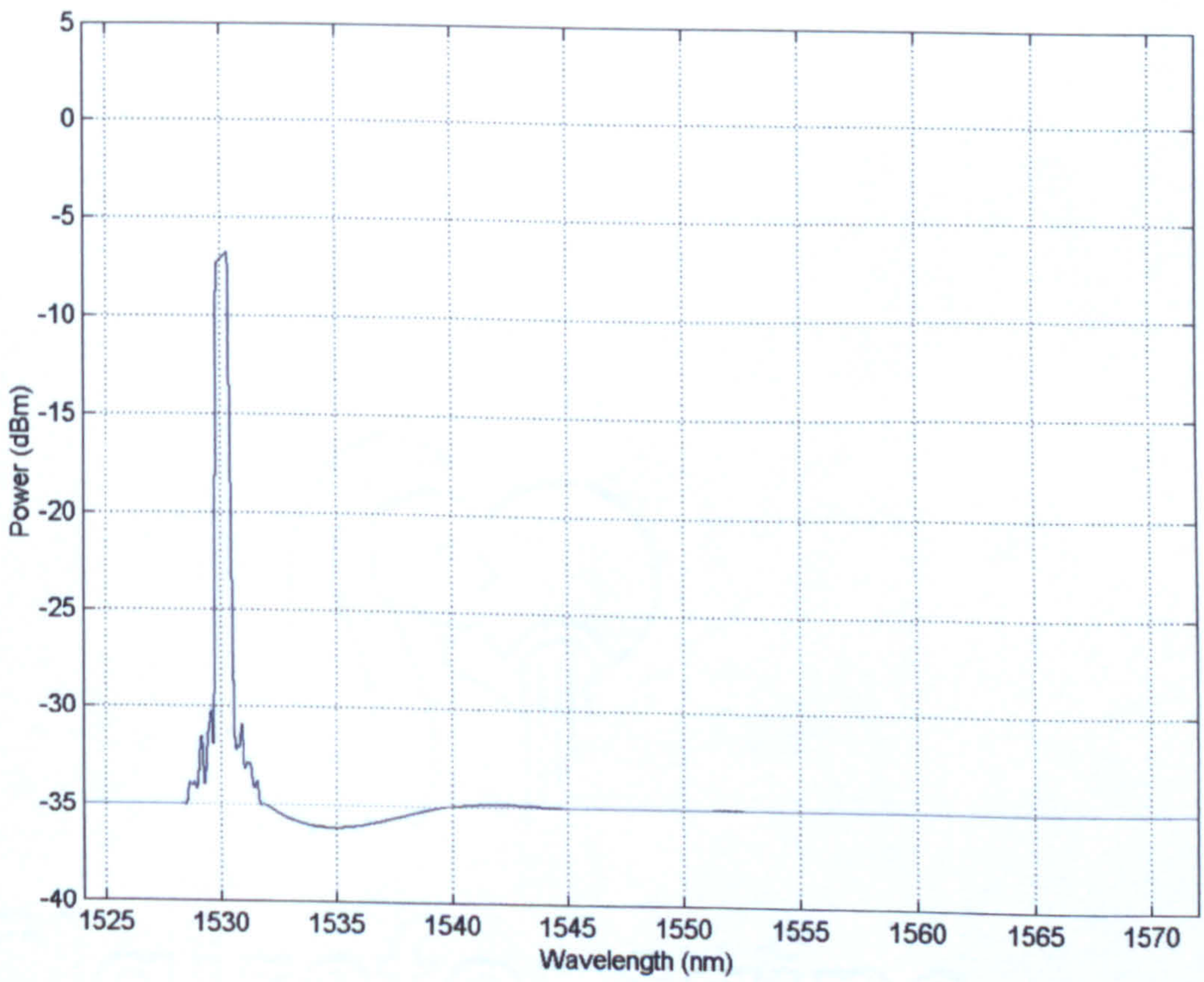

Figure 4.19.: *Optical signal at (3).*

Then the signal at port (3) can be calculated as follow:

%AT 3

tLS31=tAR2;

tAR30=10.^(tLS31/10); to transform all the units in mW.

area3 = trapz(hLS,tAR30); to calculate the surface area below the spectrum

i.e. the power at (3) in mW.

*Power3=10*log10(area3)* to transform the previous result in dBm.

This calculation gave a signal power of –9.36dBm. This result was compared against the experimental value obtained using an Optical Power Meter (-9.94dBm was measured at (3)). The calculated results agree to within 5.8% of the measured value.

From there and knowing the insertion losses of each "next" devices (<2dB in the worst case) plus adding a –1dB safety factor (which is a factor of security often use in engineering for safety reasons to prevent the unexpected to happen), it was possible to say that the light coming out any of the optical system of interest was approximately -12.36dBm (0.0581mW) minimum at the photodetectors if the optical power launched into the system at (1) was 13.7dBm.

4.7.2. Calculation of the power output of the optical system.

At this stage, it was also possible to determine how much light was output from the system and what kind of intensity changes could be expected from a change in the measurand.

The following code allowed the determination of the power out the two gratings system layout (figure 3.11.).

First, the sensing grating transmission spectrum was plotted.

```
%SECOND GRATING TRANSMITTED POWER
LambdaNGT = [1515   1520   1525   1526   1527   1528...]'; (nm)
PowerNGT =  [0      0      0      0      0      0...]'; (dB)
```

A command line was added so that the user could change the wavelength of the spectrum to simulate a change in temperature.

```
%Movement of the sensing grating
i=input('wavelength change in nm? (initial=1530.1nm)');
LambdaNGT1=LambdaNGT+i;
```

A curve was then fitted to draw the spectrum and interpolate all points.

```
%CURVE FITTING
tNGT=interp1(LambdaNGT1,PowerNGT,hLS,'spline');
```

The spectrum reflected from the reference grating (2) and the spectrum transmitted by the sensing grating, was determined. First, all the points of both spectra were compared at each wavelength interval. The smallest intensity values were kept to plot the signal curve. In other terms, the resultant curve was the result of both curves lowest intensity points. This is shown in figure 4.20..

```
%INTERSECTION GRATINGS

s4 = size(tNGT);

a4 = tNGT <= tAR3;

tAR4=tNGT;

for i=1:1:s4(2),

   if a4(1,i) == 0

      tAR4(1,i) = tAR3(1,i);

   else tAR4(1,i) = tNGT(1,i);

   end

end
```

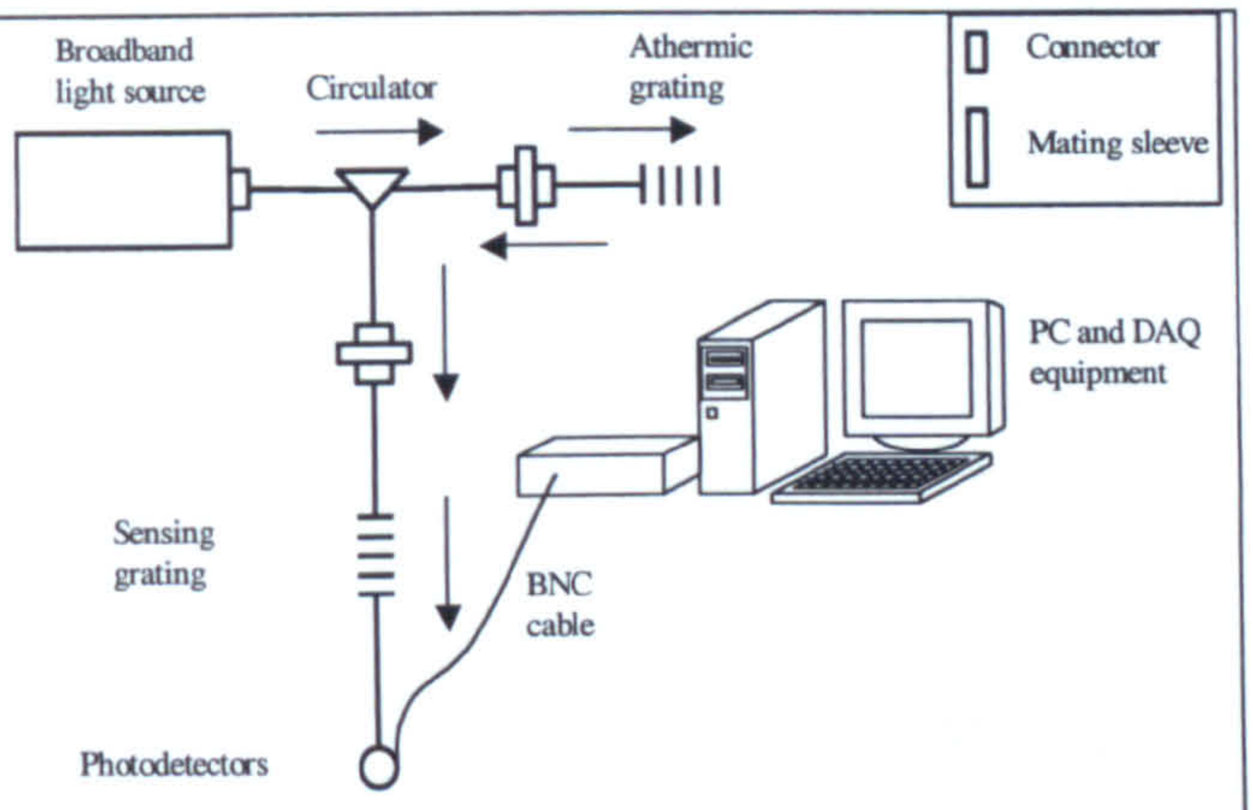

Two grating system layout reminder (figure 3.11.)

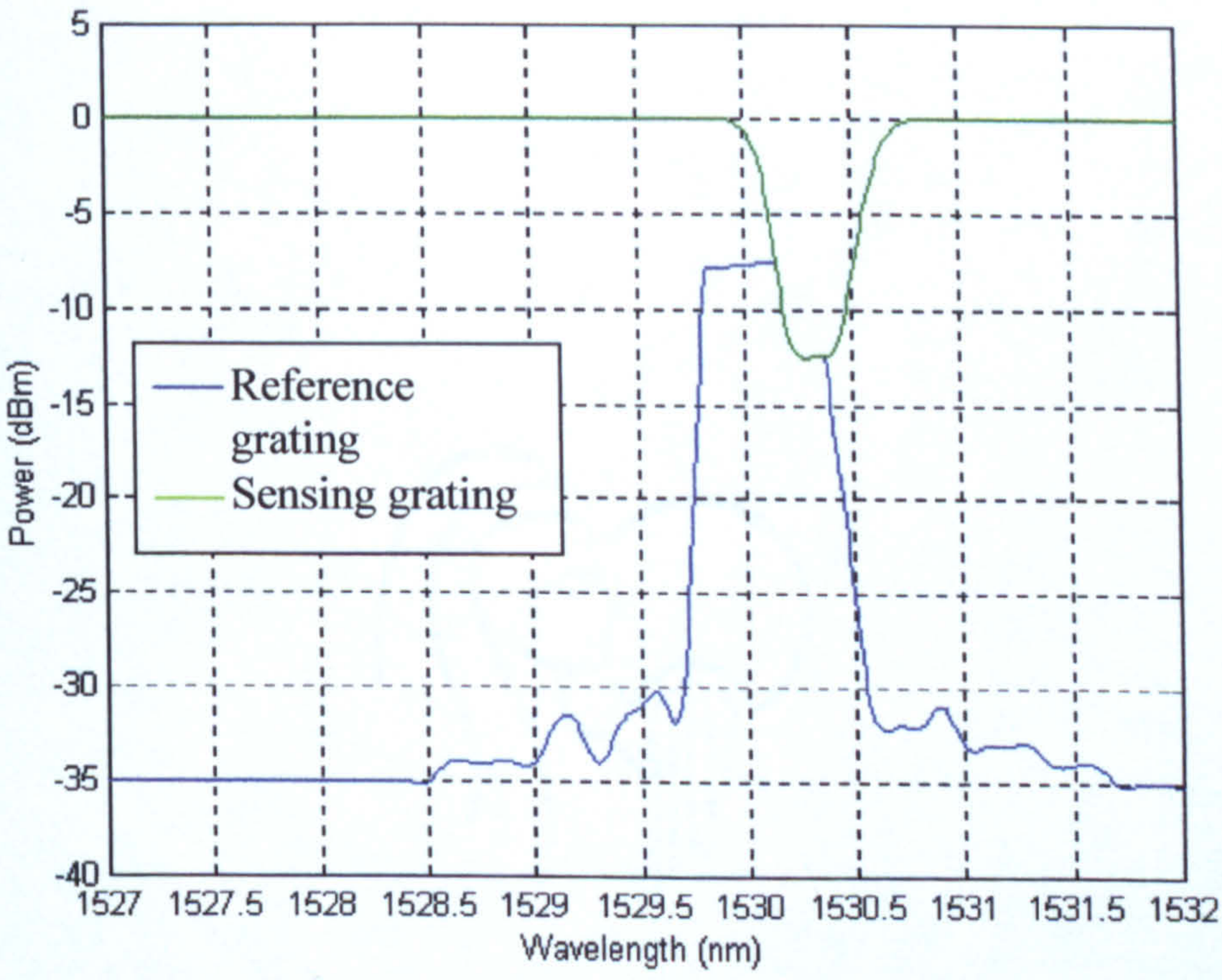

Figure 4.20.: *Signal results with no wavelength change.*

It was then possible to calculate the optical power coming out the sensing grating by integrating the new signal spectrum.

```
%OPTICAL POWER CALCULATION

%at 4

tAR40=10.^(tAR4/10);

area4 = trapz(hLS,tAR40);

Power4=10*log10(area4);
```

Power 4 is the optical power after the grating.

%at 5 Out the optical system.

Power5=Power4-(0.18) End connector loss

By shifting the wavelengths of the transmitted spectrum from the sensing grating, it was possible to simulate the temperature changes. As the temperature increased, the centre wavelength of the sensing grating increased, therefore the top spectrum in figure 4.21. moved to the right and the output power (area under the bottom spectrum) increased.

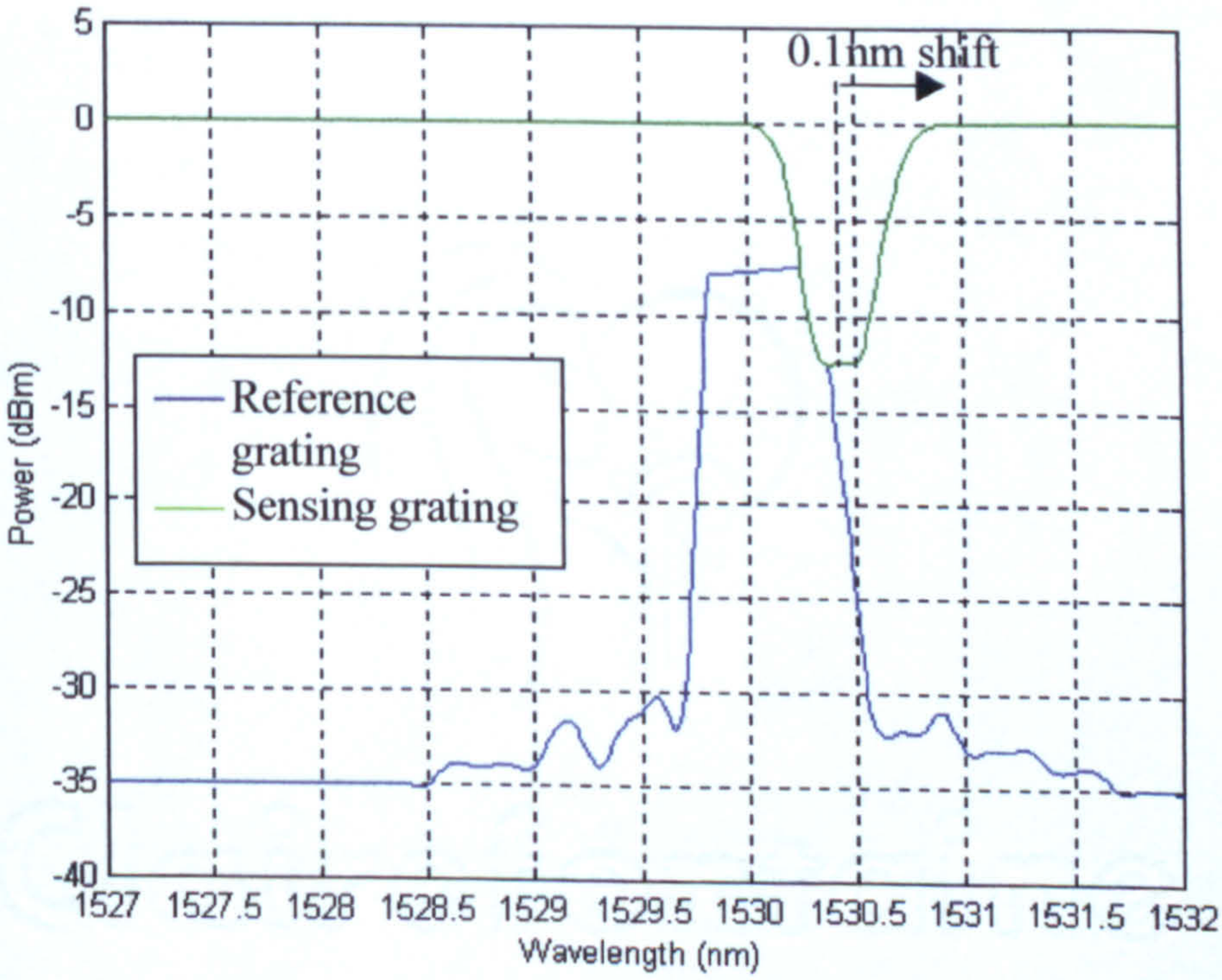

Figure 4.21.: *Signal results with a 0.1nm wavelength shift.*

Then by knowing the sensitivity of the sensing grating, it was possible to relate the change in temperature measured to a change in intensity.

Note:

The lower trace in figure 4.21. is the spectrum received at the output photodetector (figure 3.11.).

These calculations were used to select the right photodetectors and also for calibration purpose.

Test and calculations also displayed a maximum deviation from linearity of –0.0215dBm between –0.1nm and 0.15nm (corresponding to 1530.2nm to 1530.45nm) between the output power and the wavelength shift as illustrated on figure 4.22..

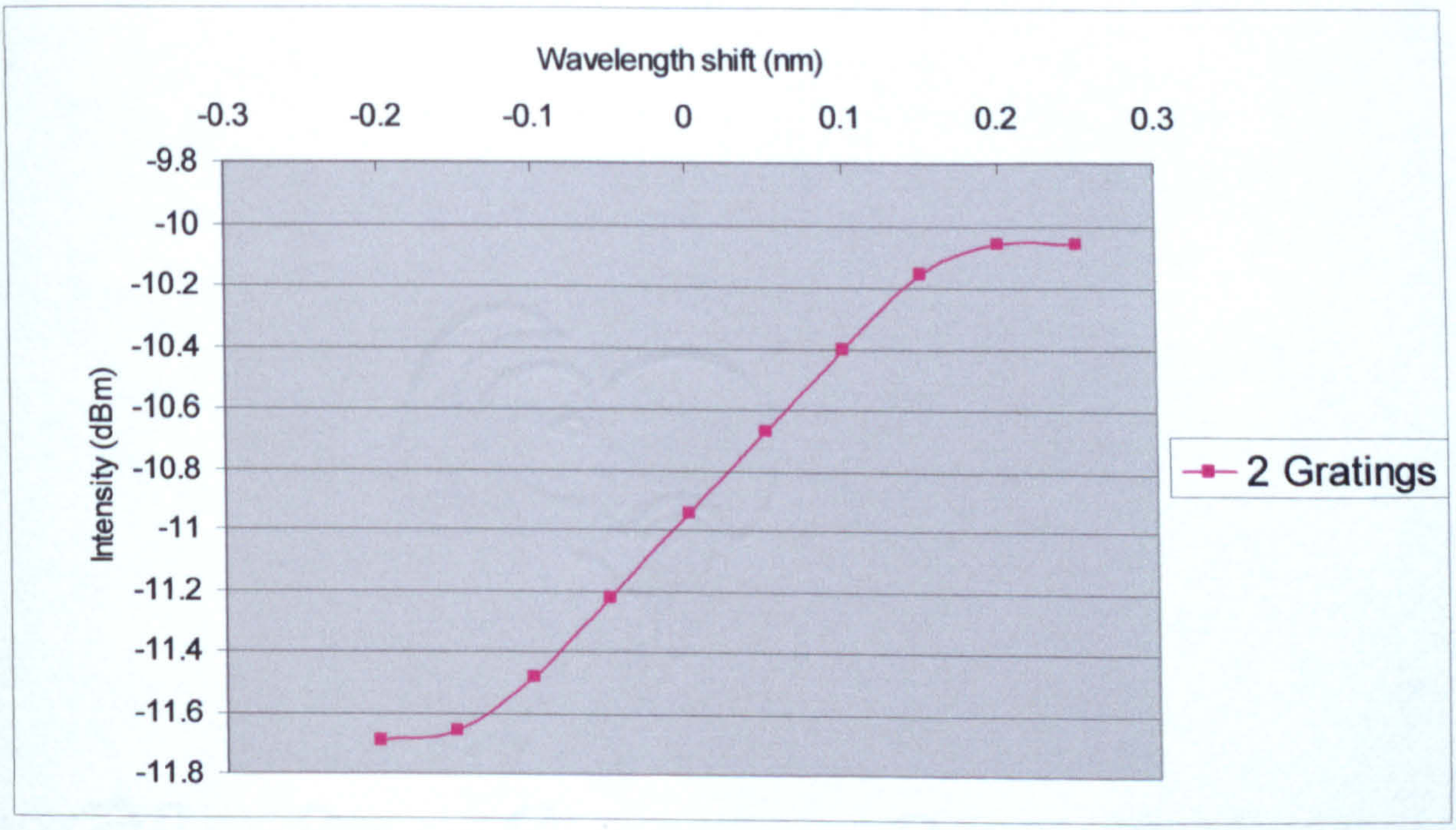

Figure 4.22.: *Two grating system response spectrum. Zero wavelength shift corresponds to 1530.3nm.*

The response spectrum of the two grating technique shows a linear response of the sensor. Therefore that sensor is easy to calibrate since the temperature change varies linearly with the intensity change over its operating range.

The same principle was used to determine the power out of the optical system for the DWDM technique. Giving the output spectrum illustrated in figure 4.23..

Tests showed that for temperature greater than 74.5°C, the sensing grating did not have any affect on the output signal. This output signal was calculated (-10.06dBm) and the same conditions were experimentally created and the maximum output power was measured (-10.13dBm). This slight difference (0.07dBm) between experimental results and calculation can be explained by losses due to fibre bending and other experimental problems.

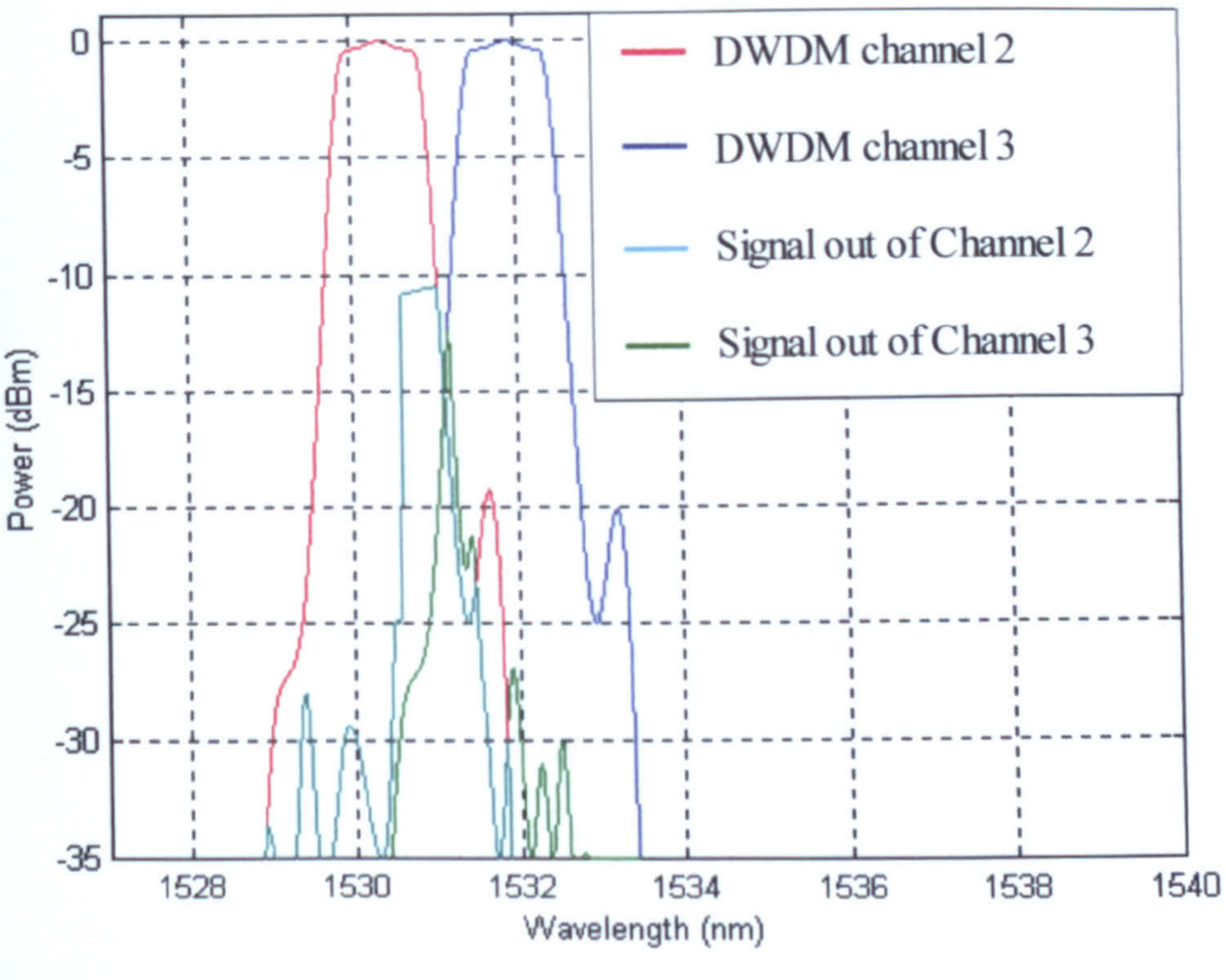

Figure 4.23.: *DWDM signal prediction spectrums.*

The DWDM simulation was mainly developed for calibration purpose and the result is shown in figure 4.24..

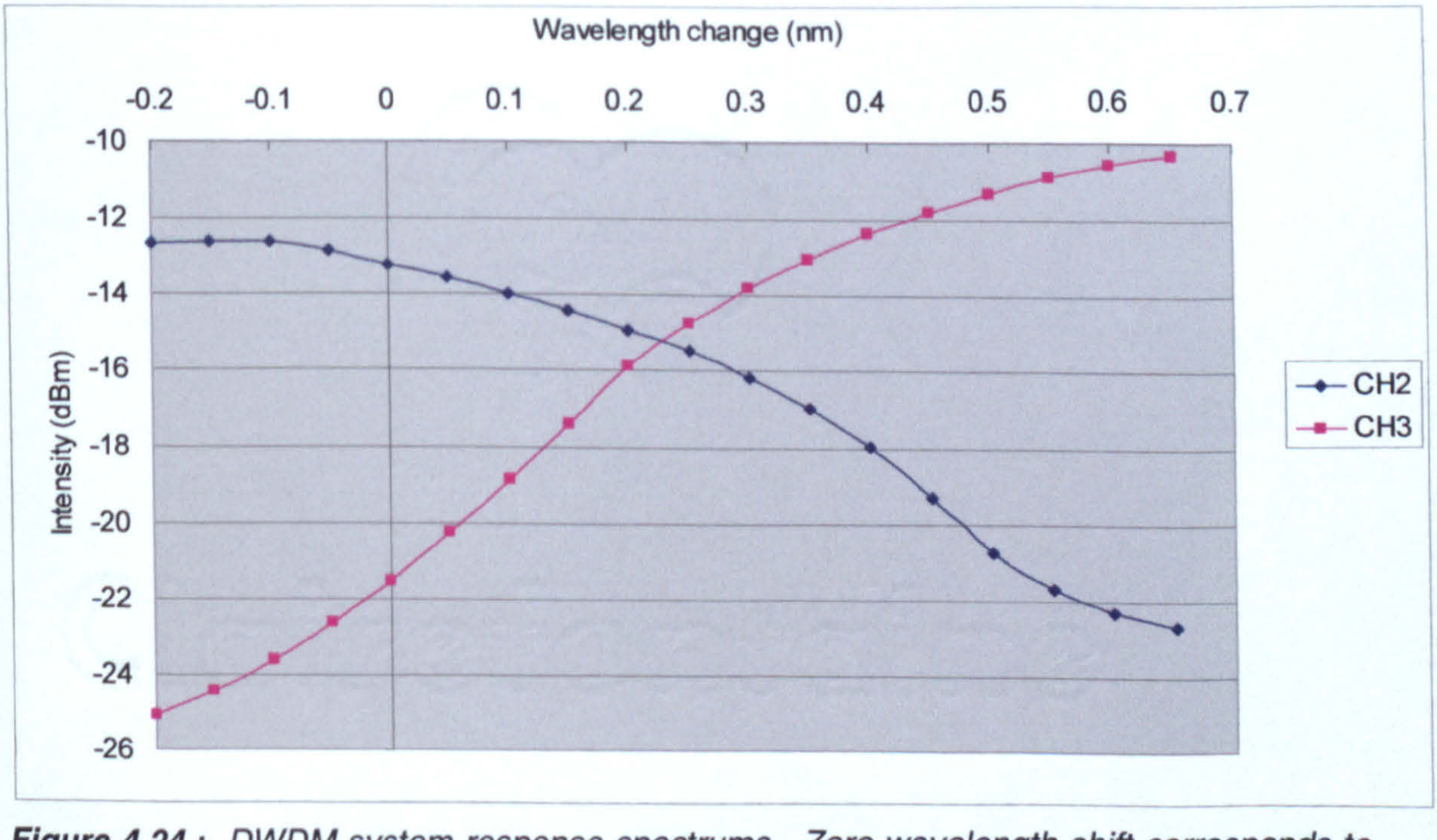

Figure 4.24.: *DWDM system response spectrums. Zero wavelength shift corresponds to 1530.8nm.*

As the DWDM system does not vary linearly when a temperature is induced, this spectrum can be used to calibrate the sensor. In other words, when intensity is recorded on the output, this spectrum allows relating that intensity to a wavelength or a wavelength change.

4.7.3. Alternative calibration technique.

Another, more experimental, way to calibrate the sensor was by using a tuneable grating. By varying the tuneable grating over a 10nm range and recording the output intensity changes, it was possible to accurately relate intensity change to wavelength changes. This principle was applied to developing the following spectrometer (figure 4.25.).

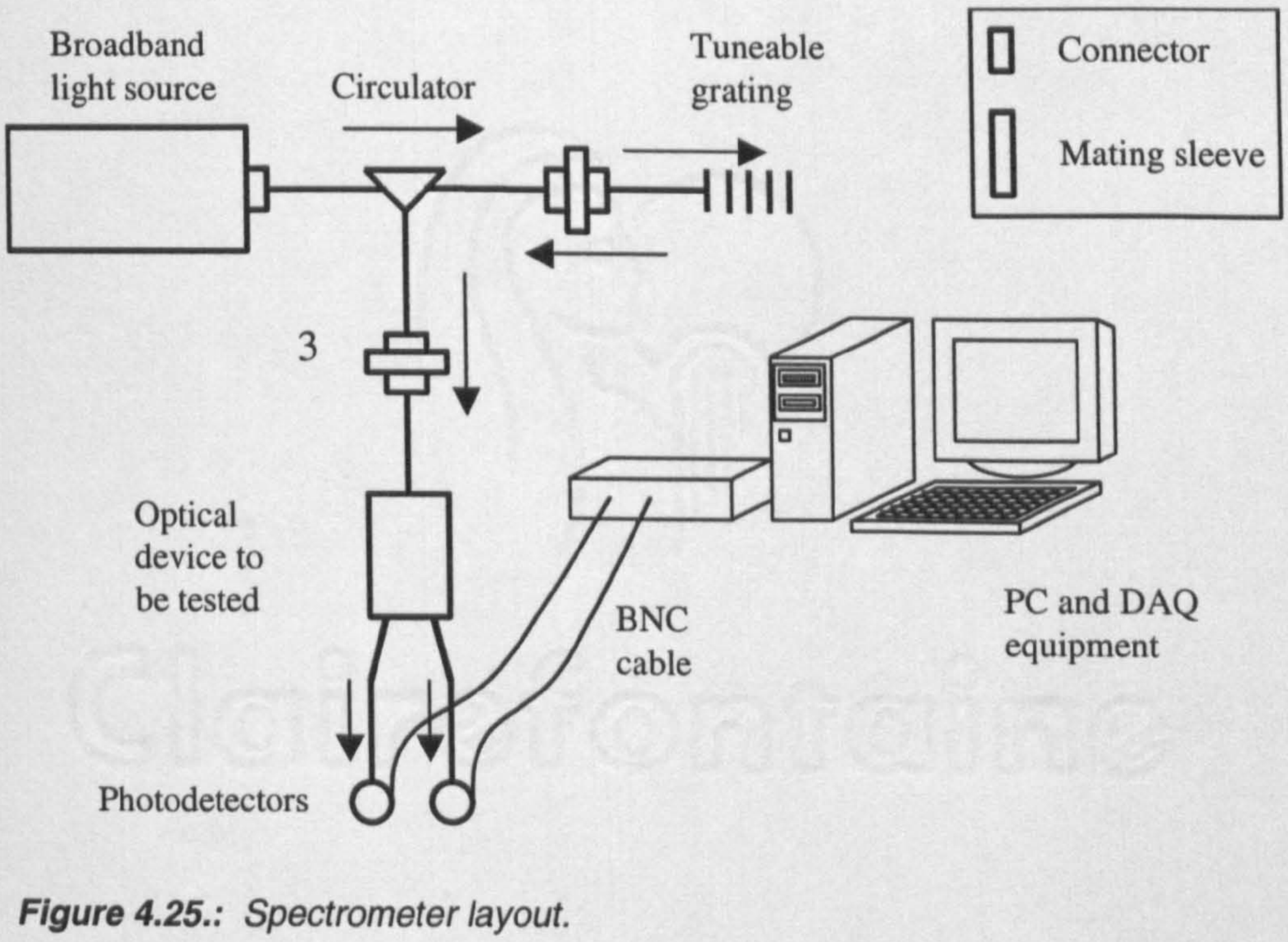

Figure 4.25.: *Spectrometer layout.*

The tuneable grating was selected so that its bandwidth and reflectivity matched the sensing grating. By using the set-up presented in figure 4.25., it was possible to plot the spectra of all the optical devices including the gratings.

Once the spectrum of the grating was plotted, it was possible to search for the minimum value to check the position of the peak and to compare the result to the value given by the manufacturer (1530.176nm). The spectrometer result gave a peak wavelength of 1530.176nm (figure 4.26.). The very good accuracy of the result is understandable since the tuneable grating offers a tuning accuracy of approximately 0.005nm and the sampling frequency used for data acquisition was relatively high (333Hz) in comparison to the speed of the tuning (18steps per second).

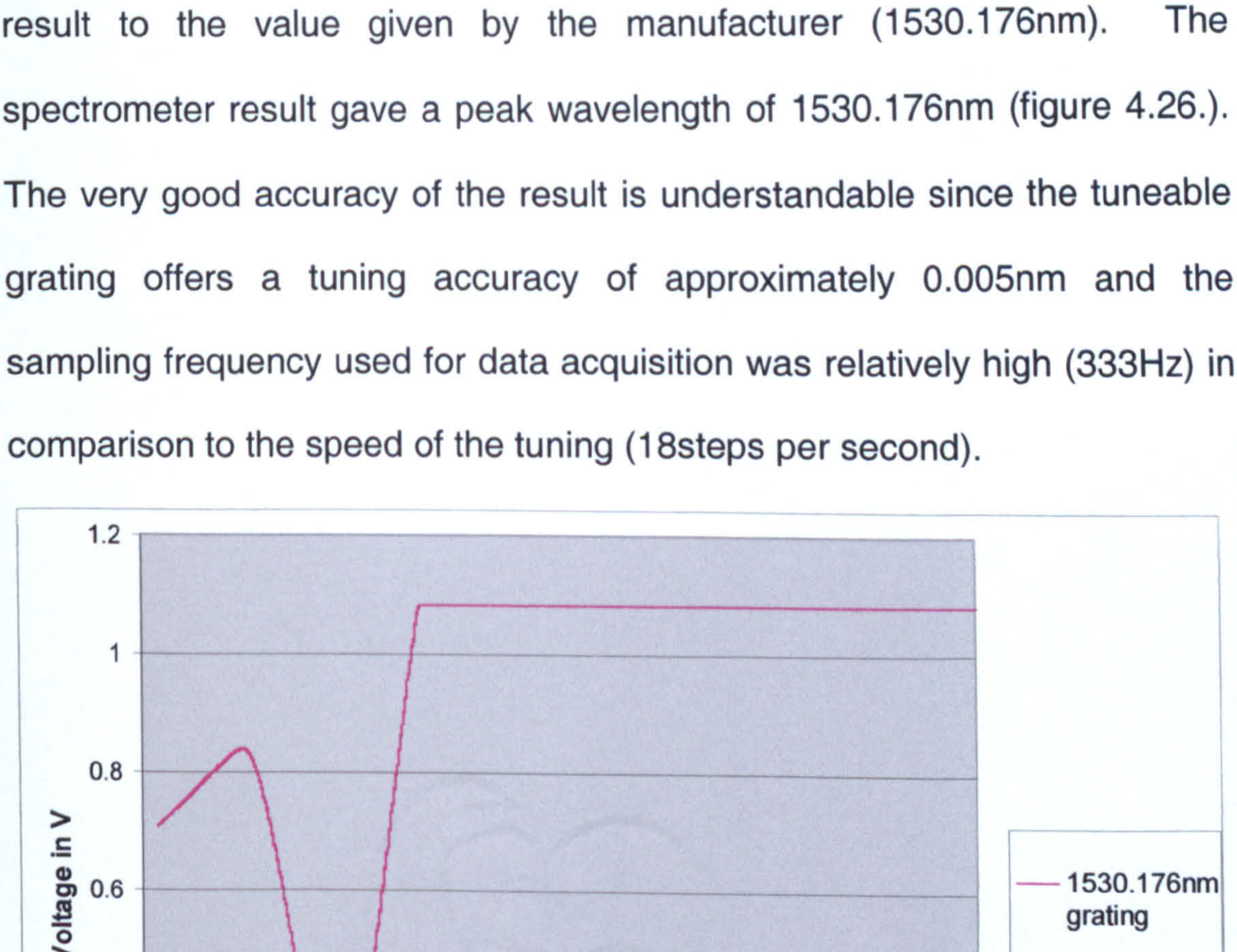

Figure 4.26.: *Grating at 1530.176nm.*

Similar tests were undertaken to test different equipment such as DWDM, WDM and coupler. These results are shown in figure 4.27., 4.28. and 4.29..

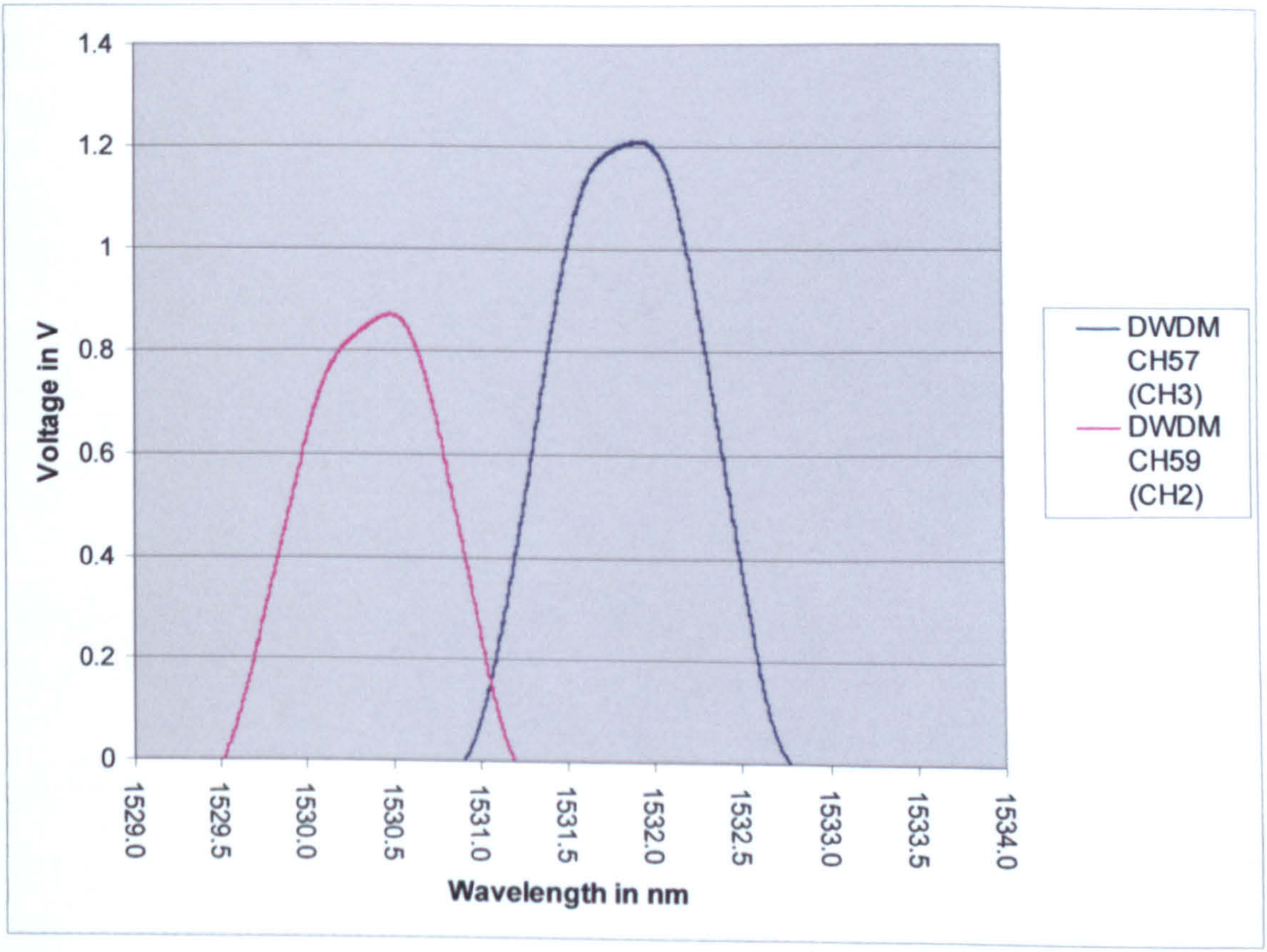

Figure 4.27.: *DWDM CH57 and CH59 spectra.*

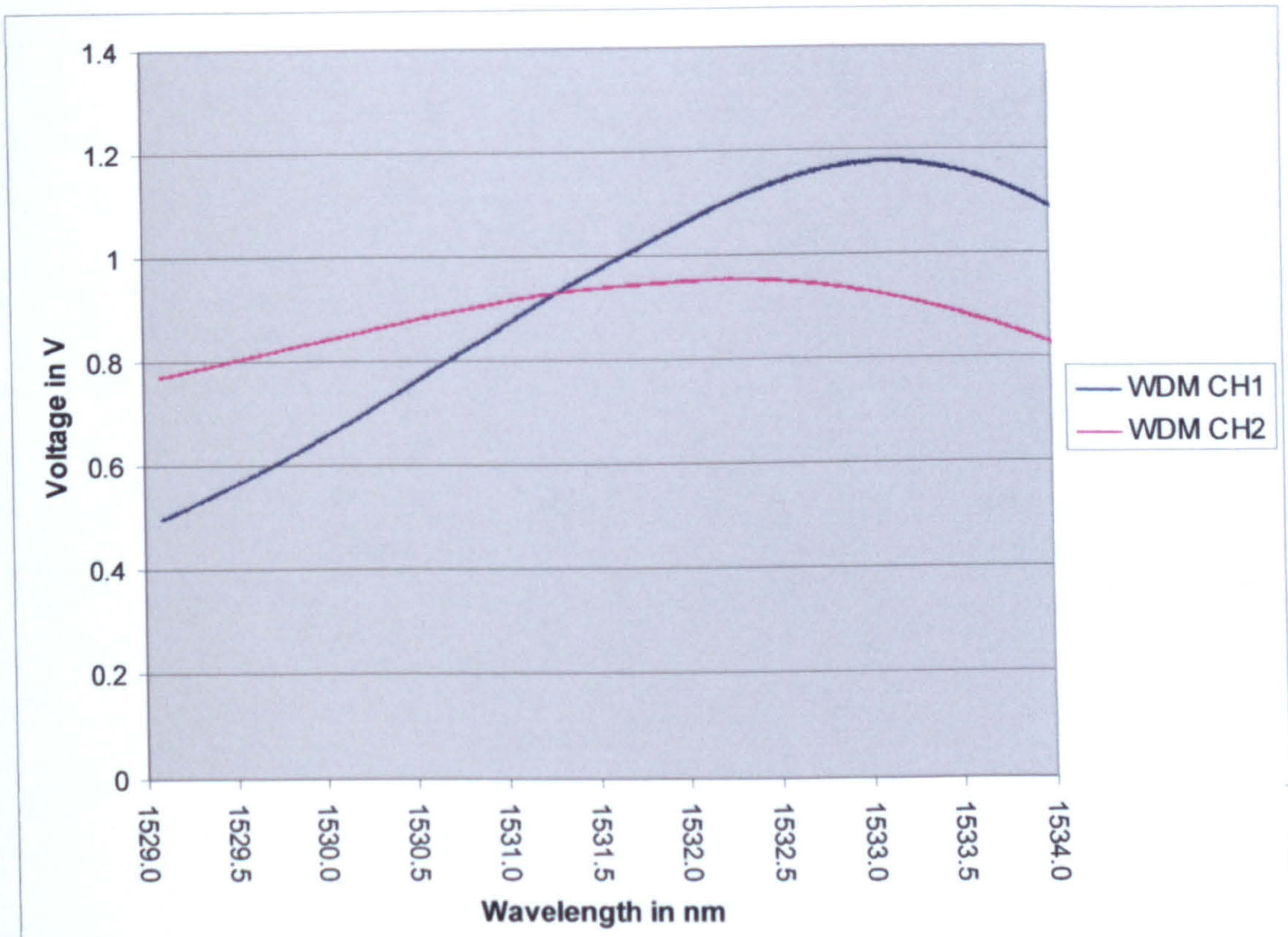

Figure 4.28.: *WDM channels spectrum.*

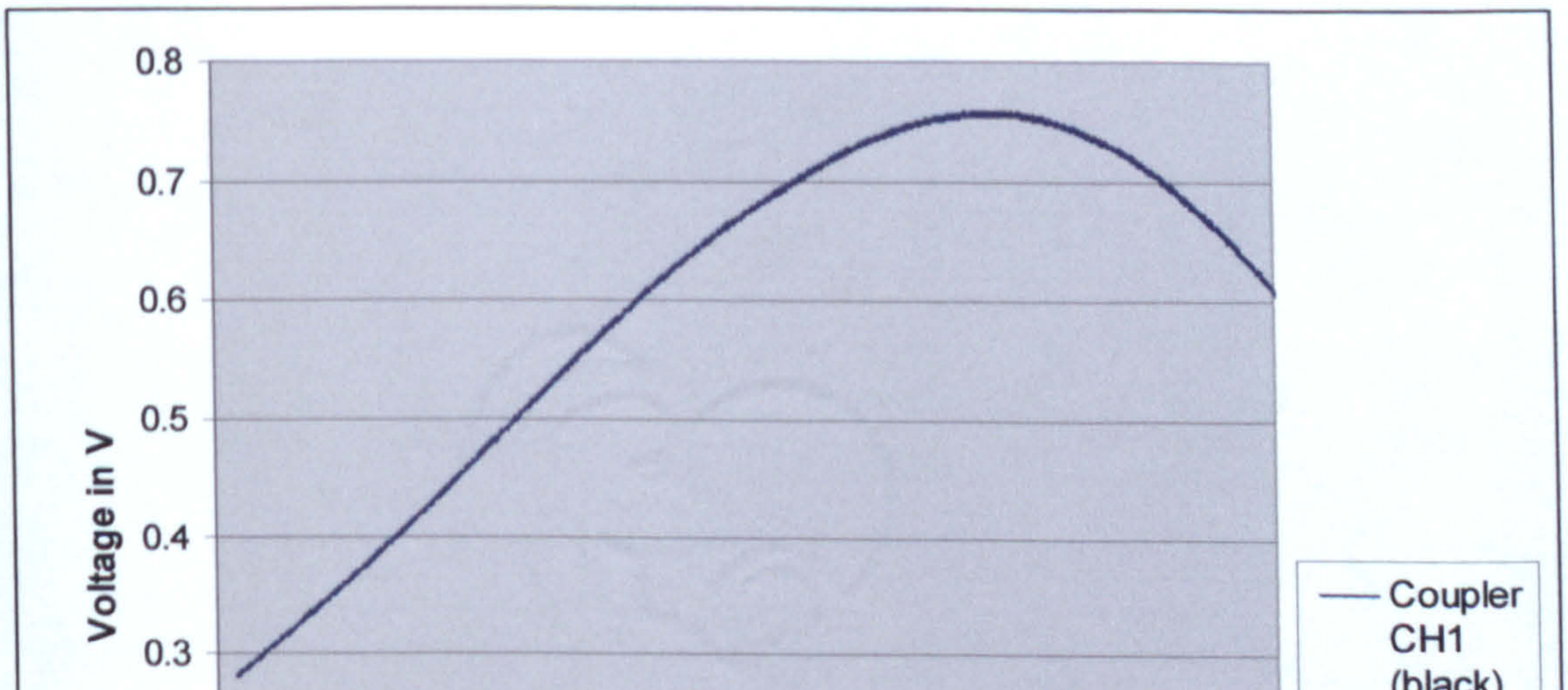

Figure 4.29.: *Coupler channel spectrum.*

These spectra were very useful because they allowed relating a wavelength change (or temperature change) to an output voltage change which corresponds to the transmitted intensity and they also allowed for checking of the manufacturer's data. The DWDM channels were centred as specified (CH59 at 1530.37nm and CH57 at 1531.92nm).

For the WDM device, the only way to position the spectrum was to check the intersection of both branches data during an experiment (chapter 6, figure 6.42.), once that intersection found, it was possible to determine at which temperature it occurred by reading it on the thermocouple data. That temperature (51.9°C) was then related to wavelength by knowing the sensitivity of the grating (11.8pm/°C). Doing so, it was possible to move the spectrum of the WDM until the channel intersection matched the wavelength of 1531.41nm determined by experiment.

This intersection technique could also be used for the DWDM technique. The intersection for the DWDM occurred at 26.78°C during the experiments (chapter 6, figure 6.38.) and 1531.0675nm for the spectroscopy (26.75°C). The intersection for the WDM occurred at 49.7°C during the experiments (chapter 6, figure 6.42.) and 1531.2968nm for the spectroscopy (49.68°C). This spectrometer allowed relating the reading during calibration directly to a temperature reading.

4.7.4. Photodetector selection.

The spectral range of the detector has to include the wavelength range discussed in the BLS selection chapter. The DET410 by Thorlabs was selected for its low price and high performance. It detects a minimum luminosity of 50μW (that is smaller than the minimal sensing signal arriving on it (58μW with safety factor of –1dB)) and a spectral range between 800 and 1800nm with a maximum and stable responsivity of 1A/W between 1500nm and 1800nm.

The detector responsivity, $\Re(\lambda)$, can be obtained from curves shown in figure 4.30. below to estimate the amount of photocurrent to expect for a given input signal. The optical power arriving at the photodetector, P_o, is then converted into a voltage. This is accomplished by adding an external load resistance, R_{LOAD}. The output voltage is derived simply from Ohm's law:

$$V_0 = P_o \times \Re(\lambda) \times R_{LOAD} \tag{4}$$

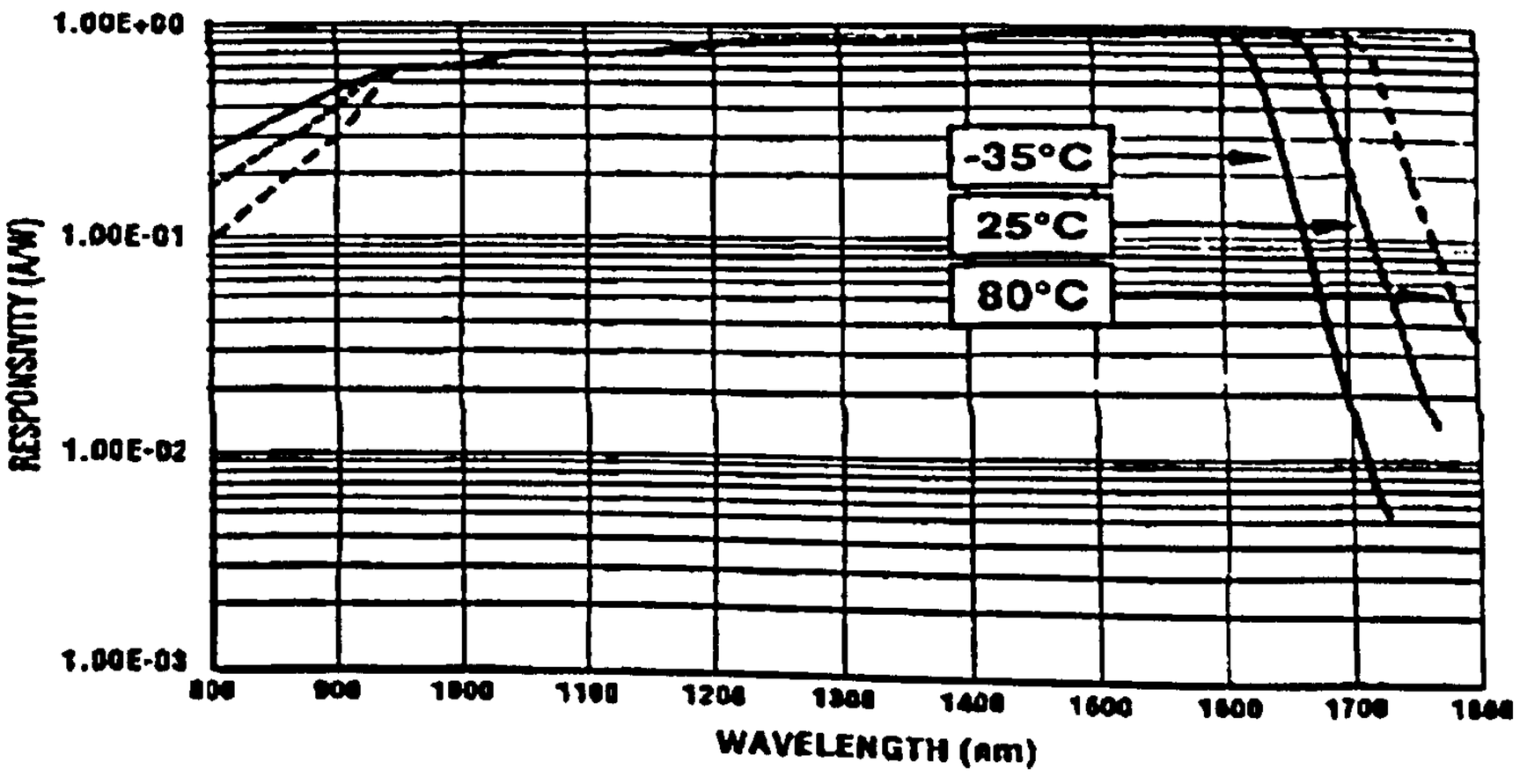

Figure 4.30.: *Photodetector responsivity versus wavelength [3].*

From the spectrum above and at the wavelength of interest (1530nm region), $\Re(\lambda) = 1$ therefore the output voltage and the intensity detected by the photodetector can be simplified as follow:

$$V_0 = P_o \times R_{LOAD} \tag{5}$$

- **Determination of R_{LOAD}.**

For maximum bandwidth, the manufacturer recommends to use a 50Ω coaxial cable with a 50Ω terminating resistor at its end. But for this temperature measurement system bandwidth is not important, the output voltage is more important. The output voltage can be increased for a given input illumination level by increasing the load resistance, R_{LOAD} up to a maximum of 10kΩ. A resistance of 10kΩ will provide the best signal/noise ratio and gives the following expression for the output voltage:

$$V_0 = P_o \times 10000 \tag{6}$$

That above expression can then be used to relate the voltage emitted from the photodetector, to the optical power arriving at the photodetector the optical power in W.

The speed of response of the DET410 under these conditions can be calculated as followed: the detector response is characterized by the rise time. It is defined as "the time difference between the points at which the detector has reached 10% of its peak output and the point at which it has

reached 90% of its peak response, when it is irradiated by a step change or relatively long pulse of light".

The rise time response, T_R, and the bandwidth, f_{BW}, are functions of the load resistance and the diode capacitance, C_J = 22pF for the DET410.

$$f_{BW} = \frac{1}{2\pi \times R_{LOAD} \times C_J} \quad (7)$$

and $T_R = \frac{0.35}{f_{BW}} = 4.83 \times 10^{-7}\, s$ equivalent to a bandwidth of $2.06 MHz$ (8)

Note:

Using the spectrometer system described above, it was possible to determine the insertion loss of some optical devices as follows.

By connecting a photodetector at (3) then recording the voltage output, and knowing the relation between voltage output and optical intensity input of a photodetector (chapter 4.7. equation (6)), it was possible to determine the optical power at (3). Then it was possible to insert any optical device at (3) and by doing the same recording (by tuning the grating so its spectrum does match the optical device spectrum at all), it was possible to determine accurately the insertion loss of the grating used for the sensing in the two grating technique. The voltage output at (3) was 0.564V (being the reference insertion loss: 0dB), when the grating is inserted the voltage output is 0.525V giving a difference of 0.039V (insertion loss of 54dB).

4.8. Data Acquisition card selection.

The Data Acquisition card was selected using the following criteria:

Price and Speed: The price of the thermocouple and equipment used to measure temperature in the same condition is reasonably low but the setting up time of the all system makes it quite expensive in labour time. The price of the optical system should be kept as low as possible since the setting up time is small and inexpensive. 2MHz cards are very expensive (a factor of six times more expensive than a 200kHz card) and such a speed is not necessary for our experiments therefore a 200KHz card was considered as "fast enough" for this type of experiment.

Number of channels input: The card should have more than five channels input: three for the thermocouples and two for the photodetectors, this will allow direct comparison of the optical systems and the thermocouple.

Resolution: The resolution is the main factor for this data acquisition application since it will determine the accuracy of the results. A resolution of 16bits was proven to give an extremely accurate representation of the actual signal [4]. Such a resolution was selected for this application.

Compatibility: Compatibility with Labview for programming virtual instruments for reading and recording data or other data acquisition

software (such as DASwizard for direct input to an Excel spreadsheet) is necessary for the acquisition and analysis of the readings.

Considering all those factors, the DAS1602/16 from Computerboards was selected.

4.9. Conclusion.

The equipment was selected for its low price and compatibility (capacity to use the same equipment in different optical systems). Once the equipment was correctly selected, it was necessary for the author to test it and to familiarize with it using a simple optical power meter. DAQ card was installed and programs were written for data acquisition and display purpose. After the tests, the optical sensing systems were built and tested in laboratory.

References.

1. Rao Y J, "In-fibre Bragg grating sensors", Meas. Sci. Technol.8, p 355-375, 1997.

2. "O-Net ASE source. User's Manual", O-Net communications (SZ) limited.

3. Thorlabs Inc., "High-speed InGaAs detector – DET410", datasheet, http://www.thorlabs.com/Thorcat/2100/2181-S01.pdf.

4. National Instruments, "Labview: Data acquisition basics manual", Part Number 320997E-01, http://www.engr.sjsu.edu/bjfurman/courses/ME120/me120pdf/DAQbasics.pdf, 2000.

Chapter 5: Heat transfer modelling: theory and tests.

5. Heat transfer modelling: theory and tests.

During a machining process, most of the energy required for material removal is transformed into heat due to the friction between the tool and the workpiece. Some of the energy is transmitted to the tool and the rest of the energy will be dissipated either by the chip or by diffusion into the workpiece [1]. Since the sensing fibre grating was not to be destroyed while measuring the temperature during the machining process, it was required that the sensing fibre and a K-type thermocouple were fitted inside the workpiece. This made the determination of the surface temperature difficult, because during the machining, the temperature inside the workpiece is different from the temperature at the machined surface. It was therefore necessary to relate the temperature inside the workpiece to the temperature at the machined surface. This was investigated theoretically and machining tests using thermocouples, were undertaken to check the theoretical results and to determine the optimal positioning of the sensing grating.

5.1. Theory.

5.1.1. Transient heat transfer.

When a solid is suddenly subject to a change in external temperature, it heats up or cools down gradually until an equilibrium temperature is reached. A typical example is cooling down of a hot metal block in a limited amount of cold water, the metal block cools down and the water heats up until they both reach the same temperature. The equilibrium condition is referred as a steady-state condition. Before the solid reaches that steady-state condition, unsteady-state conduction also known as transient conduction takes place. This transient conduction problem, in one dimension, is defined by the following differential equation:

$$\frac{\partial^2 T}{\partial y^2} = \frac{1}{\alpha}\frac{\partial T}{\partial t} \qquad (1)$$

With T, the temperature in $°C$, y, a distance in m, α, the thermal diffusivity in m^2/s and t, the time in s.

Note:

The thermal diffusivity, α, is defined by the following relation:

$$\alpha = \frac{k}{\rho c} \qquad (2)$$

with: k, the thermal conductivity in $W/m.°C$, ρ, the density in kg/m^3 and c, the specific heat capacity in $J/kg.°C$.

During machining the workpiece is fixed to the machine tool and they both reach a steady state temperature T_i, which is also, in normal conditions, the ambient temperature. Therefore, it is possible to consider the workpiece as a semi-infinite solid. The cutting tool can also be considered as a moving heat source since the cutting process generates heat. It is possible to solve the temperature field if the problem is reduced to 1D.

At an instant *t*, the heat flux is $\frac{q_0}{A}$ with q_0, the heat transfer rate in *kJ/s* and

A, the area of contact in m^2.

And the initial and boundary conditions are:

$$T(x,0) = T_i \tag{3}$$

and

$$\frac{q_0}{A} = -k\frac{\partial T}{\partial y}\Bigg]_{x=0} \quad \text{for} \quad t > 0 \tag{4}$$

And the solution can be shown to be [2]:

$$T - T_i = \frac{2q_0\sqrt{\alpha\frac{t}{\pi}}}{kA}\exp\left(\frac{-y^2}{4\alpha t}\right) - \frac{q_0 y}{kA}\left(1 - erf\,\frac{y}{2\sqrt{\alpha t}}\right) \tag{5}$$

An analytical solution of a transient heat transfer equation is hard to achieve. Many factors such as the geometry of the solid subjected to the heat source, the nature of the heat source and the boundary conditions make it difficult to accurately predict the temperature field within a real workpiece. An alternative approach to solve this transient heat transfer problem is to use a numerical solution.

The problem of calculating the surface temperatures on the basis of measured sub-surface temperatures is even more complex. For all but the simplest geometries, the most effective method is to use a numerical method. The easiest numerical method to apply to this machining case is the finite difference technique.

5.1.2. Numerical method.

The backward difference numerical method can be easily applied to solids under transient heat-flow conditions for the solution of temperature fields. Since the temperatures were monitored inside the workpiece, it was necessary to "work back" to the surface, calculating the surface temperature on the basis of the measured subsurface temperatures. To apply a numerical method such as the finite difference technique, it is required that the solution domain is broken down into a series of points at which the temperature is known or is to be determined. Figure 5.1. illustrates the temperature at three subsurface "nodes" and the nomenclature used. Each of the differentials in equation (4) can then be replaced by "backward finite difference".

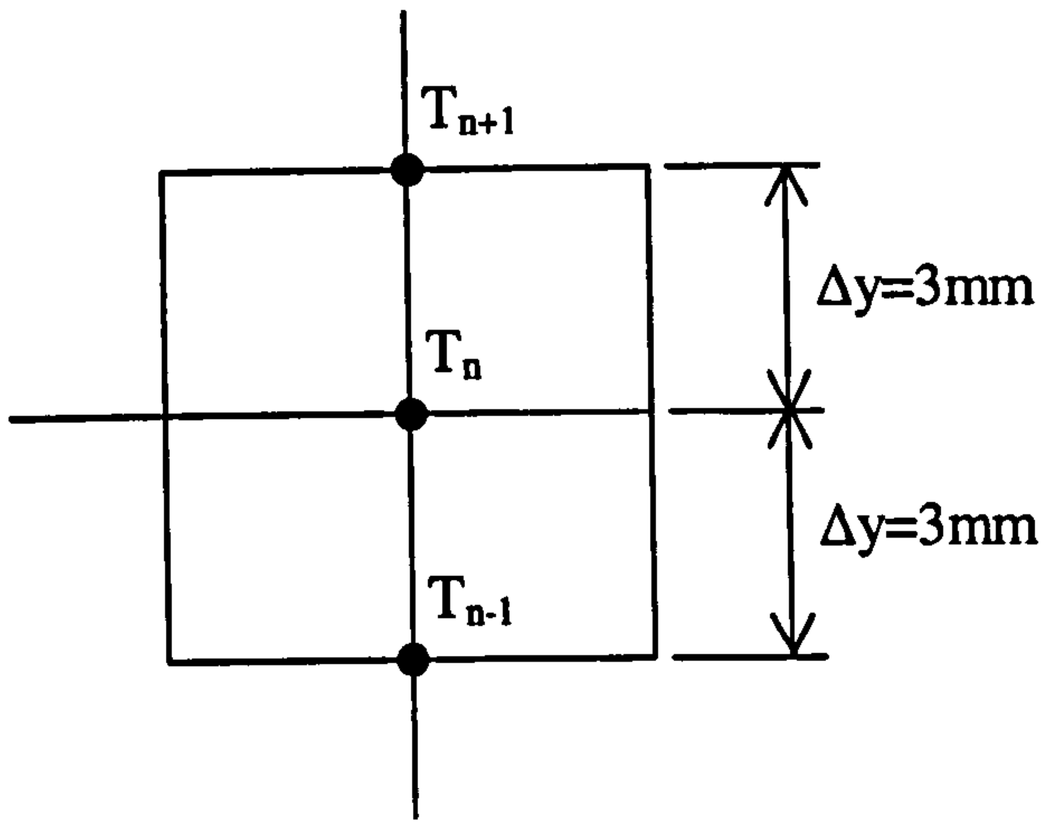

Figure 5.1: *Nomenclature for finite difference numerical method.*

The backward difference technique allows the writing of nodal temperatures T_n^{p+1} explicitly in terms of the previous nodal temperatures T_n^p with: *p*, the instant and *n*, the position. By working backward by one time increment at the time, it is possible to determine the previous temperature distribution at the desired state or position as follows:

$$\frac{\dfrac{T_{n+1}^{p+1}-T_n^{p+1}}{\Delta y}-\dfrac{T_n^{p+1}-T_{n-1}^{p+1}}{\Delta y}}{\Delta y}=\frac{1}{\alpha}\frac{\left(T_n^{p+1}-T_n^{p}\right)}{\Delta t} \tag{6}$$

$$\frac{T_{n+1}^{p+1}-2T_n^{p+1}+T_{n-1}^{p+1}}{(\Delta y)^2}=\frac{1}{\alpha}\frac{\left(T_n^{p+1}-T_n^{p}\right)}{\Delta t} \tag{7}$$

$$T_{n+1}^{p+1}=2T_n^{p+1}-T_{n-1}^{p+1}+\frac{(\Delta y)^2}{\alpha}\frac{\left(T_n^{p+1}-T_n^{p}\right)}{\Delta t} \tag{8}$$

Equation (8) can be used to calculate the temperature at node T_{n+1} on the basis of the temperatures measured at nodes T_n and T_{n-1}.

Then the properties [2] of the alumium` (Al-Mg-Si) used for the workpiece, the values of *k*, the thermal conductivity (177*W/m.°C*), ρ, the density ($2707\,kg/m^3$) and *c*, the specific heat (892*J/kg. °C*), can be used in (2) to find the thermal diffusivity, α.

$$\alpha = \frac{k}{\rho c} = \frac{177}{2707 \times 892} = 73.3 \times 10^{-6} m^2 / s$$

and knowing that $\Delta y = 3 \times 10^{-3} m$ (see figure 5.1.), (8) becomes:

$$T_{n+1}^{p+1} = \left(2T_n^{p+1} - T_{n-1}^{p+1}\right) + \frac{9}{73} \underbrace{\frac{\left(T_n^{p+1} - T_n^{p}\right)}{\Delta t}}_{\text{Temperature gradient of middle sensor/point}} \qquad (9)$$

An implicit finite difference scheme is unconditionally stable. Equation (9) allows the calculation of temperature T_{n+1}^{p+1} on the basis of the temperatures measured at the other nodal positions.

5.2. Experiments.

A series of experiments were undertaken to check the backward difference theory and the ability to calculate the surface temperature on the basis of sub-surface temperature measurement. Three thermocouples were used and the temperature measured at the third (closest to the surface) was predicted based on the temperature measured by the other two. The calculations were undertaken using Microsoft Excel.

5.2.1. Equipment setup.

K-type thermocouples were selected because they offer a wide temperature range (-200°C up to 1100°C); also their e.m.f. (ElectroMotive Force)/temperature curve is reasonably linear and they offer a sensitivity of

41μV/°C [3]. The thermocouple signal was then amplified using an amplification system built by the author. Using an AD595 Monolithic Thermocouple Amplifier with cold junction compensation, the signal of the thermocouple was amplified to approximately 10mV/°C, which gave more sensitive results and helped to reduce the effect of electrical noise on the thermocouple signal.

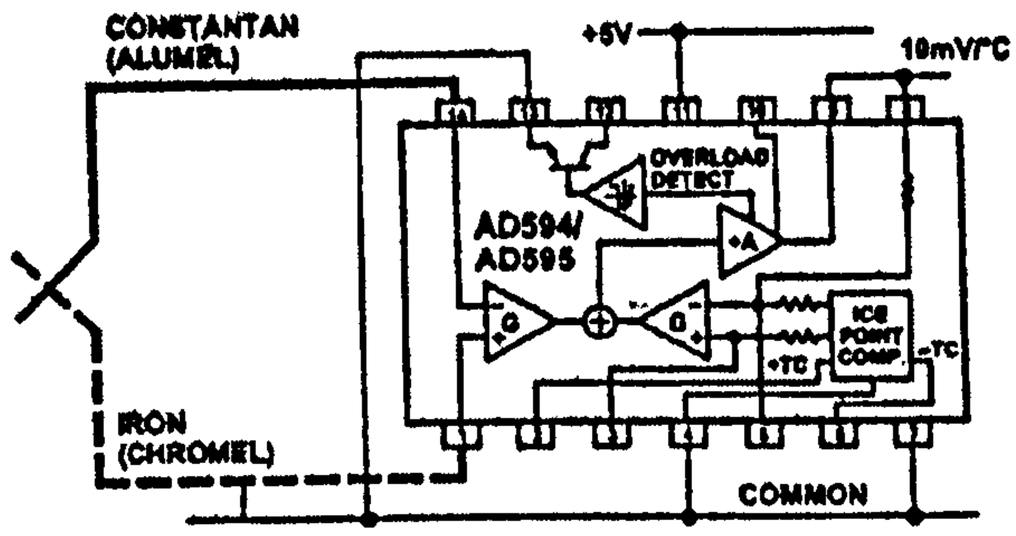

Figure 5.2.: *AD595 Basic connection, single supply operation. [3]*

A three-channel thermocouple amplifier was built. Each amplifier output was connected to a channel of the PCI data acquisition card and the voltages were measured using a DAQ software. Using the linear properties of the AD595 with a K-type thermocouple (10mV/°C), it was possible to have a real time temperature display by programming an Excel spreadsheet. The thermocouples were calibrated using ice and water (0°C) and boiling water (100°C).

Table I. Output Voltage vs. Thermocouple Temperature (Ambient +25°C, V_S = -5 V, +15 V)

Thermocouple Temperature °C	Type J Voltage mV	AD594 Output mV	Type K Voltage mV	AD595 Output mV
-200	-7.890	-1523	-5.891	-1454
-180	-7.402	-1428	-5.550	-1370
-160	-6.821	-1316	-5.141	-1269
-140	-6.159	-1188	-4.669	-1152
-120	-5.426	-1046	-4.138	-1021
-100	-4.632	-893	-3.553	-876
-80	-3.785	-729	-2.920	-719
-60	-2.892	-556	-2.243	-552
-40	-1.960	-376	-1.527	-375
-20	-.995	-189	-.777	-189
-10	-.501	-94	-.392	-94
0	0	3.1	0	2.7
10	.507	101	.397	101
20	1.019	200	.798	200
25	1.277	250	1.000	250
30	1.536	300	1.203	300
40	2.058	401	1.611	401
50	2.585	503	2.022	503
60	3.115	606	2.436	605
80	4.186	813	3.266	810
100	5.268	1022	4.095	1015
120	6.359	1235	4.919	1219
140	7.457	1445	5.733	1420
160	8.560	1659	6.539	1620
180	9.667	1873	7.338	1817
200	10.777	2087	8.137	2015
220	11.887	2302	8.938	2213
240	12.998	2517	9.745	2413
260	14.108	2732	10.560	2614
280	15.217	2946	11.381	2817
300	16.325	3160	12.207	3022
320	17.432	3374	13.039	3227
340	18.537	3588	13.874	3434
360	19.640	3801	14.712	3641
380	20.743	4015	15.552	3849
400	21.846	4228	16.395	4057
420	22.949	4441	17.241	4266
440	24.054	4655	18.088	4476
460	25.161	4869	18.938	4686
480	26.272	5084	19.788	4896

Thermocouple Temperature °C	Type J Voltage mV	AD594 Output mV	Type K Voltage mV	AD595 Output mV
500	27.388	5300	20.640	5107
520	28.511	5517	21.493	5318
540	29.642	5736	22.346	5529
560	30.782	5956	23.198	5740
580	31.933	6179	24.050	5950
600	33.096	6404	24.902	6161
620	34.273	6632	25.751	6371
640	35.464	6862	26.599	6581
660	36.671	7095	27.445	6790
680	37.893	7332	28.288	6998
700	39.130	7571	29.128	7206
720	40.382	7815	29.965	7413
740	41.647	8058	30.799	7619
750	42.283	8181	31.214	7722
760	-	-	31.629	7825
780	-	-	32.455	8029
800	-	-	33.277	8232
820	-	-	34.095	8434
840	-	-	34.909	8636
860	-	-	35.718	8836
880	-	-	36.524	9035
900	-	-	37.325	9233
920	-	-	38.122	9430
940	-	-	38.915	9626
960	-	-	39.703	9821
980	-	-	40.488	10015
1000	-	-	41.269	10209
1020	-	-	42.045	10400
1040	-	-	42.817	10591
1060	-	-	43.585	10781
1080	-	-	44.439	10970
1100	-	-	45.108	11158
1120	-	-	45.863	11345
1140	-	-	46.612	11530
1160	-	-	47.356	11714
1180	-	-	48.095	11897
1200	-	-	48.828	12078
1220	-	-	49.555	12258
1240	-	-	50.276	12436
1250	-	-	50.633	12524

Figure 5.3.: *AD595 temperature/voltage.*

5.2.2. Machining experiments.

Measurements of the subsurface temperature at different depths below the surface were undertaken during a standard milling process operated at high speed. Three thermocouples were embedded at three different depths (3, 6, 9mm from the machined surface). Before starting the milling process, it was necessary to determine the best cutting parameters.

Firstly the material of the block to be machined was identified: Aluminium alloy, Al-Mg-Si. Aluminium was selected for its high thermal conductivity

properties (177W/m.°C) and because it is widely used in the manufacturing industry. Knowing the material and that a slot machining process was to be used, it was possible to select a high-speed steel cutting tool. A standard milling cutter of 20mm in diameter (*D*) with two teeth was selected. Using the minimal number of cutting teeth will maximise the heat generated during the milling process, since a greater cutting force is required for each tooth to remove the same amount of material than would be required for a cutter with a higher number of teeth. The standard cutting parameters table was then used to determine the correct peripheral speed or surface speed. For the selected conditions, a peripheral speed *s* of 55m.min $^{-1}$ was found to be optimal. Once the peripheral speed was determined, it was possible to calculate the spindle speed using the following formula:

$$RPM = \frac{s \times 1000}{\pi \times D} = \frac{55 \times 1000}{\pi \times 20} \cong 876 rev.\min^{-1} \qquad (10)$$

The cutting parameter table for this cutter gave a feed rate per tooth *f* of 0.14mm/tooth. This parameter was then used to calculate the feed rate *F* necessary for an ideal slot milling process as followed:

$$F = f \times n \times RPM = 0.14 \times 2 \times 876 \cong 245 mm.\min^{-1} \qquad (11)$$

with *n*, the number of teeth of the cutter.

So for the selected cutter, the ideal cutting parameters were a spindle speed of 876rev.min^{-1} and a feed rate of 245mm.min^{-1}. Figure 5.4. illustrates the experiment parameters.

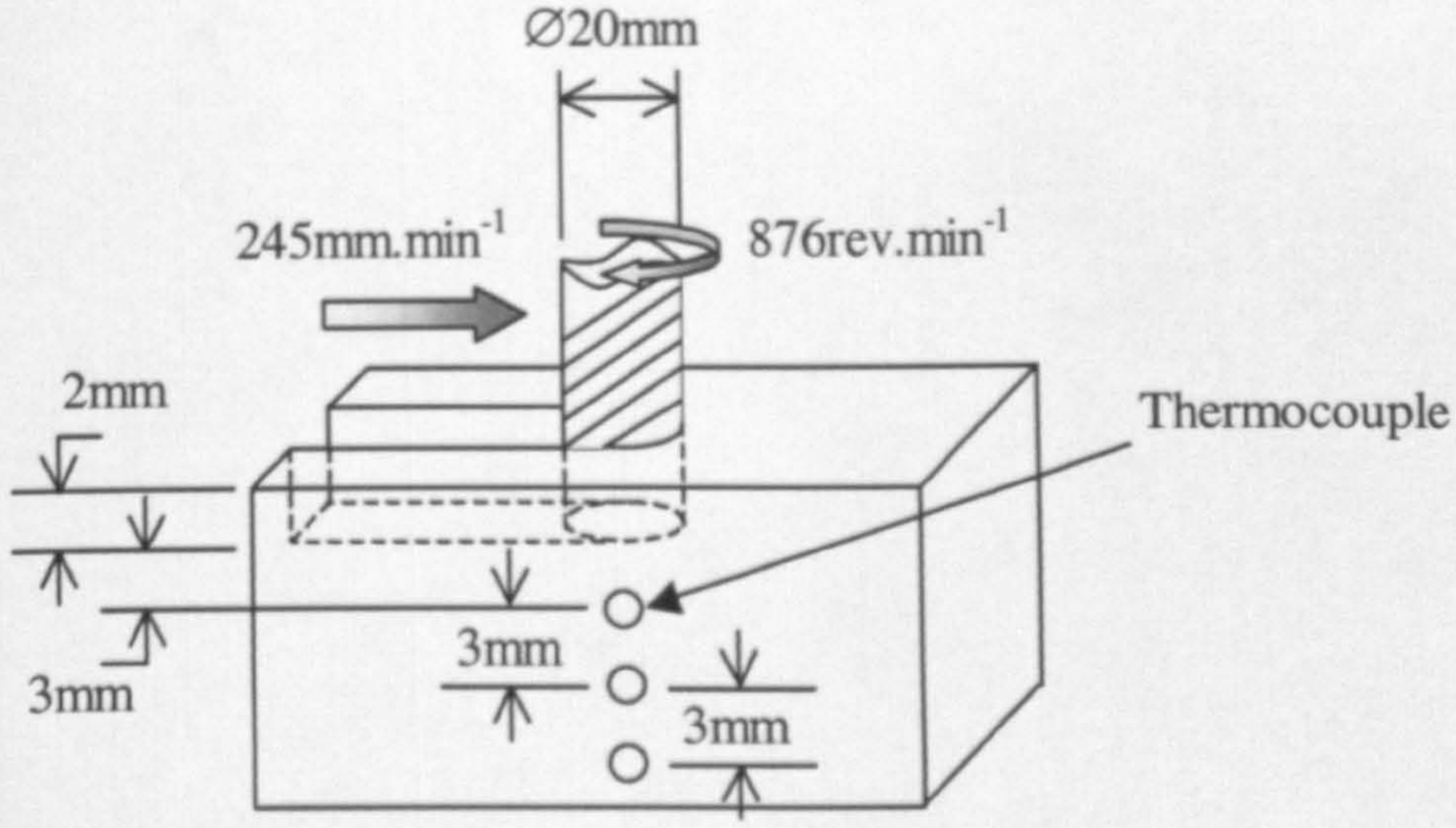

Figure 5.4.: *Diagrammatic representation of the slot milling process and the main controlling parameters.*

A series of milling tests were undertaken cutting 2mm at the time (2mm being, for this cutter, the maximum tool penetration possible without damage). During testing, the temperatures measured by the thermocouples were captured by the data acquisition card and the resulting data fed into a Microsoft Excel spreadsheet. The data captured is illustrated in figure 5.5..

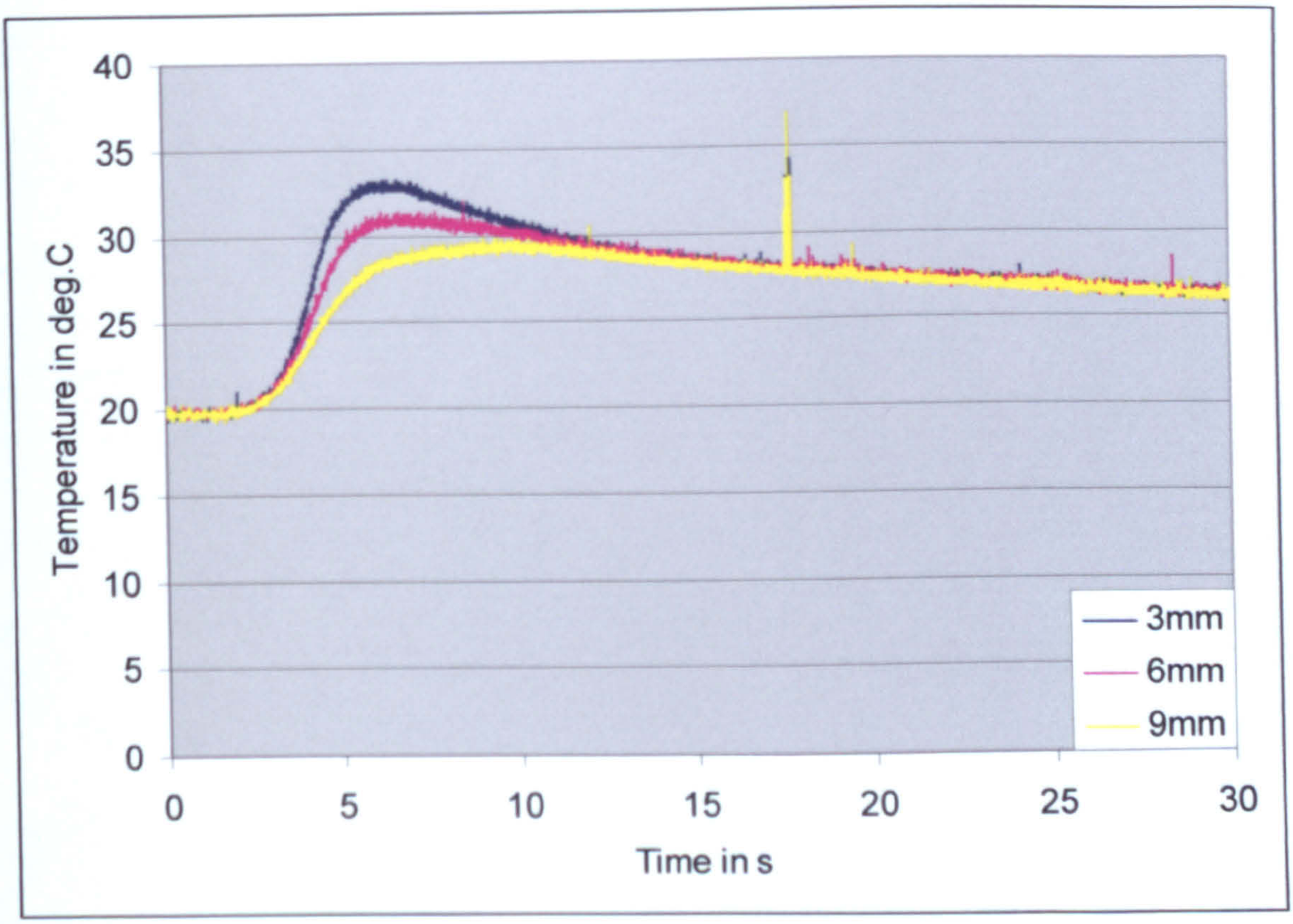

Figure 5.5: *Measurements of the temperature at different depth during a high-speed milling process.*

The aims of these experiments were:

- To check the heat penetration inside the workpiece and to obtain good idea of the temperature range at different depths during a standard milling process. If a grating were overheated, it would not shrink back into its initial state and would be permanently damaged. Therefore, it was very important to determine the maximum temperature achieved in harsh cutting conditions at the depth the fibre Bragg grating was to be placed. This way, the grating could be kept below the maximum temperature that a non-treated grating could sustain without damage (~100°C).

- To check the results calculated using the backward difference technique for relating the temperature measured at any depth with the temperature at the machined surface.

A maximum temperature of around 34°C was detected at a 3mm depth below the machined surface. The temperature range experienced at this depth is then from 18-20°C (ambient temperature) up to a maximum of 34°C. However the maximum temperature is dependant on the cutting tool used. As the tool is used, it may become damaged or worn and this will have a significant effect on the maximum temperature generated in the workpiece during machining. The more worn the cutting tool is, the higher that maximum temperature is likely to be.

Having measured the temperatures, it was necessary to investigate the use of the backward difference technique by applying it to the temperature data captured in Excel.

Using the temperature data for a depth of 9mm and 6mm, it was possible to back calculate a temperature for a depth of 3mm.

When applied to the milling experiments, the backward-difference method gives the following results:

Figure 5.6. shows the measured temperature data at respectively 9mm, 6mm and 3mm and the temperature data calculated at 3mm using the numerical method.

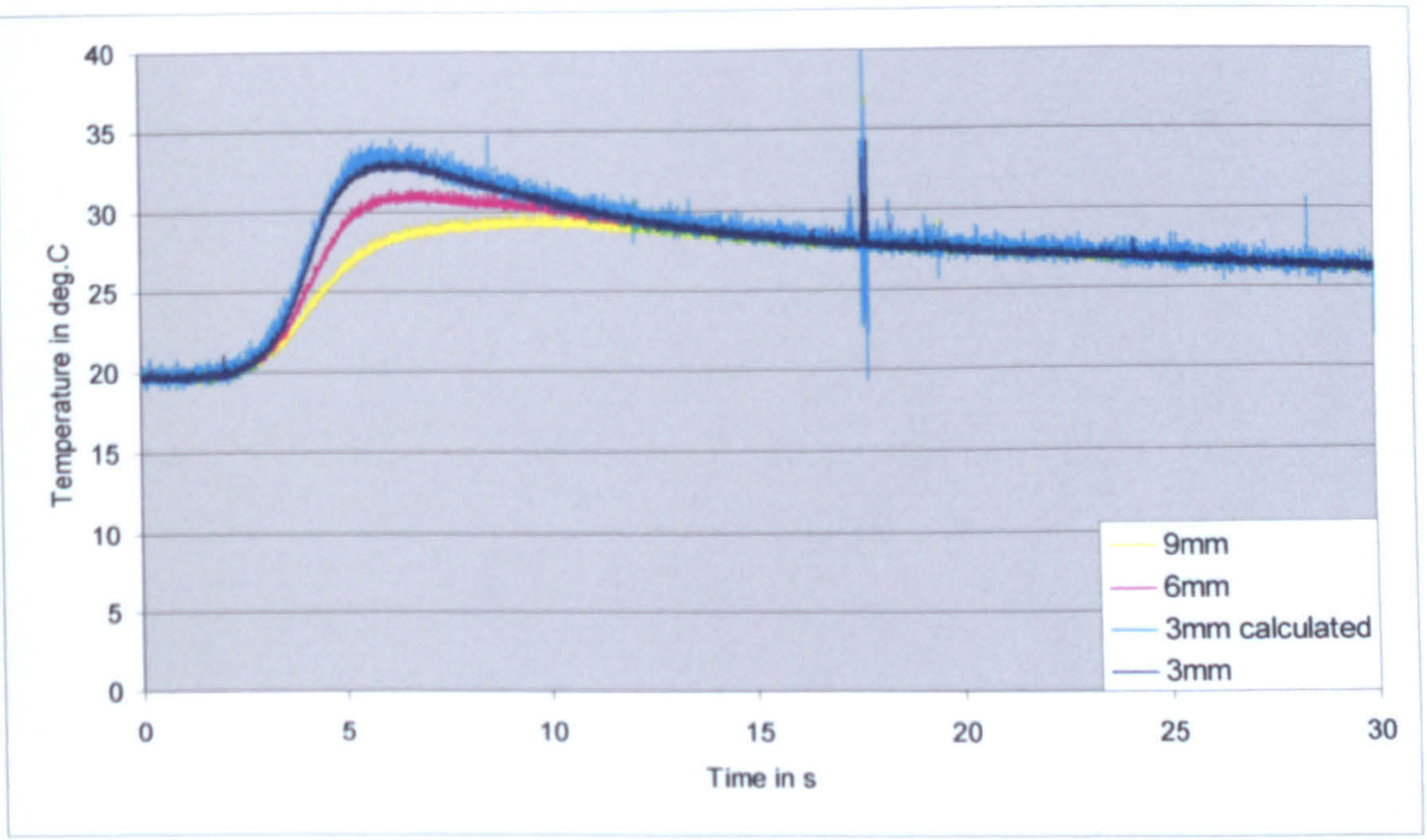

Figure 5.6: *Backward-difference method results.*

The temperature calculated for a 3mm depth was then found to be in good agreement with the temperature logged at that depth. It was therefore concluded that it would be possible to predict the temperature at the machined surface using the same technique. Figure 5.7. shows the difference between the measured temperature and the calculated temperature at the same depth. A constant error band of ±0.8°C is clearly visible. This error band is a direct result of the electrical noise generated by the thermocouple since the backward difference technique is using the measured data to predict temperature values at a different location. It should also be noted that any differencing technique is also inherently sensitive to noise in the raw data. From the first series of tests, it is known

that the optical systems will generate less noise, therefore the results of the backward difference technique applied to the optical system should be less noisy.

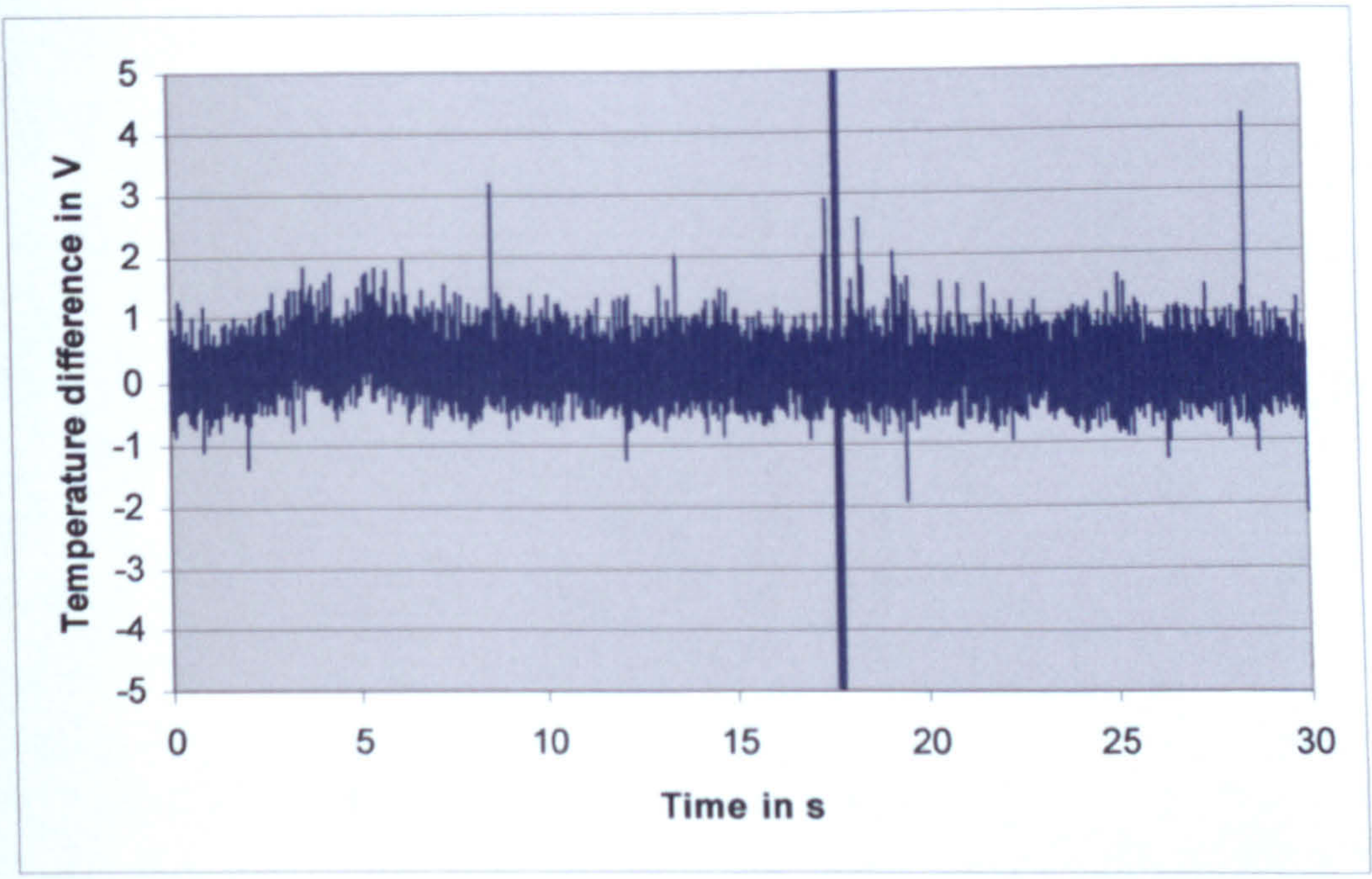

Figure 5.7.: *Backward difference error.*

5.3. Application of the backward-difference method to the fibre Bragg grating system.

Since only one fibre Bragg grating was to be used, it was necessary to complete two machining cuts in order to apply the backward difference technique. For example, by combining the data measured by the Bragg grating at 3mm and 2mm depth below the machined surface, it would be possible to predict the temperature experienced at a depth of 1mm from the tool. And also by computing the data from 2mm and 1mm from the surface

(figure 5.8.), it would be possible to have a very good estimate of the temperature at the machined surface (figure 5.9.).

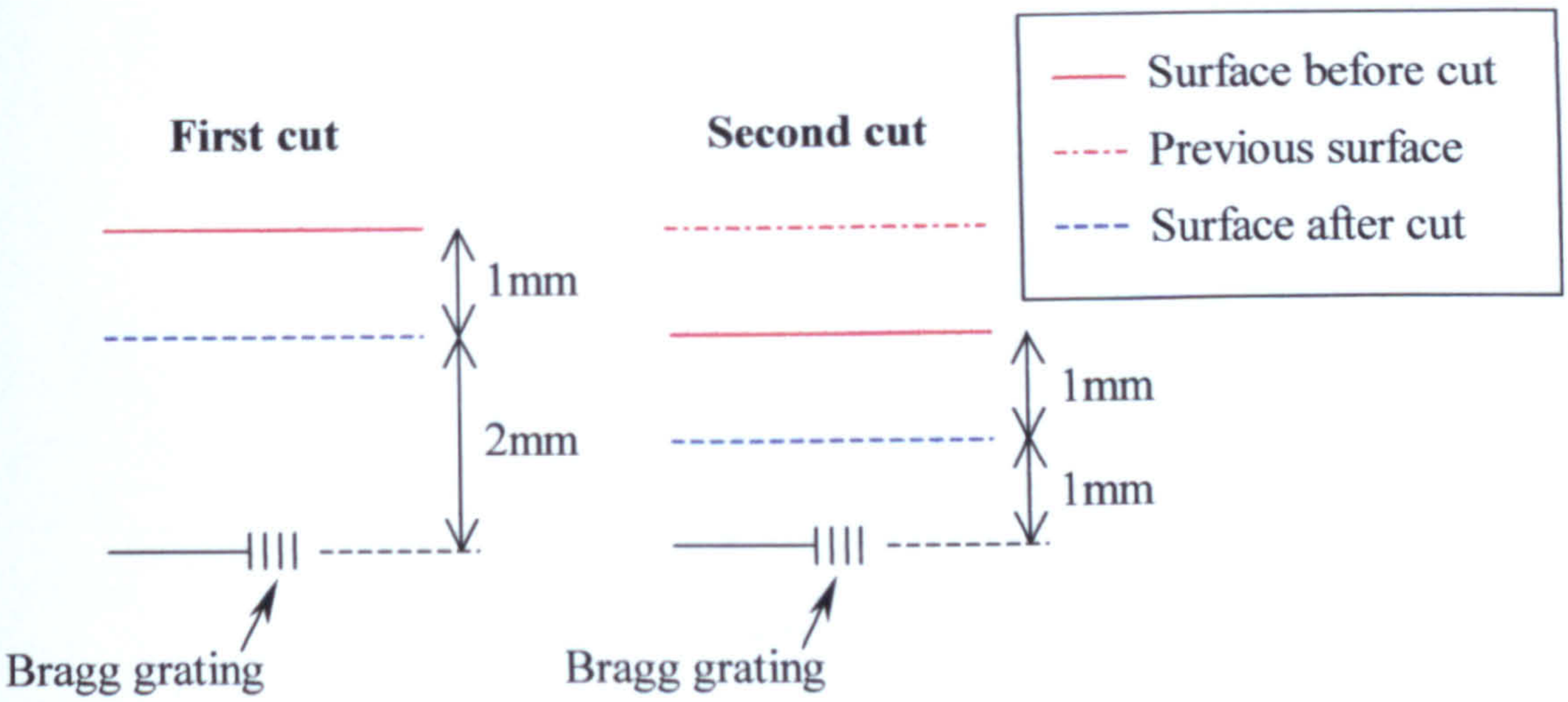

Figure 5.8.: *Backward-difference method for machining tests.*

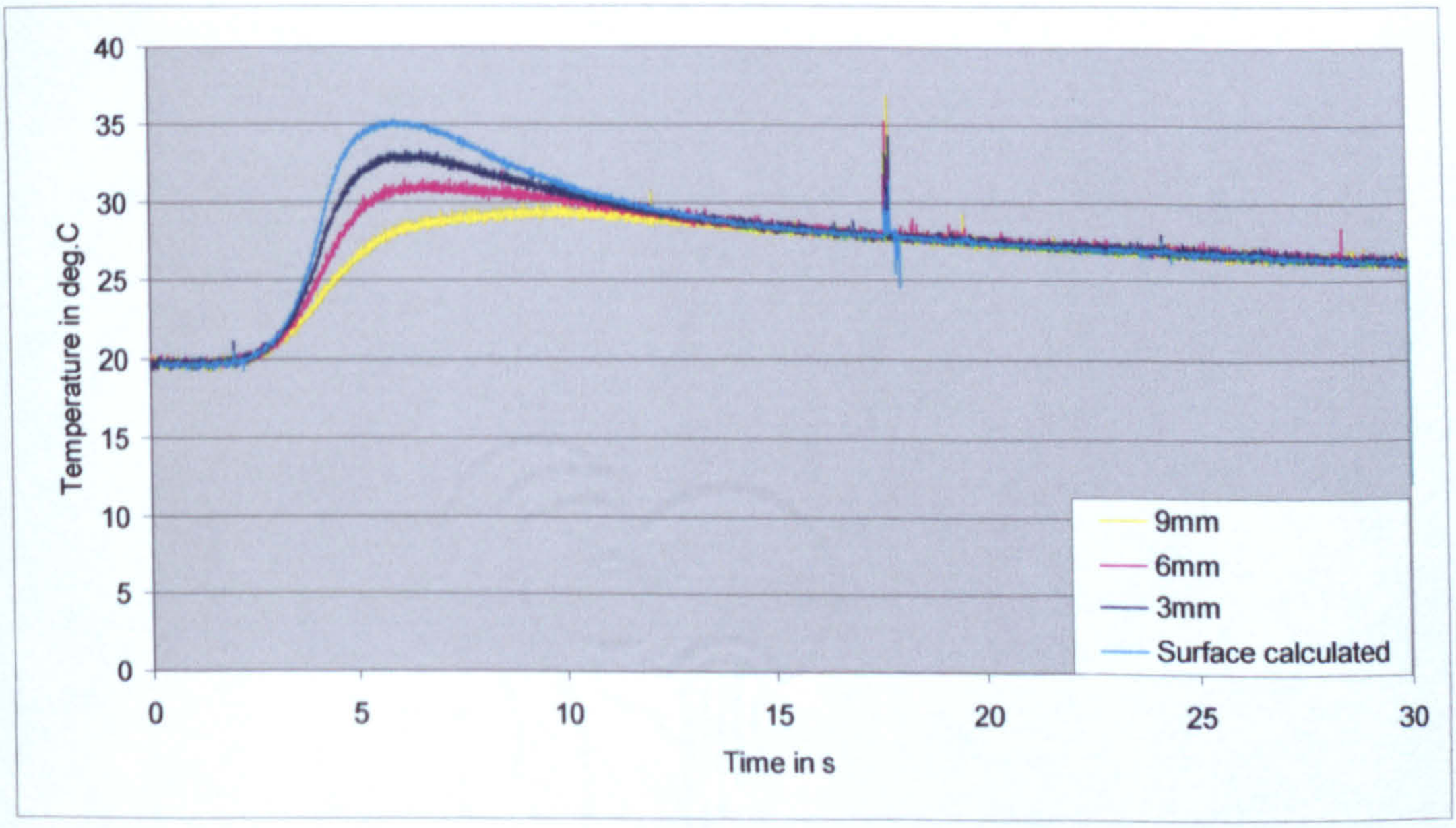

Figure 5.9.: *Backward-difference method results for surface temperature calculation.*

References.

1. Vernaza-Pena K. M., Mason J. J., and Li M., "Experimental study of the temperature field generated during orthogonal machining of an aluminium alloy", experimental mechanics, Vol. 42, No. 2, p 1-9, 2002.

2. Holman J. P., "Heat transfer", 8th edition, International edition, McGraw-Hill, 1997.

3. "Monolithic thermocouple amplifiers with cold junction compensation. AD594/AD595", Analog devices, Inc., http://www.gaw.ru/doc/AD/1188.PDF, 1999.

Chapter 6: Machining experiments.

6. Machining experiments.

6.1. Workpiece design.

In designing a workpiece for the experiments (to test the optical systems), a number of design constraints were considered:

- The workpiece should be designed in such a manner as to allow comparison of measured temperature with existing results/published data.

- The workpiece should be easily assembled and manufactured in a speedy and cost effective manner.

- It is very important to keep in mind that the workpiece is used to measure temperature at the machined surface.

In order to allow comparison of the optical temperature measurement systems with the existing thermocouple based temperature measurements, a thermocouple was embedded in close proximity to the grating. This allowed direct comparison of both sensing systems during the temperature measurement process. The thermocouple could also be used to double-check the temperature measurements and also to determine the initial temperature prior to machining.

As explained in Chapter 1, in the measurement of grinding temperature using a thermocouple, the preparation time may be up to two days and only one measurement is possible since the sensor is being destroyed. It is therefore an expensive and slow process. In order to avoid these problems, it was decided to design a workpiece with a removable and easily replaceable cap. The cap would be machined and then replaced by a new cap when needed. The idea of using a removable cap also allowed the insertion of the optical fibre within the workpiece. Adoption of this approach reduced the time required to set-up an experiment considerably and reduced cost. The new design of the workpiece is also cheaper to manufacture since the same workpiece body is reused for all the tests and only the cap is machined. The setting-up time of the new workpiece was in the region of ten minutes for the first set-up and about approximately five minutes were required to change the cap. These times compared favourably with those required for the existing thermocouple technique so it is possible to say that major improvements have been made in this respect. The workpiece body was also optimised for this specific application. The body was designed so it could be easily and solidly fixed to the machine.

Since only one fibre Bragg grating was to be used at a time for the temperature sensing, it was necessary to apply two machining cuts in order to apply the backward difference technique. To achieve this, the fibre was embedded in a slot just beneath the cap. This allowed the measurement of the temperature at different depths.

Considering the previous criteria, the following design was developed, figures 6.1. and 6.2. show the final design of the workpiece with its removable cap.

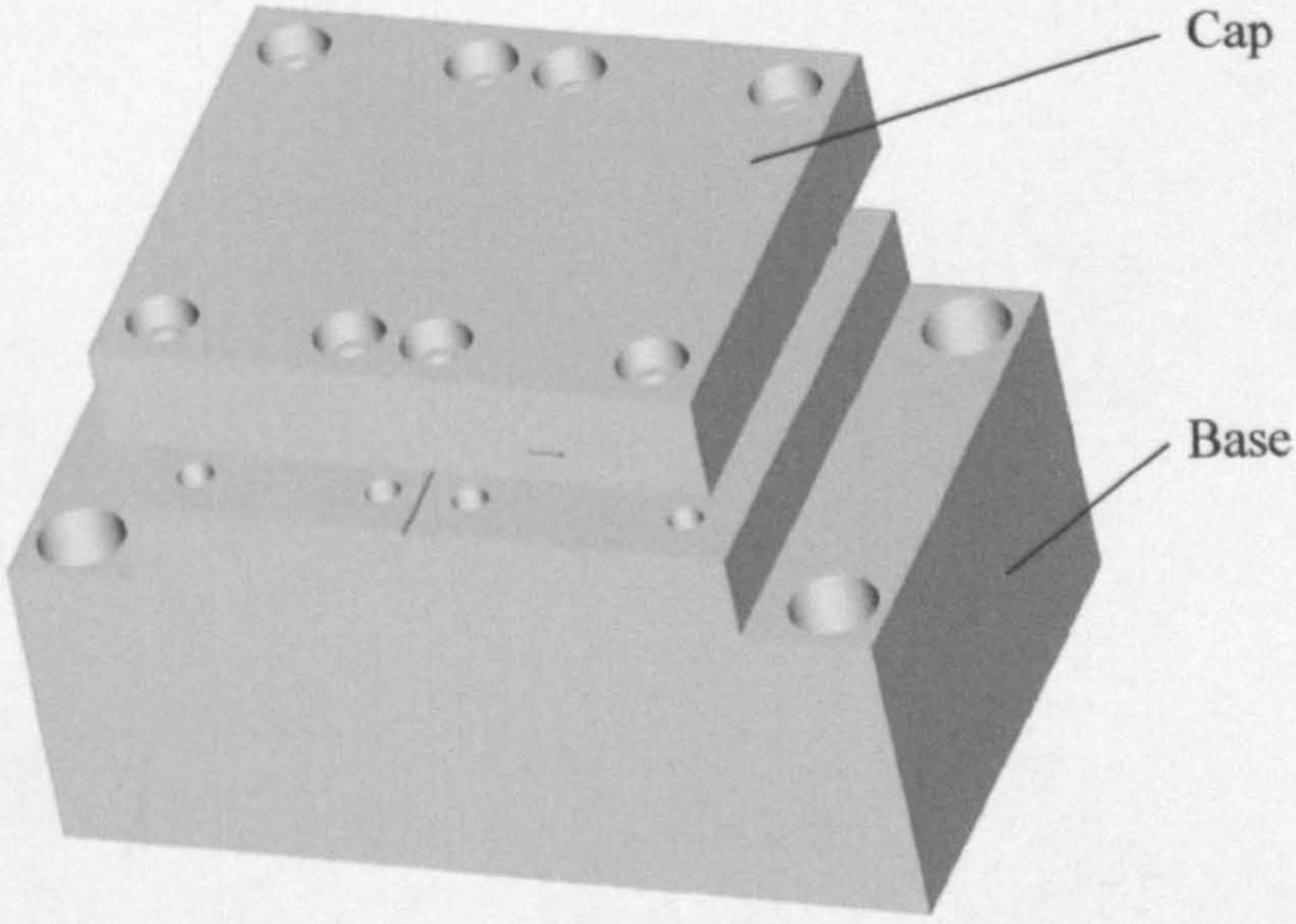

Figure 6.1.: *Workpiece design showing base and cap.*

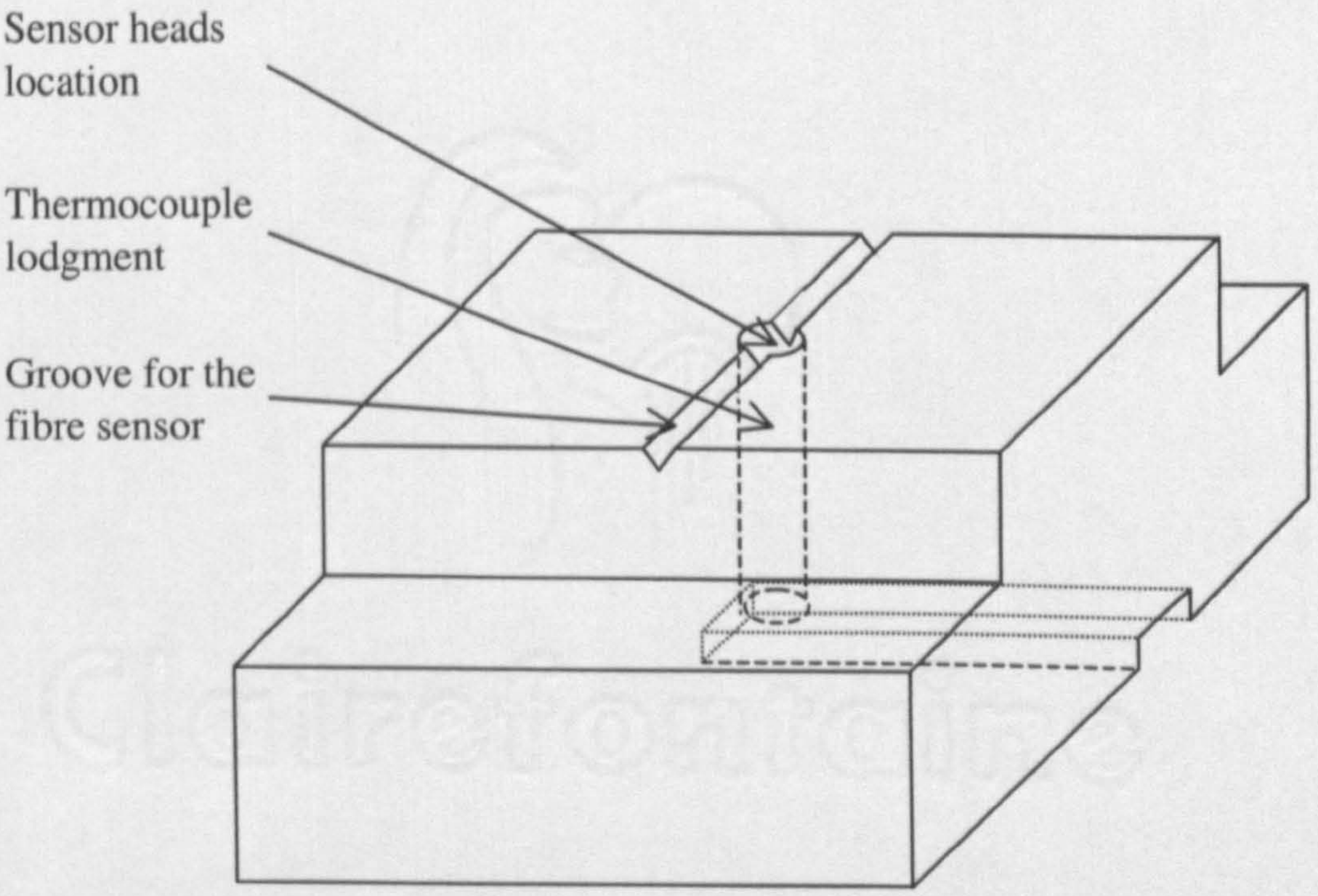

Figure 6.2.: *Details of the fibre groove and thermocouple hole in the base element.*

6.2. Milling experiments.

An initial set of milling tests were undertaken to verify the feasibility of measuring temperature during machining using optical fibres and also to check the functionality of the workpiece design.

6.2.1. Installation.

6.2.1.a. Preparation.

The workpiece, the thermocouple and the fibre were mounted in a CNC milling machine as shown in figure 6.3..

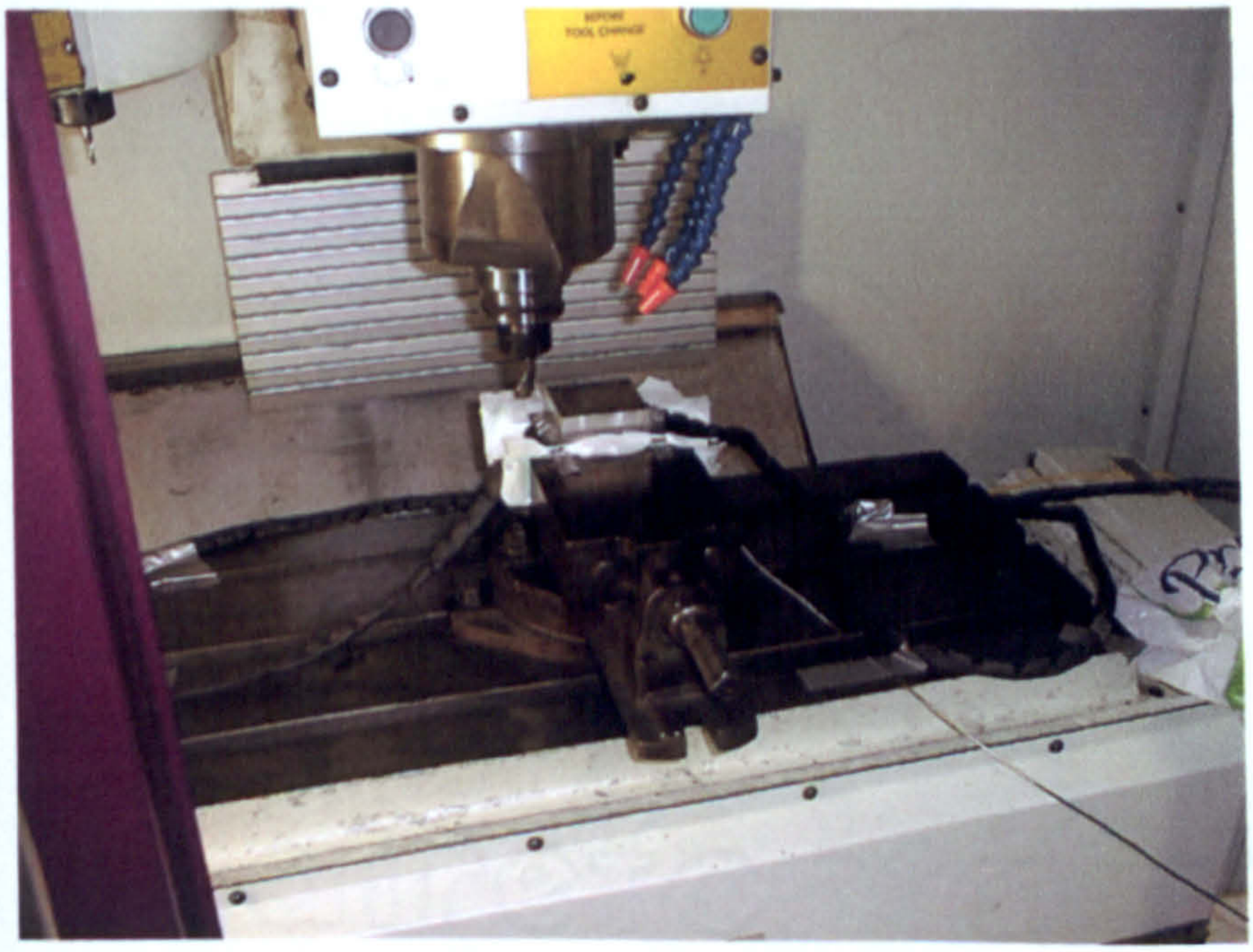

Figure 6.3.: *Workpiece and sensors installation on the Bridgeport VMC500/16 milling machine.*

A CNC milling machine was selected because it allowed good repeatability and precision in comparison to a standard manual milling machine.

To provide the necessary relative motion between the milling tool and the workpiece, the workpiece is normally mounted on a table that travels beneath the rotating tool. With a moving workpiece, it was required to transmit the temperature signals from the moving workpiece to the stationary signal processing equipment via a flexible link. However, it was found that flexure of the optical fibres gave rise to an unpredictable signal loss. Therefore, it was decided to mount the optical detectors on the moving table. In this way, the detectors moved with the workpiece and the fibres were undisturbed during the machining process. The electrical signals from the detectors were then passed to data acquisition equipment via flexible electrical cables; in this case, coaxial cables were used in order to shield the electrical signals from noise. In order to mount the detectors close to the workpiece several precautions were taken:

- The back panel of the milling machine was taken off to allow installation of the optical system.
- It was also very important to protect the photodetectors from hot chips and coolant; this was achieved by protecting them with a thin piece of light and heat resistant plastic.
- All electrical equipment, such as the light source and thermocouple amplifier, were kept outside the machine for practical reasons and to avoid contact with the cutting fluids used during some of the experiments.

Note:

The bending losses mentioned above do not have any influence on the signal launched from the light source since the signal is so strong that the losses are not visible. However, if the photodetectors were not fixed to the table the bending losses would have a bad influence on the weakened output signal.

Figure 6.4. illustrates the equipment layout.

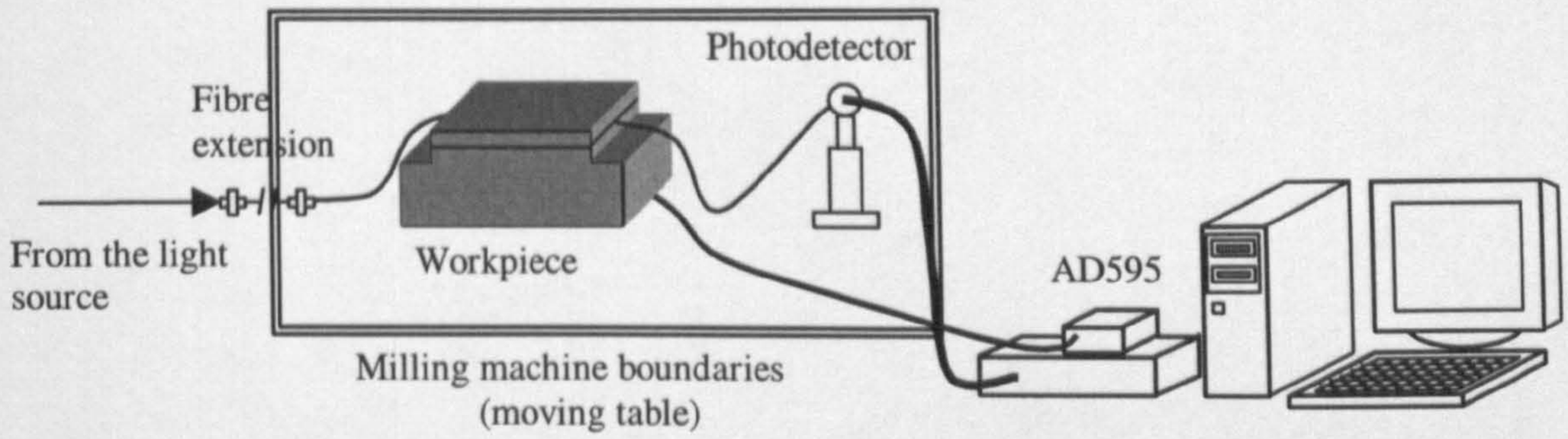

Figure 6.4.: *Equipment layout for the two gratings technique.*

6.2.1.b. Thermocouple isolation.

The electromagnetic fields produced by the electronic drive system of the milling machine gave rise to serious noise levels on the thermocouple signal. The K-type thermocouple cables used were shielded by an outer metal coating. Unfortunately when the outer coating made contact with the structure of the milling machine, electrical noise was induced onto the thermocouple signal and the noise gave rise to a large error band on the measured temperature signal. To overcome this problem, the

thermocouple cables were isolated by completely wrapping them with a plastic layer. Following is an example of a badly isolated thermocouple signal and a signal from a well-isolated thermocouple signal. Figure 6.5. shows the signals obtained from an isolated thermocouple and a thermocouple that is earthed to the machine structure. This reduction in noise achieved by isolating the thermocouple from the machine is clearly visible.

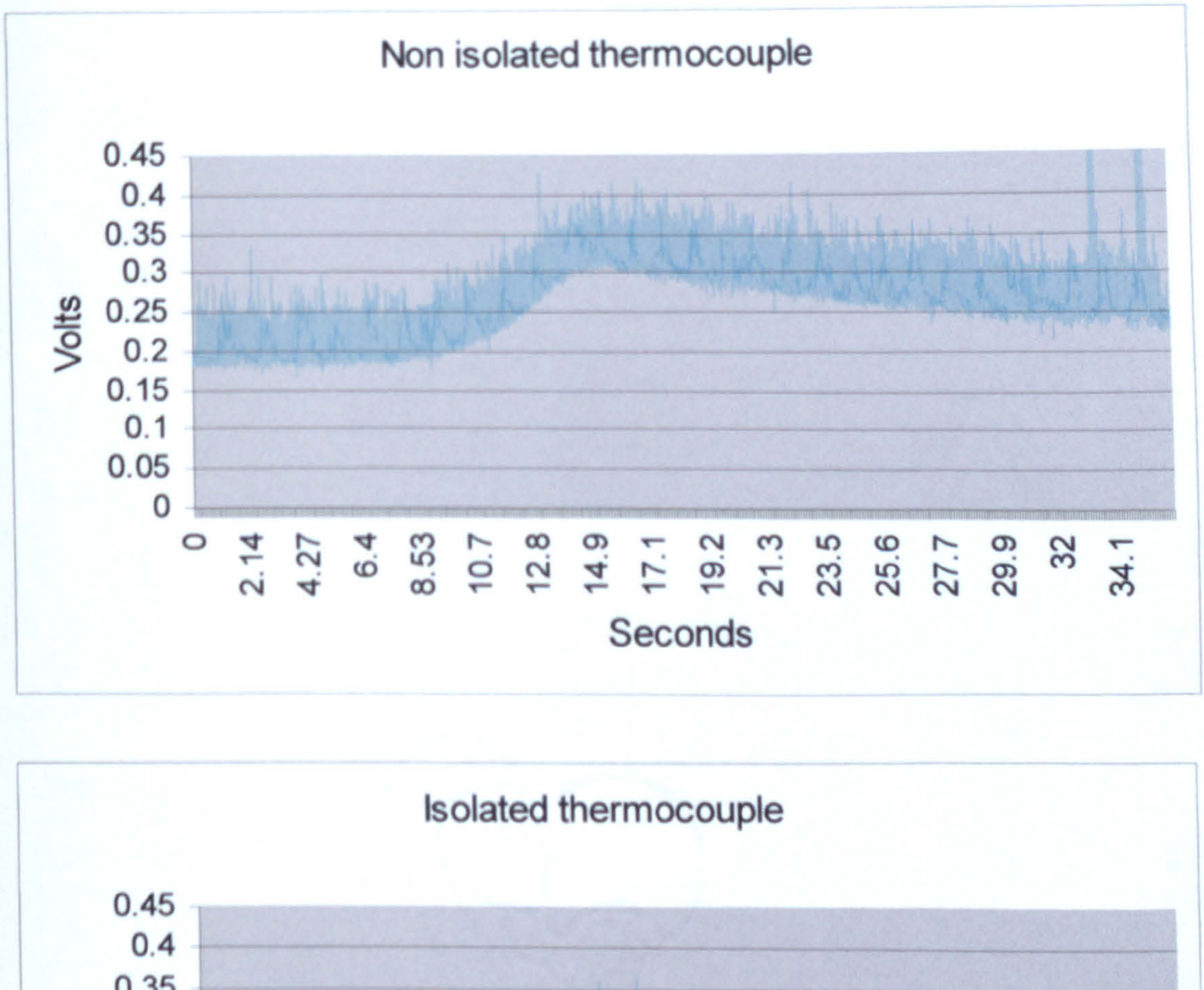

Figure 6.5: *Effect of the isolation on the thermocouple signal.*

By calculating the difference between the maximum and minimum voltage for the first forty data points (corresponding to a time interval of 0.12s when no temperature was induced on the workpiece), it was possible to compare the noise level in steady state conditions. In doing so, a peak to peak noise level of 0.076V was detected for a non-isolated thermocouple and for the isolated thermocouple the peak to peak noise level was found to be 0.0042V a reduction by a factor of 18. Since small thermocouple voltages were measured (0.01V per degree Celsius), good isolation had been shown to be a vital factor in achieving an accurate thermocouple reading.

Noise also became a problem when the thermocouple makes contact with other conductive items, such as, the workpiece and/or workpiece cap. One way to avoid this problem was to paint the surfaces of the workpiece and workpiece cap and so avoid electrical contact with the thermocouple. The paint layer created perfect noise isolation without having any significant effect on the temperature penetration within the workpiece.

6.2.1.c. Sampling rate determination.

The Nyquist sampling theorem states that: "if a signal only contains frequencies less than the cut-off frequency f_c, all the information in the signal can be captured by sampling $2f_c$" [1]. To achieve good accuracy of the readings, it is recommended to set the sampling rate between five and ten points [1]. In other words, the sampling rate was calculated so it

recorded ten points while the cutting tool was travelling above the fibre Bragg grating. So by knowing the length of a grating (1mm) and the average speed of the tool ($0.0041 m.s^{-1}$) and its diameter (20mm), it was possible to determine how long the cutting tool was above the sensor (4.88s i.e. minimal sampling rate was approximately 0.2Hz). Then knowing that 10 points were necessary during that interval, it was possible to determine the recommended sampling rate (time between two consecutive samples) (2Hz minimum).

6.2.2. Experiments.

The different optical fibre based temperature sensing systems were tested using the milling process. Data from the optical systems and the thermocouple were acquired using the DAQ software during the cutting process.

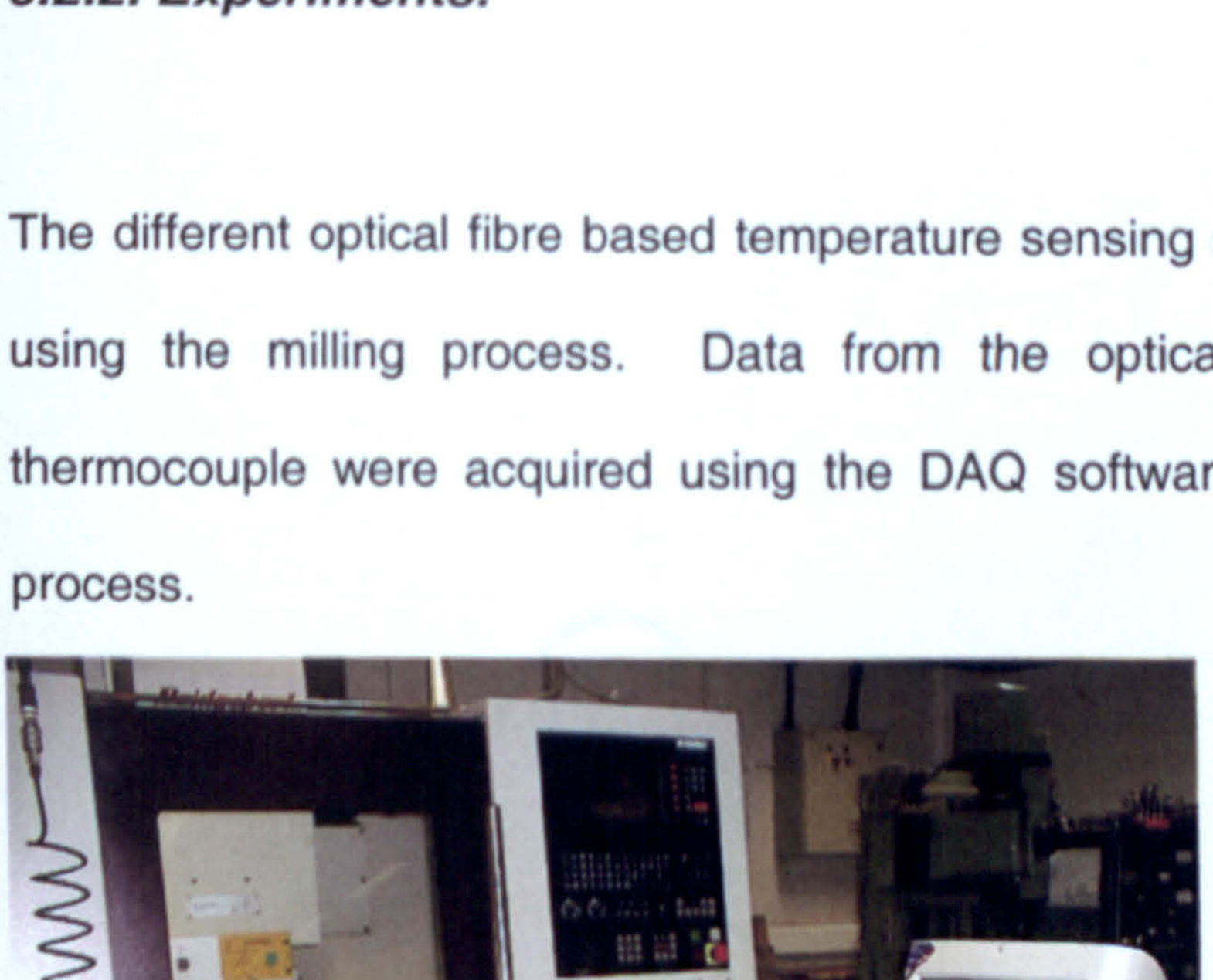

Figure 6.6.: *Equipment set-up.*

For each system, the following tests were undertaken:

The caps used during the tests had an initial thickness of 16mm. This allowed a series of cuts to be performed. As the cuts removed 2mm from the cap, the results correspond to depth of 14, 12, 10, 8, 6 and 4mm from the sensors. The experiments stopped at a distance of 4 mm from the grating and thermocouple so as to avoid damage to the optical cables. The machining parameters were the same as those previously described i.e. cutter diameter of 20mm, a spindle speed of 876rev.min^{-1} and a feed rate of 245mm.min^{-1}.

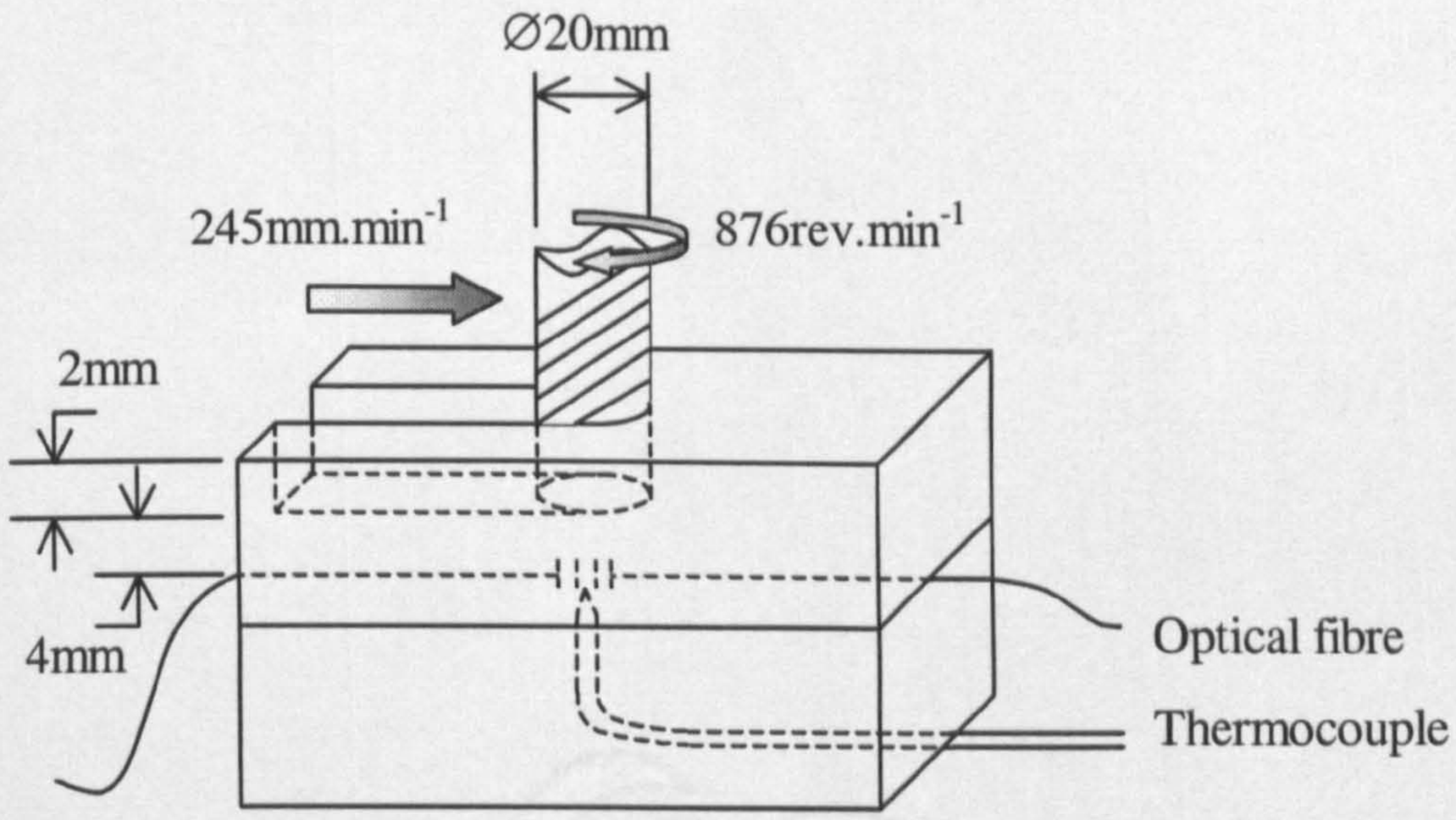

Figure 6.7.: *Parameters of the practical test.*

The raw thermocouple data of figure 6.8. were converted into temperature data by multiplying by a factor of 100 as previously described and shown in figure 6.9..

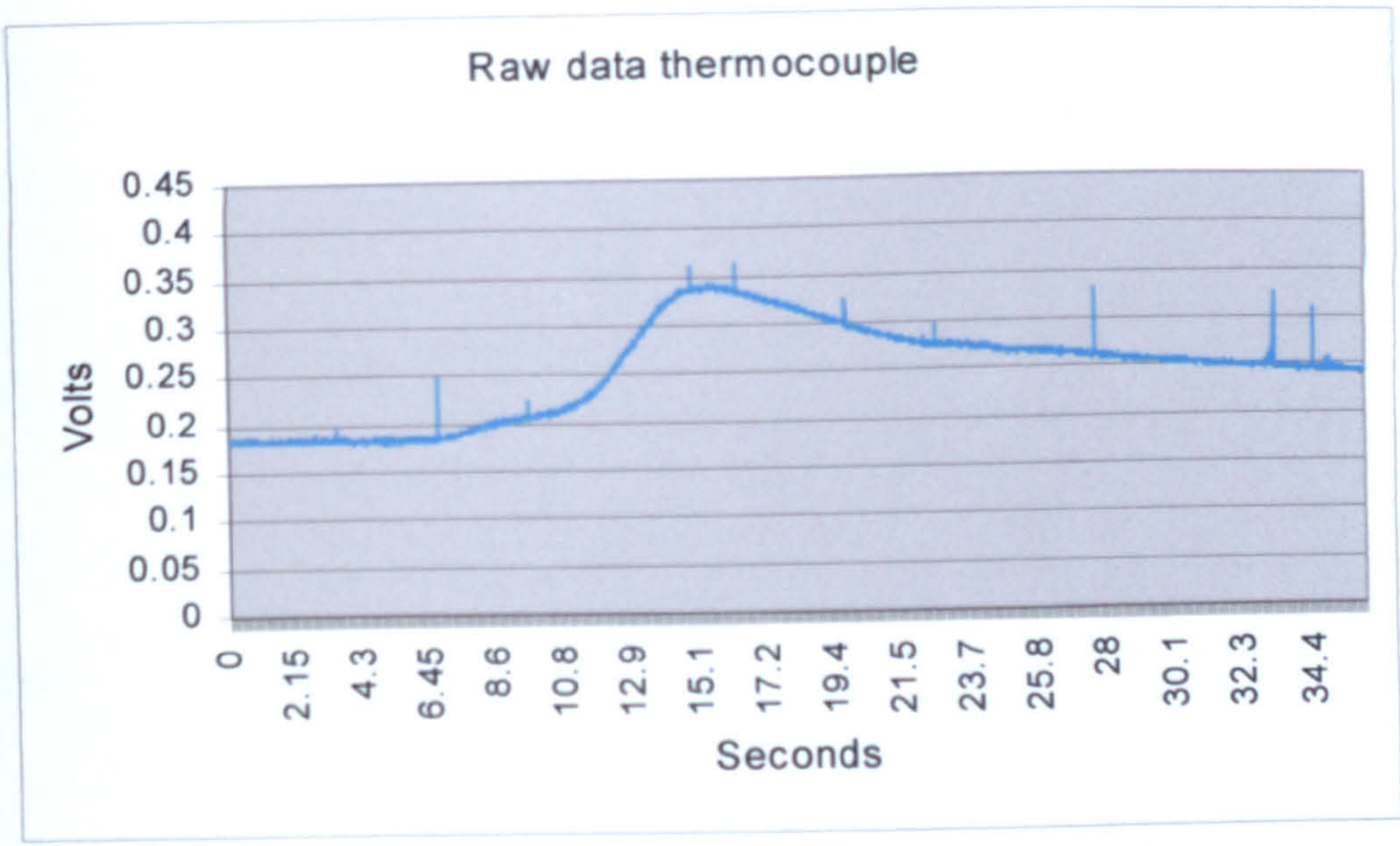

Figure 6.8.: *Raw thermocouple data.*

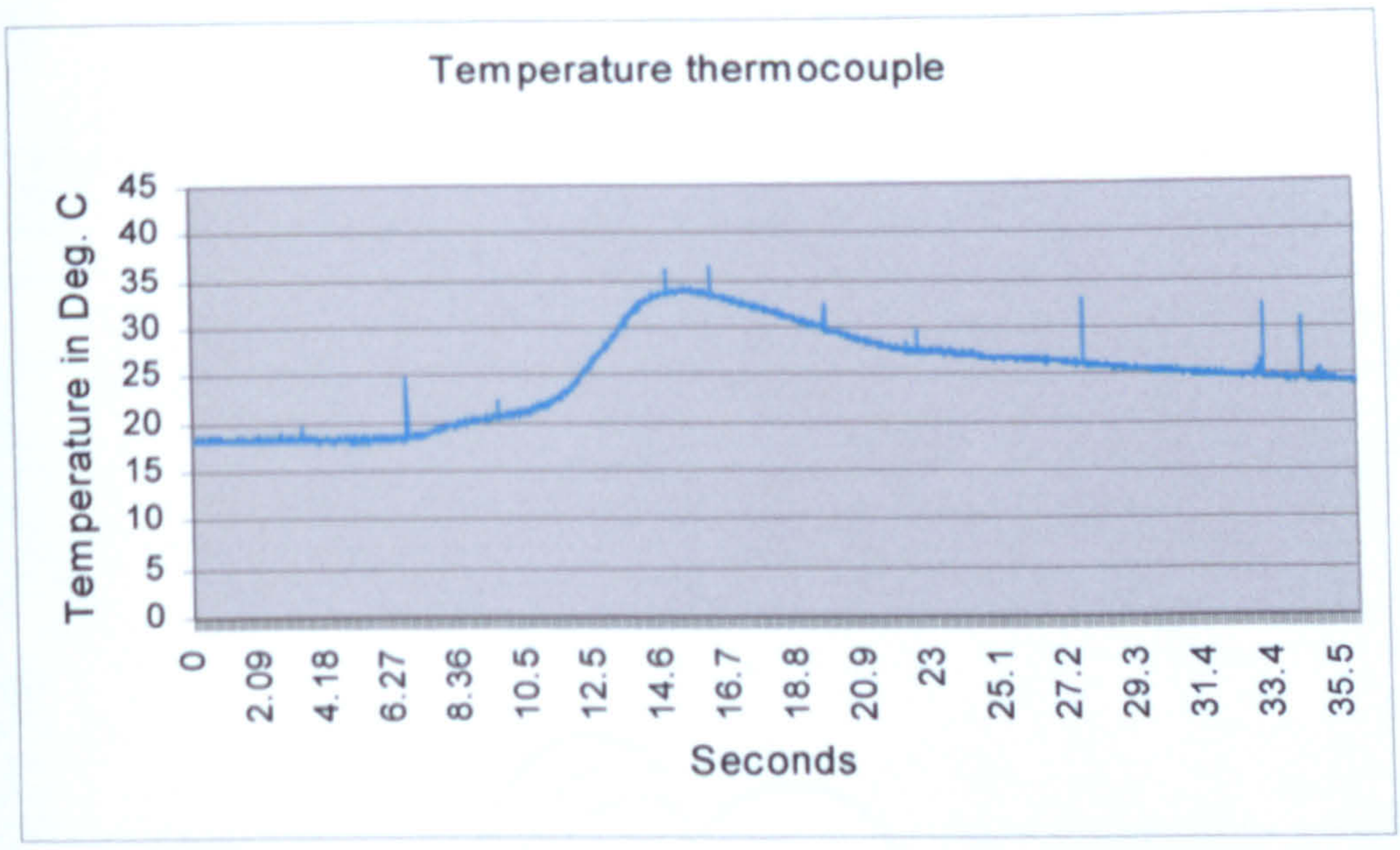

Figure 6.9.: *Translation of raw thermocouple data in temperature.*

6.2.2.a. "Cooled" experiments.

The first experiments were undertaken using coolant in order to investigate the effect of the stress induced on the Bragg grating by the cutting tool force during milling. A high coolant flow rate was used to cool down the

workpiece and cutting tool during machining so as to prevent heat transfer to the workpiece. Thus any change in grating wavelength detected during milling could be attributed to mechanical strain on the grating.

Fibre Bragg gratings are sensitive to stress because stress causes the grating to deform. The aim of that series of experiments was to check if the stresses produced by the tool on the workpiece during machining had an effect on the fibre Bragg grating. If those results were positive then a way to discriminate temperature from stress would be necessary. This problem could be solved as follow:

Since the same cutting tool, same cutting parameters and same material for the cap was used, it would possible to check the repeatability of the effects induced by the stress produced on the Bragg grating during the cutting process. If the repeatability were satisfactory, those series of data could be saved, and it would be possible to deduct them from the reading acquired during machining. By deducting the effect due to the stress, it would be possible to extract the changes in intensity induced by the temperature variation only. To verify the above, a thermocouple was used to check that the temperature inside the workpiece (at the grating position) remained constant. This test was necessary to check that the workpiece design was appropriate for these temperature measurement using optical fibre experiments and to ensure that the optical systems responded to temperature only and not to mechanical strain. If the grating was subjected to strain, then another possibility would be to change the design of the workpiece by increasing the depth and width of the groove the fibre was embedded in.

It would be an easy solution but a bigger groove that would imply an air gap between the fibre and the machined cap. This air gap would have a drastic effect on the temperature measurement since air would be isolating the sensing equipment.

However there was no need for modification of the workpiece base since no strain was induced to the fibre Bragg grating during machining.

6.2.2.b. "Dry" experiments.

Experiments were undertaken without the use of cutting fluids so as to investigate the temperature rise in the workpiece and also to determine the performance of the new temperature measurement systems. Working without coolant allowed a significant temperature rise to occur into the workpiece (a situation similar to what occurs during grinding). The use of a series of 2mm cuts provided data on the subsurface temperature distribution and could be used to calculate an estimation of the top surface using the backward difference analysis method.

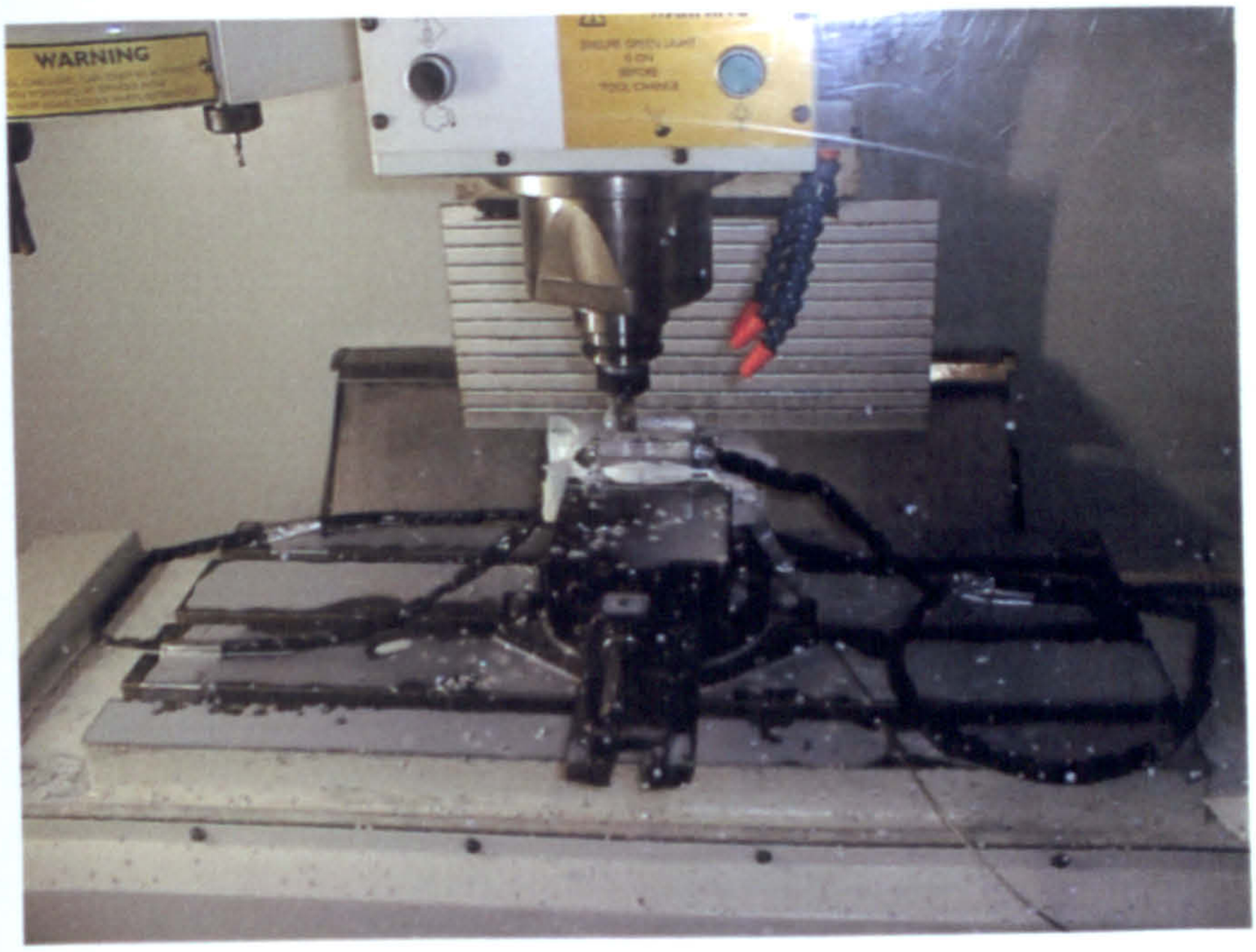

Figure 6.10.: *Milling experiment.*

Between cuts, it was necessary to cool the workpiece down to its initial conditions. The temperature was measured before the first cut and saved as the initial conditions. The temperature of the coolant was the same as the ambient temperature and therefore the same as temperature of the workpiece. The temperature during the cooling process was monitored and the cooling stopped when the initial conditions were reached.

As expected, the closer the tool to the sensors, the higher the temperature measured was. The results at 4mm from the sensors are plotted below for each different optical fibre sensing systems. The results from various tests with conditions given are shown in figure 6.11. to 6.13..

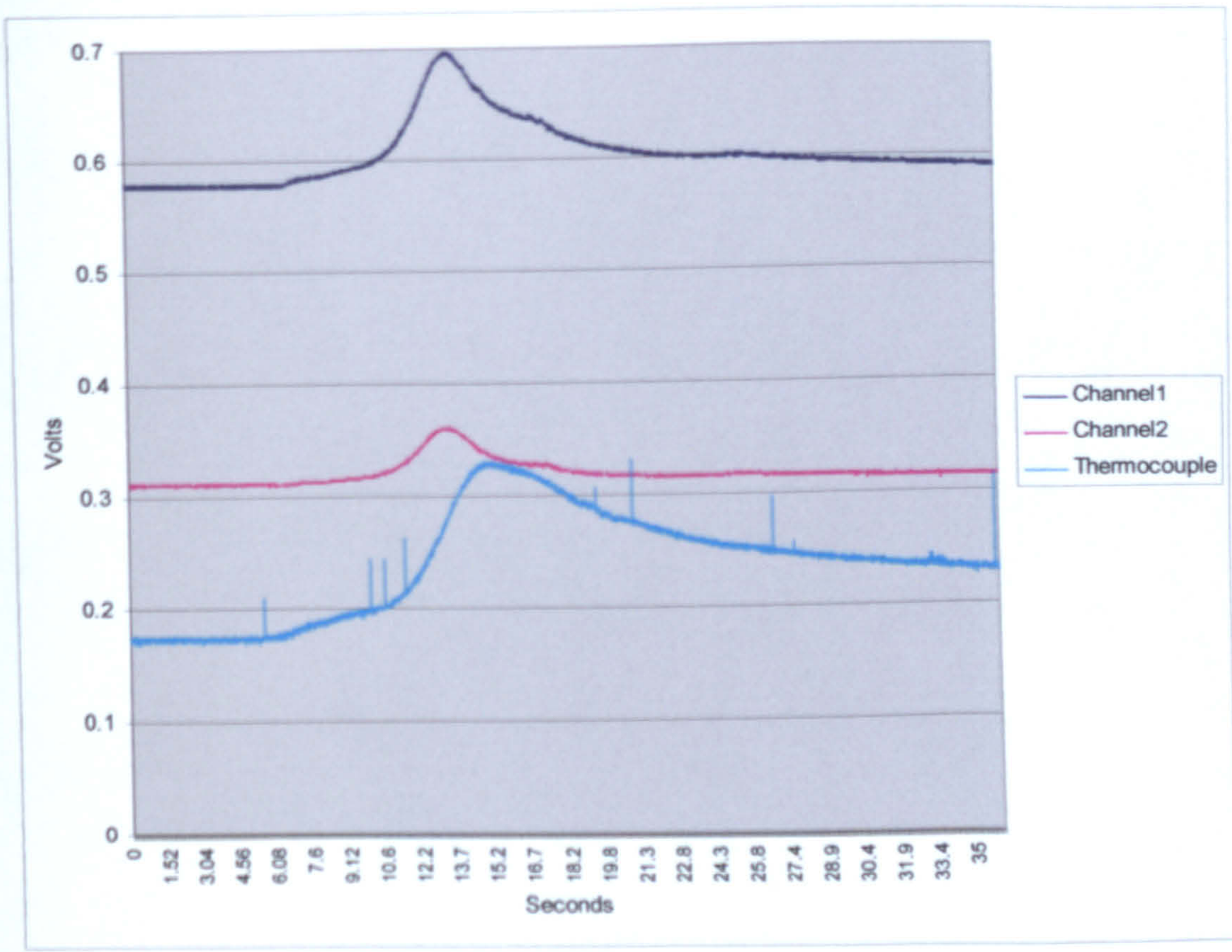

Figure 6.11.: *WDM technique results at 4mm from the sensors with a 2mm cut.*

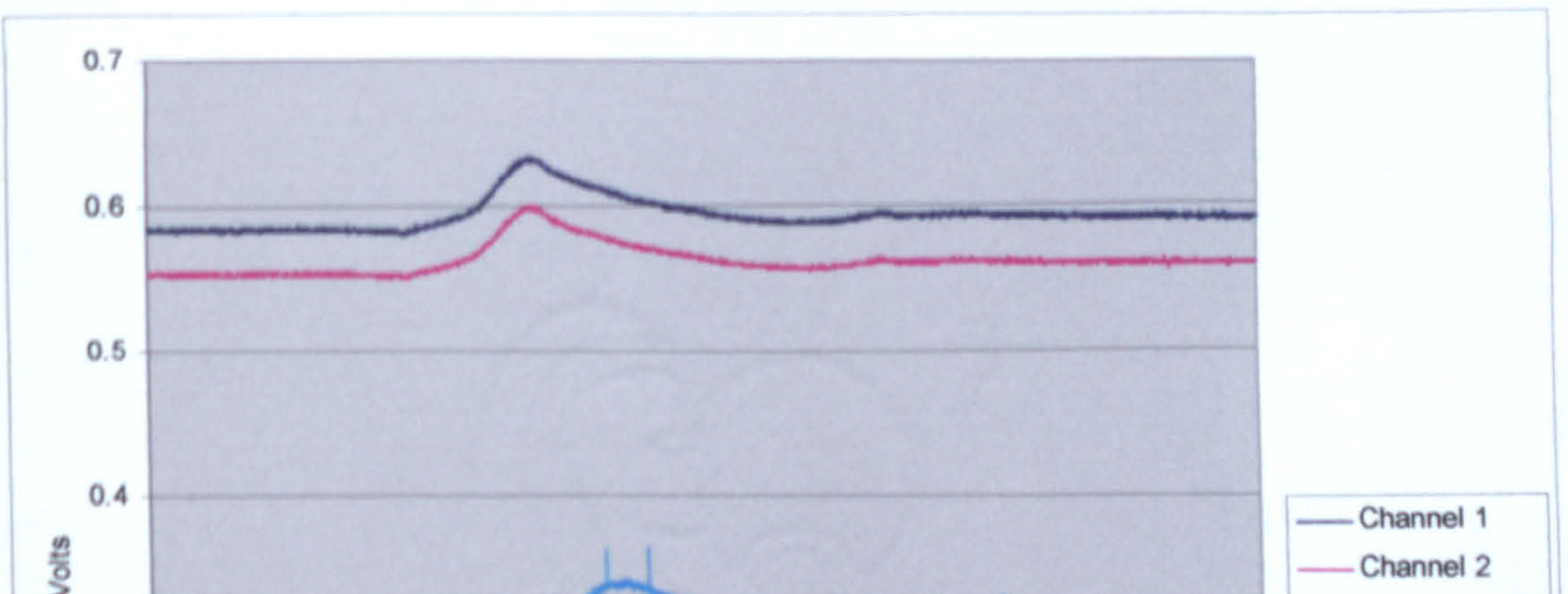

Figure 6.12.: *Coupler technique results at 4mm from the sensors with a 2mm cut.*

Note:

The thermocouple results of the results above (figures 6.11. and 6.12.) are lagging because a misalignment between the thermocouple head and the sensing Bragg grating.

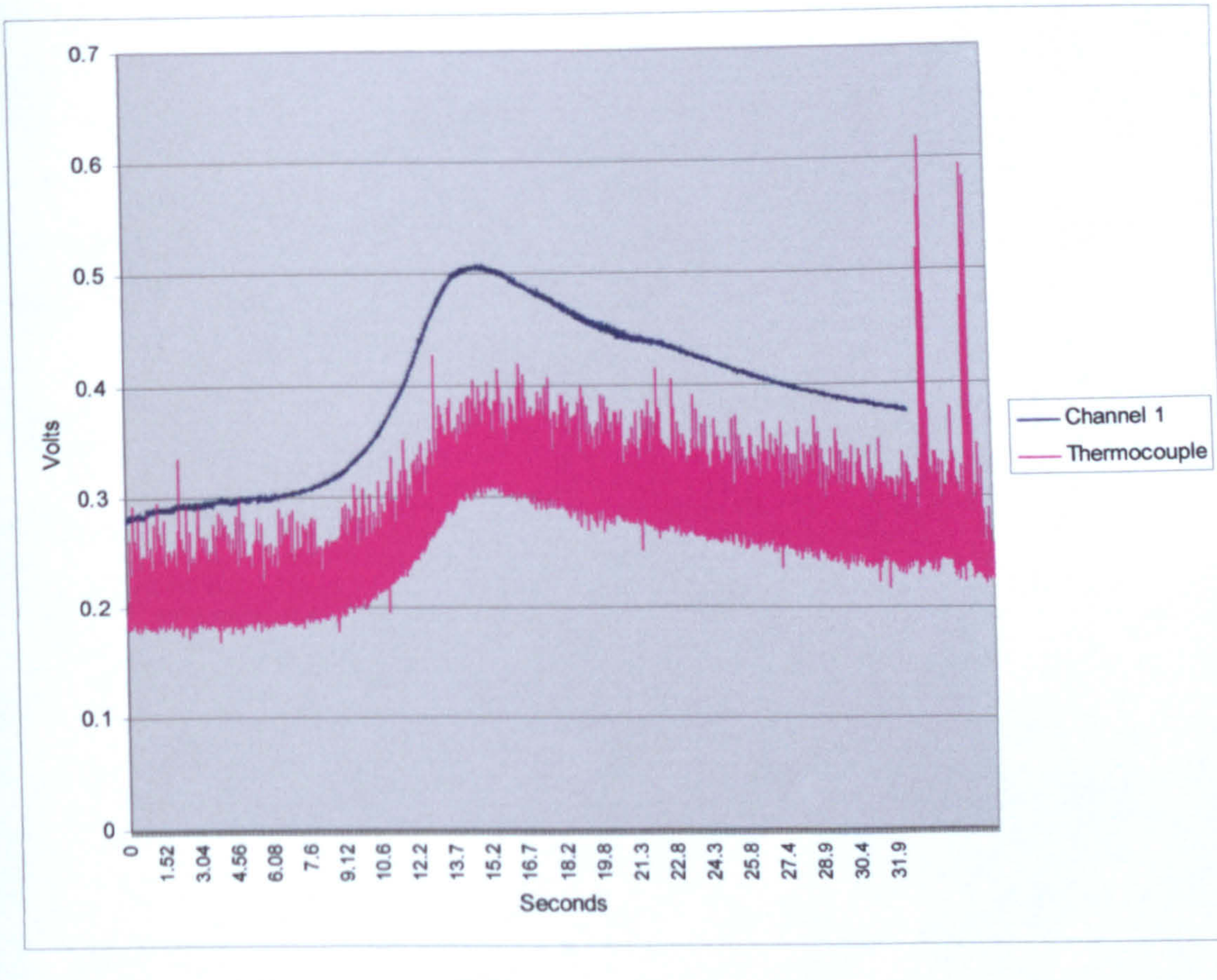

Figure 6.13.: *Two gratings technique results at 5mm from the sensors with a 2mm cut on an aluminium cap.*

Note:

The above two gratings technique experiment results show the trouble that can be encountered if the thermocouple is badly isolated (see figure 6.13.). The experiment was on a cap made of aluminium but the author noticed that the temperature profile measured on the aluminium in those conditions at 5mm from the sensors is similar to the temperature profile produced on a mild steal cap at 4mm from the sensors. This will make the comparison between all the systems easier since tests on mild steel were not

undertaken due to the destruction of the sensing fibre (explained in further detail below).

By adding a "moving average" (80 points) trend line on the thermocouple curve, it is possible to have a better reading as illustrated in figure 6.14..

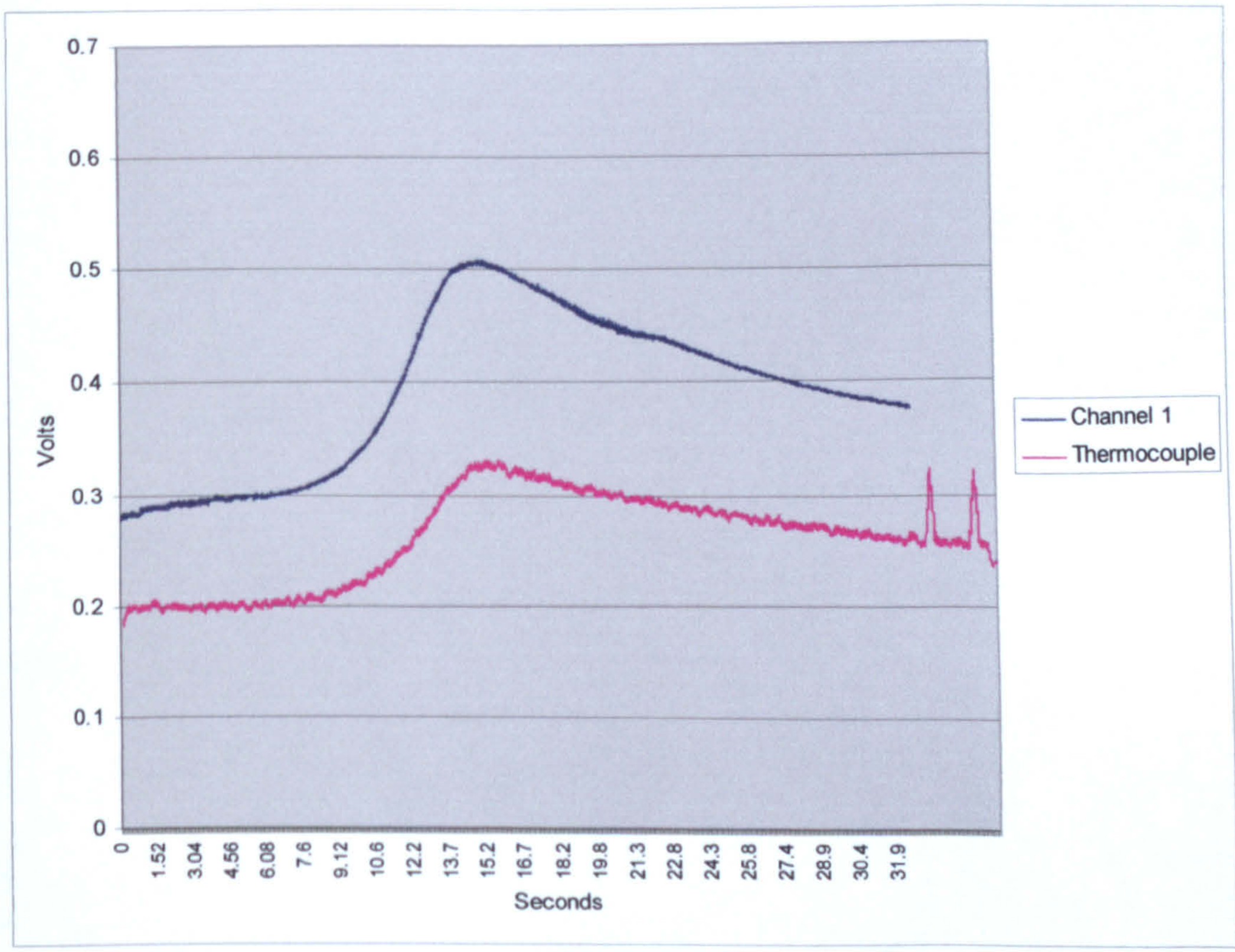

Figure 6.14.: *Two gratings technique enhanced results at 5mm from the sensors with a 2mm cut (thermocouple data has been low pass filtered and optical data is raw data).*

Note:

The DWDM was the last tested system during milling. The wear of the tool caused a rise in the measured temperature inside the workpiece. This was due to the fact that the cutting tool did not dissipate the heat as it should anymore and also it generated more heat during the machining because the cutting edges were less sharp. The results plotted in figure 6.15. showed the temperature profile at 4mm from the sensors giving a maximum temperature of 38.8°C. However for comparison purpose with the other

optical systems, the temperature profile at 6mm from the sensors was more appropriate (see figure 6.16.).

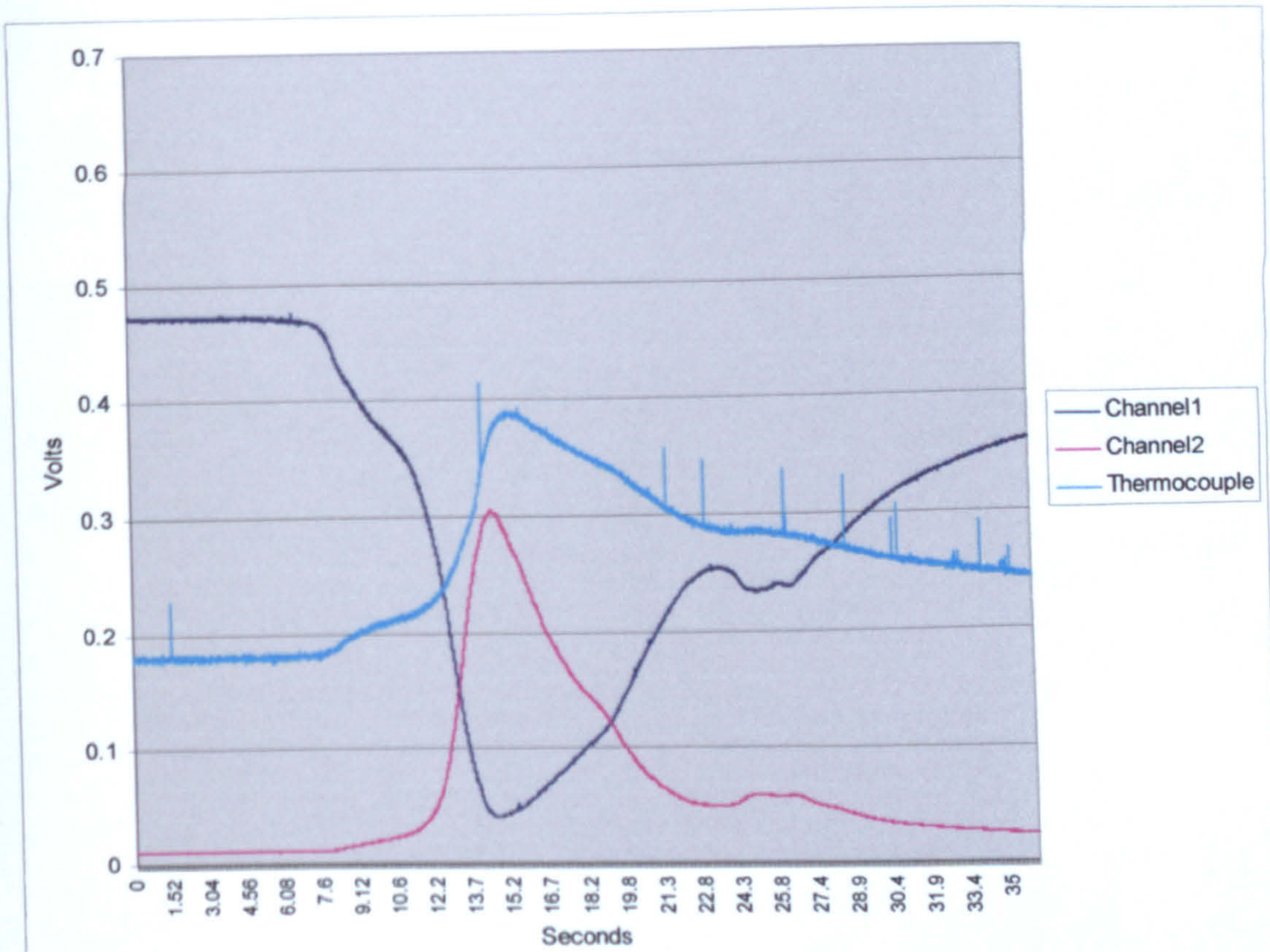

Figure 6.15.: *DWDM technique results at 4mm from the sensors with a 2mm cut.*

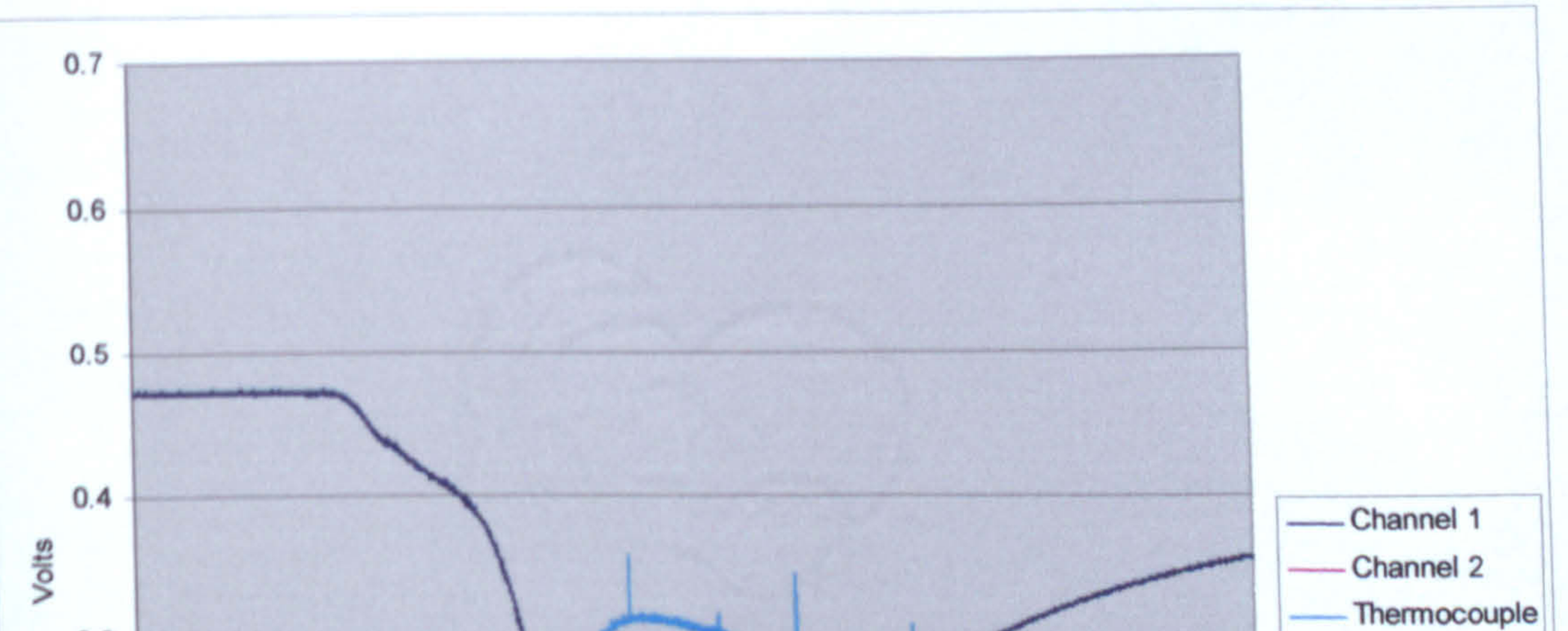

Figure 6.16.: *DWDM technique results at 6mm from the sensors with a 2mm cut.*

6.2.3. Conclusions on the milling experiments.

6.2.3.a. Problems encountered.

6.2.3.a.1. Fibre brittleness.

Fibre brittleness was always one of the main concerns during the application tests. The experiments using the two grating technique were interrupted by the destruction of the fibre during installation in the workpiece. The main inconvenience of the two gratings technique during machining is that the fibre has to go through all the workpiece since the signal transmitted through the grating is the one that is measured and not the reflected one. Another problem is that the workpiece was not mounted directly to the machine table but quite high from the table (approximately 5cm between the bottom of the workpiece and the table) in a vice for practical reasons this caused the fibre to move more freely. During changing the cap, the fibre moved slightly while mounting the cap, this caused the fibre to be squashed (figure 6.17.) when the screws holding the cap were tightened.

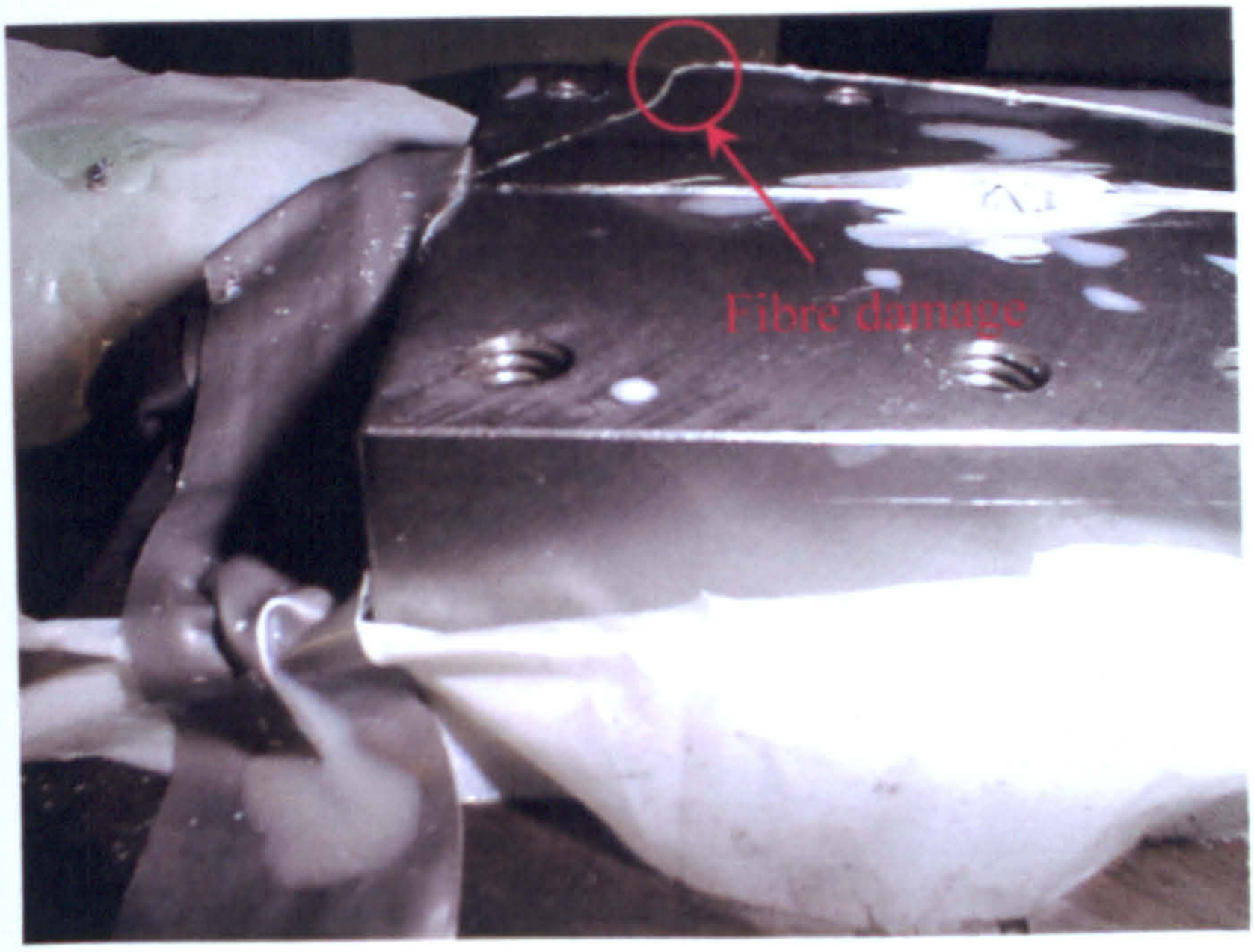

Figure 6.17.: *Damaged fibre.*

6.2.3.a.2. Metal chips.

During the dry machining tests, very hot metal chips were ejected from the machined cap onto the equipment. This could have serious consequences to the equipment if not well protected. This problem was encountered during a milling test, hot metal chips went through the fibre coating and damaged it causing destruction of the fibre Bragg grating and immediate interruption of the sensing signal.

6.2.3.a.3. Solutions to the problems.

A few workpiece modifications were necessary for the next machining tests. The workpiece was directly mounted to the machine table. Also by making the sides of the workpiece block longer on each side of the cap would allow the fibre to rest on it and also allow easier mounting of the fibre. To avoid the problems due to hot chips, the part of the fibre outside the sensor region, should be coated in some high heat resistant coating.

6.2.3.b. Comparison of the optical systems.

Before reading and comparing the data spectra, it is necessary to define a few terms:

The ***sensitivity*** of an instrument is "the ratio of response (in time and/or magnitude to a stimulus". [2]

The ***range*** of an instrument is "the difference between the largest and smallest values in a set of observations". [2]

Optical System tested	Distance sensor-cutter	Depth of cut	Material used for the cap	Coolant
WDM	4mm	2mm	Mild steel	Off
Coupler	4mm	2mm	Mild steel	Off
Two gratings	5mm	2mm	Aluminium	Off
DWDM	6mm	2mm	Mild steel	Off

Figure 6.18.: *Cutting parameters.*

The figure 6.19. shows the matching of the thermocouples' temperature data; this allows comparison of the optical systems. The main problem in this comparison was the positioning of the curves; this was due to the alignment of the sensors and also to the starting time of the recording. A slight change in position caused the peak of the temperature profile to move.

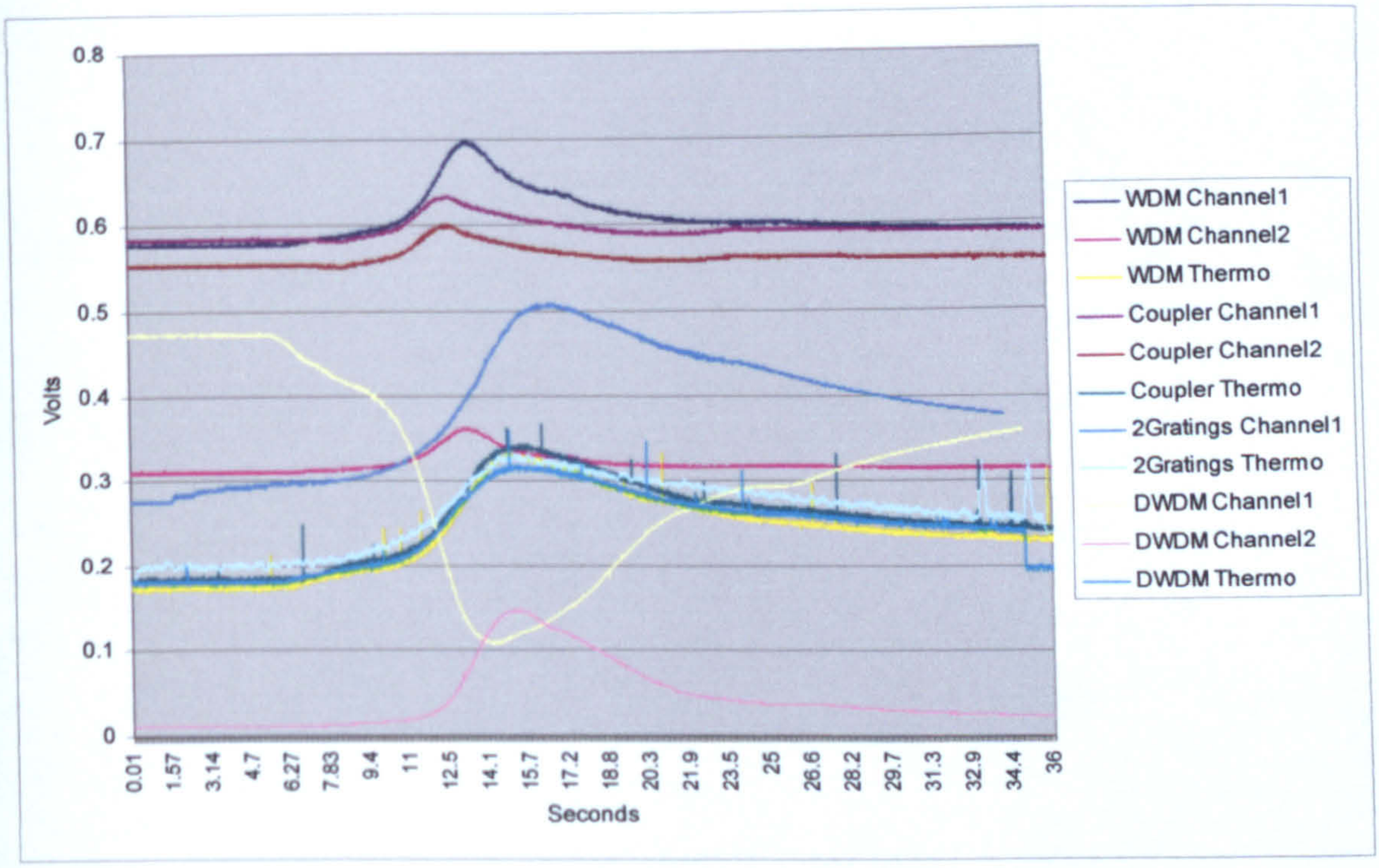

Figure 6.19.: *Comparison of the optical systems for the experiments described in figure 6.18..*

This comparison showed that the two grating and the DWDM optical systems are the most appropriate for temperature measurement since they are the most sensitive ones (figure 6.22.).

All the tables below show the different channels voltage output for each different optical system tested.

Device	Two gratings	DWDM	WDM	Coupler
Thermo-couple	0.016177	0.010797	0.009671	0.011074
CH1	0.003736	0.003087	0.00487	0.003662
CH2	N/A	0.003376	0.003967	0.00425

Figure 6.20.: *Peak to peak noise level of the sensors signals (in Volts).*

First the electrical noise on the signal was calculated by measuring the difference between maximum and minimum power before machining i.e. in a steady state.

To have a more accurate reading of the data, a moving average trend line was added. Then the minimal signal and maximum signal were found using simple spreadsheet functions and the difference was made.

Device	Two gratings	DWDM	WDM	Coupler
CH1	0.22516	0.422521	0.117379	0.047542
CH2	N/A	0.36521	0.122434	0.04519
Thermo-couple	0.14920	0.136917	0.155618	0.155788

Figure 6.21.: *Data range of the signals of the test described on figure 6.18..*

Device	Two gratings	DWDM	WDM	Coupler
Thermo-couple	10	10	10	10
CH1	15.09	30.85	7.54	3.05
CH2	N/A	26.67	7.87	2.90

Figure 6.22.: *Sensitivity of the sensors during the milling experiments in mV/°C.*

For mounting reasons in the workpiece, it was possible to say that the DWDM was the most appropriate for temperature measurement during machining. However, this optical system was harder to calibrate than the two gratings technique system. The DWDM technique allowed a wider range of temperature (up to grating destruction 300°C for treated grating used) than the two grating one that was limited to the bandwidth of the athermic-grating spectrum (approximately 74.5°C (section 4.7.2.)).

6.3. Grinding experiments.

6.3.1. Workpiece modifications.

The workpiece used for the milling experiments was used to test the measurement systems during grinding. However since fibres were

damaged during the previous experiments a few modifications of the workpiece were necessary to prevent damage of the fibres.

To prevent damage, a block was added to each side of the cap area giving the fibre more length to rest on and therefore causing it to bend less (figures 6.23., 6.24. and 6.25.). A thin protective metal plate was then applied to the top of each block to protect the fibres on each side of the cap, preventing damage from above. The extra blocks and metal plates also aided the installation of the fibres.

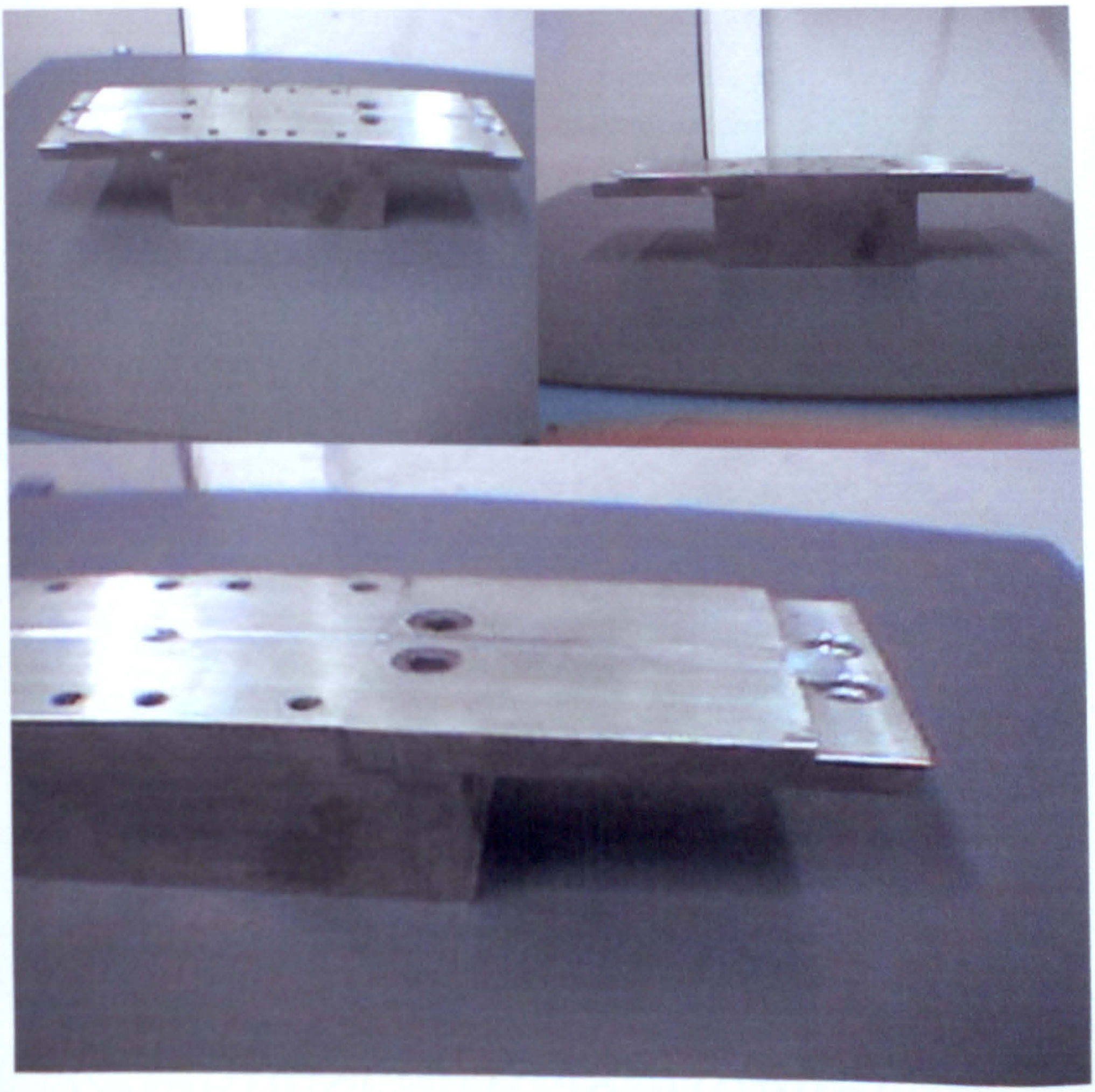

Figure 6.23., 6.24. and 6.25.: *Details of the modifications.*

6.3.2. Experimental parameters.

As the number of cutting edges on a typical grinding wheel is much greater than the number of teeth on a milling tool, grinding produces a large number of small chips and milling produces a small number of large chips. Production of a small number of large chips in milling give rise to high levels of vibration. Since the size of the grinding chips is much smaller and the typical cuts are less, the grinding process will suffer from less vibration. Therefore, it is possible to say that from a mechanical point of view, the grinding process is less harsh than the milling process and will potentially cause less damage to the fibres through the effects of vibration and the impact of hot metal chips.

Figure 6.26. shows the grinding tests general layout.

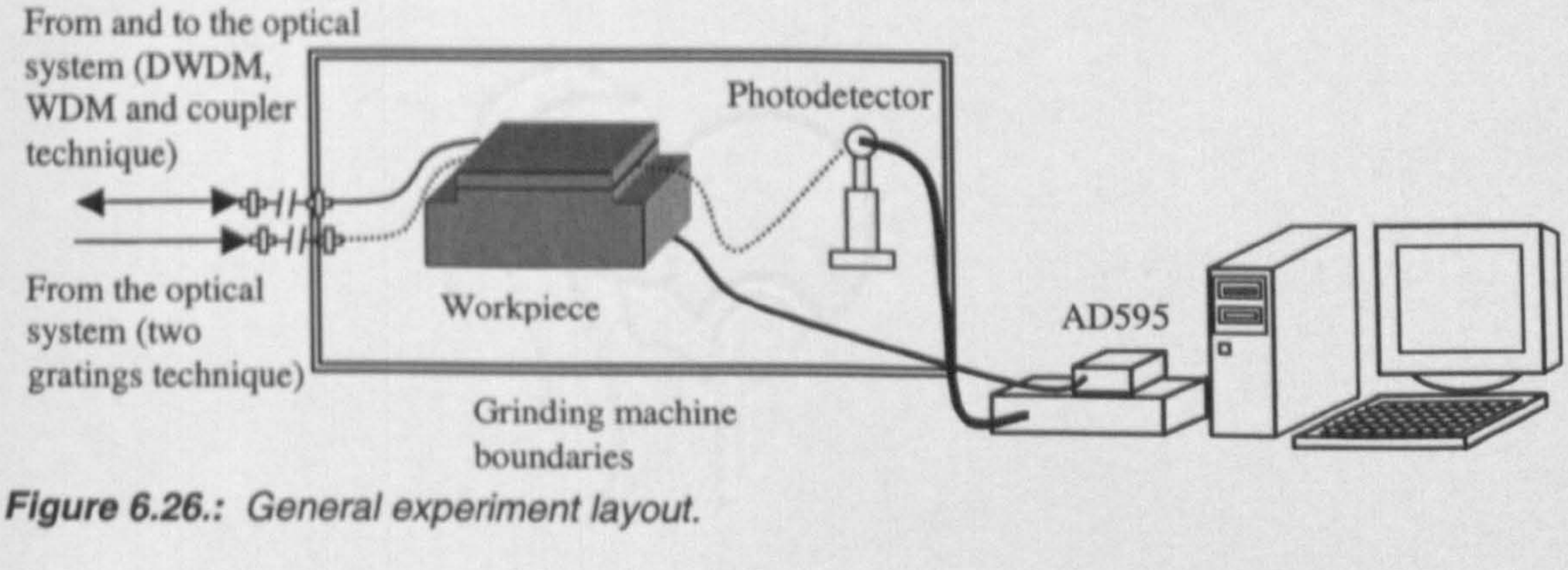

Figure 6.26.: *General experiment layout.*

To save time in setting-up and to ensure repeatable results, the optical systems were tested using the same cap without dismounting the cap or disturbing optical fibres between tests. To achieve this, an extra groove was added so that the FBG grating used for the two gratings technique and

the one used for all the other techniques were located parallel and close together (with an approximate spacing of 0.5mm), the thermocouple was then positioned so it was at the same depth as the gratings and in line with them as shown in figure 6.27..

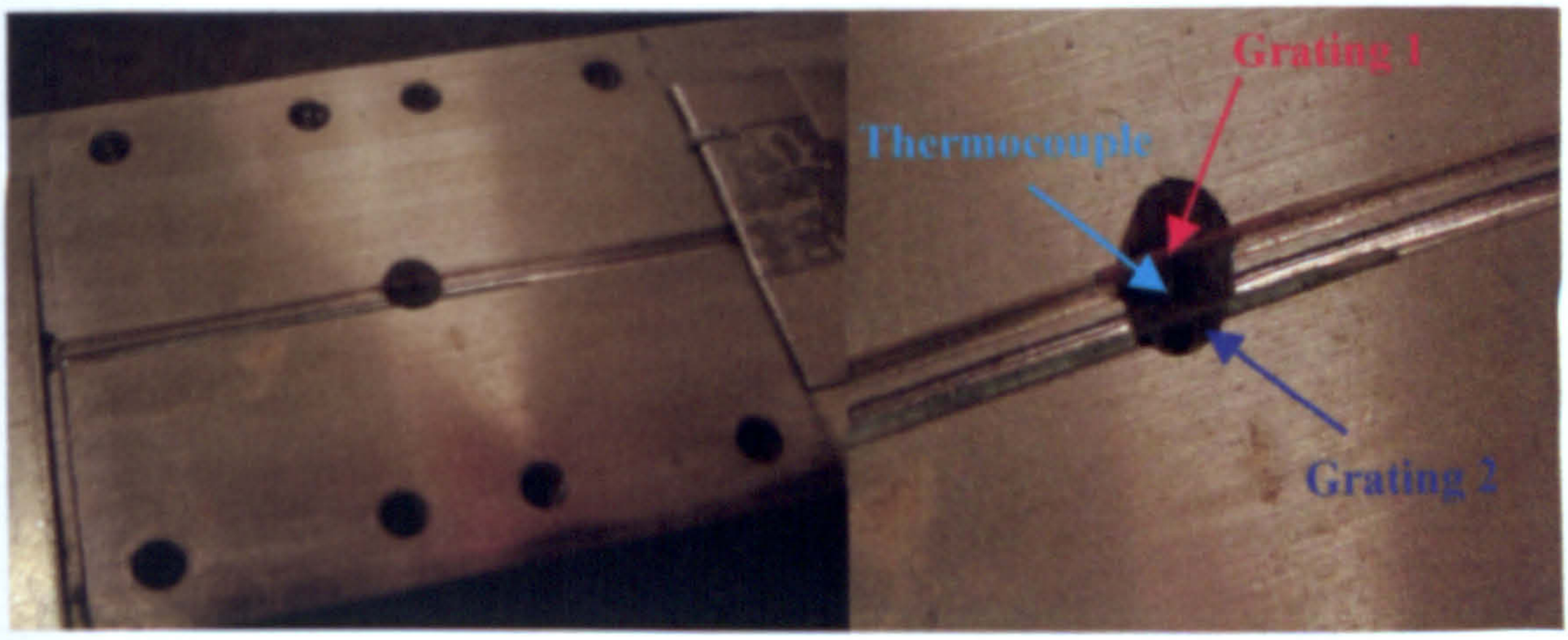

Figure 6.27.: *Sensors arrangement showing the positioning of the two Bragg gratings and of the thermocouple.*

Since the depth of cut used during grinding were very small (a few μm), the workpiece cap was first machined so that the sensors were initially at a depth of 3mm below the grinding wheel. Then each of the optical systems, two gratings, DWDM, WDM and coupler, were tested. The tests were undertaken with an applied 37.5μm depth of cut, however the real depth of cut was approximately 27μm on average. Figure 6.28. details depth of cuts achieved during the tests. Following the tests at 3mm depth the cap was ground so that the sensors were at a depth of 2mm below the surface. The tests were then repeated using an applied cut of 37.5μm for each optical system in the same order as for the first test. The cap was then ground so that the sensors were at a depth of 1mm below the surface and the tests repeated using an applied 37.5μm depth of cut.

This approach to testing allowed the tests to be carried out relatively quickly and without disturbing the sensing elements and the fibres.

Although each applied cut was 37.5µm, the actual cut achieved was significantly less. The reduction in cut was caused by the deflection of the machine tool and grinding wheel. The material remaining due to deflection was then removed prior to testing the next measurement system. This was achieved by passing the grinding wheel over the surface without applying a cut, this process is called spark out.

Test number	Optical device tested	Applied depth of cut (µm)	Actual depth of cut (µm)	Depth of cut achieved after spark out (Initial 3mm from the sensors) (µm)
1	Two gratings	37.5	37	37.5
2	DWDM	37.5	22	28
3	WDM	37.5	35	36
4	Coupler	37.5	30	Grind down to 2mm
5	Two gratings	37.5	28	30
6	DWDM	37.5	32	36
7	WDM	37.5	32	39
8	Coupler	37.5	34	Grind down to 1mm
9	Two gratings	37.5	13	34
10	DWDM	37.5	23	38
11	WDM	37.5	23	39
12	Coupler	37.5	19	41

Figure 6.28.: *Depth of cut recorded during the grinding tests.*

The cutting conditions of the experiment are illustrated on figure 6.29..

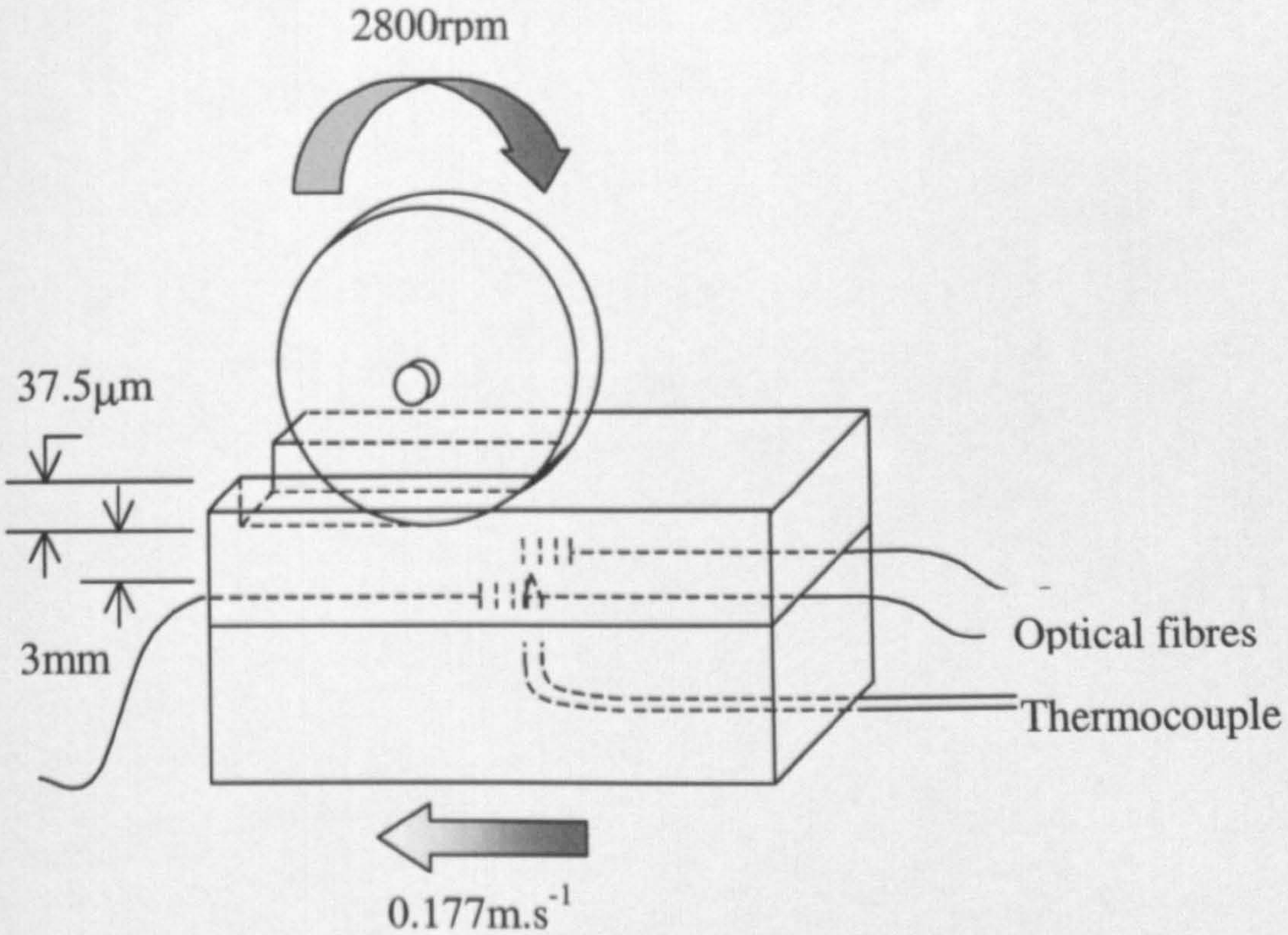

Figure 6.29.: *Grinding test parameters.*

6.3.3. Effect of depth of cut on temperature.

Figures 6.30., 6.31. and 6.32. show the raw data collected by the thermocouple during the tests conducted at a depth below the surface of 3mm, 2mm and 1mm respectively.

Assuming that an average distance difference of 37μm between 2 consecutive cuts had a minor influence on the heat penetration into the workpiece, it was possible to compare the signals recorded by the thermocouples to show the influence of the depth of cut and wheel condition on the temperature within the workpiece. The graphs clearly

showed a large variation in temperature for nominally similar grinding conditions. It was therefore necessary to record the thermocouple signal during each test of the individual optical systems.

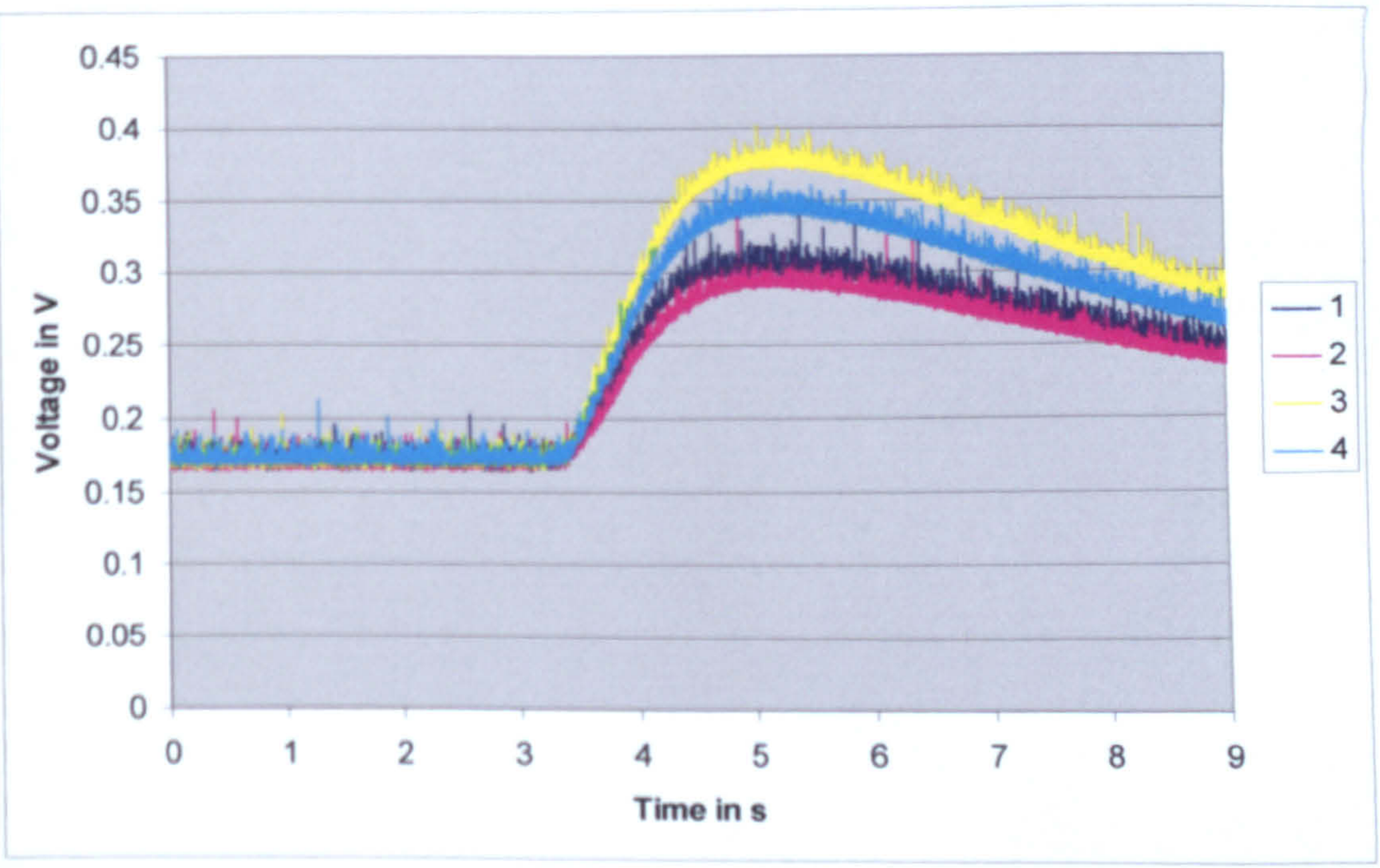

Figure 6.30.: *Effect of the depth of cut at 3mm from the sensor.*

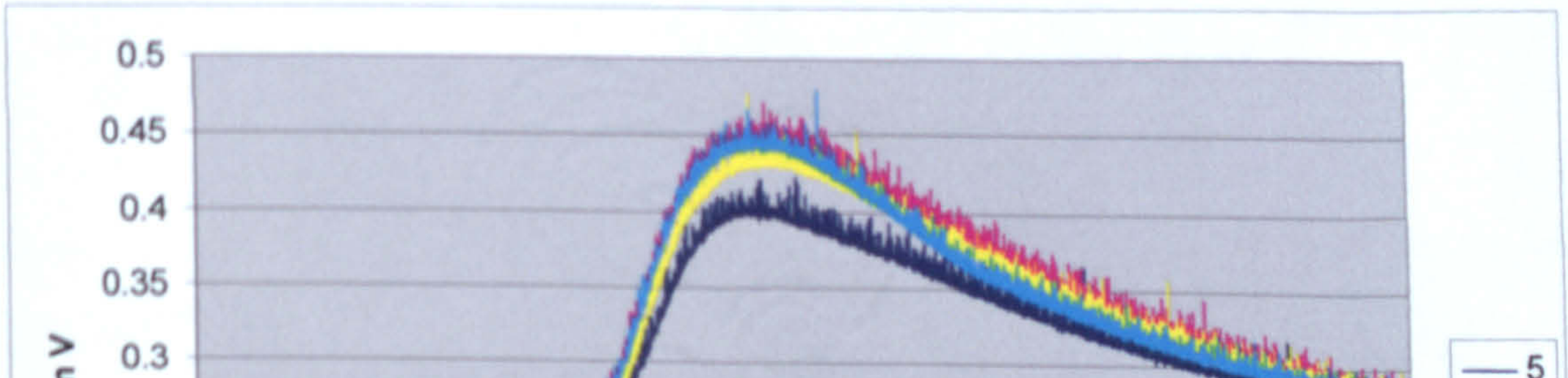

Figure 6.31.: *Effect of the depth of cut at 2mm from the sensor.*

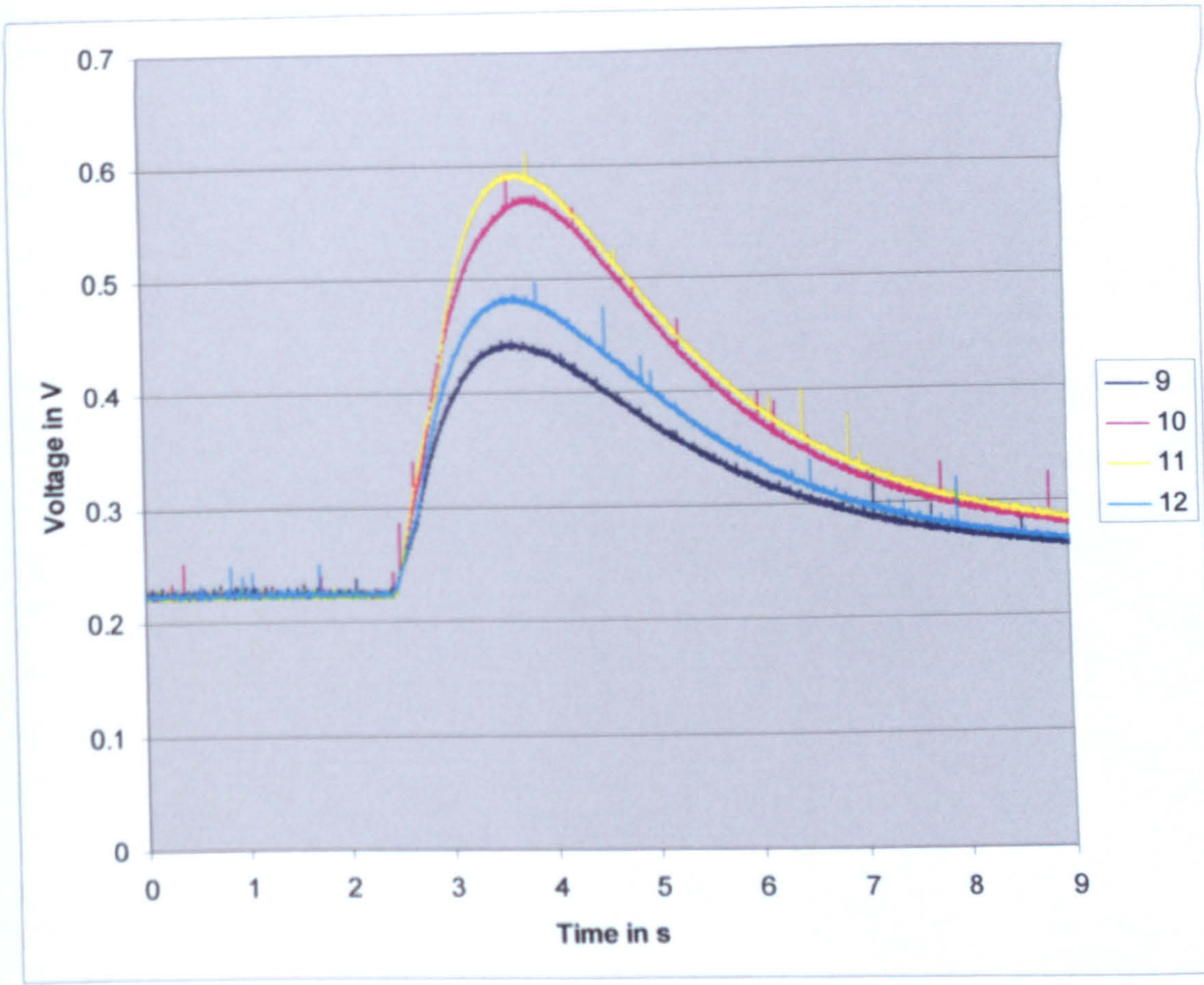

Figure 6.32.: *Effect of the depth of cut at 1mm from the sensor.*

6.3.4. Sampling rate calculation.

As explained before, the sampling rate was calculated so ten data points were recorded while the grinding wheel was travelling above the fibre Bragg grating. Knowing the length of a grating (1mm) and the average speed of the wheel ($0.177 m.s^{-1}$), it was possible to determine how long the grinding wheel was staying above the sensor, this time interval was found to be 0.00283s and corresponded to a minimal sampling rate of 177Hz. Then knowing that 10 points were necessary during that interval of time, it was

possible to determine the recommended sampling rate, this was found to be 1770Hz, which is within the capabilities of the sensing devices.

6.3.5. Effect of electrical noise.

As during the milling experiments, the electrical noise created by the machine or by other machine was found to have a great influence on the thermocouple signal. Figure 6.33. illustrates that problem.

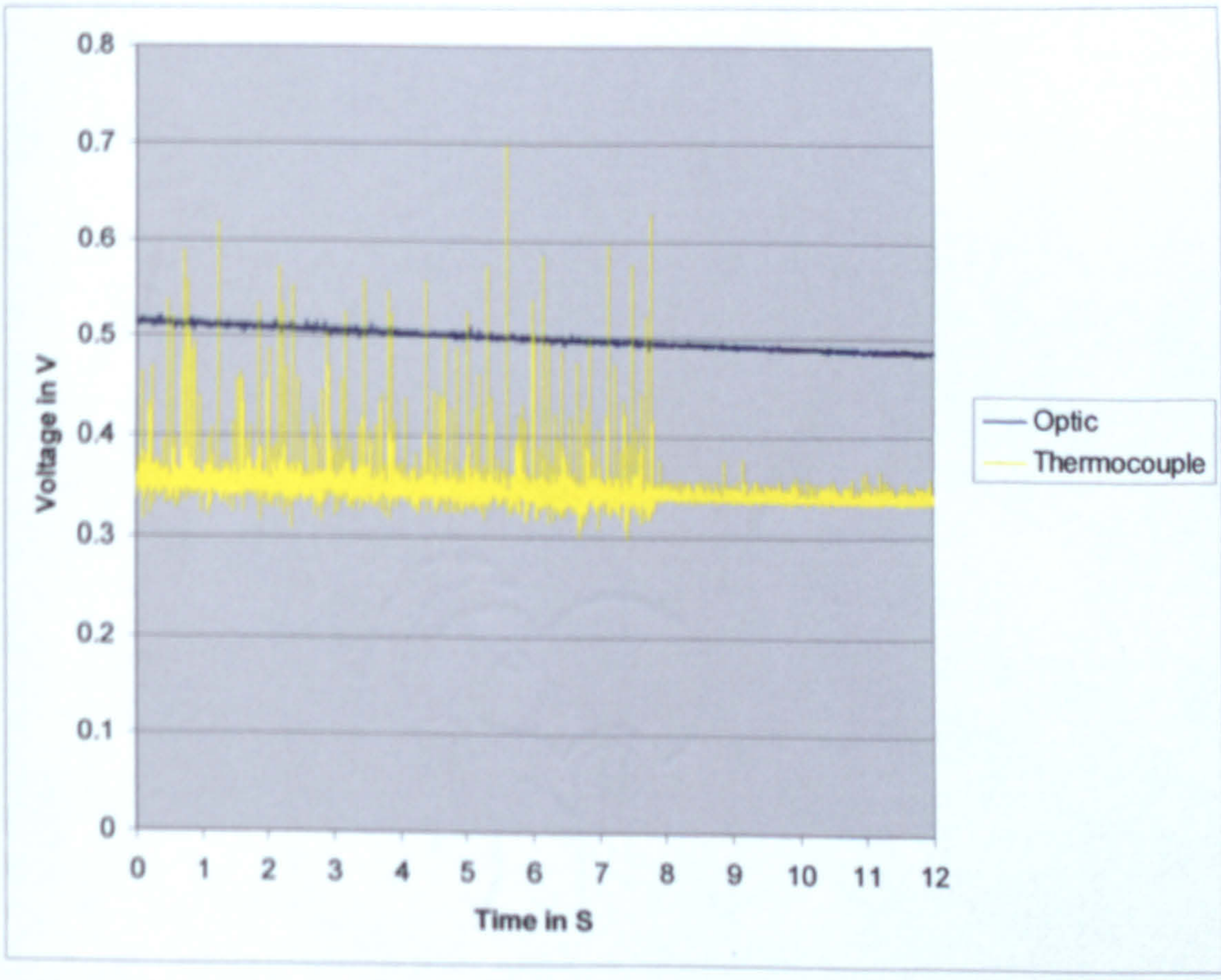

Figure 6.33.: *Other machines effect on the thermocouple signal.*

Figure 6.33. illustrates the typical noise level associated with a running electric motor. During recording of test data, another machine tool in the laboratory was inadvertently switched on and then switched off after a

further 8 seconds of recording. The effect on the thermocouple signal was dramatic and as expected the optical signal was not influenced by the changes. The noise of the thermocouple signal dramatically increased when the other machine was running, the peak-to-peak noise level increasing from 0.0146V to 0.2685V. During the same time, the peak-to-peak noise level of the optical systems stayed constant approximately 0.002V. This clearly illustrates the advantages of optical techniques over the thermocouple technique for temperature measurements in an electrically noisy environment.

6.3.6. Grinding tests results.

The following figures (figure 6.34. to figure 6.45.) present the raw data recorded for all grinding tests. The data for each of the optical systems are presented separately alongside the thermocouple data so as to allow direct comparison. Figures 6.34., 6.35. and 6.36. present the output voltage of the two gratings based measurement system and the voltage output of the thermocouple measurement system for a depth below the surface of 3mm, 2mm and 1mm respectively. Figures 6.37., 6.38. and 6.39. present the output voltage of the DWDM based measurement system and the voltage output of the thermocouple measurement system for a depth below the surface of 3mm, 2mm and 1mm respectively. Figures 6.40., 6.41. and 6.42. present the output voltage of the WDM based measurement system and the voltage output of the thermocouple measurement system for a depth below

the surface of 3mm, 2mm and 1mm respectively. Figures 6.43., 6.44. and 6.45. present the output voltage of the coupler based measurement system and the voltage output of the thermocouple measurement system for a depth below the surface of 3mm, 2mm and 1mm respectively.

6.3.6.a. Two gratings technique results.

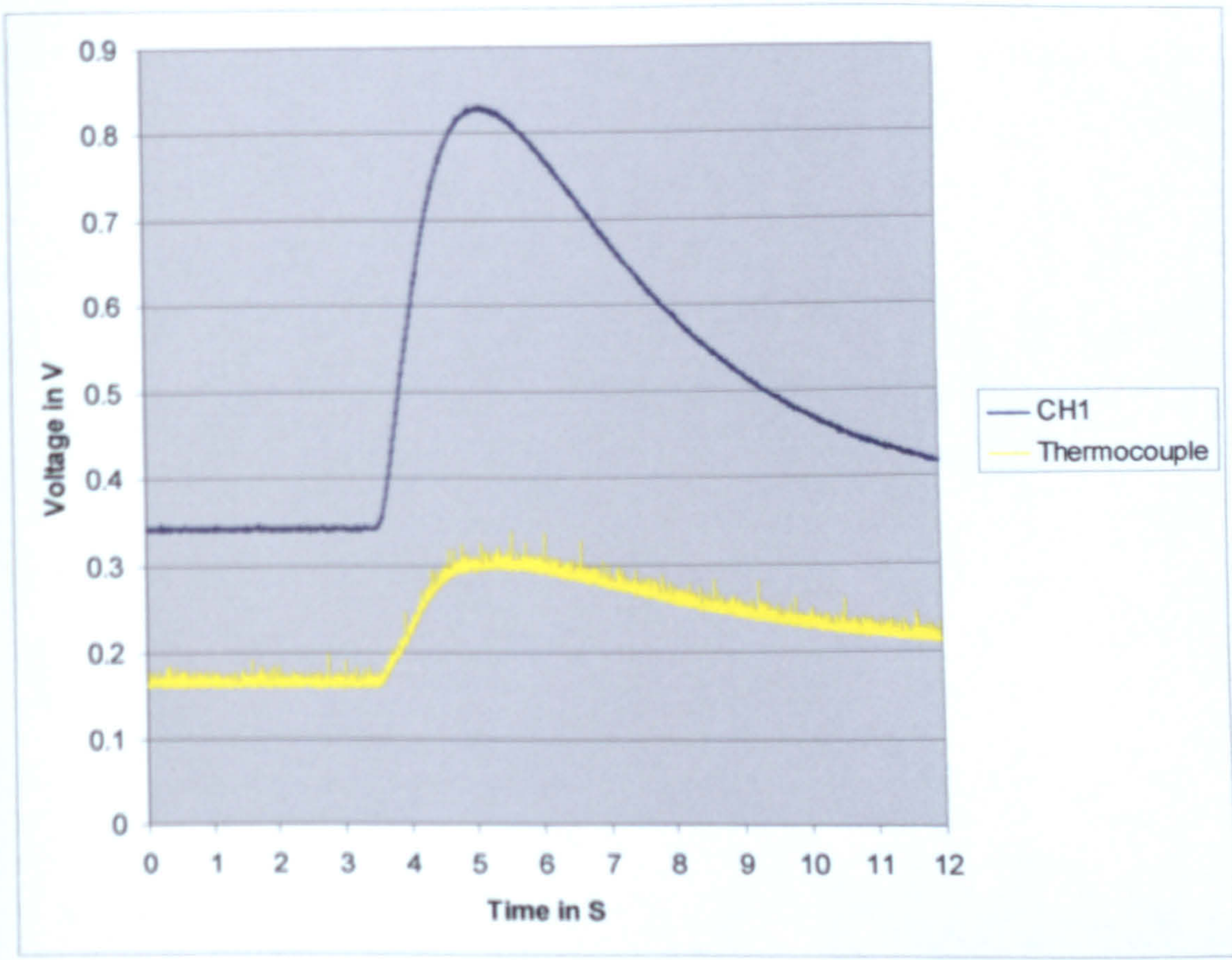

Figure 6.34.: *Raw data for the two gratings and the thermocouple techniques for test 1.*

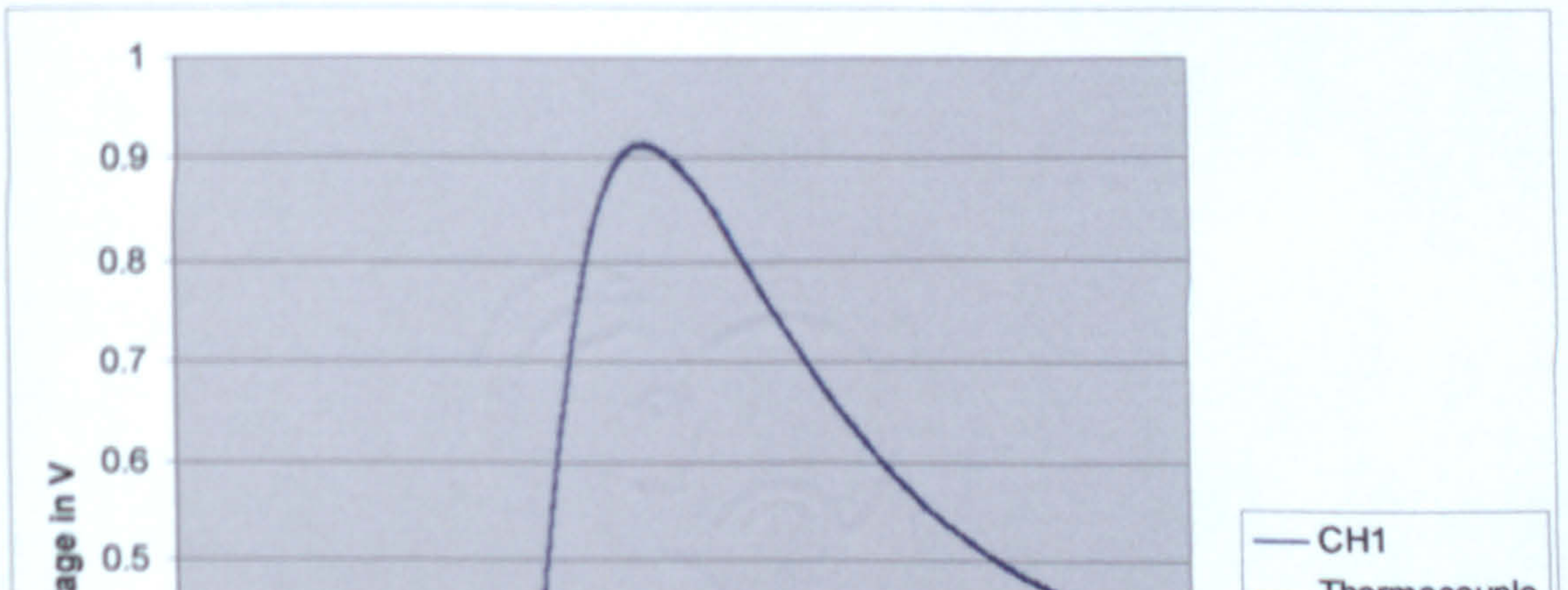

Figure 6.35.: *Raw data for the two gratings and the thermocouple techniques for test 5.*

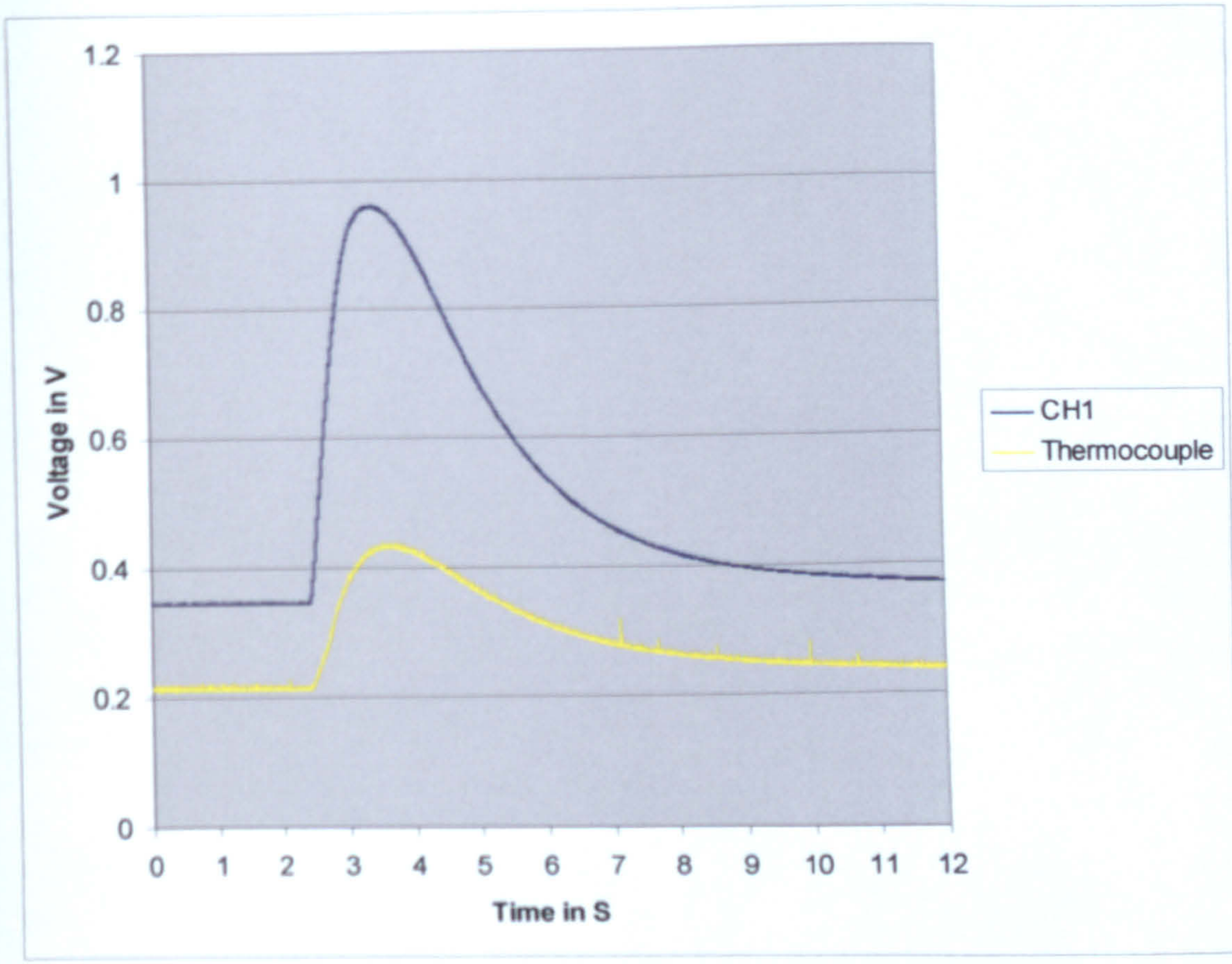

Figure 6.36.: *Raw data for the two gratings and the thermocouple techniques for test 9.*

6.3.6.b. DWDM technique results.

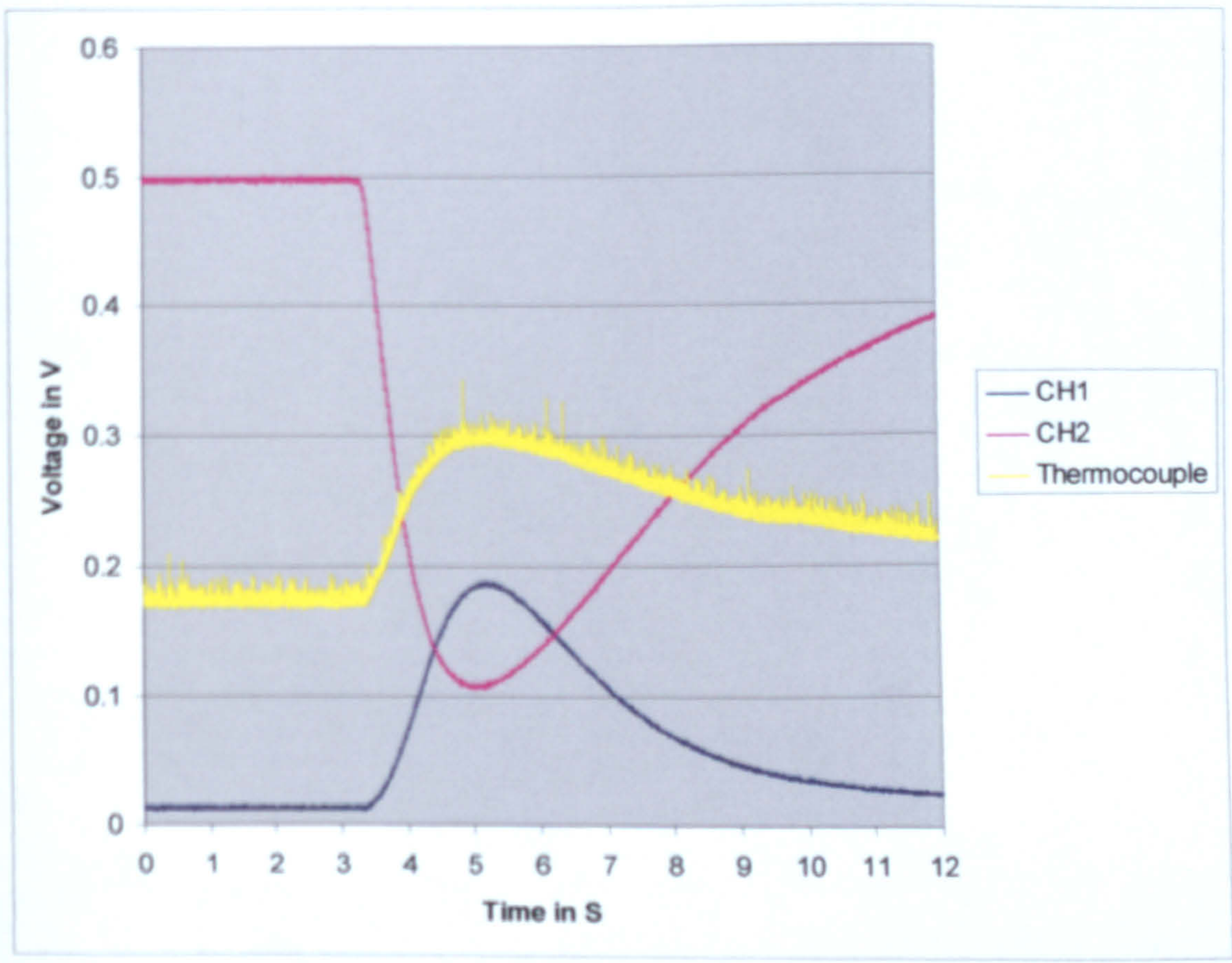

Figure 6.37.: *Raw data for the DWDM and the thermocouple techniques for test 2.*

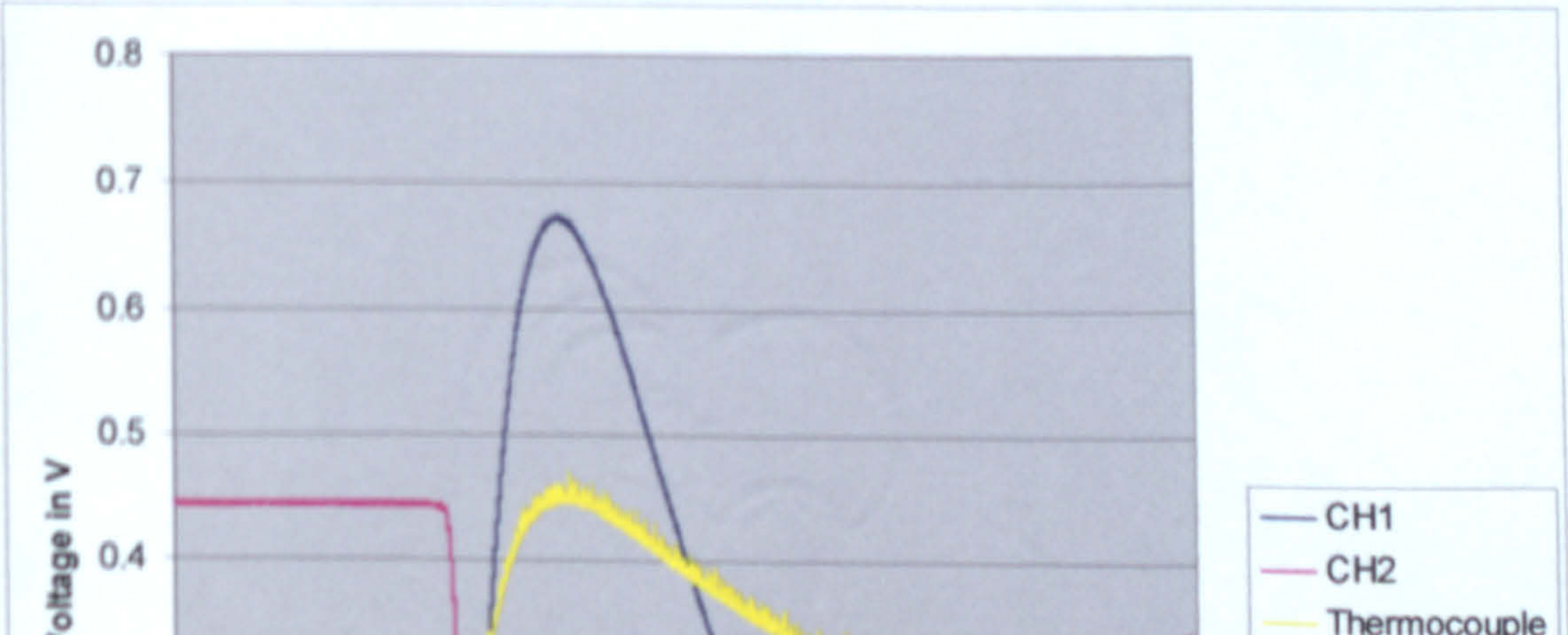

Figure 6.38.: *Raw data for the DWDM and the thermocouple techniques for test 6.*

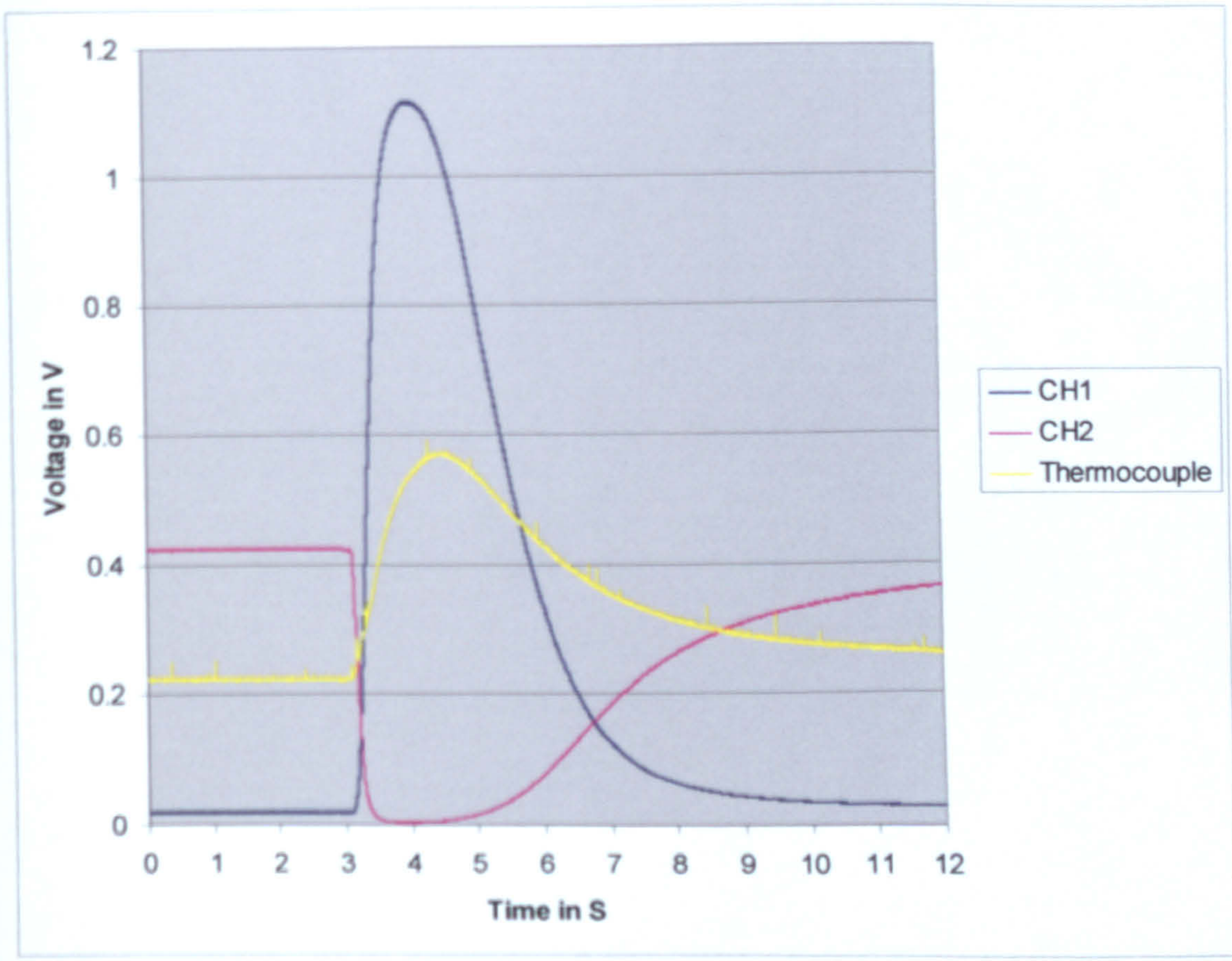

Figure 6.39.: *Raw data for the DWDM and the thermocouple techniques for test 10.*

Note:

CH1 represents the CH57 (centred at 1531.92nm) output of the DWDM and

CH2 represents the CH59 (centred at 1530.37nm) output of the DWDM.

6.3.6.c. WDM technique results.

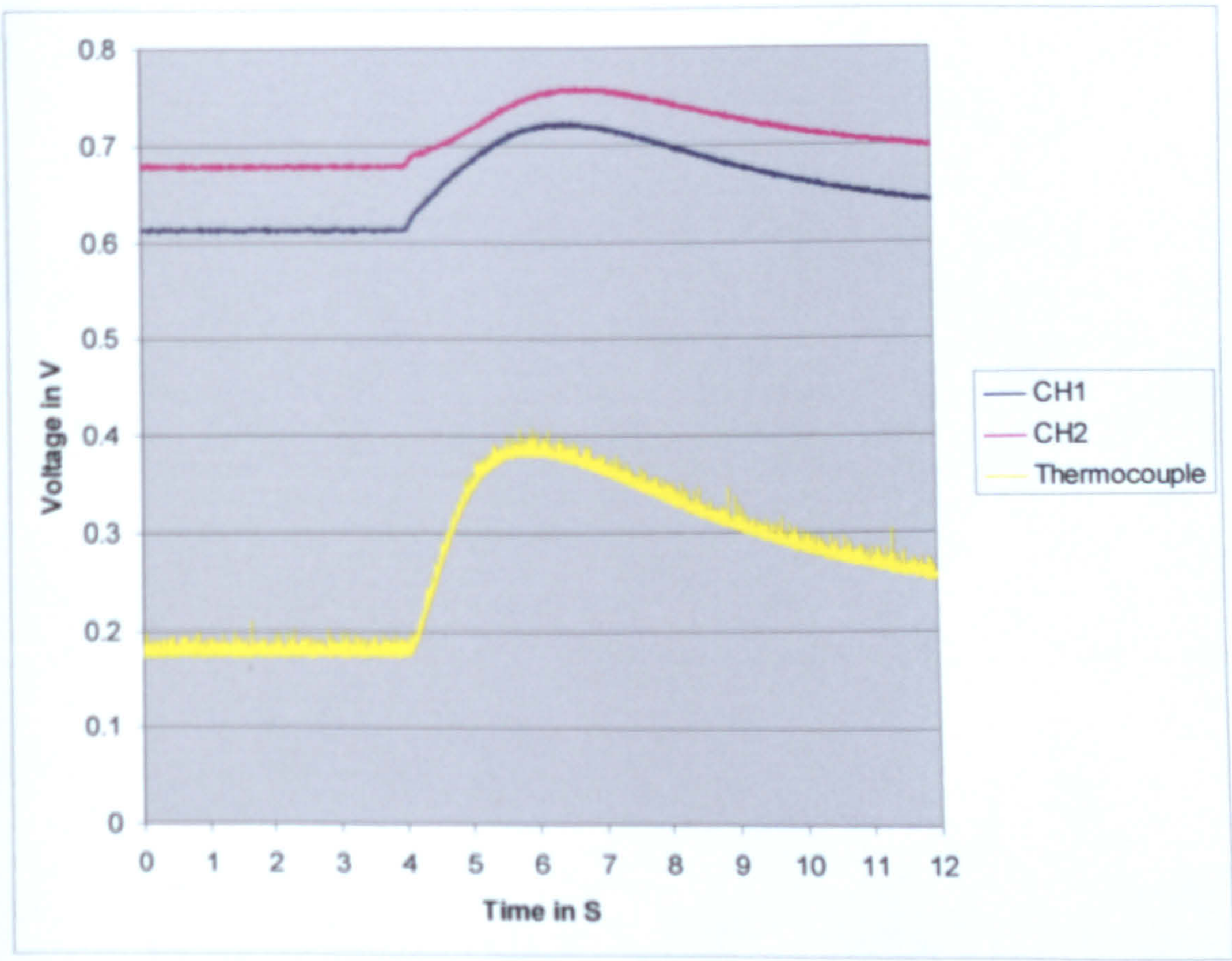

Figure 6.40.: Raw data for the WDM and the thermocouple techniques for test 3.

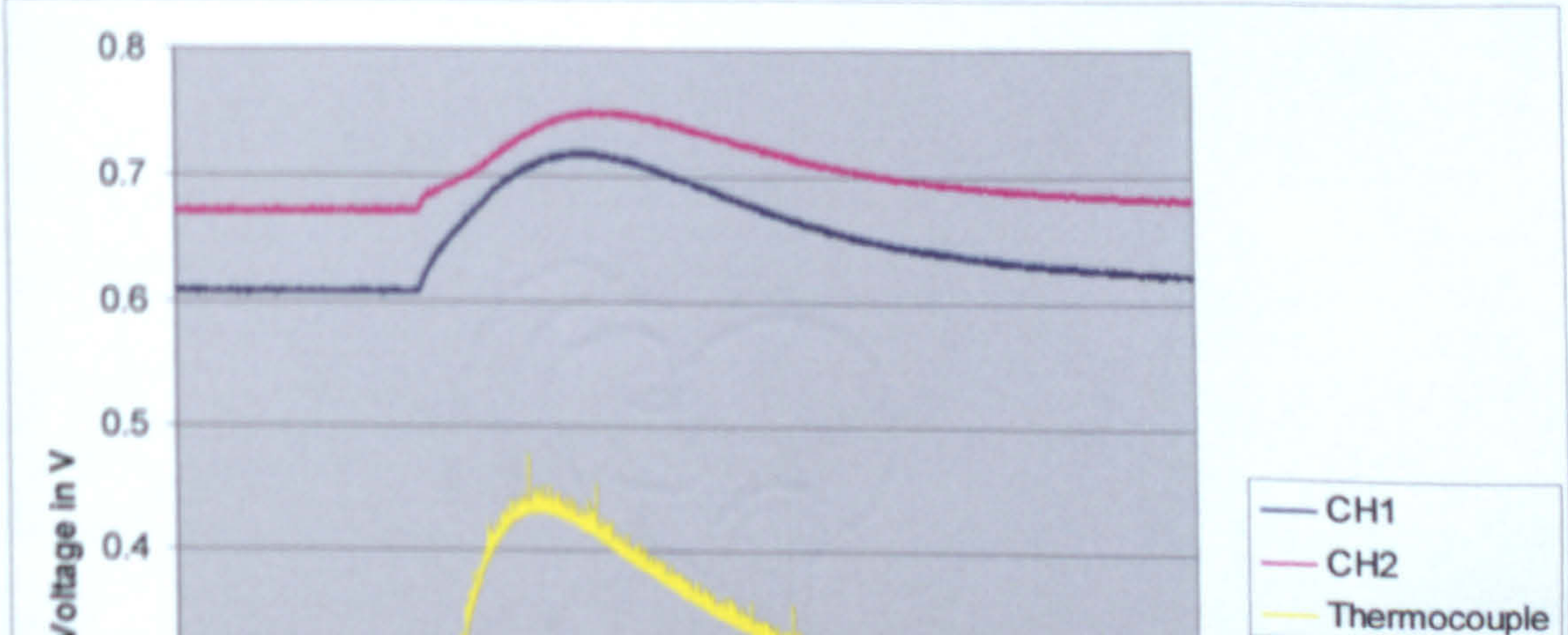

Figure 6.41.: Raw data for the WDM and the thermocouple techniques for test 7.

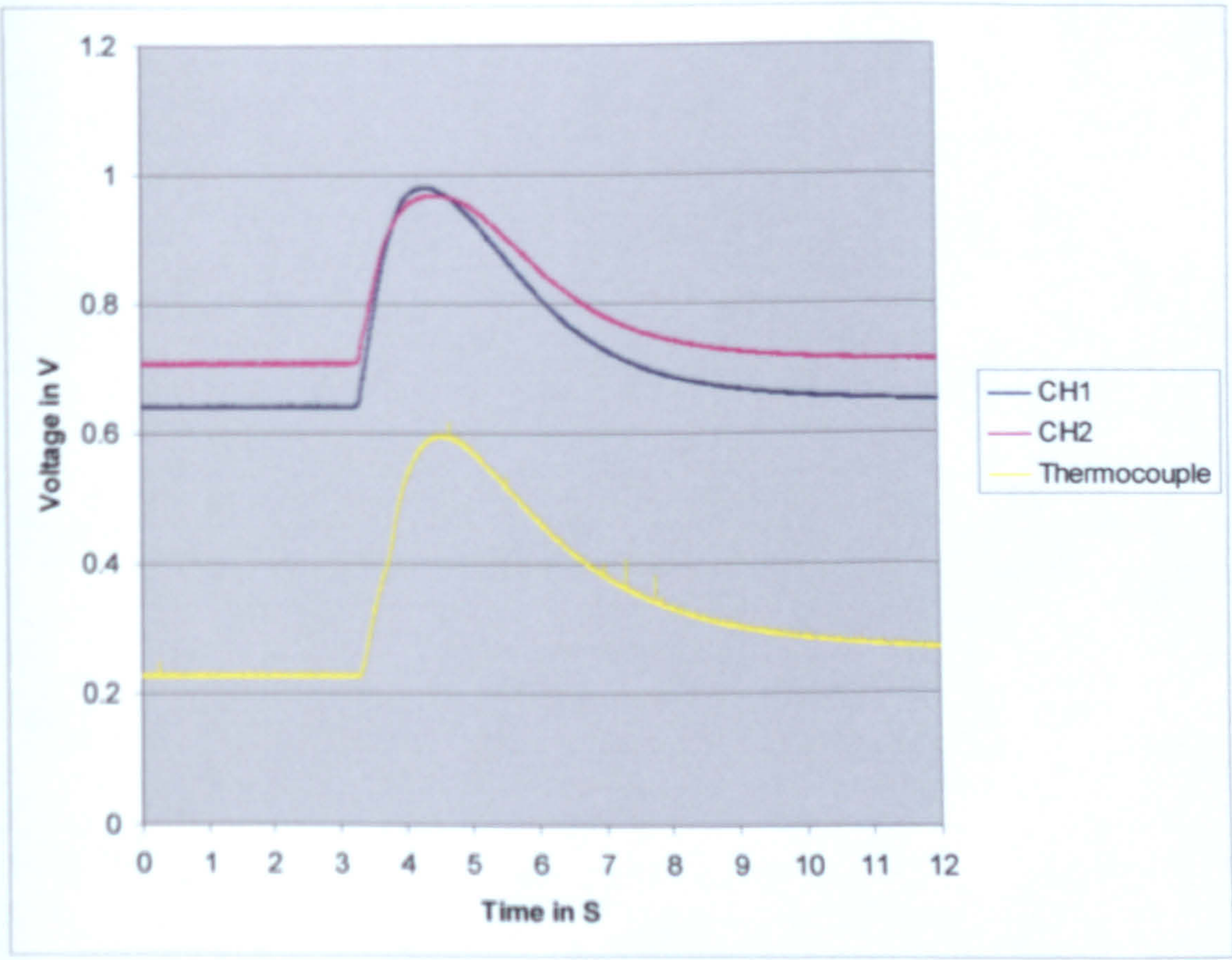

Figure 6.42.: *Raw data for the WDM and the thermocouple techniques for test 11.*

6.3.6.d. Coupler technique results.

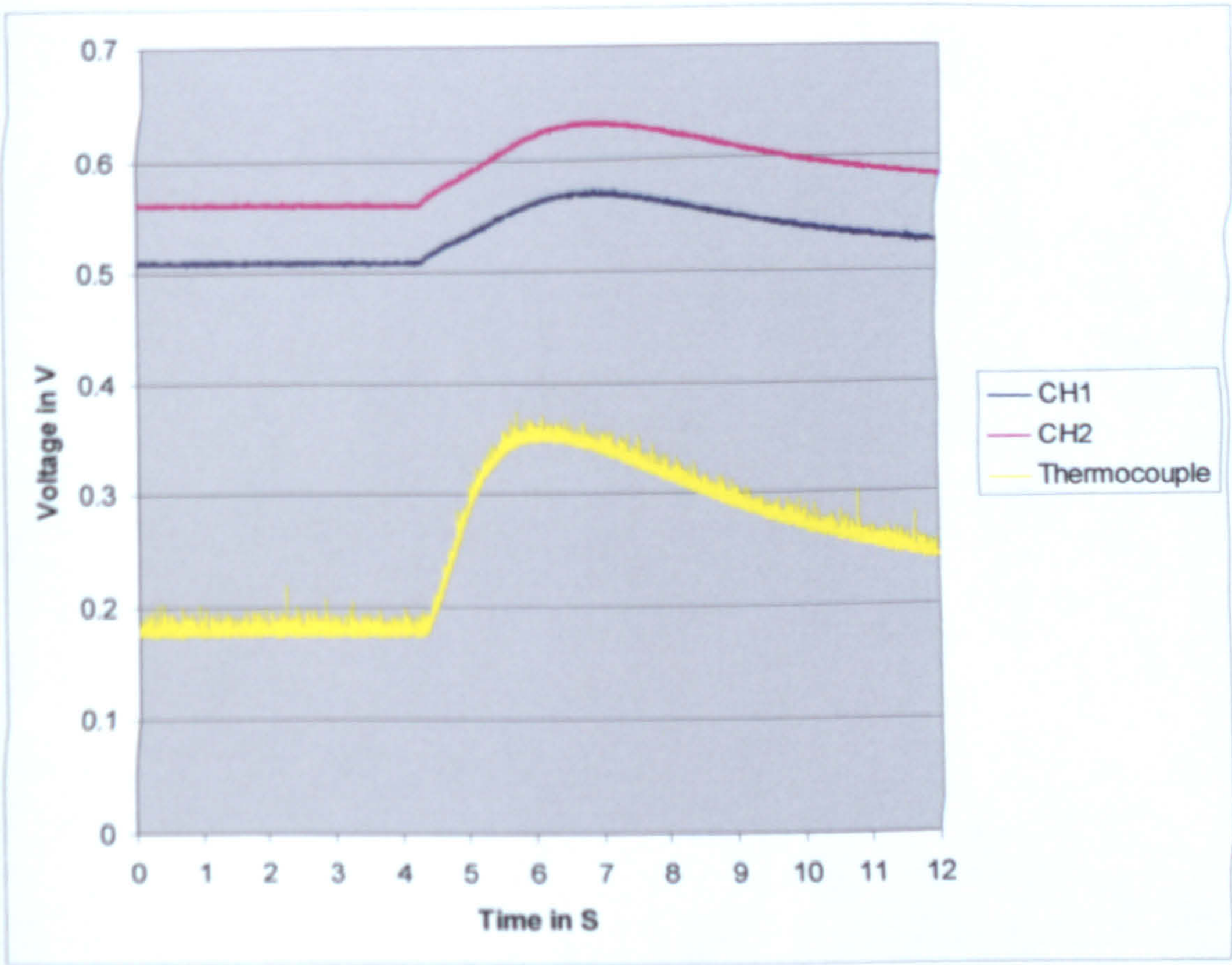

Figure 6.43.: *Raw data for the coupler and the thermocouple techniques for test 4.*

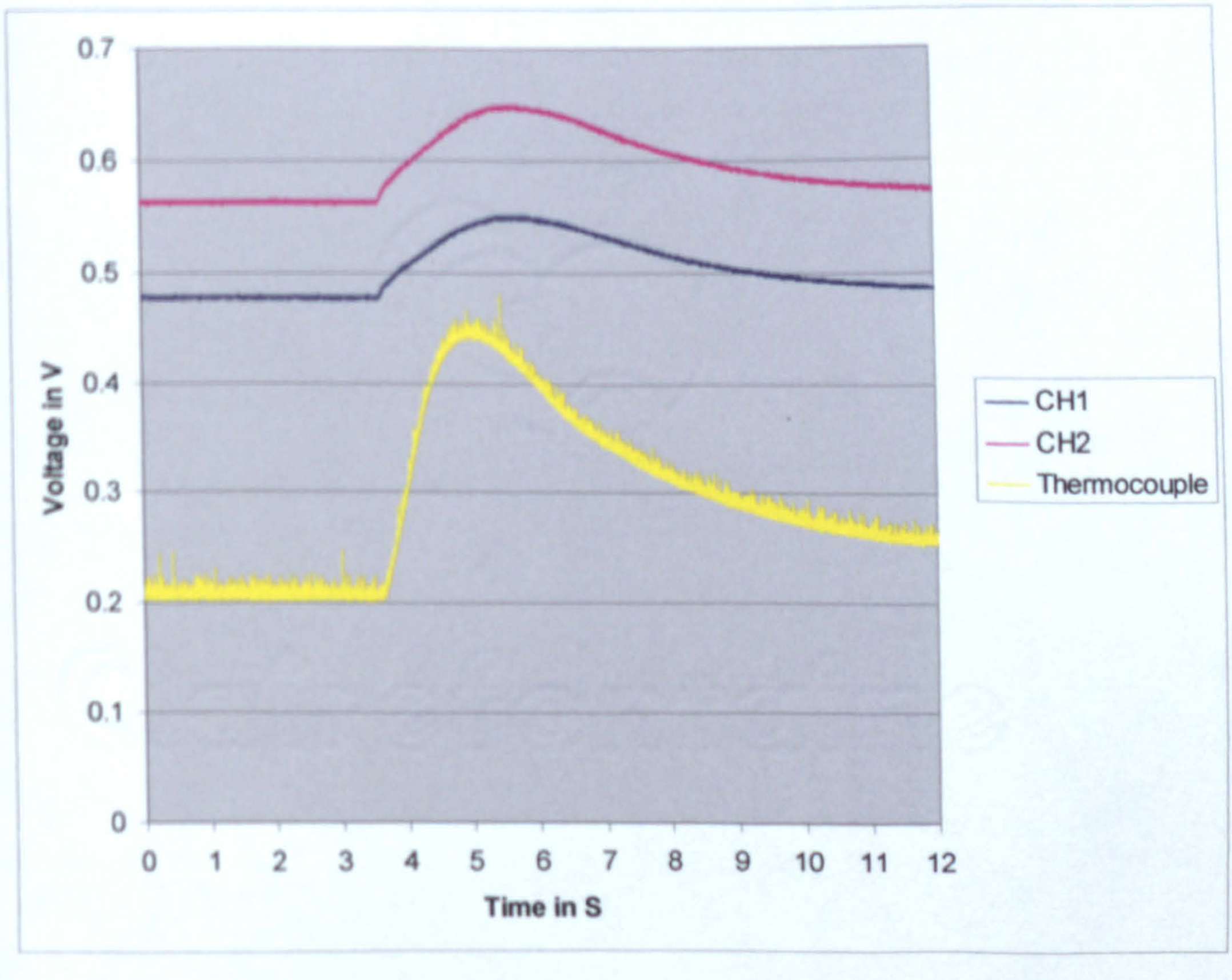

Figure 6.44.: *Raw data for the coupler and the thermocouple techniques for test 8.*

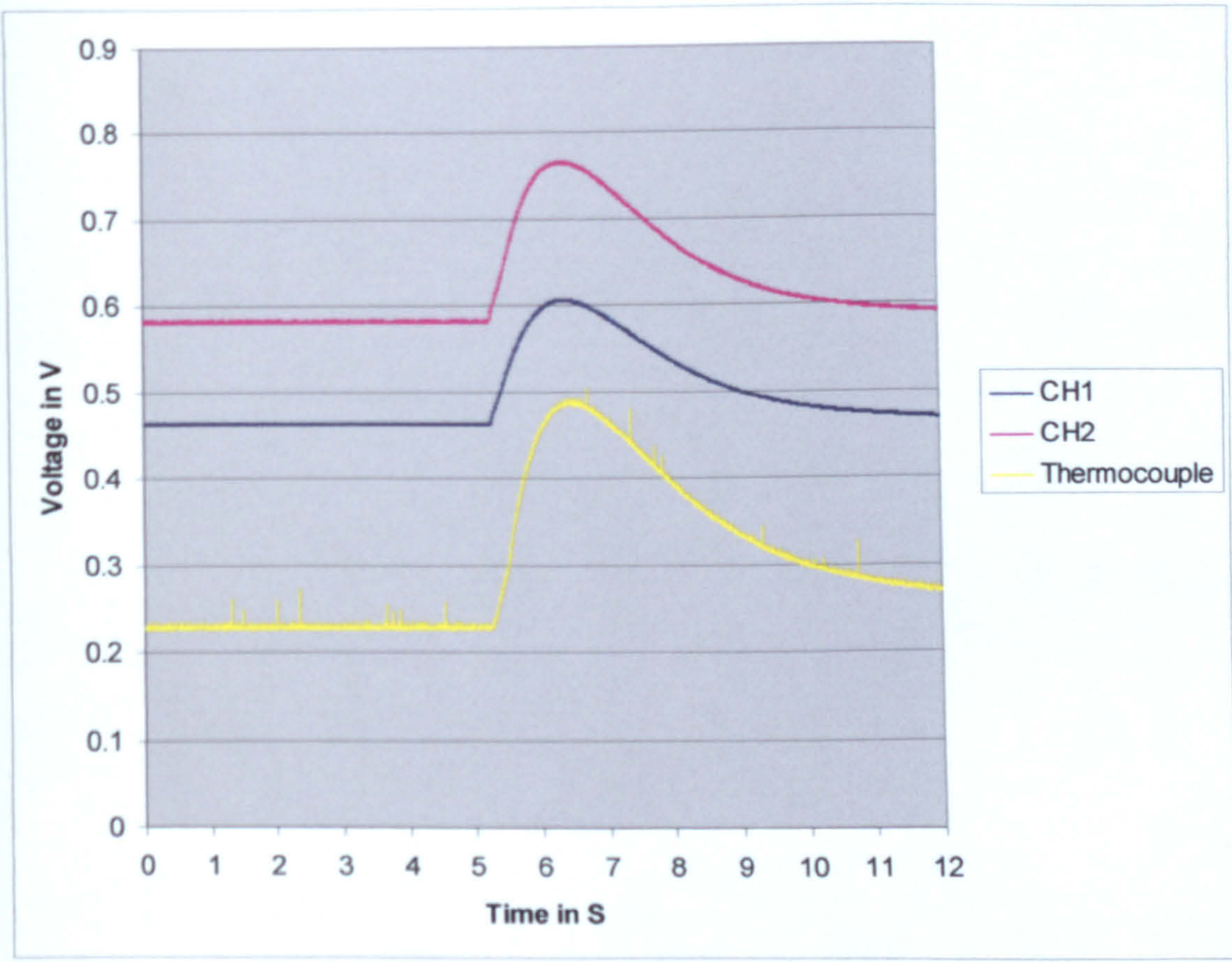

Figure 6.45.: *Raw data for the coupler and the thermocouple techniques for test 12.*

6.3.7. Summary of results.

First the peak to peak electrical noise on the signal was calculated by making the difference between maximum and minimum signal voltage before machining i.e. in a steady state.

Device	Two gratings	DWDM	WDM	Coupler
Thermo-couple (V)	0.031433	0.041351	0.037384	0.046463
CH1	0.004044	0.004654	0.005264	0.005722
CH2	N/A	0.006104	0.007095	0.006256

Figure 6.46.: *Peak to peak noise levels of the sensor signal (in Volts).*

The range of the signals was calculated as follows. First a moving average trend line was added to obtain a more accurate reading of the data. Then the minimal signal and maximum signal were found using simple spreadsheet functions and the difference was calculated.

Device	Two gratings	DWDM	WDM	Coupler
CH1	0.487725	0.173279	0.109131	0.063218
CH2	N/A	-0.38985	0.07927	0.069237
Thermo-couple	0.136025	0.127651	0.2092	0.175948

Figure 6.47.: *Range of the signals at 3mm (in Volts).*

Device	Two gratings	DWDM	WDM	Coupler
CH1	0.574409	0.655471	0.109775	0.07276
CH2	N/A	Saturated	0.077674	0.084812
Thermo-couple	0.197663	0.249779	0.230057	0.240414

Figure 6.48.: *Range of the signals at 2mm (in Volts).*

Device	Two gratings	DWDM	WDM	Coupler
CH1	0.615184	1.095062	0.338246	0.142952
CH2	N/A	Saturated	0.258629	0.183563
Thermo-couple	0.219383	0.347398	0.3691	0.259373

Figure 6.49.: *Range of the signals at 1mm (in Volts).*

Device	Two gratings	DWDM	WDM	Coupler
Thermo-couple	10	10	10	10
CH1	28.55	23.77	6.38	4.04
CH2	N/A	N/A	4.72	4.85

Figure 6.50.: *Average sensitivity in mV/°C.*

Note:

As expected the DWDM did not present a linear response, this was because the spectrum of DWDM channels were not linear at the

wavelength used (figure 4.27.). However, this problem can be compensated by choosing a Bragg grating with a slightly bigger Bragg wavelength (1530.88nm ±0.02nm). The same effect was noticeable for the WDM and coupler technique where the sensitivity was linear until the 3rd grinding test. The response spectra of the devices can be read in chapter 4.7.3.. All devices were linear for a limited wavelength range beyond which they were not so when the temperature induced to the sensing grating caused it to excess that range the sensor did not react linearly anymore. However this problem can be solved using the spectra of the optical devices plotted in chapter 4.7.3..

If a K-type thermocouple reacted at the same speed for a given heat pulse, then it would be possible to compare its response time to the response time of an optical system in the same condition to determine which one was the fastest and how much faster it was to react to that specific heat pulse.

Device	Two gratings	DWDM	WDM	Coupler
Thermo-couple	1.82	1.85	1.89	1.81
CH1	1.66	1.81	2.37	2.55
CH2	N/A	1.81	2.65	2.55

Figure 6.51.: *Response speed of the sensors for the experiments 1, 2, 3 and 4 (in seconds).*

Figure 6.51., tabulates the response time measured on the figures 6.34. to 6.45.. In these cases, it is possible to say that the two grating technique

was 8.8% faster than the thermocouple, the DWDM technique was 2.2% faster than the thermocouple, the WDM technique was 32.8% slower on average than the thermocouple and the coupler technique was 40.9% slower than the thermocouple. However, further tests need to be done using a step input heat source to quantify the real values of the reaction time of the sensors.

6.4. Conclusion.

Technique	Thermocouple	Two gratings	DWDM	WDM	Coupler
Speed	****	*****	*****	***	**
Range	***	*****	****	**	**
Noise	*	*****	*****	*****	*****
Sensitivity	***	*****	*****	**	**
Calibration	*****	****	***	**	***
Strength	****	**	****	****	****
Set-up time	****	***	****	****	****
Price	*****	****	**	***	****

Figure 6.52.: Technique comparison. *Legend:*

*****	*Very good*
****	*Good*
***	*Average*
**	*Poor*
*	*Very poor*

1. The best technique for low temperature sensing application (limited to approximately 65°C due to saturation) is the two grating technique

because it is the most sensitive of the systems tested and also offers quite simple calibration as described in chapter 4. However the main drawback of this technique is its mechanical strength according to figure 6.52. and section 6.2.3.a.1.. Since the optical signal has to travel through all the workpiece, this technique is harder to set up than the other optical techniques that offer single end-sensing capabilities. However the main advantage is that this particular sensor is so sensitive that it can detect minor temperature changes not detectable with the other systems. Another problem inherent with this technique is the requirement to manufacture two gratings to a high tolerance in Bragg wavelength and bandwidth. The wavelength accuracy required is in the order of 0.05nm. This is hard to achieve however the problem can be overcome by using a tuneable grating. The two grating technique would appear to be a major improvement of the thermocouple technique that has been used to date.

2. The second choice for sensing temperature, would be the DWDM technique because: it is very sensitive and easy to install. The DWDM based sensor is less sensitive than the two grating technique but more sensitive than the thermocouple technique (see figure 6.15. bumps in the 26s area). Since the DWDM technique offers end-sensing capability, it is very easy to install. The setting up time of the sensing grating used for this device and for the WDM and coupler technique is approximately five minutes. It is even easier to install than a thermocouple. While, as expected, channel 59 (centred at 1530.37nm) saturated quite quickly (see figure 6.37., figure 6.38. and figure 6.39), channel 57 (centred at 1531.92nm) did not saturate. In fact saturation of channel 57 would not

occur until approximately 200°C, however the test to check the saturation temperature of this device were not undertaken so as to avoid damaging the sensing fibre. The main drawback of this application is that at low temperature (up to approximately 42°C) the output should be read on channel 59 and for higher temperatures on channel 57. This can be explained by the shape of the channel spectra as previously explained in chapter 3.

3. The third choice is the thermocouple technique because, once the amplifier is built and the thermocouples are calibrated, it is very user friendly and its results are easily read. However the installation time is very long since it is hard to overcome all the electrical noise generated by the surrounding so a lot of time is spent trying to insulate the sensor, its cable, the amplifier and even the power supply. Even when everything is well insulated any changes of the environment (another machine on for example) can have devastating effects on the signal as previously discussed (see figure 6.33.). Since an expensive broadband light source is required for the optical sensor, the main advantage of the thermocouple over the other optical sensors is in its price.

4. The WDM technique would be the fourth choice. It is less sensitive than the thermocouple technique so does not improve on the existing thermocouple technique in terms of sensitivity/accuracy however it is a reliable sensor. However the main problems identified with this technique may be attributed to the choice of WDM coupler used in this instance. It would be very interesting to use a WDM coupler with another wavelength

band to see the effect the choice of the WDM coupler has on the sensing signal. Due to the WDM spectral response, the WDM technique would be more suitable for a higher temperature range (between 50°C and fibre destruction) than the one detected during this grinding application (between 20°C and 60°C).

5. As expected the coupler technique is the worst of the sensors since, as explained previously in chapter 3, in theory, the coupler should not provide an intensity change for a change in wavelength. However this technique has been shown to work correctly.

References.

1. "Signal Conditioning & PC-based Data Acquisition", Second edition handbook by Iotech, 1998.

2. P. M. B. Walker (general editor), "Chambers Science and technology dictionary", W & R Chambers ltd, 1994.

Chapter 7: Conclusion and future work.

7. Conclusion and future work.

7.1. Conclusion.

A wide range of optical fibre temperature sensors have been developed for measurement of internal temperature of a workpiece for milling and grinding process. The immunity of these sensors to harsh environments can make them ideally suited to applications where interferences from external parameters are a significant problem e.g. severe electrical noise, radiation, rf interference etc.. Direct comparison has been made to thermocouples throughout the investigations in this thesis. However the performance of the optical sensors actually supersede the performance of the thermocouple.

This work has shown that it is possible to measure temperature accurately during harsh machining processes by using optical sensors based on fibre Bragg gratings. However the main drawback of the optical systems is the price. The equipment used to build an optical sensor based on fibre Bragg grating is more expensive than the equipment used for thermocouple based sensing. But overall, some optical techniques, such as the two gratings and the DWDM based sensors, proved to be more effective than normal k-type thermocouples for measuring temperature. The optical temperature sensors developed, offer the following advantages compared to thermocouple:

- higher sensitivity (figure 6.50.).

- faster response time (figure 6.51.).
- good repeatability.
- small signal noise levels and low sensitivity to externally generated electrical noise (figure 6.33.).
- ease of use.
- possible harsh environment capabilities where other conventional sensors would fail.

Of the optical systems tested, two offered greater sensitivity and higher speed of response than thermocouples. All four optical systems exhibited less noise than the thermocouple based measurement systems. Two of the optical systems are new and the other two were improvements of existing designs.

7.2. Future work.

The ideas and techniques presented in this thesis could be further extended to allow distributed measurement.

7.2.1. Distributed sensing.

Using the same principles of signal demodulation, it is possible to achieve distributed sensing. The following optical circuit arrangements (figure 7.1.) will allow for distributed sensing.

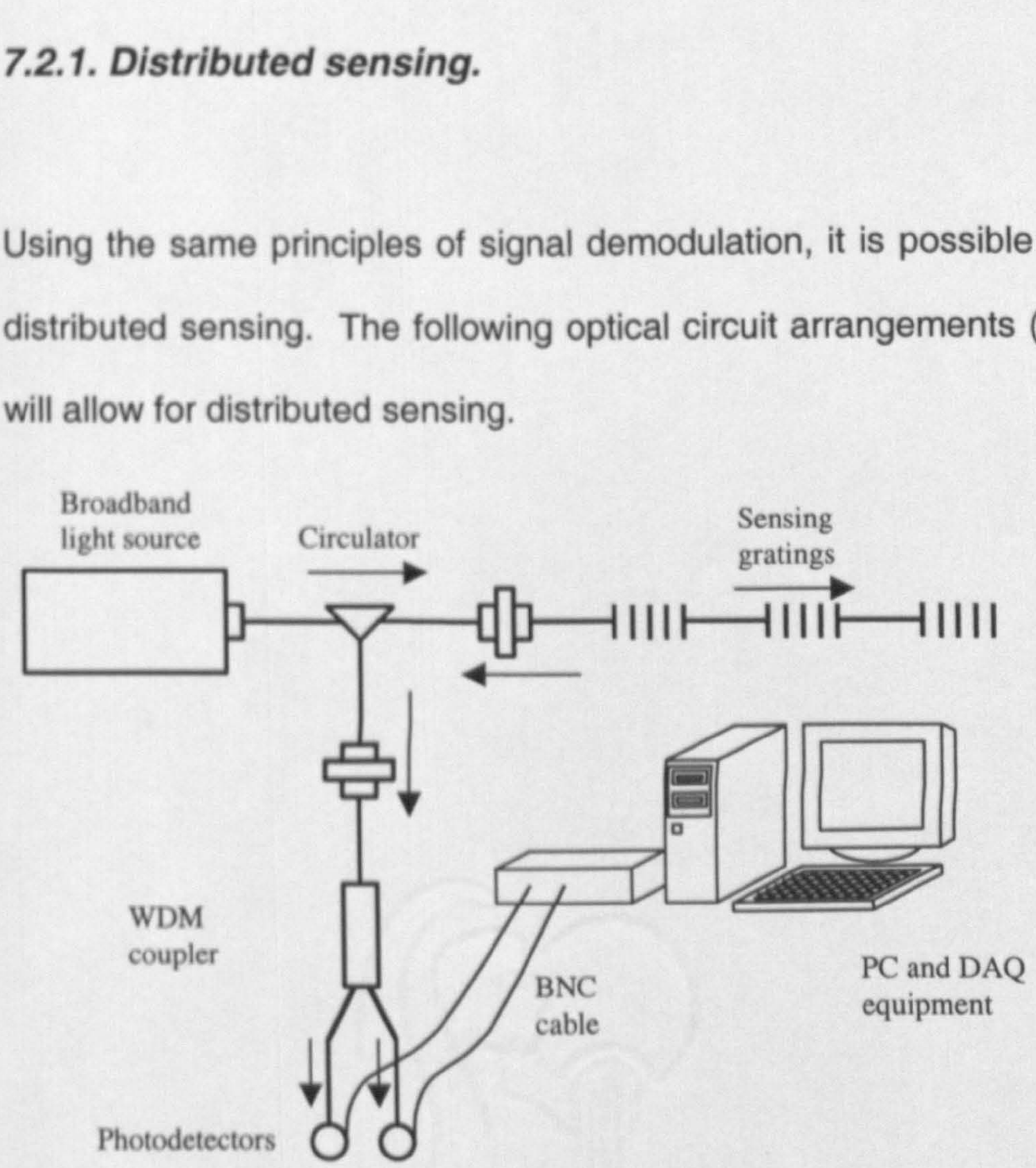

Figure 7.1.: *WDM coupler system similar to the set-up used by Lee et al [1].*

It is possible to achieve multiple sensing using the same WDM coupler. Since the wavelength range of the light source is very broad for this application and since the WDM coupler used allows a range from 1510nm to 1550nm, it is possible to achieve multiple sensing by choosing sensing

gratings at 1520nm, 1530nm, 1540nm etc. for example. Hence the gratings will not interfere with each other and clear readings are possible. Also by using different reflectivity, it is possible to determine which grating is active (reflectivity of 50%, 70% and 90% for example) since the optical power reflected will vary for each grating. However the main problem of this device is if a heat source were applied to all the gratings at the same time, then the reflected power from each grating would accumulate.

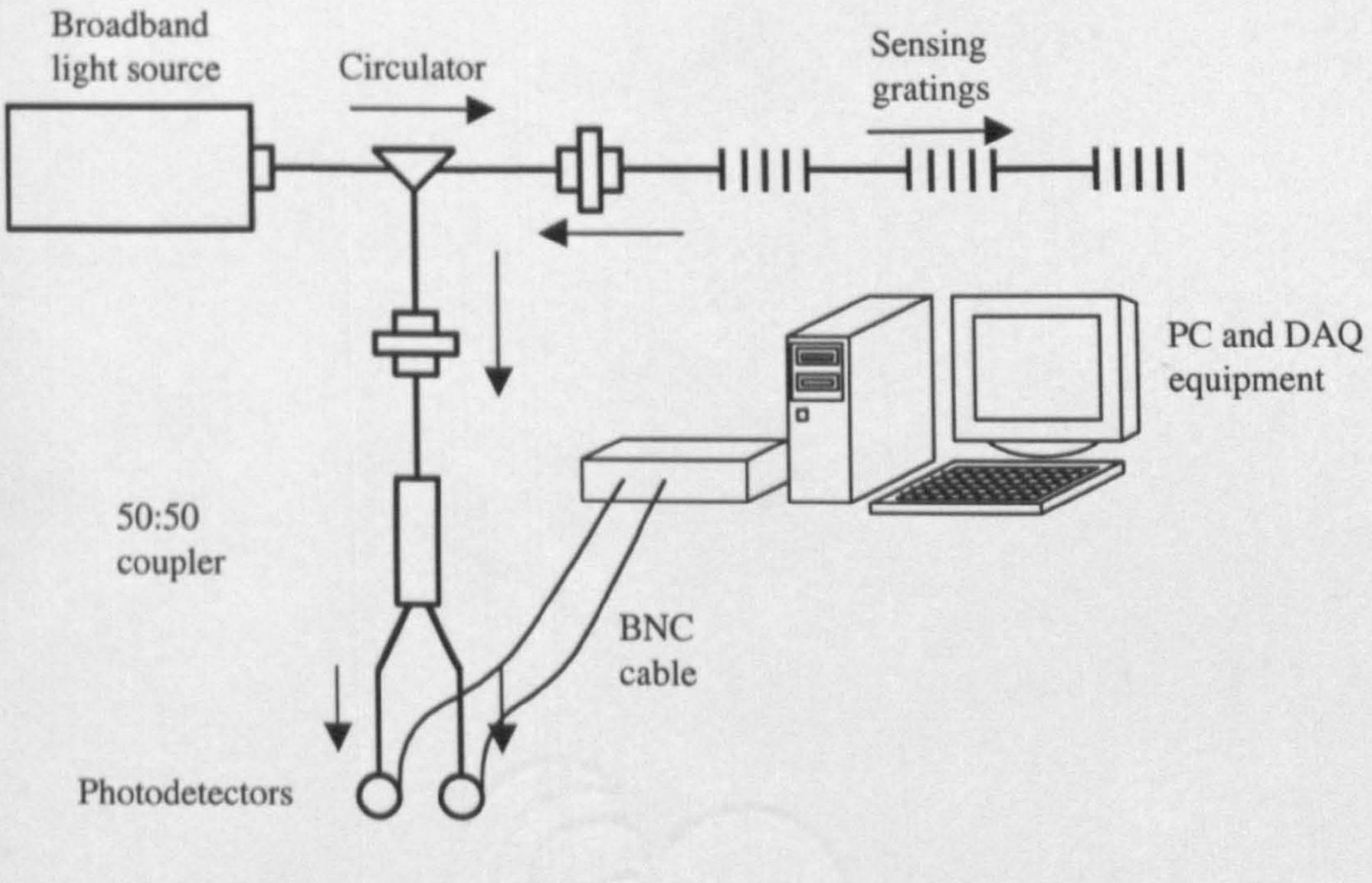

Figure 7.2.: *50:50 coupler system.*

The same principles, grating choices and restrictions are true for the coupler technique if applied for multiple sensing. The layout of the distributed sensing device is illustrated on figure 7.2..

There are two possible application of the two gratings technique for multiple sensing:

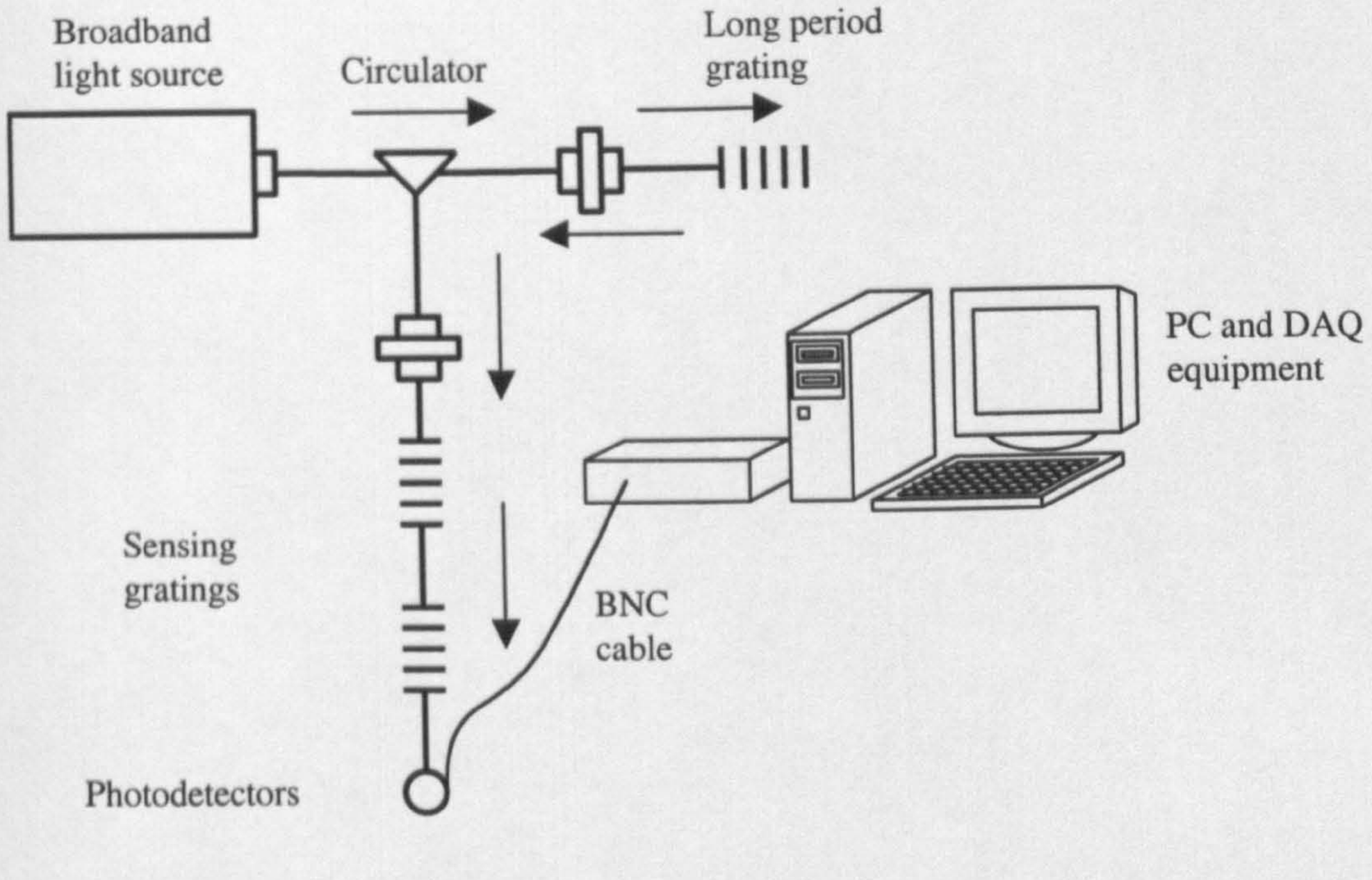

Figure 7.3.: *Two gratings system solution 1.*

Solution 1 (figure 7.3.) is based on a long period grating reflecting the optical signal. Long period gratings have broad bandwidth so therefore it is possible to "position" a few sensing gratings along that slope. However this technique is susceptible to the same problems as before. It will be hard to differentiate the signals if the sensing gratings are subjected to a heat source at the same time. Solution 2 (figure 7.4.) is based on the system used for single point sensing. Each sensing gratings will have their own "light source" (reflection of the light source signal by the first gratings). But the signal differentiation is still a problem unless a coupler is used as described in figure 7.5.. Then multiple sensing is possible at the same time on different gratings.

Note:

It is very important to select a relatively long distance between two consecutive gratings so that the changes induced by temperature on the created Fabry-Perot cavity [2] cannot be detected by the filtering system and therefore will not interfere with the Bragg grating sensors signal.

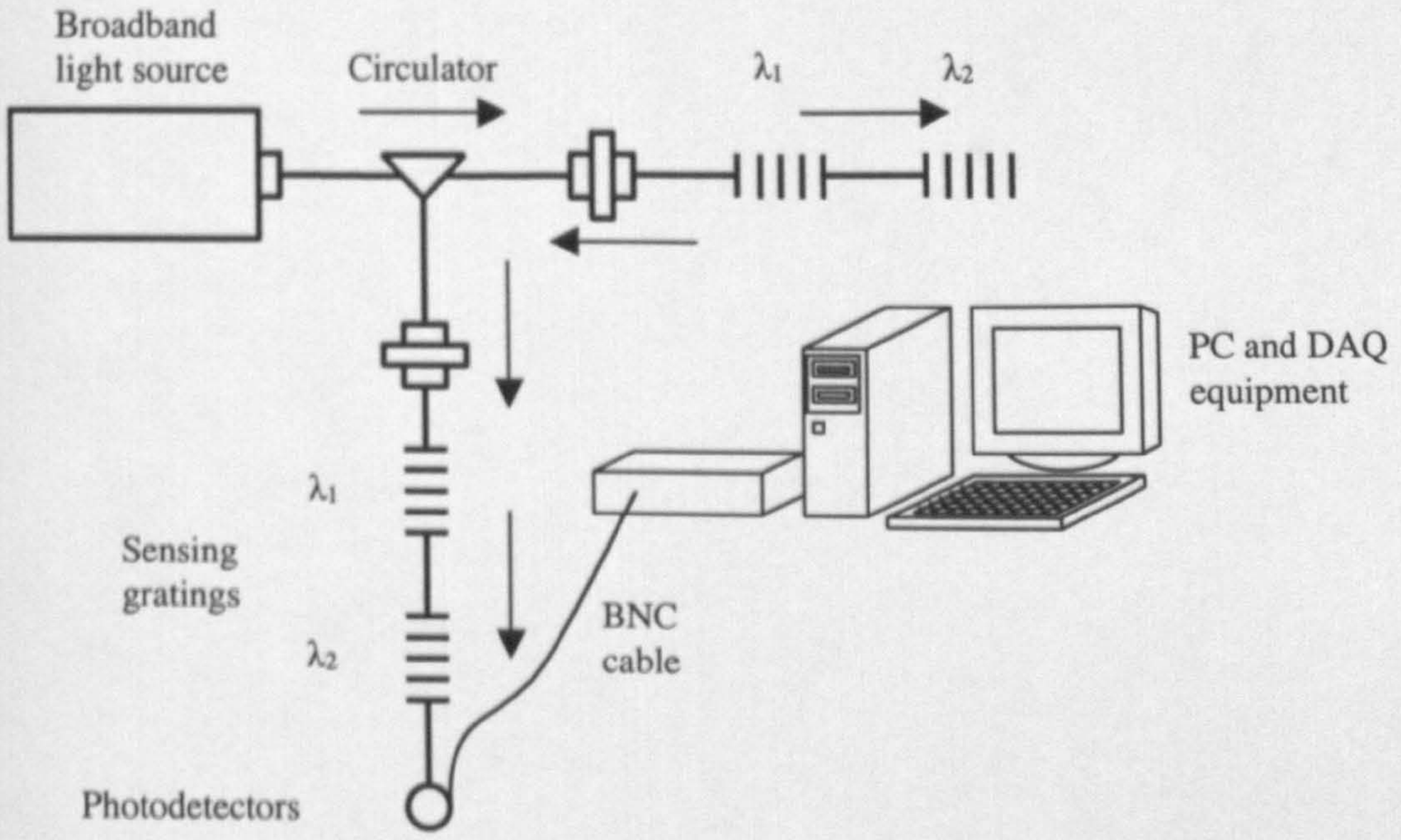

Figure 7.4.: *Two gratings system solution 2 based on the system described by Hyungdon R., Hojoon L. and Ki-Soo K. [3].*

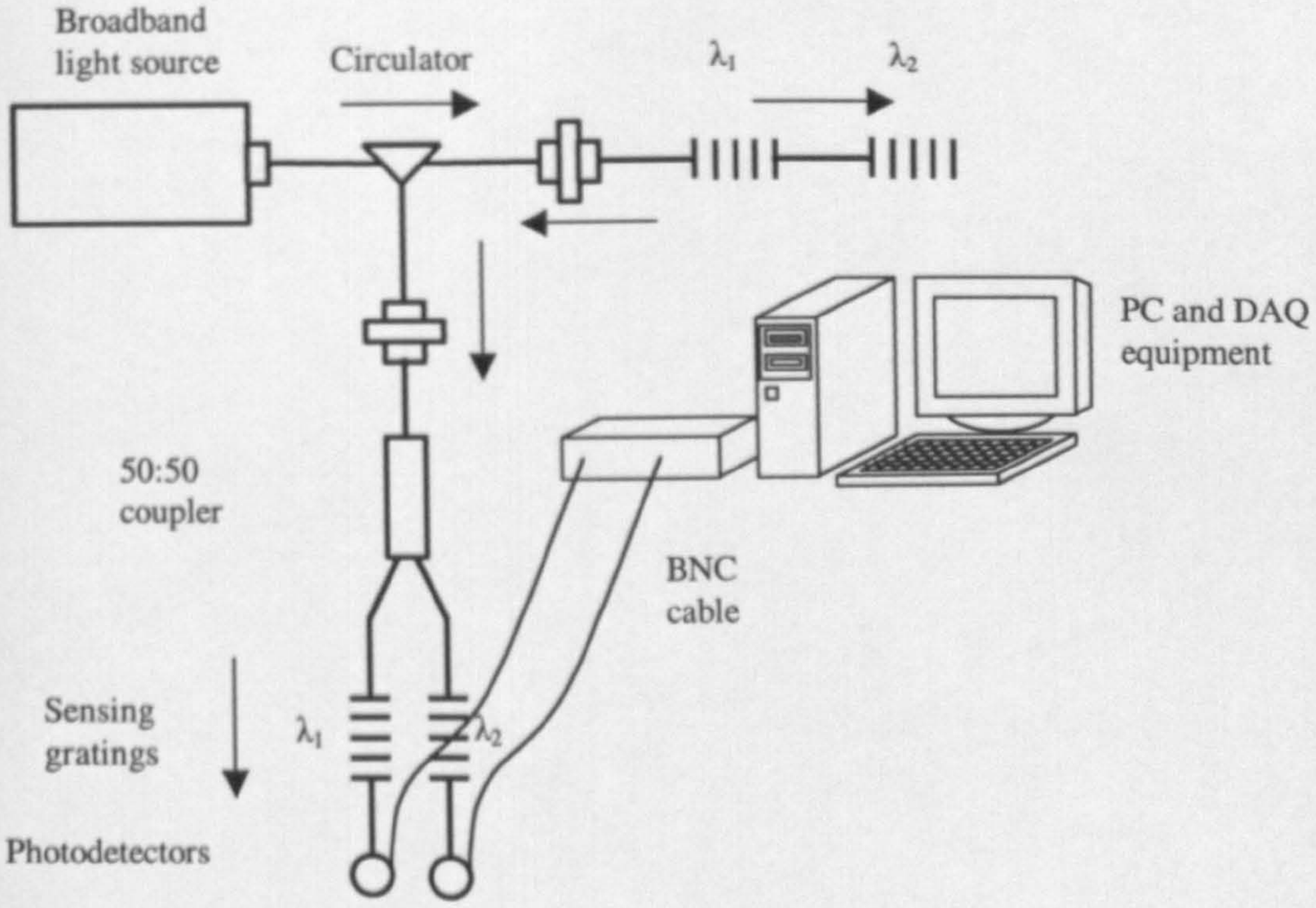

Figure 7.5.: *Two gratings system solution 3.*

The DWDM multiple sensing system (figure 7.6.) has the main advantage that it can differentiate each sensing grating. In other terms, using that technique it is possible to achieve the sensing of four gratings or more at the time if each grating is chosen so it is matching the various DWDM channels.

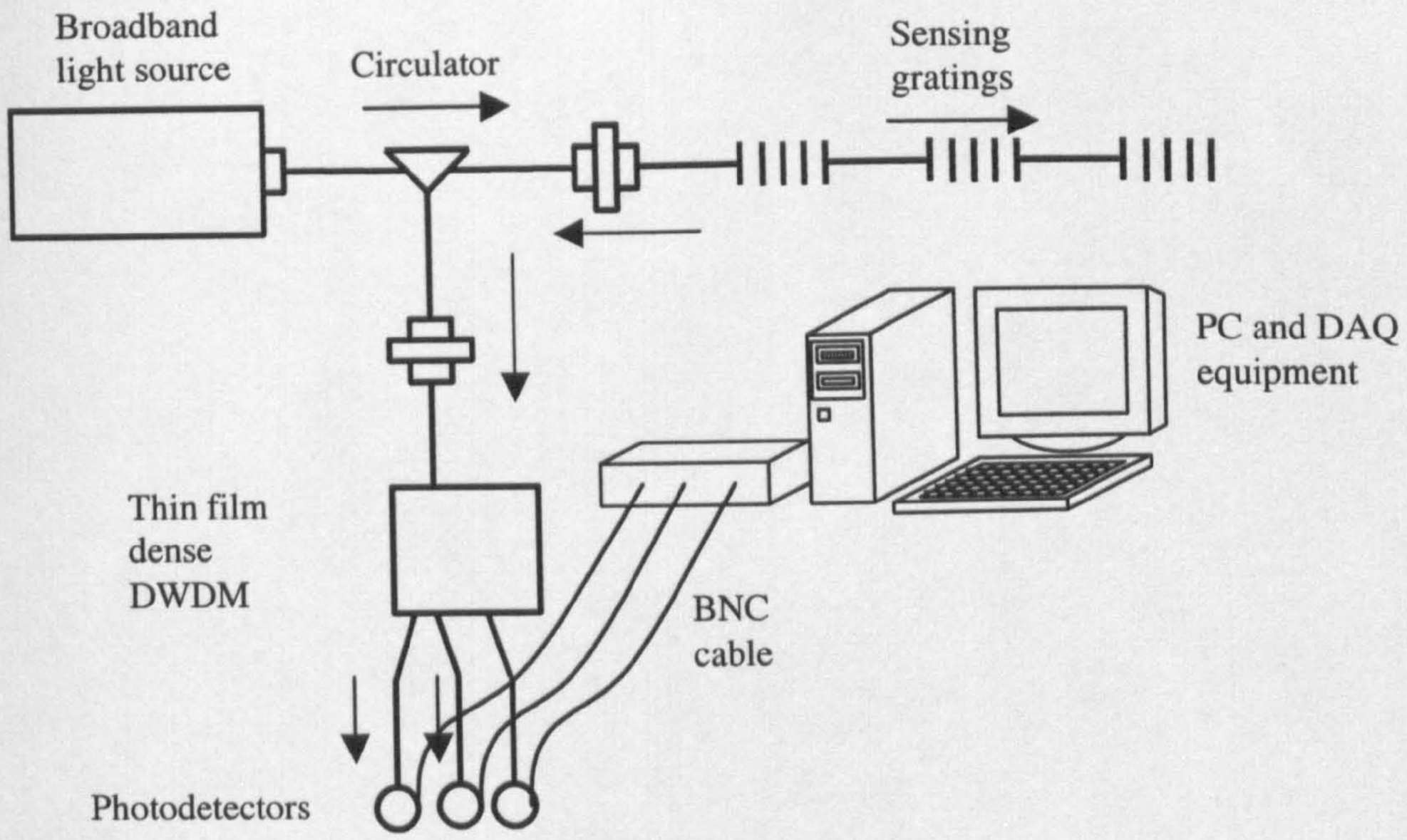

Figure 7.6.: *Thin film dense DWDM system.*

Note:

The multiple Bragg gratings do not have to be written in the same fibre, it is possible to use a multi-branches coupler to separate the signal into many different fibres each containing one or more sensing gratings as illustrated figure 7.7..

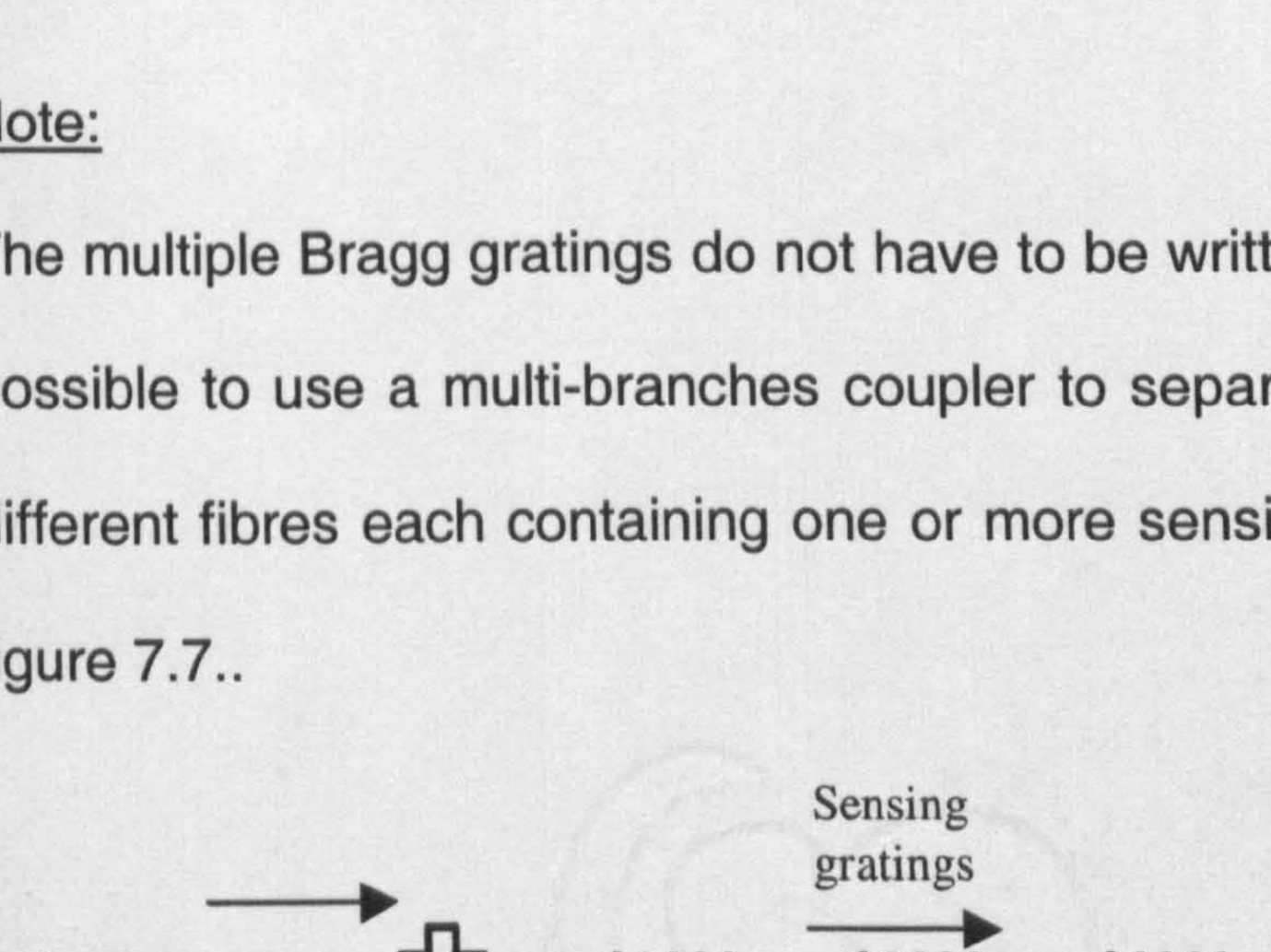

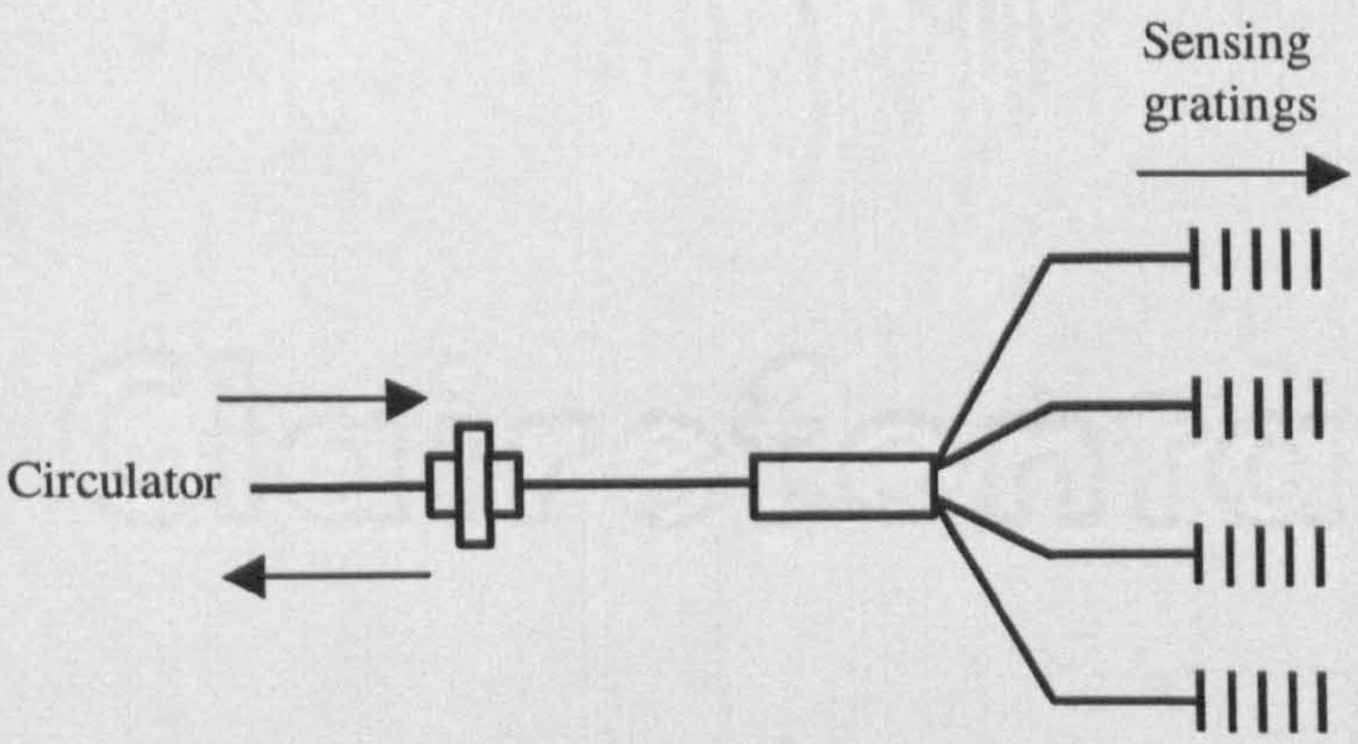

Figure 7.7.: *Different multiple FBG layout for distributed sensing application.*

7.2.3. Grinding application.

The ideas previously presented on distributed sensing could be used to monitor the heat penetration at different depths in the workpiece. This could be achieved by inclining the groove of the sensing fibre and employing a fibre with multiple gratings as illustrated on figure 7.8..

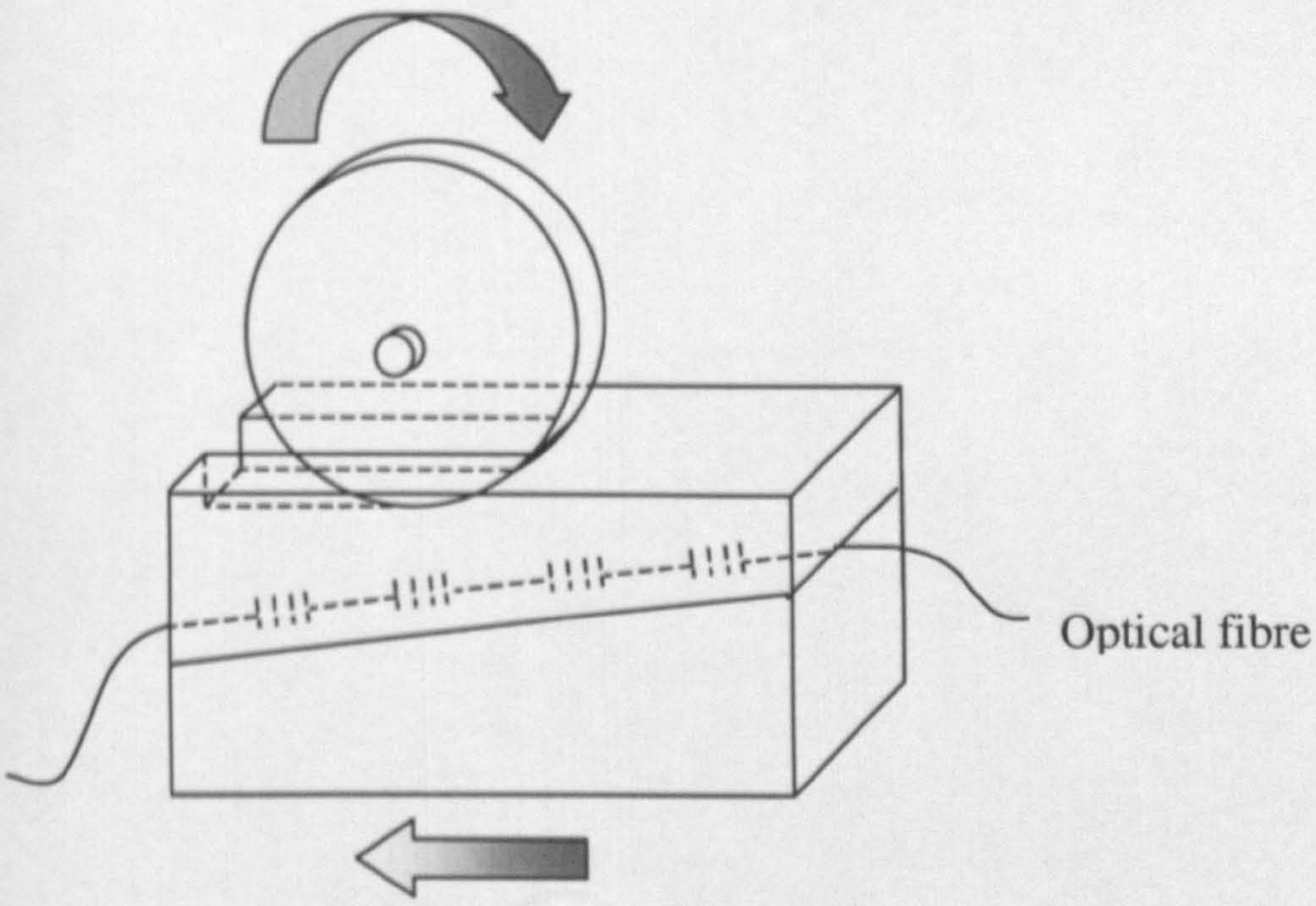

Figure 7.8.: *Grinding application of an optical distributed sensor.*

Further work is required on the inverse heat transfer calculation of surface temperatures. A 2D numerical method (finite difference) could be used for the reconstruction of the surface temperatures and the heat source.

References.

1. Lee B., "Review of the present status of optical fiber sensors", Optical Fiber Technology 9, p 57-79, 2003.
2. MacPherson W N, Kilpatrick J M, Barton J S, Jones J D C, Zhang L and Bennion I, "Heat-flux measurement using fibre-Bragg-grating Fabry-Perot sensors", Meas. Sci. Technol. 10, p 1300-1304, 1999.
3. Hyungdon R., Hojoon L. and Ki-Soo K., "Economical and multiple fiber grating sensor system with rapid response using CDMA", 14th international conference on optical fiber sensors, SPIE vol. 4185, No.3, p 712-715, 2000.

Appendix.

Publication.

F. A. Bezombes, D. R. Allanson, D. R. Burton, M. J. Lalor, "High speed temperature measurements using novel optical fibre-based systems", SPIE 5145, p 117-127, 2003.

APPENDIX NOT COPIED

ON INSTRUCTION FROM

UNIVERSITY

Further calibration.

After this thesis was written, further calibration work of the fibre Bragg grating temperature sensor was undertaken. This was possible because the equipment was not to be dismounted anymore (for demonstration etc..) resulting in canceling the possible insertion of extra losses (induced by mounting and dismounting connectors) i.e. possible errors in the calibration. The DWDM system was selected for further calibration and direct temperature measurement using fibre Bragg grating.

A techgene thermal cycler was used to calibrate the sensor. The thermal cycler allows a wide temperature range from 4°C to 99°C with a block uniformity 0.5°C and an accuracy <±0.4°C. Thermal cyclers are commonly used to conserve D.N.A.. The fibre Bragg grating and thermocouple were placed close to each over on the thermal cycler plate for comparison purpose. The first measurement was taken at 5°C and a measurement was taken for every 5°C steps up to 95°C (figure A2.1. shows the measurement achieved for a thermal cycler temperature of 40°C). Once the data wasstored an average of each channel was taken for each tests and they were plotted together in a final graph (figure A2.2.).

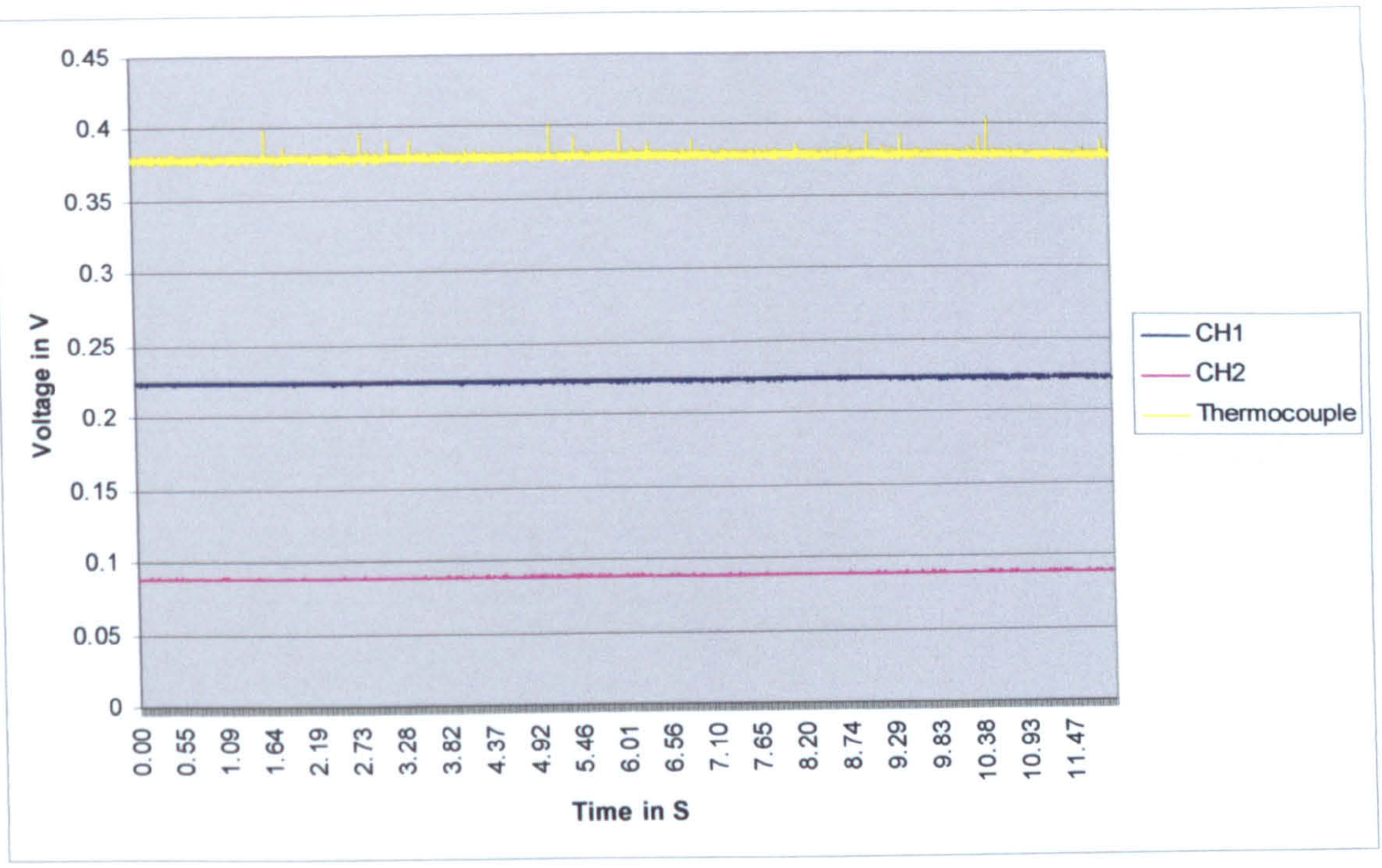

Figure A2.1.: *Measurement achieved for a thermal cycler temperature of 40°C.*

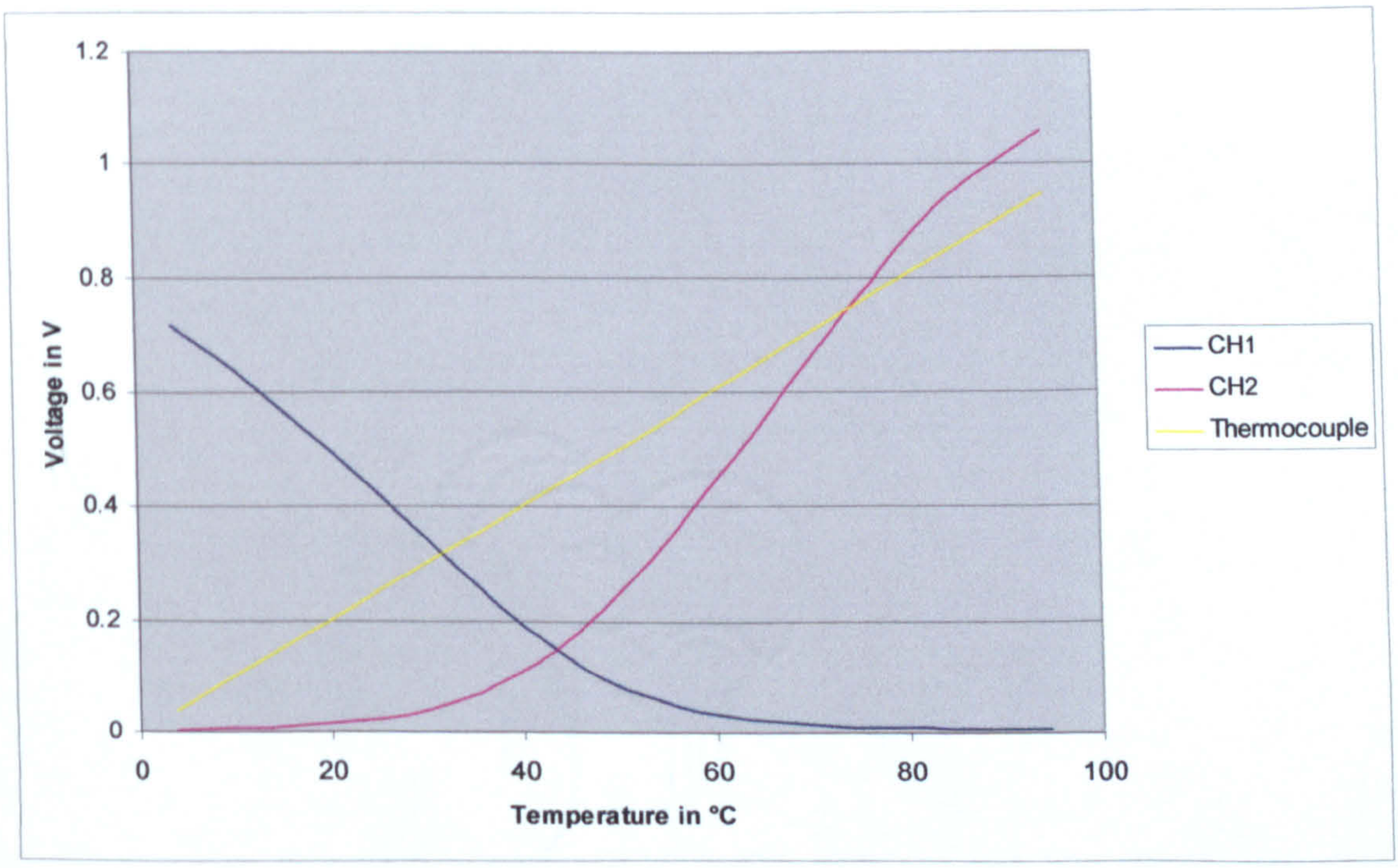

Figure A2.2.: *Compiled results from one set of experiments.*

Many tests were undertaken to check the repeatability (a maximum average error of approximately 0.0022V was calculated on CH1, 0.0032V was calculated on CH2 and 0.0038V was calculated on the thermocouple signal

between different tests (figure A2.3.)) of the DWDM based system during heating and also cooling down (from 95°C to 5°C in 5°C steps). This good repeatability allowed for effective and easy calibration of the optical temperature sensor as explain later.

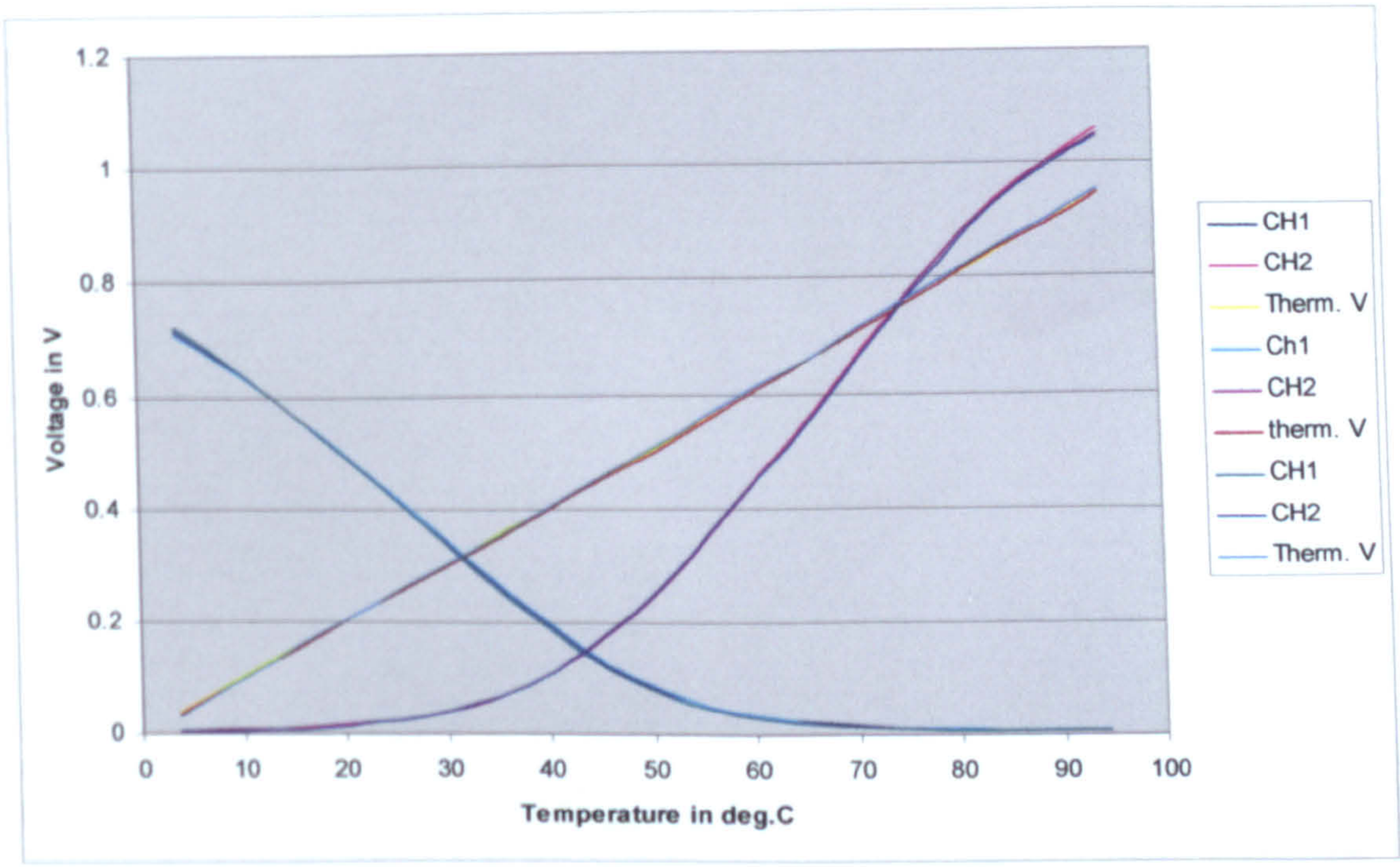

Figure A2.3.: *Repeatability tests.*

The voltage versus temperature (measured by the thermocouple) values are then entered in a Matlab program that is used for the direct calibration using cubic interpolation of the optical sensor (DWDM system). It is now possible to find the exact temperature value for each channels for a specific voltage input for example 0.1V measured on the CH1 of the optical system corresponds to approximately 47.8°C and 0.1V measured on CH2 of the optical system corresponds to approximately 39.1°C or vice versa it is possible to say that 32°C for example corresponds to 0.313V on CH1 and 0.049V on CH2. After the calibration was achieved, it was possible to input

test data from figure A2.4. into Matlab and do a program it allowing a temperature display vs. time of the Bragg sensor (figure A2.5.).

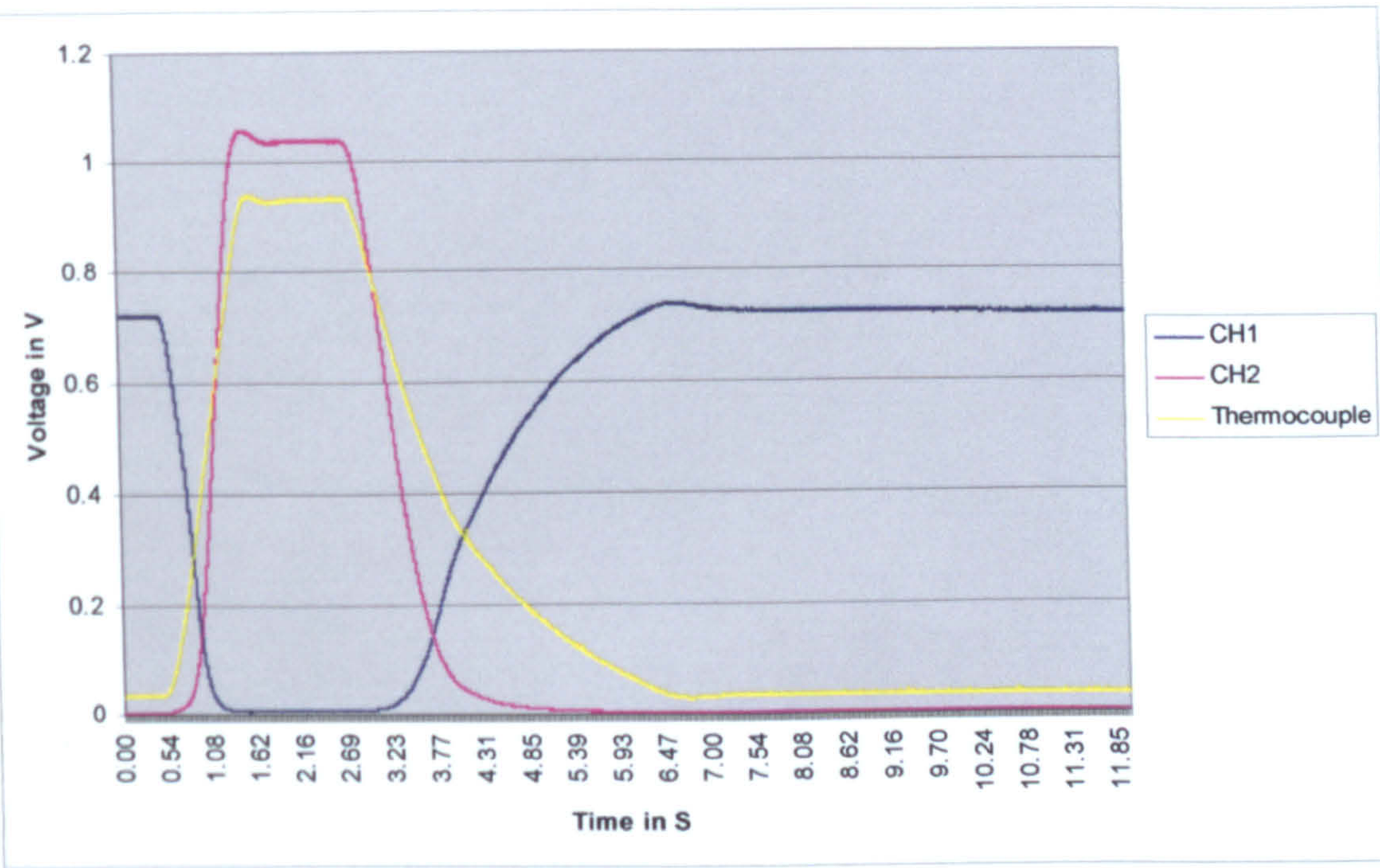

Figure A2.4.: *Test data used to calculate figure A2.5..*

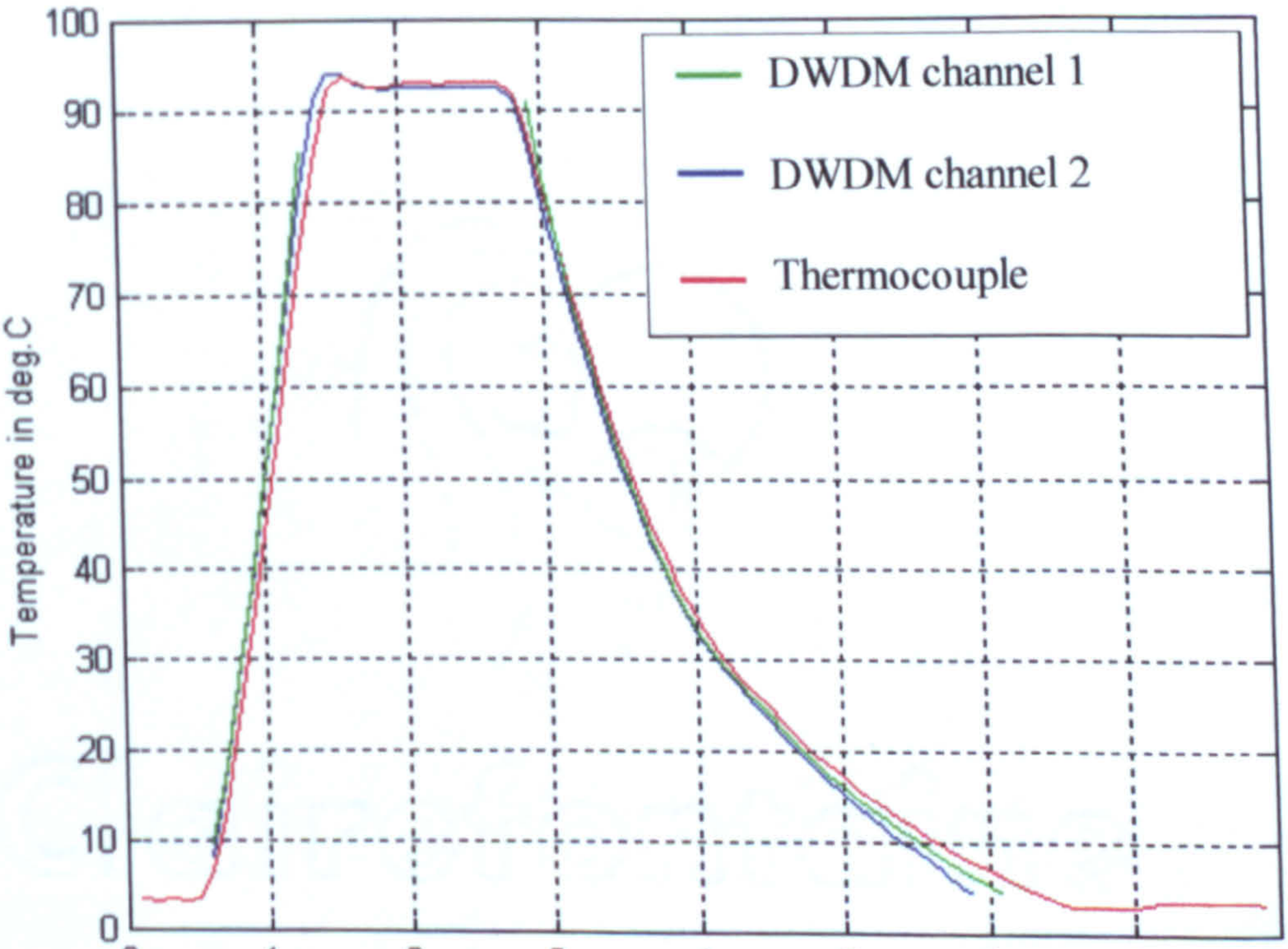

Figure A2.5.: *Temperature measurement using optical fibre Bragg grating interrogated by a DWDM.*

Note:

Channel 1 (CH1) of the optical system saturates so the curve is interrupted.

The noise on the data was removed using cubic interpolation used for calculations purpose.

Further investigations concerning the plotting of the "real" (noisy data instead of trend lines) data need to be undertaken.